Locomotion and Morphing of a Coupled Bio-Inspired Flexible System: Modeling and Simulation

by

Seyed Javad Fattahi

Thesis submitted to the
Faculty of Graduate and Postdoctoral Studies
In partial fulfillment of the requirements
For the Ph.D. degree in
Mechanical Engineering

School of Information Technology and Engineering
Faculty of Engineering
University of Ottawa

Abstract

The thesis focused on the development and analysis of a distributed parameter model that apply to a class of an autonomous hyper-redundant slender robotic systems interacting with the environment. The class of robotic devices that will be implemented based on the modelling in this thesis, is intended to be autonomously deployed in unknown, unstructured environments, in which it has to accomplish different missions by being able to robustly negotiate unknown obstacles and unpredictable and unmodelled irregularities. Therefore the mechanical models presented here are inspired by some features of a class of organisms - millipedes and centipedes - that possess many of these capabilities. Specifically, these organisms posses flexible slender bodies whose shape morphs according to the curvature of the terrain on which they operate, and possess a highly redundant system of legs that couple the body with the terrain providing propulsion for forward or backward motion, with the high number of legs ensuring a robust distributed contact even on very irregular substrates. The mechanical model that naturally captures the structure of millipede bodies is the Timoshenko beam, which is therefore adopted here. Moreover, the coupling with the environment is modeled by a system of compliant elements, that provides a distributed support analogous to the one exerted by millipedes' legs; such support provides a distributed force that in a control framework is treated as the actuation for shape morphing, so that the body of the system deforms according to the curvature of the substrate. By using a Lagrangian mechanics approach, the evolution of the system is described in a suitable product Hilbert space, in which rigid body degrees of freedom and deformations are coupled. This formulation allows to pose a distributed parameter control problem in which shape morphing and locomotion are dictated by the interaction with the substrate, which in this case is approximated as rigid (that is, the profile of the substrate is not affected by the interaction with the system).

Additionally, by modeling the material response of the substrate with a simple linear viscoelastic model, we pose an estimation problem in which, by measuring deformations and/or stresses on the body represented by the beam, we can infer the material properties of the substrate. In this case, the overall coupled system is modelled as a beam on a multilayer viscoelastic foundation. Predictions of this sensor model are in good agreement with published results, suggesting that the system can be used in a versatile way as an autonomous agent operating in a generic environment, and simultaneously as a sensor that could inform the action of the system itself, or that could be used to monitor the environment. The modeling work done in this study opens the possibility for the implementation in engineering systems applied to environmental monitoring and health

applications, in which we envision the system to be used to estimate material properties of living tissues, that can be correlated to the diagnosis of classes of diseases.

Preface

This thesis has been prepared in Thesis by article format described in the 2013 general regulations for a doctoral thesis, University of Ottawa, Faculty of Graduate and Postdoctoral Studies:

> The minimum requirements for this thesis format are three articles for a doctorate. If the research embodied in the articles required approval of an ethics board or was part of a collaboration, this must be spelled out in a preface or statement. In this preface, the student must indicate the following: a) what ethics approvals, if any, were required and when those approvals were secured; b) what are the contributions of collaborators and/or co-authors, distinguish the student's own contributions from all other contributions. The thesis by article must have: a) a general introduction, which outlines the thesis topic, and how the articles that comprise the main body of the text will address the topic. b) a general discussion and conclusion, which integrates the material addressed in the various articles and provides a global summary and analysis. The student must get permission to use copyrighted material from any co-authors (if they hold copyright) as well as from publishers.

No ethics approvals were required for this research. The contributions of coauthors are listed on subsection 1.6. Material in Chapters 5, 6, and 7 are partial duplicates of published work, as indicated in detail at the beginning of each Chapter. The chapters are not direct duplicates of the existing work. Some author original content additions and formatting changes were made to promote clarity and coherence of the presented subject matter. Concerning the material in Chapter 5, Elsevier Copyright agreement allows the authors to archive pre-print and post-print versions of the work (see `http://www.sherpa.ac.uk/romeo/issn/0022-460X` for details). For the material in Chapter 6, permission for publication has been obtained by ASME (See Appendix B). The material in chapter 7 has been published in an open access journal.

Acknowledgements

Sometimes, there comes a moment in life when no words, however appropriately chosen, can do justice to one's thoughts and feelings. This is such a time for me. I know I must personally thank many persons for this accomplishment of mine, but I am concerned I will miss some. If this does indeed happen, I will have you know that it is not intentional.

I would like to thank Dr. Necsulescu and Dr. Ahmadi for their valuable advises during my study, and I should specially thank Dr. Necsulescu, who gave me this chance to start my Ph.D. study in University of Ottawa, and none of this would have been possible without Dr. Spinello, who trained me patiently and consciously. I appreciate all of his contributions of time, ideas, and funding to make my Ph.D. stimulating. Undoubtedly, his enthusiasm for research was contagious and motivational for me, even during tough times in the Ph.D. pursuit.

Dedicated to my father

Contents

List of Tables

List of Figures

Part I

Synopsis of thesis

Chapter 1

Overview and Literature Review

1.1 Motivations

The work in this thesis is part of a project aimed at the development of a robotic device for exploration, maintenance, and non destructive testing in generic environments, that eventually can be hazardous and/or non accessible to humans. The work presented here specifically pertains to the first part of the project, which has been focused on the definition of the key characteristics that this class of devices should possess. The set of characteristics is ultimately dictated by the high level definition of the tasks that the system has to perform (desired tasks). Once the key characteristics have been defined, the next step is their translation into models that formally describe the evolution of objects and systems that suitably reproduce them. Modeling choices therefore determine a framework that allows to predict the evolution of the robotic devices, and their response in a closed loop setting, which in this case is the autonomous navigation and decision making informed by appropriate or available sensing information.

As mentioned, the class of robotic devices considered in this dissertation are intended to be able to autonomously operate in unstructured environments, or otherwise to be able to move into and explore a large (as possible) variety of terrains and substrates. Additionally, it is desirable that devices are equipped with sensing capabilities that are sophisticated and versatile enough to infer properties of the environment in which they operate. The translation of a set of desired characteristics into suitable models poses different challenges. Indeed models should be simple enough to be treatable and offer insights into the structural formal properties of modelled systems, and at the same time they should be comprehensive enough to describe and include the desired features. More-

over, robotic models have always to be developed within implementability constraints, so that modelling assumptions can realistically map to hardware and software limitations and operational conditions. This particular aspect is the object of current and future work that is the continuation of the one presented in this study, with refinements oriented to the implementability of developed theoretical tools.

From a modeling perspective, in order to develop a framework for an robust mobile system that autonomously navigate unstructured environment, we have taken inspiration from the mechanics of millipedes whose bodies morph to adapt to nonzero curvature substrates, and with forward locomotion provided by a system of legs. The redundancy of the legs ensures abundant contact in terrains with various morphologies and degrees of asperity, therefore guaranteeing the necessary thrust for locomotion.

1.2 Modelling Overview

To develop the distributed parameter modeling for a hyper redundant bio-inspired mechanism, in this thesis we present a model for the forward locomotion and shape adaptation of a slender hyper-redundant mechanism. We model the mechanism as a Timoshenko beam in plane motion with natural (force) boundary conditions, which includes a rigid body placement, kinematically described by three degrees of freedom. We assume that the characteristic length of the robot is small as compared to the radius of curvature of the substrate to which it is deployed, therefore adopting small deformations kinematics around rigid body placements. This leads to the use of the floating reference frame description [1, Chapter 5]. By reproducing the scenario of a slender robot deployed in a generic environment, the shape-tracking problem can be posed in terms of coupling with a substrate. This coupling is realized through a distributed system of spring elements that, in terms of feedback, are represented by a distributed force. We express the forward locomotion in terms of the rigid body degrees of freedom tracking a moving point on the substrate. The forward locomotion can therefore be described as a path following problem by employing a Frenet frame intrinsic description of the substrate as a parametrized curve in the two-dimensional environment [2]. The forward locomotion and shape adaptation problems are coupled by posing the problem in a distributed control framework with minimization of a suitable action functional based on the Lagrangian function of the system.

By modeling the material response of the substrate with a simple linear viscoelastic model, this study also tries to pose an estimation problem in which, by measuring

deformations and/or stresses on the beam, we can infer the material properties of the substrate. In this case, the overall coupled system is modelled as a beam on a multi-layer foundation, where different layers have different material responses. Predictions of this sensor model are in good agreement with published results, suggesting that the system can be used in a versatile way as an autonomous agent operating in a generic environment, and simultaneously as a sensor that could inform the action of the system itself, or that could be used to monitor the environment.

The model presented here is the first step towards the design and realization of a flexible hyper-redundant autonomous robotic system, which is highly adaptable to different terrains and environments. This kind of robot can be used as a machine for the non-destructive testing on out of reach facilities, or it can be used to inspect hazardous environments like gas pipes to check the overall condition of medium structure as a health monitoring tool. The class of models in this work could also be applied to the continuum description of novel healthcare systems like endoscopic tools for diagnostic in the gastrointestinal tract, and generally the engineering applications are the ultimate driving forces of this research.

1.3 Objectives and Contributions

The main objective of this thesis is the development and simulation of the closed loop dynamics of a system that is the modeling foundation of a class of robotic devices. This class of robotic devices is being designed to develop autonomous systems capable of robustly operating in unstructured environments, with applications that span environmental and structural health monitoring, and healthcare devices capable of moving in living tissues by coupling with the surroundings. Towards these objectives, the thesis study has achieved the following main contributions:

1. Develop a study of the kinematics and dynamics of a bio-inspired system based on distributed parameter modeling. We developed an appreciation of the robot's flexible body as a linearized planar Timoshenko beam theory, where the shape morphing is associated to the coupling with a substrate that models a generic environment in which the system could be deployed. This mechanical model mimics the spinal locomotion mechanisms of millipedes and centipedes in which the flexible body morphs with respect to the curvature of the substrate. The interaction with the environment has been described by a continuous distribution of spring elements

mimicking the robot legs.

2. Develop a study of millipede's locomotion. In order to cover all essential steps in the analysis of the system, we propose mathematical models, which analytically deal with both shape adaptation and forward motion modelling of a slender robot mechanism through linear Timoshenko beam theory. Systems modelled in this manner are referred to as distributed parameter (continuous) systems, in which, both forces and deformabilty are distributed throughout the extent of the system which is treated as continuous.

3. Develop a study on spinal and forward motion control algorithms, in which proposed system's Lagrangian gives an algorithm for classical and modern control framework, in order to tune the system deformability and control the forward motion. To describe the motion of the robot, we adopt the concept of floating frame that is composed of a rigid body placement and by deformation about the rigid body placement.

4. Develop a study of distributed sensor in order to find the properties of the environment that system has been deployed in. Since distributed compliant elements can act as a distributed sensor to reconstruct the kinematics of the substrate to which the robot is coupled. This work performs an inverse problem for continuous systems using distributed strain gauges. By exploiting this relation and the possible generalization, one can model the robot as a sensor to infer certain material properties of the substrate.

1.4 Literature Review

Robotics has been inspired from biological systems to reproduce some very desirable features, such as robustness and adaptability to unknown disturbances that typically arise during the operation and within the interaction with complex environments. An excursus of developments in robotic science can be found through the following references, and it is summarized in Figure 1.1.

Serial robotic manipulators, initially developed as the implementation of rigid body chains, have been applied in many industrial fields [3]. Afterwards, manipulator designers started to build the mobile robots in the framework of *wheel-platform* and *leg-platform*. In very simplistic terms, the leg-platforms mechanisms have more degree of freedom to

1495	Leonardo da Vinci designed what may be the first humanoid robot.
1645	Blaise Pascal invented a calculating machine to help his dad with taxes.
1709	Jacques de Vaucansons most famous creation was undoubtedly "The Duck."
1801	Joseph-Marie Jacquard invented a loom that could be programmed to create prints.
1865	John Brainerd created the Steam Man used to pull wheeled carts.
1903	The first patents were awarded for the construction of a printed wire
1921	The term "robot" was first used in a play called "R.U.R." by the Czech writer Karel Capek.
1937	Westinghouse creates ELEKTRO a human-like robot that could walk, talk, and smoke.
1941	Science fiction writer Isaac Asimov first used the word "robotics" to describe the technology of robots
1942	The first programmable mechanism, was designed by Willard Pollard
1946	George Devol patented a general purpose playback device for controlling machines.
1948	W. Grey Walter created his first robots; known as the turtle robots.
1951	Raymond Goertz designed the first tele-operated articulated arm.
1954	George Devol designed the first truly programmable robot, known as UNIMATE.
1960's	One of the first operational, industrial robots in North America appeared in Kitchener, Ontario.
1968	The first computer controlled walking machine was created by Mcgee the at University of South Carolina.
1968	The first manually controlled walking truck was made by R. Mosher.
1968	SRI built Shakey; a mobile robot equipped with a vision system.
1969	V. Scheinman created the Stanford Arm, which was the first successful computer-controlled robot arm.
1969	WAP-1 became the first biped robot and was designed by I. Kato.
1973	V.S. Gurfinkel and colleagues create the first six-legged walking vehicle.
1973	I. Kato created WABOT I which was the first full-scale anthropomorphic robot.
1973	C. Milacron released the T3, the first commercially available minicomputer-controlled industrial robot
1975	V. Schenman developed the Programmable Universal Manipulation Arm (Puma).
1977	The V. Masha, a six-legged walking machine.
1978	S. Hirose created ACMVI (Oblix) robot. It had snake-like abilities.
1979	H. Makino designed the Selective Compliant Articulated Robot Arm (SCARA)
1980	Quasi-dynamic walking was first realized by WL-9DR.
1981	S. Hirose developed Titan II.
1985	RB5X was Created by the General Robotics Corp.
1985	A four legged walking machine, Collie1.
1988	The first HelpMate robot went to work at Danbury Hospital in Connecticut.
1989	Aquarobot, a walking robot for undersea use.
1989	The WL12RIII was the first biped walking robot, by Kato Corporation
1993	Dante explored Mt. Erebrus. The 8-legged walking robot.
1996	RoboTuna was created by D. Barrett at MIT. The robot was used to study how fish swim.
1996	Honda created the P2, which was the first step in creating ASIMO.
1998	NASA's PathFinder landed on Mars.
1998	LEGO released their MINDSTORMS robotic.
1998	Campbell Aird was fitted with the first bionic arm called the Edinburg Modular Arm System (EMAS).
1999	Mitsubishi created a robot fish.
2000	Sony unveiled the SDR at Robodex.
2001	iRobot Packbots searched through the rubble of the world Trade Center.
2002	iRobot released the first generation of Roomba.
2005	Cornell University created self-replicating robots.

Figure 1.1: The overview of the evolution and growth of robotic science and applications [4–12].

control and technically they are more complicated than the wheeled-platform robots, but in the unstructured environment legs are more adapted than wheels. However, the complexity for modeling and control grows with additional degree of freedom, and also dynamics of multi body system differ from those robots which are operating in a fixed station and without the capability to reconfigure or movement. To address the kinetics and dynamics of multi body systems, the classical dynamics are usually described by setting up the equations of motion through common methods like Newton-Euler, Lagrange or Hamilton. Furthermore other modern methods for the dynamic analysis of multibody systems could be in form of differential algebraic equations (DAEs) and/or ordinary differential equations (ODEs). Apparently, both conventional and modern methods in dynamic analysis point of view employ a maximal set of constraint and degree of freedom to describe the dynamic relations of the system.

The evolution of multi-body systems is described by a set of differential equations, algebraic constraints, and variables depending on the state of the system. Occasionally the performance of the system depends on geometric constraints of the robot that allocates the task. This kind of problem can be solved by considering a system with many degrees of freedom and the idea of discrete concurrent computation and acting in the system like mechanisms which we can be seen in many biological systems. In the application framework, the multi-body robots are widely used in many fields such as general industrial application, health monitoring, inspecting hazardous or inaccessible environments, and health care inspectors, or they are used as probes for smart drug delivery or in surgical applications. There are two main approaches in modelling the kinematics and dynamics of robotic manipulators. The first one is based on multi-body mechanics, in which the manipulator is comprised of a chain of rigid bodies interconnected in such a way that relative degrees of freedom are permitted among subsets (typically pairs). In this case the system has a finite number of degrees of freedom, whose evolution is described by a system of ordinary differential equations in which torques acting as duals of kinematic degrees of freedom are treated as control inputs. This approach has been historically used in the development of robotic manipulators with a relatively low number of degrees of freedom, and in which the interaction between parts can be well approximated by rigid body mechanics.

The other approach is based on distributed parameter modeling, in which the evolution of infinite dimensional system (for example a beam) is used to describe the dynamics of a manipulator. The continuous description is introduced to approximate a class of systems with many degrees of freedoms, or systems for which the flexibility can be con-

sidered as distributed in describing the interaction between parts. For these reasons the related class of modeled systems is often referred as hyper-redundant. The advantage of this approach in modeling systems with many degrees of freedom is that an otherwise large system of coupled ordinary differential equations is replaced by a more compact system of partial differential equations describing the evolutions of spatial fields. However, the solution of distributed parameter systems is in general more difficult as it requires specific techniques (often numerical) to deal with the spatial dependence of the field equations. Solution techniques are usually based on separation of variables and subsequent spatial projection on a finite dimensional subspace of the set in which the solution of the original problem is defined. In this work we use a standard Galerkin projection on linear modal basis functions of the beam that models the body of the robot.

In the field of robotics, it is crucial to investigate the effects on multibody robots of the environment's interaction variations, and from the point of view of dynamics and motion, physics based multibody simulations have gained more importance due to their versatility [14–16]. Another relatively recent branch of robotics research is biomechanics, which is concerned with mechanical modeling of features characterizing biological systems ,where the kinetics and dynamics of multibody systems are often used as modeling frameworks [17–20].

Common to all multibody systems is the need for reliable computation for dynamic analysis of the motion, which is an important factor in determining the best design. Reliable computation for dynamic analysis has led to remarkable developments within the fields of structural dynamics in the last two decades, in which use of Lie groups and differential geometry has gained importance in the robot technology, structural mechanics and control system [21–25].

In the same framework, the biomechanics field the symmetries and geometric features, like the symplectic structure of Hamiltonian and Lagrangian systems, play a main role in stability analysis and in the evaluating the system's physical characteristics [26–28].

In the field of flexible manipulators and articulated multi-link flexible robots, several studies have recently considered the different beam models and various constitutive models, as well as time-varying boundary conditions [29]. The dynamics of single robotic flexible manipulators have been studied in [30, 31]. Ower and Van de Vegte [32] discussed the vibrations of a flexible manipulator model based on the linearization and transfer function matrix of an Euler-Bernoulli beam model; their analysis did not involve large displacements. De Luca and Siciliano in [33] introduced simplifying assumptions in end mass-boundary conditions in order to derive the governing equations. Moreover,

Lagrangian and Ritz methods have been used in [34] to study a flexible manipulator. Recently Chaolan et al. [35] analyzed a flexible hub-beam system by accounting for the influence of shear and axial deformations. Chen [36] established a generalized dynamic model for a planar n-link flexible manipulator, and Lee [37] proposed a new link deflection model to fix the incompatibilities dealing with modeling of flexible robots with bending mechanism in the hypothesis of an Euler-Bernoulli beam through the conventional Lagrangian approach. Therewith, Zhang et al. [38] obtained a system of partial differential equations for a two-link Euler-Bernoulli manipulator from an Hamiltonian formulation in order to design reliable control techniques. Milford and Asokanthan [39] presented the modal analysis of a two-link flexible manipulator by using the Timoshenko beam theory from partial differential equations governing the free vibrations. di Castri et al. [40] investigated modal analysis of a two-link flexible manipulator, and they showed how it can recover large discrepancies associated with the model proposed in [39]. In general, when local deformations are not small, it may be desirable instead to formulate the equations of motion with respect to an inertial frame of reference. However, this introduces a number of difficulties, mainly associated with the proper handling of translations and rotations. Furthermore, the development of flexible elements accommodating finite rotations usually results in rather complex formulations, and particularly numerous formulations for flexible beams can be found in [41–44].

By taking inspiration from the mechanics of several biological systems, the robotics field started to develop mechanisms with more degrees of freedom, often referred as hyper-redundant systems, Often, researchers are focused on the effort of reproducing animal's body capability in adapting to unstructured environments. Animals have indeed developed a wide diversity of mechanisms in moving which are in fact remarkable things that allow them to exploit the physical properties of their environmental leaning, and their amazing quick control switch to take a smooth locomotion for different patterns. Also, modern robotic systems technology has made available joints that are capable of reproducing kinematic actions inherently possessed by biological systems, such as free rotation or drawbacks. Several studies have been devoted to hyper redundant morphologies [45–47]. In order to catch robustness and system adaptability with respect to different environments, mobile multibody robots have been developed from classical manipulators by considering rigid body chains interacting with the environment in a variety of modes. In the framework of flexible members, several researches have recently proposed finite dimensional (with large number of degrees of freedom) and distributed systems capable of high deformability and large displacement of the end effector, still considering

higher speed than traditional manipulators along with low energy consumption [48–51]. This applies, on an evolutionary scale, to biological systems and therefore to bio-inspired robots [52–54]. Furthermore several studies have been devoted to path planning and control of mobile robots [55–57]. Hirose [58–60] studied the motion of snakes on various types of surfaces, the elastic elephant trunk like, and soft grippers. Furthermore the tendon-driven robots and octopus tentacle-like gripper were investigated by Hirose in [61, 62]. Clement and Ifiigo [63] discussed a snake-like manipulator with obstacle avoidance. The model of an articulated mobile robot whose joints are pinned has been studied in [64]; Verriest [65] presented the kinematics and dynamics of a planar multiple link robot and proposed a non-conventional control method based on differential friction. Sen [66] proposed a motion algorithm for a snake-like manipulator robot, and an algorithms for control of hyper-redundant robots by parametrizing their backbone curves in [67]. The first bio-inspired serpentine robot called *Active Cord Mechanism* is presented in [68, 69].

For this class of system, a major challenge in control design is the mapping of distributed sensor inputs to actions for actuators. Additional challenges arise when the system is coupled with environments (for example the problem of warm locomotion) with complex material responses. This has led to the development of advanced technologies in real-time perception in uncontrolled environments applied to hyper-redundant systems [70–76]. In the framework of the multi-link robotic manipulators and dynamic inverse problem, the interaction with the environment strongly affects the performance of mobile robots as environmental conditions and morphology are coupled with locomotion techniques [77–81]. For force control of multi-link manipulators, several researchers have recently proposed the optimal distributed force for mobile robot using generalized inverse kinematics and dynamics algorithms to optimize control forces that have been developed in the manipulator robots for generating redundant robot joint trajectories [82–85]. Many researchers have studied the inverse vibration problem to find out displacement, crack identification, health monitoring of the mechanism or to estimate the material properties or axial external forces with different active or passive approach [86–98]. As the forward vibration solution of a mechanism deal with many kinetic and dynamic terms like initial condition, applied external force in time to find the displacement, velocity and other dynamic relations, in inverse vibration problem also we seek to estimate a time dependent force or material properties. Therefore in order to optimize these estimated time dependent parameters we can use different optimization methods; among all in [99–105] the inverse vibration problem for the linear and non-linear systems

has been addressed considering different optimization methods. General solution of an inverse vibration problem using a linear least-squares error method is presented in [106], a non-linear inverse vibration problem for estimating the time-dependent stiffness by a linear matrix equations and least square error method is presented in [107].

In this thesis, we considered (i) shape tracking with a slender mechanism coupled with a substrate. Shape tracking is based on the flexibility of the mechanism, that is modeled as a Timoshenko beam. The interaction with the environment is described by a distributed system of deformable elements. By considering the initial configuration to be locally parallel to the substrate, in the sense that it is parallel to the tangent to the substrate at the nearest point, we focus on the coupling with the environment and specifically on the deformation induced by the shape of the substrate. (ii) the Lagrangian dynamics formulation of the problem of an hyper-redundant mechanism coupled with a substrate, that encodes the salient features of the mechanics of locomotion and shape morphing of millipedes and centipedes organisms, as elucidated in the recent work [108]. In these organisms, a highly redundant system of legs couples an elongated body with substrates/environment, and the distribution of the contact between the extremities of the legs and the environment results into a peristaltic wave traveling axially, which ultimately provides the propulsive action. In our model, suitable kinematic descriptors allow to link the control of the system with the autonomous operation of a class of devices, that will be implemented based on the model presented here, with bio-inspired features giving the desirable robustness and adaptability to operate in unstructured and unknown environments. With respect to existing literature treating the dynamics and control of hyper-redundant systems, the model developed in this work couples locomotion and shape morphing by describing them respectively as a global rigid body placement and a deformation around current rigid body configurations, with analytical treatment based on the adoption of the floating reference frame; moreover, time scales separation between deformations and rigid body motion capture the very fast shape morphing with respect to forward/backward motion of millipedes; (iii) a well posed distributed parameter control formulation, in which the state variables are defined in a product Hilbert space that allows directly to obtain approximated convergent solutions by projection in its finite dimensional sub-spaces. This permits to simulate salient features of the systems, and to inform future design directions. In current and future hardware implementations based on the model proposed here, actuation is provided by the coupling elements mimicking the legs of millipedes, consistently with the mechanisms characterizing the biological systems investigated in [108]. (iv) a sensor model comprised of a Timoshenko beam coupled

with a linear viscoelastic substrate via a distributed system of compliant elements. The system of governing equations includes the evolution of the kinematic descriptors of the Timoshenko beam and of the interface between the coupling elements and the viscoelastic substrate. This model is used to pose an inverse problem aimed at estimating the constitutive parameters of the substrate from deformation measurements of the beam induced by different input forces and torques.

1.5 Organization of the Thesis

Part I contains the statement of motivation, objectives, and contributions of the thesis, along with a brief discussion of some theoretical tool used in the study. Part II contains journal papers either published in technical journals, through which the main results and contributions of the study are presented. Moreover, we proposed (i) shape tracking with a hyper-redundant slender mechanism coupled with a substrate. Shape tracking is based on the flexibility of the mechanism, that is modeled as a Timoshenko beam, and the interaction with the environment is described by a distributed system of deformable elements. (ii) a governing evolution of the shape morphing and forward locomotion of an hyper-redundant mechanism coupled with a substrate, that encodes the salient features of the mechanics of locomotion and shape morphing of millipedes. In this model, suitable kinematic descriptors allow to link the control of the system with the autonomous operation of a class of devices with bio-inspired features giving the desirable robustness and adaptability to operate in unstructured and unknown environments. (iii) a well posed distributed parameter formulation, in which the system of governing equations includes the evolution of the kinematic descriptors of the Timoshenko beam and of the interface between the coupling elements and the viscoelastic substrate. This model is used to pose an inverse problem aimed at estimating the constitutive parameters of the substrate from deformation measurements of the beam induced by different input forces and torques. Part III summarizes the main results and concludes the thesis.

1.6 Summary of Research Papers in the Thesis

The core part of this thesis are three research papers. For each of them, the abstract is given below.

Paper A: A Timoshenko Beam Reduced Order Model for Shape Tracking with a Slender Mechanism

This work is published in Journal of Sound and Vibration [109].

Summary: We consider a flexible bio-inspired slender mechanism, modeled as a Timoshenko beam. It is coupled to the environment by a continuous distribution of compliant elements. We derive a reduced order model by projecting the governing partial differential equations along the linear modal basis of the Timoshenko beam. The coupling with the substrate allows to formulate the problem in a control framework, and therefore to track the profile of the substrate through the deformation of the body. Distributed coupling elements are modeled in the framework of two parameters elastic foundations. A closed loop force control is simulated for shape morphing when the system is coupled with a smooth substrate.

Background: The basic idea of this work is to introduce a bio-inspired model for an hyper-redundant slender mechanism based on Timoshenko beam. The system is inspired by the mechanics of millipedes, and is developed through a detailed technical description of kinetics and dynamics of the system. From the mechanical point of view, the system can be considered as a continuous system having an infinite number of degrees of freedom and the adaptation to the shape of the substrate is achieved through the deformation of the body. Here we specifically focus on the deformation of the body and the coupling with the substrate.

Paper B: Path following and shape tracking with a continuous slender robot

This paper is under revision in the ASME Journal of Dynamic Systems, Measurement and Control. It has been resubmitted after a minor revision recommendation from the associated editor in charge.

Summary: We present the continuous model of a mobile slender mechanism that is intended to be the structure of an autonomous hyper-redundant slender robotic system. Rigid body degrees of freedom and deformability are coupled through a Lagrangian weak formulation that includes control inputs to achieve forward locomotion and shape tracking. The forward locomotion and the shape tracking are associated to the coupling with a substrate that models a generic environment in which the mechanism could be deployed, and mimic the spinal locomotion mechanisms of millipedes and centipedes in which the forward motion is propelled by a system of legs, and the flexible body adapts to non-zero curvature of the substrate. The assumption of small deformations around

rigid body placements allows to adopt the floating reference kinematic description. By posing the distributed parameters control problem in a weak form, we naturally introduce an approximate solution technique based on Galerkin projection on the linear mode shapes of the Timoshenko beam model, that is adopted to describe the body of the robot. Simulation results illustrate coupling among forward motion and shape tracking as described by the dynamics governing the system.

Background: Introducing a model for the forward locomotion and shape tracking with a slender hyper-redundant robot is the basic motivation for this work. Considering Paper A, the robot is modeled as a Timoshenko beam in plane motion with natural (force) boundary conditions, which allows rigid body motion to the system, kinematically described by three degrees of freedom. By reproducing the scenario of a slender robot deployed in a generic environment, the shape-tracking problem is posed in terms of coupling with a substrate. We adopt the concept of floating frame to describe the motion of the robot that is composed by a rigid body placement and by a small deformation about the rigid body placement. The forward motion of robot is coupled with the robot's body deformation and with respect to the rigid body placement. Model is expressed in terms of the rigid body degrees of freedom, which tracks a moving point on the substrate, eventually with a given offset.

Paper C: Sensing linear viscoelastic constitutive parameters with a Timoshenko beam on a multi-layer foundation: modeling and simulation

This work is under revision in the Journal of Sensing and BioSensing Research.

Summary: We present a sensor model comprised of a Timoshenko beam coupled with a linear viscoelastic substrate via a distributed system of compliant elements. The system of governing equations includes the evolution of the kinematic descriptors of the Timoshenko beam and of the interface between the coupling elements and the viscoelastic substrate. This model is used to pose an inverse problem aimed at estimating the constitutive parameters of the substrate from deformation measurements of the beam induced by different input forces and torques. The sensing model is demonstrated by comparing its prediction with published experimentally obtained constitutive parameters identifying standard linear viscoelastic material models, showing good agreement between model estimations and experimental results.

Background: The basic idea in this work is presenting an inverse problem for the proposed system in Paper A, and deploying a bio-inspired hyper-redundant model as a distributed sensor. We derive the forward problem using a coupled Timoshenko beam

with a standard solid viscoelastic substrate. We propose an explicit solution for the forward and inverse problems, through a reduced order model by projecting the governing partial differential equations along the linear basis functions. In sensor framework, we consider the coupling with the substrate as a sensor to estimate the mechanical properties of the substrate through the inverse problem of the deformations of the system. To assess the validity of a inverse problem, the convergence of the least square minimizing has validated through an iterative procedure of Nedler method.

Chapter 2

Modelling Frameworks

2.1 Millipedes Locomotion

Animals locomotion often is based on simple principles; moving forward/backward and shape morphing due to the reaction of exerted force form the environment. Obviously the interacting forces depend on the material and geometric properties of the animal body in a wide diversity of mechanisms. A lot of work including multi-legged robots, snake-like robots, and robotic fish has been done on bio-inspired mobile robotic technology recently [30–32, 34, 35, 58–60]. From the point of view of animal's morphology, locomotion can be classified in three classes;

1) Endoskeleton body

2) Exoskeleton body

3) No skeleton body,

In all these cases, the body can be represented by a chain of rigid elements connected by spherical joints (three degree of freedom). Considering that animal bodies, in adapting to environments, use a complicated nervous control system, they have ability to change the locomotion pattern to another according to the physical changes of the substrate, by fact of having high number of internal degrees of freedom. Therefore, natural modeling framework to describe key bio-inspired locomotion features is the beam model.

Among six main class of Arthropods; Chilopoda or the centipedes; Pauropoda or the pauropods; Symphyla or the symphylans; Entognatha or the collembolans, proturans, and diplurans; and Insecta or the insects, Millipedes belong to Diplopoda class in the Subphylum Atelocerata of the Phylum Arthropoda [110], and as it is schematized in Fig. 2.1 they have two legs per segment [111]. The slender body is comprised of an ex-

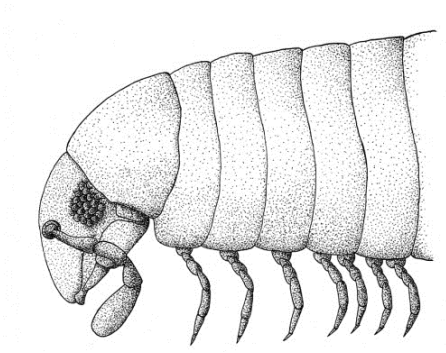

Figure 2.1: Schematics of the external anatomy of a generalized juliform millipede (Fig. 2 from [13])

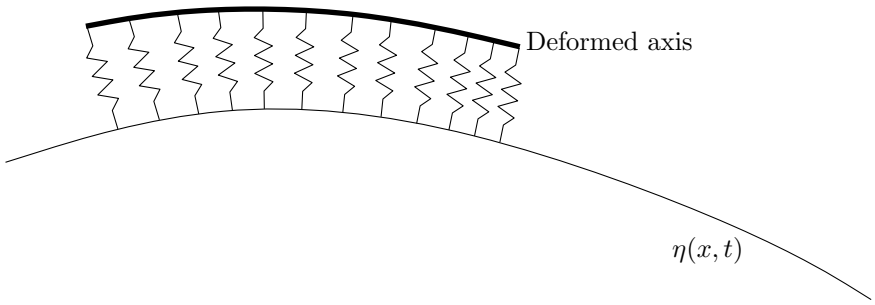

Figure 2.2: Sketch of the mechanism coupled with the substrate with profile described by the curve $\eta(x;t)$

oskeleton which can be schematized as a chain of coaxial rings, which possesses an internal cartilaginous spine with spinal elements connected by three degrees of freedom joints. The locomotion can be characterized by two mechanisms, namely the spinal locomotion and the concertina locomotion [112–116], and it is achieved by the two stages kinematics illustrated in Fig. 2.3, comprised of a stage in which the leg is in contact with the ground (dense phase) moving backward to create the thrust associated to friction, and a recovery stage (sparse phase) in which the leg is not in contact and moves forward. Constant phase difference between adjacent legs makes an overall wave like forward motion in the system [108, 116]. In order to model the millipede's locomotion, we consider compliant elements between beam and substrate to be part of the moving robot (See Fig. 4.5), as they mimic the function of millipedes legs in providing the distributed support to the

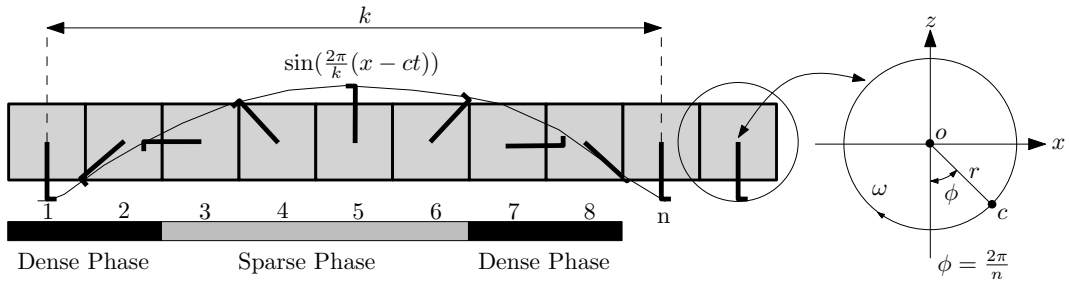

Figure 2.3: Schematic of the millipede motion in the mechanical nature of wave propagated walking.

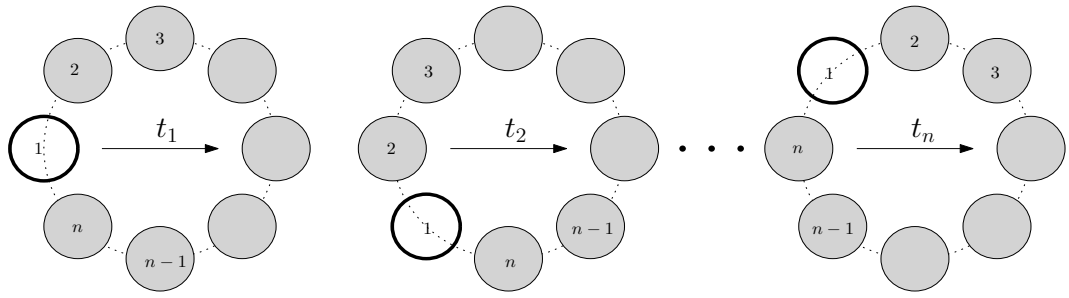

Figure 2.4: Schematic of arrangement of body segments with respect to waves.

body resulting from the coupling with the environment, which in turn determines the shape morphing to adapt to nonzero curvature of the substrate. Additionally, the profile of the legs' extremities can be described by a metachronal wave propagating along the axis x that is aligned with the axis of the body when it is rectilinear [57, 117],

$$\sin\left(\frac{2\pi}{k}(x-ct)\right) \tag{2.1}$$

where k and c are the wave length and the speed of propagation of the wave, respectively. As it is illustrated in Fig. 4.5, in multi-legged animals, the leg tip is the interface between the body and the substrate. Therefore, considering the natural projection of the circular movement of the leg tip with respect to the body axis, it can be envisaged as to-and-fro motion along the body axis, in which the constant phase difference between adjacent legs can be expressed as [108],

$$\phi = \frac{2\pi}{n} \tag{2.2}$$

where n is the number of leg's in one wave. We consider motion of the legs described by the schematics in Fig. 2.3 and Fig. 2.4, to be characterized by constant angular velocity $\boldsymbol{\omega}$, which is an axial vector perpendicular to the plane of motion. By assuming that the bending of the legs is negligible with respect to the rigid body rotation, the velocity a point c in contact with the ground is therefore given by the relation, (see Fig. 2.3)

$$\mathbf{v}_c = \mathbf{v}_o + \boldsymbol{\omega} \wedge \mathbf{r}_{oc} \tag{2.3}$$

where $\mathbf{r}_{oc}$ is the position vector from point o to point c. We consider an equal length for all limbs, and the positive direction of the body axis is taken from tail to head. By assuming that the contact is rolling without slipping, we have $\mathbf{v}_c = \mathbf{0}$, and therefore the velocity of the body point o is tangential with respect to the body axis and has magnitude

$$v_o = \omega r_{oc} \tag{2.4}$$

Therefore, v_o is a rigid body forward speed generated by a limb in contact with the ground.

This locomotion mechanism, that directly relates to the kinematics of the limbs, is the object of current work that extends the model in Paper B by linking the kinematics of the mechanism to the bio-inspired nature of the locomotion. Simulation studies are informing design choices that are being implemented in the first generation of hardware devices related to the work in this thesis.

2.2 Timoshenko Beam Theory

For several years dynamics of vibrating beams has been investigated by using different engineering beam theories. Euler-Bernoulli beam theory is the most commonly used, as it is simple and it provides reasonable engineering approximations for many problems. Because of a constitutive assumptions on shear stiffness (i.e., the beam is infinitely rigid with respect to shear actions), natural frequencies calculated through of the Euler-Bernoulli beam theory are overestimated. Lord Rayleigh (John William Strutt) presented a beam theory that includes the effect of the rotary inertia to Euler-Bernoulli beam theory into Euler-Bernoulli beam theory. In Rayleigh beam theory neglecting shear distortion was still a remaining assumption, and this causes some overestimation natural frequencies. In the shear beam theory, shear effects have been considered, but rotary inertia has been neglected by Timoshenko, Young and Weaver [118]. This theory gives accurate results only at high frequency vibrations. Shear beam could violate the principles of conservation of momentum for pinned-free and free-free boundary conditions [119]. In Timoshenko beam theory, rotary inertia and shear distortion are both included, and among all, Timoshenko beam theory is more applicable for beams with various thicknesses or slenderness ratios, it is therefore considered a good correction of Euler-Bernoulli beam theory by including both shear distortion and rotary inertia. Based on all above facts, this thesis considers Timoshenko beam as a continuous model. Moreover, organisms like centipedes and polychaete worms can be modeled as a Timoshenko beam, which represent the limit of a rigid body chain with pinned elements.

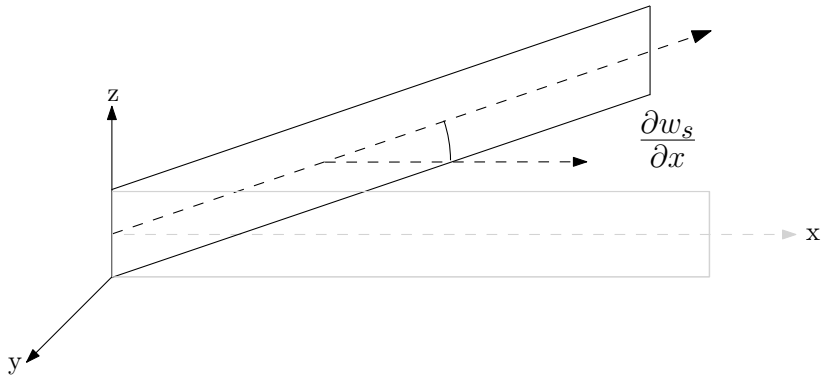

Figure 2.5: Shear deformation on a cantilever beam

In the Timoshenko beam theory, for an undeformed beam, strain components can be

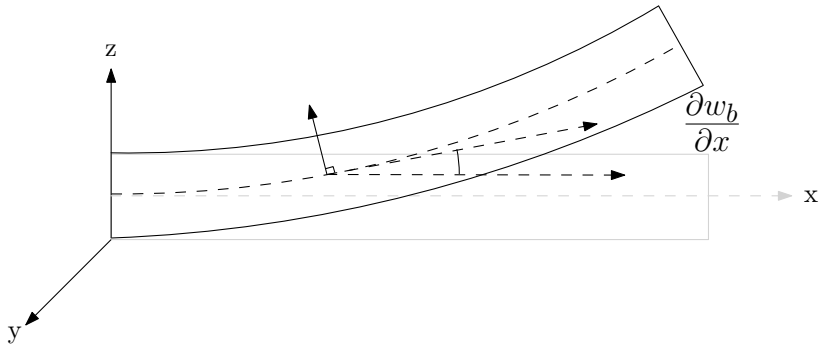

Figure 2.6: Bending deformation on a cantilever beam

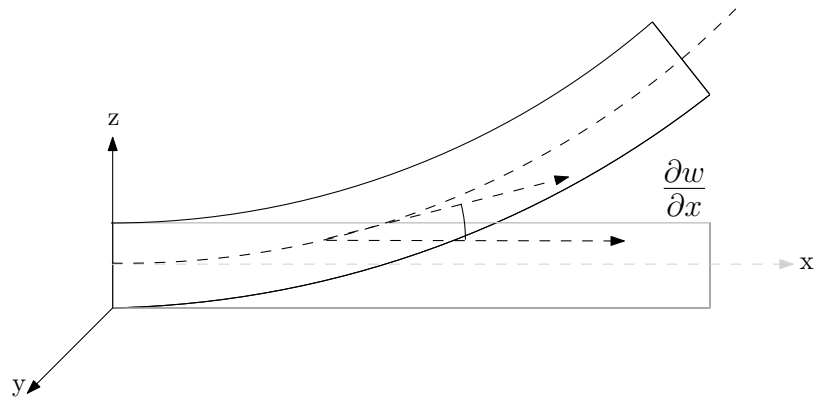

Figure 2.7: Shear bending deformation on a cantilever beam

found as:

$$\varepsilon_{xx} = \frac{\partial u_1}{\partial x} = 0, \qquad \varepsilon_{yy} = \frac{\partial u_2}{\partial y} = 0, \qquad \varepsilon_{zz} = \frac{\partial u_3}{\partial z} = 0 \tag{2.5}$$

$$\varepsilon_{xy} = \frac{\partial u_1}{\partial y} + \frac{\partial u_2}{\partial x} = 0, \qquad \varepsilon_{yz} = \frac{\partial u_2}{\partial z} + \frac{\partial u_3}{\partial y} = 0, \qquad \varepsilon_{zx} = \frac{\partial u_1}{\partial z} + \frac{\partial u_3}{\partial x} = \frac{\partial w}{\partial x} \tag{2.6}$$

The components of stress corresponding to the strains presented by (2.5) are given by,

$$\sigma_{xx} = \sigma_{yy} = \sigma_{zz} = \sigma_{xy} = \sigma_{yz} = 0 \tag{2.7a}$$

$$\sigma_{zx} = G\frac{\partial w}{\partial x} \tag{2.7b}$$

where G is the shear modulus, and equation (2.7) states that the shear stress σ_{zx} is uniform at every point in the cross section of the beam. Timoshenko introduced a

constant k, as the shear correction factor, in the expression for the shear stress,

$$\sigma_{zx} = kG\frac{\partial w}{\partial x} \tag{2.8}$$

Figures (2.5),(2.6) and (2.7) show that the total transverse displacement of the beam's centreline can be defined by $w = w_s + w_b$. Hence, the total slope of the detected centreline of the beam is approximated by,

$$\frac{\partial w}{\partial x} = \frac{\partial w_b}{\partial x} + \frac{\partial w_s}{\partial x} \tag{2.9}$$

The rotation of the cross section considering the effect of bending can be expressed as

$$\psi = \frac{\partial w_b}{\partial x} = \frac{\partial w}{\partial x} - \frac{\partial w_s}{\partial x} = \frac{\partial w}{\partial x} - \beta \tag{2.10}$$

where β is the shear deformation or shear angle. Then the components of displacement of a point in the beam are given by:

$$u_1 = u - z\left(\frac{\partial w}{\partial x} - \beta\right) = u - z\psi(x,t), \qquad u_2 = 0, \qquad u_3 = w(x,t) \tag{2.11}$$

For the motion of a particle under shear and bending deformation the strain components will change in the following,

$$\varepsilon_{xx} = \frac{\partial u_1}{\partial x} = \frac{\partial u}{\partial x} - z\frac{\partial \psi}{\partial x}, \qquad \varepsilon_{yy} = \frac{\partial u_2}{\partial y} = 0, \qquad \varepsilon_{zz} = \frac{\partial u_3}{\partial z} = 0$$
$$\varepsilon_{xy} = \frac{\partial u_1}{\partial y} + \frac{\partial u_2}{\partial x} = 0, \qquad \varepsilon_{yz} = \frac{\partial u_2}{\partial z} + \frac{\partial u_3}{\partial y} = 0, \qquad \varepsilon_{zx} = \frac{\partial u_1}{\partial z} + \frac{\partial u_3}{\partial x} = -\psi + \frac{\partial w}{\partial x} \tag{2.12}$$

and for stress components,

$$\sigma_{xx} = E\left(\frac{\partial u}{\partial x} - z\frac{\partial \psi}{\partial x}\right); \qquad \sigma_{yy} = \sigma_{zz} = \sigma_{xy} = \sigma_{yz} = 0; \qquad \sigma_{zx} = kG\left(\frac{\partial w}{\partial x} - \psi\right) \tag{2.13}$$

where E is the young modulus. Therefore the strain energy of the beam can be determined as

$$\pi = \frac{1}{2}\iiint_V \left(\sigma_{xx}\varepsilon_{xx} + \sigma_{yy}\varepsilon_{yy} + \sigma_{zz}\varepsilon_{zz} + \sigma_{xy}\varepsilon_{xy} + \sigma_{yz}\varepsilon_{yz} + \sigma_{zx}\varepsilon_{zx}\right) dV$$
$$\frac{1}{2}\int_l \iint_A \left[Ez^2\left(\frac{\partial u}{\partial x}\right)^2 + Ez^2\left(\frac{\partial \psi}{\partial x}\right)^2 + kG\left(\frac{\partial w}{\partial x} - \psi\right)^2\right] dA dx =$$
$$\frac{1}{2}\int_0^l \left[EI\left(\frac{\partial \psi}{\partial x}\right)^2 + kAG\left(\frac{\partial w}{\partial x} - \psi\right)^2\right] dx \tag{2.14}$$

and kinetic energy of the beam including rotary inertia can be represented as,

$$T = \frac{1}{2}\int_0^l \left[\varrho A\left(\frac{\partial u}{\partial t}\right)^2 + \varrho A\left(\frac{\partial w}{\partial t}\right)^2 + \varrho I\left(\frac{\partial \psi}{\partial t}\right)^2\right] dx \tag{2.15}$$

The work done by the external distributed force $p_w(x,t)$ and external distributed torque $p_\psi(x,t)$ is given by

$$W = \int_0^l p_w(x,t)w(x,t) + p_\psi(x,t)\psi(x,t)dx \tag{2.16}$$

Therefore using the extended Hamilton's principle

$$\delta\int_{t_1}^{t_2}(\pi - T - W)\,dt = 0 \tag{2.17}$$

and by substituting the strain and kinetic energy and the work done, we obtain

$$\int_{t_1}^{t_2}\Bigg\{\int_0^l \left[EI\frac{\partial u}{\partial x}\delta\left(\frac{\partial u}{\partial x}\right) + EI\frac{\partial \psi}{\partial x}\delta\left(\frac{\partial \psi}{\partial x}\right) + kAG\left(\frac{\partial w}{\partial x} - \psi\right)\delta\frac{\partial w}{\partial x} - kAG\left(\frac{\partial w}{\partial x} - \psi\right)\delta\psi\right] dx$$
$$- \int_0^l \left[\varrho A\frac{\partial w}{\partial t}\delta\left(\frac{\partial w}{\partial t}\right) + \varrho I\frac{\partial \psi}{\partial t}\delta\left(\frac{\partial \psi}{\partial t}\right)\right] dx - \int_0^l p_w\delta w dx - \int_0^l p_\psi\delta\psi dx\Bigg\}dt \tag{2.18}$$

By evaluating part by part of this integral with the help of partial integration with respect to t and x,

$$\int_{t_1}^{t_2}\int_0^l EI\frac{\partial u}{\partial x}\delta\left(\frac{\partial u}{\partial x}\right)dxdt = \int_{t_1}^{t_2}\left[EI\frac{\partial u}{\partial x}\delta u\Big|_0^l - \int_0^l \frac{\partial}{\partial x}\left(EI\frac{\partial u}{\partial x}\right)\delta u dx\right]dt \tag{2.19}$$

$$\int_{t_1}^{t_2}\int_0^l EI\frac{\partial \psi}{\partial x}\delta\left(\frac{\partial \psi}{\partial x}\right)dxdt = \int_{t_1}^{t_2}\left[EI\frac{\partial \psi}{\partial x}\delta\psi\Big|_0^l - \int_0^l \frac{\partial}{\partial x}\left(EI\frac{\partial \psi}{\partial x}\right)\delta\psi dx\right]dt \tag{2.20}$$

$$\int_{t_1}^{t_2}\int_0^l kAG\left(\frac{\partial \psi}{\partial x} - \psi\right)\delta\frac{\partial w}{\partial x}dxdt =$$
$$\int_{t_1}^{t_2}\left[kAG\left(\frac{\partial \psi}{\partial x} - \psi\right)\delta w\Big|_0^l - \int_0^l kAG\frac{\partial}{\partial x}\left(\frac{\partial \psi}{\partial x} - \psi\right)\delta w dx\right]dt \tag{2.21}$$

$$-\int_{t_1}^{t_2}\int_{0}^{l} \varrho A\frac{\partial u}{\partial t}\delta\left(\frac{\partial u}{\partial t}\right)dxdt = -\int_{t_1}^{t_2}\int_{0}^{l} \varrho A\frac{\partial^2 u}{\partial t^2}\delta u dxdt \tag{2.22}$$

$$-\int_{t_1}^{t_2}\int_{0}^{l} \varrho A\frac{\partial w}{\partial t}\delta\left(\frac{\partial w}{\partial t}\right)dxdt = -\int_{t_1}^{t_2}\int_{0}^{l} \varrho A\frac{\partial^2 w}{\partial t^2}\delta w dxdt \tag{2.23}$$

$$-\int_{t_1}^{t_2}\int_{0}^{l} \varrho I\frac{\partial \psi}{\partial t}\delta\left(\frac{\partial \psi}{\partial t}\right)dxdt = -\int_{t_1}^{t_2}\int_{0}^{l} \varrho I\frac{\partial^2 \psi}{\partial t^2}\delta \psi dxdt \tag{2.24}$$

substitution of the equations (2.19) (2.20),(2.21),(2.22), (2.23) and (2.24) into (2.18) results into

$$\begin{aligned}\int_{t_1}^{t_2}\Bigg\{ kAG\left(\frac{\partial w}{\partial x}-\psi\right)\delta w\Big|_0^l + EI\frac{\partial u}{\partial x}\delta u\Big|_0^l + EI\frac{\partial \psi}{\partial x}\delta\psi\Big|_0^l + \\ \int_0^l\left[-\frac{\partial}{\partial x}\left(EI\frac{\partial u}{\partial x}\right)+\varrho I\frac{\partial^2 u}{\partial t^2}\right]\delta u dx + \\ \int_0^l\left[\frac{\partial}{\partial x}\left(kAG\left(\frac{\partial w}{\partial x}-\psi\right)\right)+\varrho A\frac{\partial w^2}{\partial t^2}-p_w\right]\delta w dx + \\ \int_0^l\left[-\frac{\partial}{\partial x}\left(EI\frac{\partial \psi}{\partial x}\right)-kAG\left(\frac{\partial w}{\partial x}-\psi\right)+\varrho I\frac{\partial^2 \psi}{\partial t^2}-p_\psi\right]\delta\psi dx\Bigg\}dt = 0\end{aligned} \tag{2.25}$$

Applying homogeneous boundary conditions, the first term goes to zero, and the evaluation of w and ψ is described by the coupled field equation

$$\rho I\frac{\partial^2 u}{\partial t^2} - \frac{\partial}{\partial x}(EI\frac{\partial u}{\partial x}) = 0 \tag{2.26a}$$

$$\rho A\frac{\partial^2 w}{\partial t^2} + \frac{\partial}{\partial x}(kAG(\psi - \frac{\partial w}{\partial x})) = p_w \tag{2.26b}$$

$$\rho I\frac{\partial^2 \psi}{\partial t^2} - \frac{\partial}{\partial x}(EI\frac{\partial \psi}{\partial x}) + kAG(\psi - \frac{\partial w}{\partial x}) = p_\psi \tag{2.26c}$$

where ρ refers mass density, E is Young's modulus and G shear modulus or modulus of rigidity. These above partial differential equations are used for finding the normal modes

and frequency of free vibration. In the case of a uniform beam, by eliminating ψ from the (2.26b) and (2.26c), a single form equation can be obtained;

$$\frac{EI}{\rho A}\frac{\partial^4 w}{\partial x^4} - \left(\frac{EI}{kAG} + \frac{I}{A}\right)\frac{\partial^4 w}{\partial x^2 \partial t^2} + \frac{\rho I}{kGA}\frac{\partial^4 w}{\partial t^4} + \frac{\partial^2 w}{\partial x^2} = 0 \tag{2.27}$$

When the shear and rotational terms are small and neglected, the equation reduces to that of the Euler-Bernoulli beam.

2.3 Elastic Foundation Model

This section provides an overview of models for foundations and different elastic substrates. Subsequently, the modelling of the elastic substrate structure (could be soil media), and the interaction between a system of distributed springs under a Timoshenko beam and elastic foundation as two mediums is the point of discussion. Finding material properties of soil, is very important and complicated to deal with as the variety of its material properties could make it elastic, plastic, nonhomogeneous, and anisotropic. The main approach in foundation designing is finding material parameters and presenting an adequate model for the foundation structure which describes reality. Therefore, it is essential to estimate the properties of the supporting foundation and its mechanical behavior through a constitutive model mathematically.

2.3.1 One parameter model

A comprehensive survey in foundation models that contains a study in different elastic foundation models and development of some models is presented in [120]. Generally, considering the response of the foundation surface with respect to applied loads is a common attitude in the study of foundation models, that passive stresses, caused within the foundation, are not considered in the calculation. The primitive model of the elastic foundation is Winkler elastic foundation, in which the exerted force caused by the foundation is proportional to the vertical displacement of the beam. As it is shown in the Figure.2.8, the displacement of the foundation outside the beam boundaries (loaded region) is zero. The governing equation for Winkler elastic foundation is given by,

$$p_\eta = \kappa_w w(x,t) \tag{2.28}$$

where $p_\eta(x,t)$ is the force per unit length exerted by the foundation, $w(x,t)$ is the transverse displacement of the beam, and κ_w is Winkler foundation constant. Winkler foun-

dation behaves like an array of independent springs as shown in Figure.2.8, where dimension κ_w is force per unit length per unit displacement, which is in the studies made by [121–123] and [124].

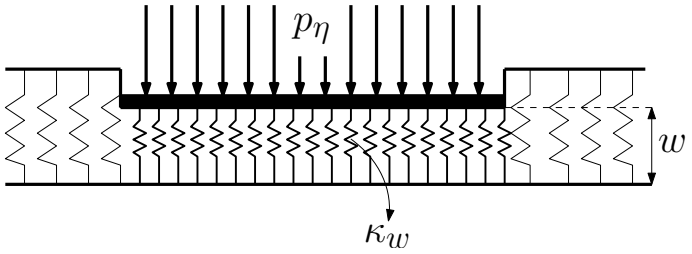

Figure 2.8: One parameter model(Winkler Model) of elastic foundation

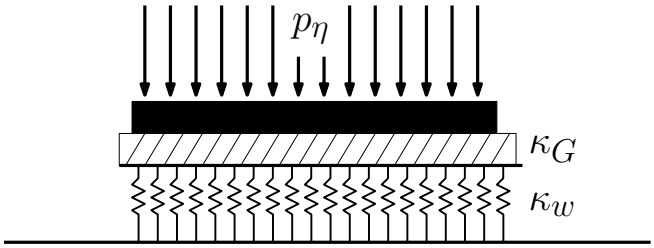

Figure 2.9: Two parameter model(Pasternak Model) of elastic foundation

2.3.2 Two parameter model

The first parameter of the foundation in all two parameter foundation models, is still Winkler elastic foundation parameter, and there are different mathematical models for the second elastic foundation layer. Shearing stiffness of the elastic foundation, which is neglected in Winkler model is taken into consideration as the parameter of second layer of the elastic foundation [120]. The vibration characteristics of Timoshenko beam on two parameters with shear modulus of the elastic foundation has been studied in [125]. Also a comprehensive definition for the second parameter of the elastic foundation has been presented in [126], and the mathematical model for the elastic foundation is expressed as,

$$p_\eta = \kappa_w w(x,t) + \kappa_{w_1} \frac{\partial w(x,t)}{\partial x} \tag{2.29}$$

where p_η is foundation reaction, κ_w is Winkler foundation parameter, and κ_{w_1} is second elastic foundation parameter which has the dimension of force. Four different models for κ_{w_1} depending on the foundation type have been studied in [126]. In the generalized foundation model, a moment has been assumed between the beam and foundation besides pressure,

$$p_\eta = \kappa_w w(x,t), \quad M_\eta = \kappa_{w_1} \frac{\partial w(x,t)}{\partial n} \tag{2.30}$$

where n is any direction at a point in the plane of the foundation surface; κ_w is Winkler parameter and κ_{w_1} is corresponding proportionality factor in direction of n [120], which can define dimensionally as, reaction moment per unit length per unit rotation that is relatively arbitrary is proportional with the angle of rotation of the beam.

In Vlasov model foundation is assumed to be a semi-infinite medium [120], and κ_{w_1} is obtained in terms of elastic constants and the dimensions of beam and foundation by,

$$\kappa_{w_1} = \frac{E_s B}{4\mu(1+\nu_s)} \tag{2.31}$$

where, E_s and ν_s are Young's modulus and Poisson's ratio of foundation respectively, B is width of the beam and μ is a decay rate of vertical deformation of foundation.

Curvature of the elastic foundation is also considered in Pasternak foundation model, as well as the displacement of the foundation. As it is shown in Figure. 2.9, in the Pasternak foundation model; the second parameter of the foundation has been defined with κ_G, as a shear modulus [120, 126], so the governing equation of Pasternak elastic foundation can be shown as,

$$p_\eta = \kappa_w w(x,t) + \kappa_G \frac{\partial^2 w(x,t)}{\partial x^2} \tag{2.32}$$

A generalized Pasternak viscoelastic foundation has been studied in [127] with investigating vibration of Timoshenko beam under moving load, in which a damping effect was also included in the governing equation as,

$$p_\eta = -\kappa_w w(x,t) + C\frac{\partial w(x,t)}{\partial t} + \mu \frac{\partial^3 w(x,t)}{\partial t \partial^2 x} \tag{2.33a}$$

$$M_\eta = -\kappa_\psi \psi(x,t) - C\frac{\partial \psi(x,t)}{\partial t} \tag{2.33b}$$

where M_η and p_η are moment and pressure induced by the viscoelastic foundation, κ_w and κ_ψ are substrate parameters for vertical and rotational loading respectively, C is damping coefficients and μ is shear viscosity coefficient of the foundation.

Other foundation models like Hetenyi foundation and Reissner foundations have been discussed in [120]. In Hetenyi foundation interaction between two layer springs has been studied by embedding an elastic beam and a plate for two dimensional and three dimensional cases respectively. In Reissner foundation, the equations of continuum and in-plane stresses have been considered when the foundation layers are small [120]. Same other models for two parameter foundation model, with different name, have been studied in [128, 129].

2.4 Viscoelastic Foundation Model

There are different groups of materials such as biological tissues, polymers, soil, and metals at high temperatures, that have the gradual deformation and recovery by subjecting to loading and unloading. The duration of the loading and unloading plays a main role in the response of these materials, in which the amount of deformation depends upon how quickly the force is applied, and is dependent upon the rate at which the deformation is changing with time with respect to applied loads. This time-dependent material behavior is called viscoelasticity.

For viscoelastic materials, stress σ, is not only a function of strain ε, but is also a function of the strain rate $\dot{\varepsilon} = \frac{d\varepsilon}{dt}$, where t is time. Therefore, the relationship between stress and strain can be expressed as,

$$\sigma = \sigma(\varepsilon, \dot{\varepsilon}) \tag{2.34}$$

In the viscoelasticity point of view, the Boltzmann superposition theory state that: firstly, the creep in a viscoelastic material is a function of the entire loading history, which means the long past deformations influence on present behavior; secondly, increasing load makes an independent and additive contribution to the total deformation, which means if a viscoelastic material is loaded and creeps under certain amount of load, then applying an extra load will produce additional creep, which the final creep is exactly same as creep if that total load had been applied once to the unloaded viscoelastic material within same total creep time [130]. A brief review of viscoelasticity can be found in [131].

Generally the analogy of the viscoelastic material is based on combination of springs and dashpots, where springs represent the elastic solid behavior and dashpots are used to present the viscous response. The deformation is completely recoverable in the spring upon removing of applied forces, whereas we have a permanent deformation when the dashpot undergoes.

2.4.1 Kelvin-Voigt Model

The simplest forms of experimental models for the viscoelastic materials are obtained by combining a spring and a dashpot together in parallel and/or in series configurations. The Kelvin-Voigt model schematic is shown in Figure. 2.10, which is a system consisting of a spring and a dashpot connected in a parallel arrangement. The stress σ, applied to the entire system produces stresses σ^s and σ^d in the spring and the dashpot respectively. The total applied stress to the system is equal to stress applied to the spring and the dashpot such that,

$$\sigma = \sigma^s + \sigma^d \tag{2.35}$$

where subscripts "s" and "d" denote the spring and dashpot, respectively. The deformation caused by the applied stress in the spring and dashpot are equal, because of their parallel arrangement. Therefore, the total strain of the system ε, is equal to both strains ε^s and ε^d, occurring in the spring and the dashpot as,

$$\varepsilon = \varepsilon^s = \varepsilon^d \tag{2.36}$$

The stress-strain relationship for the spring and the stress-strain rate relationship for the dashpot are,

$$\sigma^s = \kappa\varepsilon^s \tag{2.37a}$$

$$\sigma^d = \mu\dot{\varepsilon}^d \tag{2.37b}$$

where κ_1, and μ are stiffness and damping parameters of the elements. Substituting (2.37) into (2.35), and considering (2.36), the general stress-strain relation for the Kelvin-Voigt cen be represented as,

$$\sigma = \kappa\varepsilon + \mu\dot{\varepsilon} \tag{2.38}$$

which is a two-parameter viscoelastic model.

2.4.2 Maxwell Model

Maxwell model for the viscoelastic material is illustrated in Figure. 2.11, which consists of connecting a spring and a dashpot in a series. Therefore, for the Maxwell model, the applied stress σ to the entire system is applied equally on the spring σ^s, and the dashpot σ^d, and the total system deformation (strain) ε, is equal to the sum of the strains in

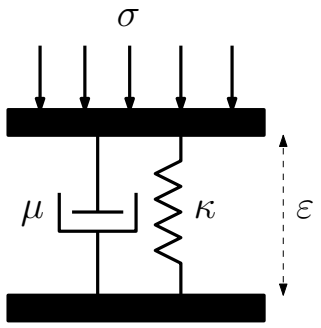

Figure 2.10: Kelvin-Voigt model

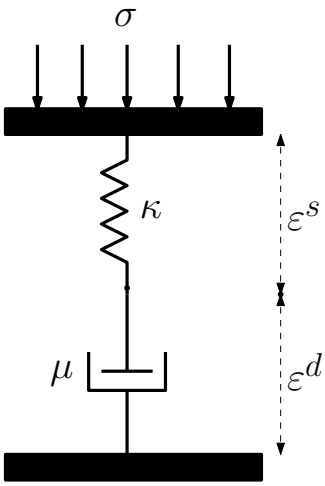

Figure 2.11: Maxwell model

the spring ε^s, and the dashpot ε^d. Considering stress-strain analyses similar to analogy carried out for the Kelvin-Voigt model, a constitutive equation for the stresses and strains response of the Maxwell model, can be derived as,

$$\mu\dot{\sigma} + \kappa\sigma = \kappa\mu\dot{\varepsilon} \tag{2.39}$$

where κ, and μ are stiffness and damping parameters of the Maxwell model. This expression is a constitutive differential equation, which contains time derivatives, so that simple constant of proportionality between stress and strain does not exist. The concept of "modulus", the ratio of stress to strain, can be defined as Creep Moduli and Relaxation Moduli, and they must be broadened for more complicated behavior.

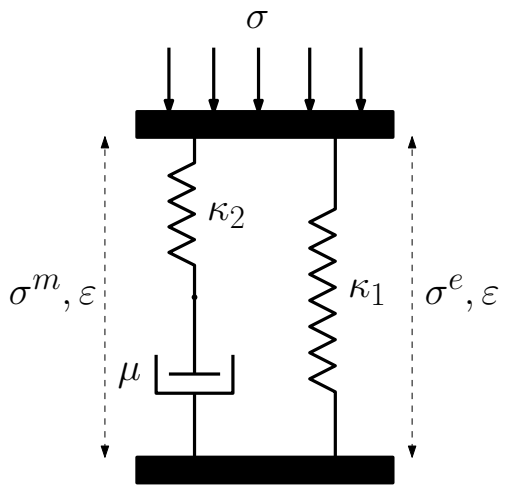

Figure 2.12: Standard Linear Solid model

2.4.3 Standard Linear Solid Model

The Kelvin-Voigt and Maxwell are the basic viscoelastic models, which are normally used for the modelling of some viscoelastic solid and fluid respectively, constructed by connecting a spring and a dashpot together, but they do not represent completely the viscoelastic behavior of any known real material. However, adding springs and/or dashpots to one of these models, they can be used to reconstruct the behavior of more realistic viscoelastic materials. Standard Linear Solid model, also referred to as Zener model, provides a good approximate representation of the behavior response of biomaterials, polymers, and soil, in their viscoelastic range, and it can also describe stress relaxation and creep behavior of real viscoelastic material as well. As it is illustrated in Figure. 2.12, the standard linear solid model is a combination of the Maxwell branch and a parallel spring κ_1, which experience the same strain in the system. The total stress σ is equal to the sum of the stress in each branch, which is decomposed into rate independent equilibrium stress σ^e in the spring κ_2 and the rate dependent overstress components σ^m in the spring κ_1 and dashpot μ as,

$$\sigma = \sigma^e + \sigma^m \tag{2.40}$$

and the strain in the Maxwell element and in the parallel elastic spring element is,

$$\varepsilon = \varepsilon^e = \varepsilon^m \tag{2.41}$$

Considering Hooke's law, the linear elastic constitutive equation in the spring is,

$$\sigma^e = \kappa_2 \varepsilon \tag{2.42}$$

and considering the governing equation for the Maxwell element in (2.39) the stress-strain relation for Maxvel branches can be rewritten as,

$$\sigma^m + \frac{\mu}{\kappa_1}\dot{\sigma}^m = \mu\dot{\varepsilon} \tag{2.43}$$

Substituting (2.43) and (2.42) into (2.40), and considering (2.41), the governing equation for the total stress in standard linear solid model can be obtained as:

$$\sigma + \frac{\mu}{\kappa_1}\dot{\sigma} = \kappa_2 \varepsilon + \frac{\mu}{\kappa_1}\left(\kappa_1 + \kappa_2\right)\dot{\varepsilon} \tag{2.44}$$

Then by integrating the solution of (2.44) defines the stress-strain relation at a constant strain rate for the standard linear solid model is given by:

$$\sigma = \kappa_2 \varepsilon + \mu\dot{\varepsilon}\left[1 - \exp\left(\frac{\kappa_1 \varepsilon}{\mu\dot{\varepsilon}}\right)\right] \tag{2.45}$$

There is other models that consisted of combination of springs and doshpots which can be found in [130].

Chapter 3

Discretization

3.1 Galerkin Estimation

Galerkin finite element method was proposed by Walther Ritz for the numerical solution of partial differential equations, but this approach is usually credited to Boris Galerkin. In general, Galerkin method is the projection of a infinite dimensional function space on a finite dimensional one, and it is a class of methods for converting a continuous multi operator problem to a discrete problem. Owing to finite element nature, the Galerkin method has main advantages like;

- Accuracy of Galerkin methods depends on the exact solution,
- High formal order of accuracy can be obtained by suitably choosing basis functions,
- Galerkin is very well suited to handle different geometries,
- Galerkin requires a simple treatment of the boundary conditions in order to achieve uniformly high accuracy.

When the analytical solution of governing equation (2.26), is hard to obtain precisely due to complicated geometry or boundary conditions, the Galerkin method is an approximation tool for finding the solution of PDE equations through a spatial discretization and a weighted residual formulation to transform the strong form of PDE into a weak form or integral equation. Hence, the Galerkin estimation is a method to solve PDE by splitting the governing strong form of PDE into weak form. Galerkin uses orthogonality of a set of basis functions to turn PDEs into coupled sets of ODEs as temporal-spatial

separation. We consider a decomposition of the spatial bases component of PDE in terms of time-dependent coefficients as the following variational equation,

$$(Lx, \vartheta) = (f, \vartheta), \qquad f \in \mathbf{H}, \tag{3.1}$$

where x is a regular solution of $Lx = f$, where L is a positive definite operator in the Hilbert space $\mathbf{H}$. Then, we choose a complete set of elements in the energetic space $\mathbf{H}_L$ as,

$$\phi_1, \phi_2, \phi_3, \cdots, \phi_n, \cdots; \quad \phi_i \in \mathbf{H}_L, \quad i = 1, 2, \cdots \tag{3.2}$$

Therefore, we can approximate the element $u \in \mathbf{H}_L$ by a linear combination,

$$a_1\phi_1 + a_2\phi_2 + \cdots + a_N\phi_N \tag{3.3}$$

where the number N satisfies the inequality,

$$\|(x - a_1\phi_1 + a_2\phi_2 + \cdots + a_N\phi_N)\|_L < \epsilon \tag{3.4}$$

for a given $\epsilon > 0$. Therefore, $x \in \mathbf{H}_L$ is a solution of variational (3.1), if and only if the equation holds for the coordinates ϕ_k, $k = 1, 2, \cdots$;

$$(Lx, \phi_k) = (f, \phi_k), \quad k = 1, 2, \cdots; \tag{3.5}$$

In order to approximate the solution $x \in X_L \subseteq \mathbf{H}_L$, we consider the subspace

$$\mathbf{X}_N = \{\phi_1, \phi_2, \cdots, \phi_N\} \tag{3.6}$$

of the space $\mathbf{H}_L$. Then, we find the approximate solution

$$x_N = a_1\phi_1 + a_1\phi_1 + \cdots + a_N\phi_N \in \mathbf{X}_N \tag{3.7}$$

through solving the system of linear equations

$$(Lx_N, \phi_k) = (f, \phi_k), \quad k = 1, 2, \cdots, N \tag{3.8}$$

which takes the explicit form

$$\sum_{i=1}^{N} (L\phi_i, \phi_k)a_i = (f, \phi_k), \quad k = 1, 2, \cdots, N \tag{3.9}$$

Considering (3.9), as a system of linear equations, Galerkins methods produce an approximate solution x_N, provided that L is a positive definite operator.

3.2 Basis functions for weak form of Timoshenko beam theory

In this work we use Galerkin projections of the fields u, w and ψ on suitable bases. In order to separate variables, the displacement and rotation fields can be expressed as

$$u(x,t) = \tilde{\mathbf{u}}^{\mathsf{T}}(x)\mathbf{a}(t), \tag{3.10a}$$

$$w(x,t) = \tilde{\mathbf{w}}^{\mathsf{T}}(x)\mathbf{b}(t), \tag{3.10b}$$

$$\psi(x,t) = \tilde{\boldsymbol{\psi}}^{\mathsf{T}}(x)\mathbf{c}(t) \tag{3.10c}$$

where $\tilde{\mathbf{u}} = (\tilde{u}_1 \cdots \tilde{u}_n)^{\mathsf{T}}$, $\tilde{\mathbf{w}} = (\tilde{w}_1 \cdots \tilde{w}_n)^{\mathsf{T}}$ and $\tilde{\boldsymbol{\psi}} = \left(\tilde{\psi}_1 \cdots \tilde{\psi}_n\right)^{\mathsf{T}}$ are $n-$dimensional sets of spatial basis functions, and $\mathbf{a} = (a_1 \cdots a_n)^{\mathsf{T}}$, $\mathbf{b} = (b_1 \cdots b_n)^{\mathsf{T}}$ and $\mathbf{c} = (c_1 \cdots c_n)^{\mathsf{T}}$ are time dependent vectors of amplitudes. The Galerkin projection technique dictates the substitution of (4.6) into Timoshenko governing equations, with the premultiplication a set of test functions $\tilde{\mathbf{u}}$, $\tilde{\mathbf{w}}$ and $\tilde{\boldsymbol{\psi}}$, respectively. Here we set the basis functions for the weak form (reduced order model) to be the linear eigenfunctions of a Timoshenko beam.

3.2.1 Transverse Mode shape

In order to obtain the natural frequencies and associated eigenfunctions we follow the approach in [132], which is based on the solution of a vector eigenvalues problem for the system of two coupled second order differential equations for the transverse displacement and for the rotation of the cross section. In our case, the nondimensionalized form of equations (2.26b) and (2.26c) are,

$$\frac{\partial^2 w}{\partial t^2} - \frac{\partial^2 w}{\partial x^2} + \frac{\partial \psi}{\partial x} = 0 \tag{3.11a}$$

$$\alpha_1 \frac{\partial^2 \psi}{\partial t^2} - \frac{\partial^2 \psi}{\partial x^2} - \alpha_1\alpha_2 \left(\frac{\partial w}{\partial x} - \psi\right) = 0 \tag{3.11b}$$

where the nondimensional variables

$$\hat{x} = \frac{x}{\ell}, \quad \hat{t} = \frac{t}{\tau}, \quad \hat{u} = \frac{u}{\ell} \quad \hat{w} = \frac{w}{\ell}$$

where ℓ is the total length of the undeformed body, that by adopting the linearized beam theory equals the length of the deformed body (by neglecting second order terms), and τ is the characteristic time. By defining the characteristic time

$$\tau^2 = \frac{\varrho \ell^2}{kG}$$

and dropping the hat to indicate nondimensional quantities, we have introduced the nondimensional coefficients,

$$\alpha_1 = \frac{kG}{E}, \quad \alpha_2 = \frac{A\ell^2}{I} \tag{3.12a}$$

Therefore $\alpha_1\alpha_2$ is a measure of the shear stiffness versus the bending stiffness. The consideration of two separate evolution equations for w and ψ allows to enforce boundary conditions for free ends in a direct way.

To determine the eigenvalues, we follow the general procedure that consists on the time-space separation of variables followed by substitution in the homogeneous governing equations (2.26). The general solution of the second and third equations (4.4) is therefore assumed to be of the form

$$\begin{pmatrix} w(x,t) & \psi(x,t) \end{pmatrix}^{\mathsf{T}} = \exp(\mathrm{i}\omega t) \begin{pmatrix} W(x) & \Psi(x) \end{pmatrix}^{\mathsf{T}}$$

where ω is the frequency of oscillation, $i = \sqrt{-1}$ is the imaginary unit, and $W(x)$, $\Psi(x)$ are functions in $[0,1]$ that express the dependency on x. By substituting into the second and third equations (4.4) and by separating the variables we obtain the spatial eigenvalue problem

$$\begin{aligned} \frac{\mathrm{d}^2 W}{\mathrm{d}x^2} + \omega^2 W - \frac{\mathrm{d}\Psi}{\mathrm{d}x} &= 0 \\ \frac{\mathrm{d}^2 \Psi}{\mathrm{d}x^2} + \alpha_1 \left(\omega^2 - \alpha_2\right) \Psi + \alpha_1\alpha_2 \frac{\mathrm{d}W}{\mathrm{d}x} &= 0 \end{aligned}$$

The free ends boundary conditions are

$$\begin{aligned} \frac{\mathrm{d}\Psi}{\mathrm{d}x}(0) = \frac{\mathrm{d}\Psi}{\mathrm{d}x}(1) &= 0 \\ \frac{\mathrm{d}W}{\mathrm{d}x}(0) - \Psi(0) = \frac{\mathrm{d}W}{\mathrm{d}x}(1) - \Psi(1) &= 0 \end{aligned}$$

The general solution of the eigenvalues problem is sought by considering the vector valued function $\exp(\lambda x) \begin{pmatrix} \bar{W} & \bar{\Psi} \end{pmatrix}^{\mathsf{T}}$, where $\bar{W}$ and $\bar{\Psi}$ are constants. Such function is a solution for some positive constant λ if and only if

$$\begin{pmatrix} \lambda^2 + \beta_1 & -\lambda \\ \beta_3\lambda & \lambda^2 + \beta_2 \end{pmatrix} \begin{pmatrix} \bar{W} \\ \bar{\Psi} \end{pmatrix} = \begin{pmatrix} 0 \\ 0 \end{pmatrix}$$

with nondimensional parameters β_i defined by

$$\beta_1 = \omega^2, \quad \beta_2 = \alpha_1 \left(\omega^2 - \alpha_2\right), \quad \beta_3 = \alpha_1\alpha_2$$

The roots λ^2 of the characteristic polynomial $\lambda^4 + (\beta_1 + \beta_2 + \beta_3)\lambda^2 + \beta_1\beta_2 = 0$ are

$$\lambda_{1,2}^2 = -\frac{1}{2}\left(\beta_1 + \beta_2 + \beta_3\right)\left(1 \pm \sqrt{\Delta}\right)$$
$$\Delta = 1 - \frac{4\beta_1\beta_2}{\left(\beta_1 + \beta_2 + \beta_3\right)^2}$$

In order for λ^2 to be real it must be $\Delta > 0$, which is satisfied for $\beta_1\beta_2 < \gamma^2/4$, where $\gamma = \beta_1 + \beta_2 + \beta_3$. The special case $\lambda^2 = 0$ occurs when $\Delta = 1$, that is $\beta_1\beta_2 = 0$ or

$$\beta_1 = 0 \Rightarrow \omega^2 = 0,$$
$$\beta_2 = 0 \Rightarrow \omega^2 = \alpha_2 \text{ or } \alpha_1 = 0$$

This corresponds to rigid body motions of the system [132].

The condition $\Delta > 0$ dictates $\omega > 0$; therefore it must be $\gamma > 0$ since this is the case when γ is evaluated for $\omega > 0$. For $\Delta > 0$ and $\gamma > 0$ we have

$$\lambda_1 = \pm i\theta, \quad \theta^2 = \frac{\gamma}{2}\left(\sqrt{\Delta} + 1\right)$$

Moreover the condition $\Delta > 0$ implies

$$\beta_1\beta_2 = \alpha_1\omega^2\left(\omega^2 - \alpha_2\right)\begin{cases} < 0 & \text{for } \omega^2 < \alpha_2 \\ > 0 & \text{for } \omega^2 > \alpha_2 \end{cases}$$

For $\beta_1\beta_2 < 0$ we have $\sqrt{\Delta} > 1$ and

$$\lambda_2 = \pm\mu, \quad \mu^2 = \frac{\gamma}{2}\left(\sqrt{\Delta} - 1\right)$$

For this case the general solution is therefore given by [132]

$$\Phi(x) = C_1\begin{pmatrix} \sin\theta x \\ -\frac{\beta_1 - \theta^2}{\theta}\cos\theta x \end{pmatrix} + C_2\begin{pmatrix} \cos\theta x \\ \frac{\beta_1 - \theta^2}{\theta}\sin\theta x \end{pmatrix}$$
$$+C_3\begin{pmatrix} \sinh\mu x \\ \frac{\beta_1 + \mu^2}{\mu}\cosh\mu x \end{pmatrix} + C_4\begin{pmatrix} \cosh\mu x \\ \frac{\beta_1 + \mu^2}{\mu}\sinh\mu x \end{pmatrix}$$

Imposing the free end boundary conditions at $x = 0$ we obtain

$$C_1 = C_3\frac{\theta}{\mu}$$
$$C_2 = -C_4\frac{\beta_1 + \mu^2}{\beta_1 - \theta^2}$$

By imposing the free end boundary conditions at $x = 1$ we obtain the following linear algebraic relations involving C_3 and C_4

$$\mathbf{A}\begin{pmatrix} C_3 \\ C_4 \end{pmatrix} = \begin{pmatrix} 0 \\ 0 \end{pmatrix}$$

with coefficients matrix $\mathbf{A}$ given by

$$\mathbf{A} = \begin{pmatrix} \frac{\theta}{\mu}\left(\beta_1 - \theta^2\right)\sin\theta + \left(\beta_1 + \mu^2\right)\sinh\mu & \left(\beta_1 + \mu^2\right)\left(\cosh\mu - \cos\theta\right) \\ -\frac{\beta_1}{\mu}\cosh\mu & -\frac{\beta_1}{\mu}\sinh\mu \end{pmatrix}$$

The nontrivial solutions of the system are obtained by investigating the condition for rank deficiency of the coefficients matrix, which translates to the determinant being zero

$$-\cos\theta\cosh\mu + \frac{\theta(\theta^2 - \beta_1)}{\mu(\mu^2 + \beta_1)}\sin\theta\sinh\mu + 1 = 0 \tag{3.13}$$

All parameters in the characteristic equation depend on ω and on the material and geometric parameters of the system. Therefore, once the material and the geometry are defined the characteristic equation is a nonlinear function of ω only.

The first seven roots of the characteristic equation that determine the corresponding modes are given in Table 3.1. The roots are computed for $\alpha_1 = 0.1$ (shear modulus ten times smaller than the Young's modulus) and $\alpha_1\alpha_2 = 100$ (shear stiffness $kGA\ell^2$ to one hundred times larger than the bending stiffness EI). The mode shapes are normalized with respect to the maximum amplitude. The plots of the first three modes W and Ψ normalized with respect to the maximum value are given in Figure 3.1 and Figure 4.7 respectively. Here we consider α_2 large enough so that all modes included as basis functions have eigenfrequency ω_n satisfying $\omega_n^2 < \alpha_2$; therefore we do not consider the general solution for $\omega^2 > \alpha_2$ for which $\sqrt{\Delta} < 1$ and $\lambda_2 = \pm i\bar{\mu}$, with $\bar{\mu}^2 = -\mu^2$.

Table 3.1: First seven roots of the characteristic equation (4.11) with nondimensional material parameters $\alpha_1 = 0.1$ and $\alpha_2 = 100$

n	1	2	3	4	5	6	7
ω	2.07	4.96	8.32	11.8	15.3	18.7	22.0

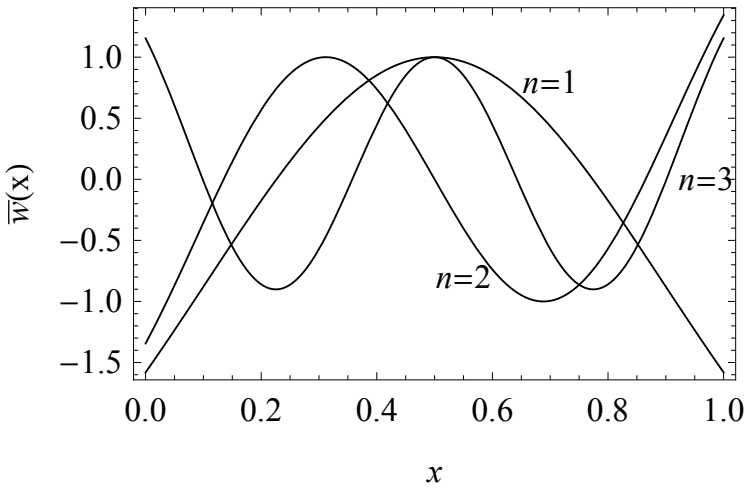

Figure 3.1: First three flexural modes, normalized with respect to the value at $x = 0.5$.

3.2.2 Axial Mode shape

Considering same nondimensional variables, the nondimensionalized form of equations (2.26a) is,

$$\alpha_1 \frac{\partial^2 u}{\partial t^2} - \frac{\partial^2 u}{\partial x^2} = 0 \tag{3.14}$$

and the boundary value problem of (3.14) can be expressed as,

$$\frac{\partial^2 U}{\partial x^2} - \beta U(x) = 0 \tag{3.15}$$

where has a solution in form of,

$$U(x) = C_1 \cos \beta x + C_2 \sin \beta x \tag{3.16}$$

where C_1 and C_2 are arbitrary constants to be determined form boundary conditions, and the free-free boundary condition in this case is;

$$\frac{\partial U}{\partial x}(0) = \frac{\partial U}{\partial x}(1) = 0 \tag{3.17}$$

then substituting for $\frac{\partial U}{\partial x}$ from (3.16), gives

$$C_2 = 0, \quad C_1 \sin \beta = 0 \tag{3.18}$$

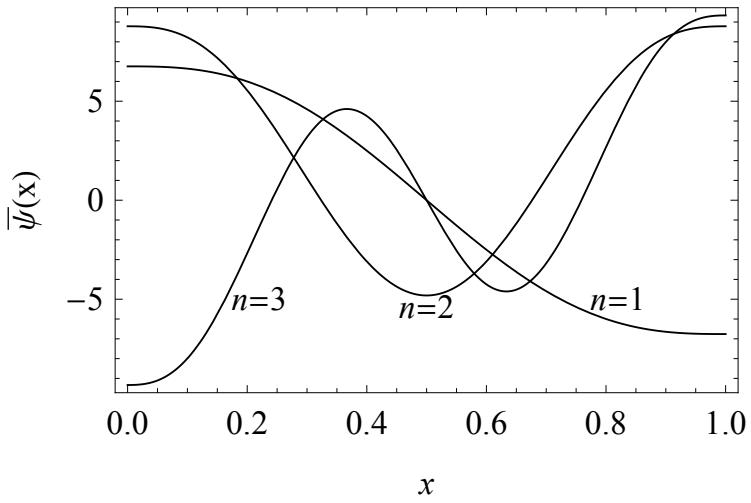

Figure 3.2: First three rotational modes, normalized with respect to the value at $x = 0.5$.

which yields,

$$\beta = n\pi \qquad n = 1, 2, \ldots, \infty \tag{3.19}$$

For $\beta = 0$ the (3.15) reduces to $\frac{\partial^2 U}{\partial x^2} = 0$, which has a solution of,

$$U(x) = D_1 + D_2 x \tag{3.20}$$

Applying boundary conditions, the eigenfunction for zero the frequency is $U(x) = D_1$ and considering (3.16) for $C_2 = 0$ the rest of eigenfunction can be expressed as,

$$U_n = \cos \beta_n x \tag{3.21}$$

The plots of the first three axial modes U, normalized with respect to the maximum value are given in Figure 3.3.

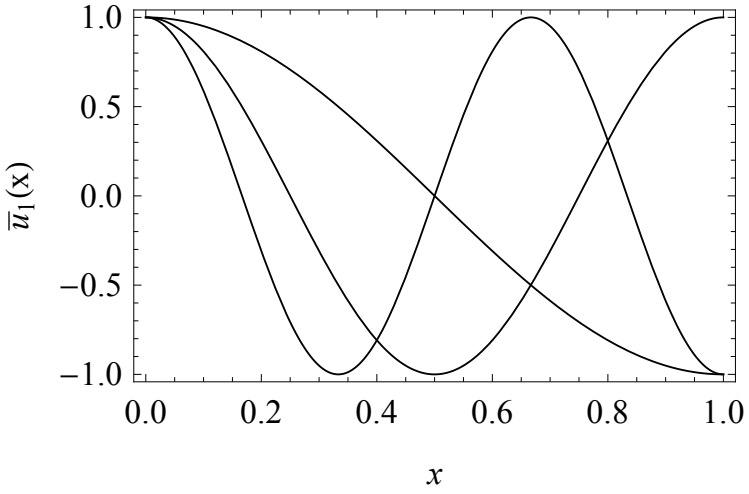

Figure 3.3: First three axial modes, normalized with respect to the maximum.

References

[1] A. A. Shabana, *Dynamics of Multibody Systems*. Cambridge University Press, 3 ed., 2010.

[2] C. Altafini, "Following a path of varying curvature as an output regulation problem," *IEEE Transactions on Automatic Control*, vol. 47, pp. 1551–1556, SEP 2002.

[3] F. L. Lewis, D. M. Dawson, and C. T. Abdallah, *Robot manipulator control: theory and practice*. CRC Press, 2003.

[4] R. Bogue, "Exoskeletons and robotic prosthetics: a review of recent developments," *Industrial Robot- An International Journal*, vol. 36, no. 5, pp. 421–427, 2009.

[5] M. Kassler, "Robotics for health care: a review of the literature," *Robotica*, vol. 11, pp. 495–516, NOV-DEC 1993.

[6] K. Doty, C. Melchiorri, and C. Bonivento, "A theory of generalized inverses applied to robotics," *International Journal of Robotics Research*, vol. 12, pp. 1–19, FEB 1993.

[7] S. Dubowsky and E. Papadopoulos, "The kinematics, dynamics, and control of free-flying and free-floating space robotic systems," *IEEE Transactions on Robotics and Automation*, vol. 9, pp. 531–543, OCT 1993.

[8] R. Van Ham, T. G. Sugar, B. Vanderborght, K. W. Hollander, and D. Lefeber, "Compliant Actuator Designs Review of Actuators with Passive Adjustable Compliance/Controllable Stiffness for Robotic Applications," *IEEE Robotics & Automation Magazine*, vol. 16, pp. 81–94, SEP 2009.

[9] P. Darie, E. Guglielmelli, B. Allotta, and M. Carrozza, "Robotics for medical applications," *IEEE Robotics & Automation Magazine*, vol. 3, pp. 44–56, SEP 1996.

[10] M. Hoffmann, H. G. Marques, A. H. Arieta, H. Sumioka, M. Lungarella, and R. Pfeifer, "Body Schema in Robotics: A Review," *IEEE Transactions on Autonomous Mental Development*, vol. 2, pp. 304–324, DEC 2010.

[11] N. Tejima, "Rehabilitation robotics: a review," *Advance Robotic*, vol. 14, no. 7, pp. 551–564, 2000.

[12] S. A. Green, M. Billinghurst, X. Chen, and J. G. Chase, "Human-Robot Collaboration: A Literature Review and Augmented Reality Approach In Design," *International Journal of Advanced Robotic Systems*, vol. 5, pp. 1–18, MAR 2008.

[13] R. Janssen, N.-M. Prpic, and W. G. M. Damen, "A review of the correlation of tergites, sternites, and leg pairs in diplopods," *Frontiers in Zoology*, vol. 3, pp. 1–10, Feb 2006.

[14] M. Wojtyra and J. Fraczek, "Comparison of Selected Methods of Handling Redundant Constraints in Multibody Systems Simulations," *Journal of Computational and Nonlinear Dynamics*, vol. 8, APR 2013.

[15] M. A. Sherman, A. Seth, and S. L. Delp, "Simbody: multibody dynamics for biomedical research," in *IUTAM Symposium on Human Body Dynamics* (McPhee, J and Kovecses, J, ed.), vol. 2 of *Procedia IUTAM*, pp. 241–261, Int Union Theoret & Appl Mech (IUTAM), 2011. IUTAM Symposium on Human Body Dynamics - From Multibody Systems to Biomechanics, Univ Waterloo, Waterloo, CANADA, JUN 05-08, 2011.

[16] G. Schultz and K. Mombaur, "Modeling and Optimal Control of Human-Like Running," *IEEE/ASME Transactions on Mechatronics*, vol. 15, pp. 783–792, OCT 2010.

[17] A. Carvalho and A. Suleman, "Multibody simulation of the musculoskeletal system of the human hand," *Multibody System Dynamics*, vol. 29, pp. 271–288, MAR 2013.

[18] T. M. Guess, "Forward dynamics simulation using a natural knee with menisci in the multibody framework," *Multibody System Dynamics*, vol. 28, pp. 37–53, AUG 2012.

[19] A. Stops, R. Wilcox, and Z. Jin, "Computational modelling of the natural hip: a review of finite element and multibody simulations," *Computer Methods in Biomechanics and Biomedical Engineering*, vol. 15, no. 9, pp. 963–979, 2012.

[20] M. E. Lund, M. de Zee, M. S. Andersen, and J. Rasmussen, "On validation of multibody musculoskeletal models," *Proceedings of the Institution of Mechanical Engineers Part H Journal of Engineering in Medicine*, vol. 226, no. H2, SI, pp. 82–94, 2012.

[21] F. Naets, T. Tamarozzi, G. H. K. Heirman, and W. Desmet, "Real-time flexible multibody simulation with Global Modal Parameterization," *Multibody System Dynamics* , vol. 27, pp. 267–284, MAR 2012.

[22] V. Sonneville and O. Bruls, "Sensitivity analysis for multibody systems formulated on a Lie group," *Multibody System Dynamics*, vol. 31, pp. 47–67, JAN 2014.

[23] A. Muller and Z. Terze, "On the choice of configuration space for numerical Lie group integration of constrained rigid body systems," *Journal of Computational and Applied Mathematics*, vol. 262, pp. 3–13, MAY 15 2014. 13th Seminar Numerical Solution of Differential and Differential-Algebraic Equations (NUMDIFF), Martin Luther Univ Halle Wittenberg, Halle, GERMANY, SEP 10-14, 2012.

[24] Z. Terze, M. Vrdoljak, and D. Zlatar, "Geometric Mathematical Framework for Multibody System Dynamics," in *Numerical Analysis and Applied Mathematics, VOLS I-III* (Psihoyios, G and Tsitouras, C, ed.), vol. 1281 of *AIP Conference Proceedings*, pp. 1288–1291, European Soc Comp Methods Sci & Engn, 2010. International Conference on Numerical Analysis and Applied Mathematics, Rhodes, GREECE, SEP 19-25, 2010.

[25] O. Bruls and A. Cardona, "On the Use of Lie Group Time Integrators in Multibody Dynamics," *Journal of Computational and Nonlinear Dynamics*, vol. 5, JUL 2010.

[26] A. Wynn, Y. Wang, R. Palacios, and P. J. Goulart, "An energy-preserving description of nonlinear beam vibrations in modal coordinates," *Journal of Sound and Vibration*, vol. 332, pp. 5543–5558, OCT 14 2013.

[27] J. Ding and Z. Pan, "Higher Order Variational Integrators for Multibody System Dynamics with Constraints," *Advances in Mechanical Engineering*, 2014.

[28] P. Betsch, C. Hesch, N. Saenger, and S. Uhlar, "Variational Integrators and Energy-Momentum Schemes for Flexible Multibody Dynamics," *Journal of Computational and Nonlinear Dynamics*, vol. 5, JUL 2010.

[29] M. Pascal, "Some open problems in dynamic analysis of flexible multibody systems," *Multibody System Dynamics*, vol. 5, no. 4, pp. 315–334, 2001.

[30] F. Bcllezza, L. Lanari, and G. Ulivi, "Exact modeling of the slewing flexible link," in *Proc of IEEE International Conference on Robotics and Automation*, pp. 734–739, 1990.

[31] M. White and G. Heppler, "A timoshenko model of a flexible slewing link," in *American Control Conference, Proceedings of the 1995*, vol. 4, pp. 2815–2819, IEEE, 1995.

[32] J. Ower and J. de Vegte, "Classical control design for a flexible manipulator: modeling and control system design," *Robotics and Automation, IEEE Journal of*, vol. 3, no. 5, pp. 485–489, 1987.

[33] A. De Luca and B. Siciliano, "Closed-form dynamic model of planar multilink lightweight robots," *Systems, Man and Cybernetics, IEEE Transactions on*, vol. 21, no. 4, pp. 826–839, 1991.

[34] P. Tomei and A. Tornambe, "Approximate modeling of robots having elastic links," *Systems, Man and Cybernetics, IEEE Transactions on*, vol. 18, no. 5, pp. 831–840, 1988.

[35] Y. Chaolan, H. Jiazhen, and C. Guoping, "Modeling study of a flexible hub–beam system with large motion and with considering the effect of shear deformation," *Journal of sound and vibration*, vol. 295, no. 1, pp. 282–293, 2006.

[36] W. Chen, "Dynamic modeling of multi-link flexible robotic manipulators," *Computers & Structures*, vol. 79, no. 2, pp. 183–195, 2001.

[37] H.-H. Lee, "New dynamic modeling of flexible-link robots," *Journal of dynamic systems, measurement, and control*, vol. 127, no. 2, pp. 307–309, 2005.

[38] X. Zhang, W. Xu, S. S. Nair, and V. Chellaboina, "Pde modeling and control of a flexible two-link manipulator," *Control Systems Technology, IEEE Transactions on*, vol. 13, no. 2, pp. 301–312, 2005.

[39] R. Milford and S. Asokanthan, "Configuration dependent eigenfrequencies for a two-link flexible manipulator: experimental verification," *Journal of sound and vibration*, vol. 222, no. 2, pp. 191–207, 1999.

[40] C. di Castri and A. Messina, *Modeling effects on free vibration of a two-link flexible manipulator*. Springer, 2010.

[41] P. Pai and A. Palazotto, "Large-deformation analysis of flexible beams," *International Journal of Solids and Structures*, vol. 33, pp. 1335–1353, APR 1996.

[42] S. Von Dombrowski, "Analysis of large flexible body deformation in multibody systems using absolute coordinates," *Multibody System Dynamics*, vol. 8, pp. 409–432, NOV 2002.

[43] J. Gerstmayr and H. Irschik, "On the correct representation of bending and axial deformation in the absolute nodal coordinate formulation with an elastic line approach," *Journal of Sound and Vibration*, vol. 318, pp. 461–487, DEC 9 2008.

[44] H. Yoo, R. Ryan, and R. Scott, "Dynamics of flexible beams undergoing overall motions," *Journal of Sound and Vibration*, vol. 181, pp. 261–278, MAR 23 1995.

[45] R. Kang, D. T. Branson, T. Zheng, E. Guglielmino, and D. G. Caldwell, "Design, modeling and control of a pneumatically actuated manipulator inspired by biological continuum structures," *Bioinspiration & Biomimetics*, vol. 8, Sep 2013.

[46] G. Chirikjian and J. Burdick, "Kinematically optimal hyper-redundant manipulator configurations," *IEEE Transactions on Robotics and Automation*, vol. 11, pp. 794–806, DEC 1995.

[47] B. Atakan, A. Erkmen, and I. Erkmen, "3-D grasping during serpentine motion with a snake-like robot," in *Proceedings of the Sixth IASTED International Conference on Robotics and Applications* (Gerhardt, LA, ed.), pp. 46–51, Int Assoc

Sci & Technol Dev, 2005. 6th IASTED International Conference on Robotics and Applications, Cambridge, MA, Oct 31-Nov 02, 2005.

[48] D. Bopearatchy and G. Hatanwala, "State space control of a multi link robot manipulator by a translational modelling technique," in *Intelligent Control, 1990. Proceedings., 5th IEEE International Symposium on*, pp. 285–290, IEEE, 1990.

[49] T. Nanayakkara, K. Watanabe, K. Kiguchi, and K. Izumi, "Controlling multi-link manipulators by fuzzy selection of dynamic models," in *Industrial Electronics Society, 2000. IECON 2000. 26th Annual Confjerence of the IEEE*, vol. 1, pp. 638–643 vol.1, 2000.

[50] M. Moallem, K. Khorasani, and R. Patel, "An inverse dynamics sliding control technique for flexible multi-link manipulators," in *American Control Conference, 1997. Proceedings of the 1997*, vol. 3, pp. 1407–1411 vol.3, 1997.

[51] J.-X. Xu, Y.-J. Pan, and T.-H. Lee, "A gain shaped sliding mode control scheme using filtering techniques with applications to multi-link robotic manipulators," in *American Control Conference, 2001. Proceedings of the 2001*, vol. 6, pp. 4363–4368 vol.6, 2001.

[52] C. Wright, A. Johnson, A. Peck, Z. McCord, A. Naaktgeboren, P. Gianfortoni, M. Gonzalez-Rivero, R. Hatton, and H. Choset, "Design of a modular snake robot," in *Intelligent Robots and Systems, 2007. IROS 2007. IEEE/RSJ International Conference on*, pp. 2609–2614, IEEE, 2007.

[53] M. Tesch, K. Lipkin, I. Brown, R. Hatton, A. Peck, J. Rembisz, and H. Choset, "Parameterized and scripted gaits for modular snake robots," *Advanced Robotics*, vol. 23, no. 9, pp. 1131–1158, 2009.

[54] R. L. Hatton and H. Choset, "Generating gaits for snake robots: annealed chain fitting and keyframe wave extraction," *Autonomous Robots*, vol. 28, no. 3, pp. 271–281, 2010.

[55] Z. Shiller and Y.-R. Gwo, "Dynamic motion planning of autonomous vehicles," *Robotics and Automation, IEEE Transactions on*, vol. 7, no. 2, pp. 241–249, 1991.

[56] B. d'Andrea Novel, G. Bastin, and G. Campion, "Modelling and control of non-holonomic wheeled mobile robots," in *Robotics and Automation, 1991. Proceedings., 1991 IEEE International Conference on*, pp. 1130–1135, IEEE, 1991.

[57] J. Gray and H. Lissmann, "Studies in animal locomotion vii. locomotory reflexes in the earthworm," *Journal of Experimental Biology*, vol. 15, no. 4, pp. 506–517, 1938.

[58] S. Hirose, T. Kado, and Y. Umetani, "Tensor actuated elastic manipulator," in *Proceedings of the Sixth World Congress on Theory of Machines and mechanisms*, 1983.

[59] B. C. Jayne, "Kinematics of terrestrial snake locomotion," *Copeia*, pp. 915–927, 1986.

[60] Y. Umetani and S. Hirose, "Biomechanical study of serpentine locomotion," in *On Theory and Practice of Robots and Manipulators*, pp. 171–184, Springer, 1974.

[61] S. Hirose, K. Ikuta, M. Tsukamoto, and K. Sato, "Considerations on design of the actuator based on the shape memory effect," in *The Theory of Machines and Mechanisms (Proc. 7th World Congr., Seville, Spain)*, pp. 1549–1556, Pergamon Oxford, 1987.

[62] S. Hirose and Y. Umetani, "The kinematics and control of a soft gripper for the handling of living or fragile objects," in *Proc. of the Fifth World Congress on the Theory of Machines and Mechanisms*, pp. 1175–1178, 1979.

[63] W. Clement and R. Inigo, "Design of a snake-like manipulator," *Robotics and Autonomous Systems*, vol. 6, no. 3, pp. 265–282, 1990.

[64] S.-C. Chiang, "Path planning for an articulated transporter/manipulator system," 1993.

[65] E. Verriest, "Efficient motion planning for a planar multiple link robot, based on differential friction," in *American Control Conference, 1989*, pp. 2364–2365, IEEE, 1989.

[66] D. Sen and T. Mruthyunjays, "Studies of a new snake-like manipulator," in *ASME Conf. Robotics, Spatial Mechanisms, and Mechanical Systems*, vol. 45, pp. 423–438, 1992.

[67] G. S. Chirikjian and J. W. Burdick, "The kinematics of hyper-redundant robot locomotion," *Robotics and Automation, IEEE Transactions on*, vol. 11, no. 6, pp. 781–793, 1995.

[68] S. Hirose, "Biologically inspired robots: Snake-like locomotors and manipulators,(1993)."

[69] H. Yamada, S. Chigisaki, M. Mori, K. Takita, K. Ogami, and S. Hirose, "Development of amphibious snake-like robot acm-r5," *Proc. ISR2005*, 2005.

[70] A. Motahari, H. Zohoor, and M. H. Korayem, "A New Inverse Kinematic Algorithm For Discretely Actuated Hyper-redundant Manipulators," *Latin American applied research*, vol. 43, pp. 161–168, APR 2013.

[71] A. Chibani, C. Mahfoudi, T. Chettibi, and R. Merzouki, "Conceptual Study of a Class of Hybrid Hyper-Redundant Robot," in *IEEE International Conference on Robotics and Biomimetics (ROBIO)*. Guangzhou, P R China, DEC 11-14, 2012.

[72] M. G. Marcos, J. A. T. Machado, and T. P. Azevedo-Perdicoulis, "A fractional approach for the motion planning of redundant and hyper-redundant manipulators," *Signal Processing*, vol. 91, pp. 562–570, MAR 2011.

[73] S. Yahya, H. A. F. Mohamed, M. Moghavvemi, and S. S. Yang, "A Geometrical Inverse Kinematics Method for Hyper-Redundant Manipulators," in *10th International Conference on Control, Automation, Robotics and Vision, VOLS 1-4*, pp. 1954–1958. Hanoi, Vietnam, DEC 17-20, 2008.

[74] F. Fahimi, H. Ashrafiuon, and C. Nataraj, "An improved inverse kinematic and velocity solution for spatial hyper-redundant robots," *IEEE Transactions on Robotics and Automation*, vol. 18, pp. 103–107, FEB 2002.

[75] H. Mochiyama, E. Shimemura, and H. Kobayashi, "Shape control of manipulators with hyper degrees of freedom," *International Journal of Robotics Research*, vol. 18, pp. 584–600, JUN 1999.

[76] G. Chirikjian and J. Burdick, "A modal approach to hyper-redundant manipulator kinematics," *IEEE Transactions on Robotics and Automation*, vol. 10, pp. 343–354, JUN 1994.

[77] C. Huang, C. Shih, and S. Kim, "An inverse vibration problem in estimating the spatial and temporal-dependent external forces for cutting tools," *Applied Mathematical Modelling*, vol. 33, pp. 2683–2698, Jun 2009.

[78] W. Chen, Y. Yang, W. Chang, and H. Lee, "Inverse problem of estimating transient heat transfer rate on external wall of forced convection pipe," *Energy Conversion and Management*, vol. 49, pp. 2117–2123, Aug 2008.

[79] D. T. Lin, W.-M. Yan, and H.-Y. Li, "Inverse problem of unsteady conjugated forced convection in parallel plate channels," *International Journal of Heat and Mass Transfer*, vol. 51, no. 5, pp. 993–1002, 2008.

[80] M. Girault and D. Petit, "Resolution of linear inverse forced convection problems using model reduction by the Modal Identification Method: application to turbulent flow in parallel-plate duct," *International Journal of Heat and Mass Transfer*, vol. 47, pp. 3909–3925, AUG 2004.

[81] C. Huang and W. Chen, "A three-dimensional inverse forced convection problem in estimating surface heat flux by conjugate gradient method," *International Journal of Heat and Mass Transfer*, vol. 43, pp. 3171–3181, SEP 2000.

[82] L. Righetti, J. Buchli, M. Mistry, M. Kalakrishnan, and S. Schaal, "Optimal distribution of contact forces with inverse-dynamics control," *International Journal of Robotics Research*, vol. 32, pp. 280–298, MAR 2013.

[83] K. Nagasaka, Y. Kawanami, S. Shimizu, T. Kito, T. Tsuboi, A. Miyamoto, T. Fukushima, and H. Shimomura, "Whole-body Cooperative Force Control for a Two-Armed and Two-Wheeled Mobile Robot Using Generalized Inverse Dynamics and Idealized Joint Units," IEEE International Conference on Robotics and Automation ICRA, pp. 3377–3383. AK, May 03-08, 2010.

[84] C. Guarino L Bianco and O. Gerelli, "Trajectory scaling for a manipulator inverse dynamics control subject to generalized force derivative constraints," in *IEEE/RSJ International Conference on Intelligent Robots and Systems*, pp. 5749–5754. St Louis, MO, Oct 10-15, 2009.

[85] S. Ider, "Inverse dynamics of redundant manipulators using a minimum number of control forces," *Journal of Robotic Systems*, vol. 12, pp. 569–579, Aug 1995.

[86] K. M. Dolatshahi and F. R. Rofooei, "Inverse vibration problem for un-damped 3-dimensional multi-story shear building models," *Journal of Sound and Vibration*, vol. 333, pp. 99–113, Jan 6 2014.

[87] C. Liu, "An iterative GL(n, R) method for solving non-linear inverse vibration problems," *Nonlinear Dynamics*, vol. 74, pp. 685–699, Nov 2013.

[88] A. Maciag and A. Pawinska, "Solving direct and inverse problems of plate vibration by using the Trefftz functions," *Journal of Theoretical and Applied Mechanics*, vol. 51, no. 3, pp. 543–552, 2013.

[89] G. F. Safina, "Analysis of Direct and Inverse Problems on Transverse Vibrations of a Supported Shaft," *Russian Journal of Nondestructive Testing*, vol. 46, pp. 302–313, APR 2010.

[90] Q. S. Wang, Y. Wang, and L. H. Zhang, "Inverse mode problem in the discrete model of circular plate axial symmetry vibration," *Applied Mechanics and Materials*, vol. 34, pp. 71–78, 2010.

[91] B. N. Datta and V. Sokolov, "Quadratic Inverse Eigenvalue Problems, Active Vibration Control and Model Updating," *Applied and Computational Mathematics*, vol. 8, no. 2, pp. 170–191, 2009.

[92] L. D. Chiwiacowsky, H. F. De Campos Velho, and P. Gasbarri, "A variational approach for solving an inverse vibration problem," *Inverse Problems in Science and Engineering*, vol. 14, no. 5, pp. 557–577, 2006. Symposium on Inverse Problems, Design and Optimization, Rio de Janeiro, Brazil, Mar 17-19, 2004.

[93] H. Ressing and M. Gadala, "A practical investigation to solving the inverse problem of crack identification through vibration measurements," *Engineering Computations*, vol. 23, no. 1-2, pp. 32–56, 2006.

[94] N. Khiem, "Crack detection for structure based on the dynamic stiffness model and the inverse problem of vibration," *Inverse Problems in Science and Engineering*, vol. 14, pp. 85–96, Jan 2006.

[95] C. Huang, "A generalized inverse force vibration problem for simultaneously estimating the time-dependent external forces," *Applied Mathematical Modelling*, vol. 29, pp. 1022–1039, Nov 2005.

[96] C. Huang, "A nonlinear inverse problem in estimating simultaneously the external forces for a vibration system with displacement-dependent parameters," *Journal of The Franklin Institute. Engineering and Applied Mathematics*, vol. 342, pp. 793–813, NOV 2005.

[97] C. Huang, "A non-linear inverse vibration problem of estimating the external forces for a system with displacement-dependent parameters," *Journal of Sound and Vibration*, vol. 248, pp. 789–807, Dec 13 2001.

[98] C. Huang, "An inverse non-linear force vibration problem of estimating the external forces in a damped system with time-dependent system parameters," *Journal of Sound and Vibration*, vol. 242, pp. 749–765, May 17 2001.

[99] D. Moss and H. Benaroya, "A discrete inverse vibration problem with parameter uncertainty," *Applied Mathematics and Computation*, vol. 69, pp. 313–333, May 1995.

[100] L. Starek, D. Iman, and A. Kress, "A Symmetric Inverse Vibration Problem," *Journal of Vibration and Acoustics*, vol. 114, pp. 564–568, OCT 1992.

[101] M. Yamamoto, "Inverse eigenvalue problem for a vibration of a string with viscous drag," *Journal of Mathematical Analysis and Applications*, vol. 152, pp. 20–34, OCT 1990.

[102] H. Banks, R. Powers, and I. Rosen, "Inverse problems in the modeling of vibrations of flexible beams," *Lecture Notes in Control and Information Sciences*, vol. 102, pp. 1–22, 1987.

[103] A. Tsaune and V. Golovko, "Anharmonic vibration-rotation inverse problem with reconstruction of Hamiltonian terms," *Journal of Molecular Spectroscopy*, vol. 108, no. 1, pp. 82–98, 1984.

[104] M. Hamada, Y. Seguchi, and Y. Tada, "Shape Determination Problems of Structures by the Inverse Variational Principle : 2nd Report, Buckling and Vibration Problems," *The Japan Society of Mechanical EngineersBulletin of the JSME*, vol. 23, no. 184, pp. 1581–1588, 1980.

[105] N. Stepanov, G. Koptev, and Y. Panchenko, "Uniqueness of solution of an inverse vibration problem," *Optika i spektroskopiya*, vol. 38, no. 4, pp. 657–662, 1975.

[106] C. Yang, "Solution of an inverse vibration problem using a linear least-squares error method," *Applied Mathematical Modelling*, vol. 20, pp. 785–788, Oct 1996.

[107] D. Hua and P. Lancaster, "Linear matrix equations from a non-linear inverse vibration problem of estimating the time-dependent stiffness coefficnverse problem

of vibration theory," *Linear Algebra and its Applications* , vol. 246, pp. 31–47, Oct 1996.

[108] S. Kuroda, I. Kunita, Y. Tanaka, A. Ishiguro, R. Kobayashi, and T. Nakagaki, "Common mechanics of mode switching in locomotion of limbless and legged animals," *Journal of The Royal Society Interface*, vol. 11, no. 95, p. 20140205, 2014.

[109] J. Fattahi and D. Spinello, "A timoshenko beam reduced order model for shape tracking with a slender mechanism," *Journal of Sound and Vibration*, vol. 333, no. 20, pp. 5165 – 5180, 2014.

[110] J. L. Capinera, *Insects and Wildlife: Arthropods and their Relationships with Wild Vertebrate Animals*. Wiley-Blackwell, 2010.

[111] J. L. Capinera, *Encyclopedia of Entomology*, vol. 4. Springer, 2008.

[112] R. W. Cahn, "Biomimetics: Biologically inspired technologies," *Nature*, vol. 444, pp. 425–426, NOV 23 2006.

[113] L. Drago, G. Fusco, E. Garollo, and A. Minelli, "Structural aspects of leg-to-gonopod metamorphosis in male helminthomorph millipedes (Diplopoda)," *Frontiers in Zoology*, vol. 8, Aug 22 2011.

[114] M. Golubitsky, I. Stewart, P. Buono, and J. Collins, "A modular network for legged locomotion," *Phisica D*, vol. 115, pp. 56–72, APR 15 1998.

[115] H. Enghoff, "Adaptive radiation of the millipede genus cylindroiulus on madeira: habitat, body size, and morphology (diplopoda, iulida: Iulidae)," *Revue d'écologie et de biologie du sol*, vol. 20, no. 3, pp. 403–415, 1983.

[116] D. Avirovik, B. Butenhoff, and S. Priya, "Millipede-inspired locomotion through novel U-shaped piezoelectric motors," *Smart Materials and Structures*, vol. 23, Mar 2014.

[117] F. Boyer and S. Ali, "Recursive inverse dynamics of mobile multibody systems with joints and wheels," *Robotics, IEEE Transactions on*, vol. 27, no. 2, pp. 215–228, 2011.

[118] W. Weaver Jr, S. P. Timoshenko, and D. H. Young, *Vibration problems in engineering*. John Wiley & Sons, 1990.

[119] E. Kausel, "Nonclassical modes of unrestrained shear beams," *Journal of engineering mechanics*, vol. 128, no. 6, pp. 663–667, 2002.

[120] A. D. Kerr, "Elastic and viscoelastic foundation models," *Journal of Applied Mechanics*, vol. 31, no. 3, pp. 491–498, 1964.

[121] Y. Shin, J. Yun, K. Seong, J. Kim, and S. Kang, "Natural frequencies of euler-bernoulli beam with open cracks on elastic foundations," *Journal of mechanical science and technology*, vol. 20, no. 4, pp. 467–472, 2006.

[122] M.-H. Hsu, "Vibration analysis of edge-cracked beam on elastic foundation with axial loading using the differential quadrature method," *Computer Methods in Applied Mechanics and Engineering*, vol. 194, no. 1, pp. 1–17, 2005.

[123] M. De Rosa, "Free vibrations of timoshenko beams on two-parameter elastic foundation," *Computers & Structures*, vol. 57, no. 1, pp. 151–156, 1995.

[124] S. Lee, Y. Kuo, and F. Lin, "Stability of a timoshenko beam resting on a winkler elastic foundation," *Journal of sound and vibration*, vol. 153, no. 2, pp. 193–202, 1992.

[125] T. Wang and J. Stephens, "Natural frequencies of timoshenko beams on pasternak foundations," *Journal of Sound and Vibration*, vol. 51, no. 2, pp. 149–155, 1977.

[126] A. G. Razaqpur and K. Shah, "Exact analysis of beams on two-parameter elastic foundations," *International Journal of Solids and Structures*, vol. 27, no. 4, pp. 435–454, 1991.

[127] M. Kargarnovin and D. Younesian, "Dynamics of timoshenko beams on pasternak foundation under moving load," *Mechanics Research Communications*, vol. 31, no. 6, pp. 713–723, 2004.

[128] L. G. Arboleda-Monsalve, D. G. Zapata-Medina, and J. D. Aristizabal-Ochoa, "Timoshenko beam-column with generalized end conditions on elastic foundation: Dynamic-stiffness matrix and load vector," *Journal of Sound and Vibration*, vol. 310, no. 4, pp. 1057–1079, 2008.

[129] X. Ma, J. Butterworth, and G. Clifton, "Static analysis of an infinite beam resting on a tensionless pasternak foundation," *European Journal of Mechanics-A/Solids*, vol. 28, no. 4, pp. 697–703, 2009.

[130] J. Vincent, *Structural biomaterials*. Princeton University Press, 2012.

[131] H. T. Banks, S. Hu, and Z. R. Kenz, "A brief review of elasticity and viscoelasticity," tech. rep., DTIC Document, 2010.

[132] N. Van Rensburg and A. Van der Merwe, "Natural frequencies and modes of a timoshenko beam," *Wave motion*, vol. 44, no. 1, pp. 58–69, 2006.

Part II

Publications

Chapter 4

A Timoshenko Beam Reduced Order Model for Shape Tracking with a Slender Mechanism

The work in this chapter is published in the Journal of Sound and Vibration. [91]

4.1 Abstract

We consider a flexible bio-inspired slender mechanism, modeled as a Timoshenko beam. It is coupled to the environment by a continuous distribution of compliant elements. We derive a reduced order model by projecting the governing partial differential equations along the linear modal basis of the Timoshenko beam. The coupling with the substrate allows to formulate the problem in a control framework, and therefore to treat the system as a sensor to reconstruct the profile of the substrate through the deformation of the body. The coupling is modeled in the framework of two parameters elastic foundations. The convergence of the reduced order model with increasing number of basis functions is addressed in a suitable H^1 error norm. A closed loop force control is simulated for shape morphing when the system is coupled with a smooth substrate.

Keywords: Flexible Mechanism, Reduced Order Modeling, Timoshenko Beam, Modal Analysis

4.2 Introduction

In this paper we consider shape tracking with a slender mechanism coupled with a substrate. Shape tracking is based on the flexibility of the mechanism, that is modeled as a Timoshenko beam. The interaction with the environment is described by a distributed system of deformable elements. By considering the initial configuration to be locally parallel to the substrate, in the sense that it is parallel to the tangent to the substrate at the nearest point, we focus on the coupling with the environment and specifically on the deformation induced by the shape of the substrate. Based on the linear eigenfunctions of a Timoshenko beam on elastic foundations a reduced order model of the distributed evolution equations is obtained by Galerkin projection. The reduced order model allows to formulate a control problem for the slender mechanism coupled with a substrate, and considers the shape of the substrate as desired input to be tracked. The model presented here is the first step towards the development of a flexible hyper-redundant autonomous robotic system highly adaptable to different terrains and environments, through a locomotion system inspired by the spinal mechanics of millipedes- and centipedes-like organisms.

A crucial characterization for the class of mechanisms studied here is the model of the distributed coupling with the environment through the system of deformable elements that mimic the functions of the legs of millipedes. This distributed system is modeled as an elastic foundation. Several foundation models can be found in the literature to describe thin structures on soft elastic continua. Typically such models constitutively relate the response of the bed to the kinematics of the structure resting on it. The simplest is the Wrinkler model, in which the foundation is described as a system of independent springs reacting to the deflection of the body [1, 2]. Two parameters extensions of the Wrinkler model have been proposed by Filolenko-Borodich [3] and Pasternak [4–6] respectively by considering membrane like interactions (with constant tension) and shear interactions among springs. Alternatively to this family of models that are based on interactions between mechanical elements, continuum medium based model have been proposed based on variational formulations that include assumed kinematics of the foundation elastic medium [1, 7]. The Vlasov model [8] is based on the assumption that the in-plane displacement of the structure is identically zero, and the displacement on the transverse direction is controlled by the structure's deflection through a shape function that expresses the dependency on the dept of the elastic medium. A rigorous derivation of the shape function of the Vlasov model is presented in [7]. The generalized

Vlazov-Jones model is presented in [9] to account for non-vanishing in-plane structural displacements, and adapted in [10] to to describe the isotropic matrix material in syntactic foams particulate composites. All two parameter models are equivalent in the sense that they are described by the same constitutive relation, except for the computation of the parameters [11]. Here we adopt a two parameter model to describe the distributed system of elastic elements mimicking the functions of the legs, and therefore the coupling between the system and the environment in which the slender mechanism is deployed. Parameters of the model depend on the actual material employed and on the geometry. The coupling determines shape morphing and forward locomotion; in this work we restrict our attention to shape morphing with respect to a substrate described by a given profile. Millipedes' bio-inspired forward locomotion has been recently implemented through piezo-electric motors that reproduce the characteristic kinematics of the organism' walk [12]. In future developments of the system studied here we plan to explore different directions, such as those offered by electrically and thermally actuated memory foams [13, 14]. By looking at the reaction of the bed (that depends on the structural deflection and on the geometry of the substrate) as feedback, the constitutive parameters are treated as control gains and therefore considered as tunable parameters to control the shape adaptation with respect to the substrate. Further developments include the description of the elasticity of the substrate, with the adoption of a multi-parameters foundation model that includes the properties of the coupling (legs mimicking) system, and the properties of the substrate, allowing to use the device as a sensor to estimate the material properties of the surroundings to which it is coupled.

In the framework of multi-link robotic manipulators, several researches have recently proposed finite dimensional (with large number of degrees of freedom) and distributed systems capable of high deformability and large displacement of the end effector, still considering higher speed than traditional manipulators along with low energy consumption [15–18]. Mobile multibody robots have been developed from classical manipulators by considering rigid body chains interacting with the environment in a variety of modes. The interaction with the environment strongly affects the performance of mobile robots as environmental conditions and morphology are coupled with locomotion techniques. This applies, on an evolutionary scale, to biological systems and therefore to bio-inspired robots [19–21]. Multibody mobile mechanisms with large number of degrees of freedom can be modeled as continuous systems by introducing the appropriate approximations. Often models of one dimensional continua with local Euclideian structure (beam models) are naturally adopted, due to the slenderness of the system [22]. The vibrations of

a flexible manipulator based on the linear Euler-Bernoulli beam model are discussed in [23]. The governing equations of a continuous manipulator with distributed end mass boundary conditions are derived in [24]. Lagrangian and Ritz methods are used in [25] to study a flexible manipulator. A flexible hub-beam system has been analyzed in [26] by accounting for the influence of shear and axial deformation. Modeling of flexible manipulators with different geometric and dynamic conditions can be found in [27–32], among others. The Lagrangian approach has been used in [33] to model bending of flexible robots modeled as Euler-Bernoulli beams, whereas an Hamiltonian formulation has been adopted in [34] to obtain the governing equations for the same class of systems and design associated controllers. The modal analysis of a two-link flexible manipulator modeled as a Timoshenko beam has been presented in [35]. Examples of modeling and control of flexible mechanisms and chains with flexible links can be found in [36–38]. Locomotion and control techniques for bio-inspired and bio-mimetic robots have been proposed in [39–45] among others. Neural locomotion controllers for a central pattern generator of lamprey is developed in [46]. A survey on control in bio-inspired robotic systems can be found in [47]. Wheeled bio-inspired mobile robots control with non-holonomic constraints is discussed in [48]. The locomotion mechanism of worms is studied in [49–52]. Studies of the motion of snakes on various types of surfaces, the elastic elephant trunk like, and soft grippers are presented in [53–55]; tendon-driven robots and octopus tentacle-like gripper are investigated in [56–58]. Control of a snake-like manipulator with obstacle avoiding is proposed in [59]. Modeling and control of a wheel-less articulated mobile bio-inspired robot is presented in [60]; the kinematics and dynamics of a planar multiple link robot with non-conventional control method based on differential friction is discussed in [61]. Motion control based on inverse kinematics is presented in [62], and control of hyper-redundant robots by parametrization of the backbone curves is presented in [63].

The mechanical model based on the linear Timoshenko beam adopted here is valid under the hypothesis of length of the mechanism small as compared to the radius of curvature of the substrate to which it is coupled, so that a first order (linearized) kinematics is sufficiently accurate to describe the shape morphing, or otherwise the change in curvature induced by the substrate. When this hypothesis fails, it is appropriate to use higher order theories that include geometric nonlinearities. Boyer et al. [22] considered a general dynamic modeling approach that applies to elongated bodies continuous robots with distributed strain actuation. The body is modeled as a geometrically exact beam, and different bio-inspired locomotion mechanisms of hiper-redundant elongated organisms are reproduced. The Geometrically Exact Beam Theory proposed in [64, 65], and

based on Cosserat medium theory [66], has been used to model passive steerable needles [67, 68], soft robotics arms [69], and bio-inspired elongated (eel like) continua [70]. With the linear analysis presented here we want to set a basic modeling framework for the coupling effects of the substrate, the associated feedback interactions, and the role of the feedback gains as representative of lumped physical characteristics of the coupling material systems. This the first step towards the inclusion of geometrically nonlinear kinematics, and double curvature substrates for which out of plane deformation modes are relevant [22]. Out of plane deformation modes, and more generally three dimensional effects, need to be included to study locomotion and morphing on unstructured terrains; moreover, bio-inspired forward locomotion in incoherent terrains such as sand is efficiently achieved by serpentine mode (lateral undulation) [55] in which lateral motion is used for propulsion. A combination of undulatory and pedundulatory (through systems of legs) motions with planar and three dimensional characteristics have been implemented in multibody elongated robots [71, 72]. Three dimensional displacement modes that include the torsion of the body are investigated in [22].

The rest of the paper is organized as follows. In Section 4.3, we briefly describe the locomotion mechanics of millipedes that is characterized by various mechanisms, with specific attention to the spinal locomotion part that inspires this work. In Section 4.4 we present the continuous model, based an Timoshenko beam, of a slender mechanism with sensing system that is represented by a continuous distribution of compliant elements mimicking the function of the legs with respect to shape tracking; the compliant elements can act as a distributed sensor to reconstruct the kinematics of the substrate to which the system is coupled. Section 4.5 includes a reduced order model of the system based on the Galerkin projection on the modal basis of a Timoshenko beam on a bed of springs. A simple degree-of-freedom approximation is considered and validated through a convergence analysis with increasing number of basis functions in the Galerkin projection. In Section 4.6 we formulate a control problem to track the shape of the substrate by considering a closed loop system with feedback given by the legs used as force transducers, therefore naturally embedding the coupling between the mechanism and the substrate through the stiffness of the legs. Simulation results presented in Section 6.5 illustrate the tracking by considering constant and time varying inputs, and show the influence of the stiffness of the coupling elastic elements. Despite its simplicity, a single degree-of-freedom system captures the salient features of the closed loop system in terms of deflection. Conclusions and final remarks are given in Section 4.8.

4.3 Spinal Locomotion Mechanics and Modelling

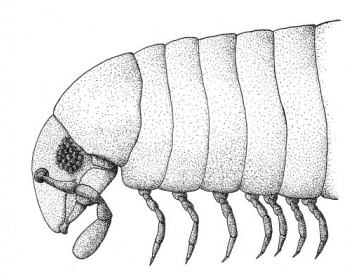

Figure 4.1: Schematics of the external anatomy of a generalized juliform millipede (Fig. 2 from [73])

Figure 4.2: Details of the dorsal structure of selected millipedes (By Animalparty (Own work) [CC-BY-SA-3.0 (`http://creativecommons.org/licenses/by-sa/3.0`)], via Wikimedia Commons)

Millipedes belong to Diplopoda class that is one of the six classes (Chilopoda or the centipedes; Pauropoda or the pauropods; Symphyla or the symphylans; Entognatha or the collembolans, proturans, and diplurans; and Insecta or the insects) in the Subphylum Atelocerata of the Phylum Arthropoda [74]. They are arthropods that have two legs per segment [75], see schematics in Fig. 4.1. The slender body is comprised of an exoskeleton which can be schematized as a chain of coaxial rings as shown in Fig. 4.2, with length commonly varying between 2 mm to 35 cm, see Fig. 4.3 for an example of a large specimen. It possesses an internal cartilaginous spine with spinal elements connected by three degrees of freedom joints. The locomotion can be characterized by two mechanisms, namely the spinal locomotion and the concertina locomotion [12, 76–79]. The latter consists of the axial stretching and folding of the body to achieve forward

Figure 4.3: Giant millipede (longer than 20 cm) from south bank of river Periyar near Kodanadu. (By Irvin calicut (Own work) [CC-BY-SA-3.0 (`http://creativecommons.org/licenses/by-sa/3.0`)], via Wikimedia Commons)

motion; this kind of locomotion is rarely employed, mainly to move through very narrow passages. The former is the most commonly used, and it is achieved by the the two stages kinematics schematized in Fig. 4.4, comprised of a stage in which the leg is in contact with the ground (larger semicicle) moving backward to create the thrust associated to friction, and a recovery stage (smaller semicircle) in which the leg is not in contact and moves forward. Pairs of contiguous legs are 90° phase shifted, giving to the overall system a characteristic wave like forward motion [12]. The wave motion with characteristic phase shift ensures interference avoidance and high robustness in unstructured terrains, due to the many contact points even when local irregularities are met. When the millipede walks on a flat surface the bending of the spine is negligible; therefore the shape morphing is mainly associated to changes in shape of the substrate.

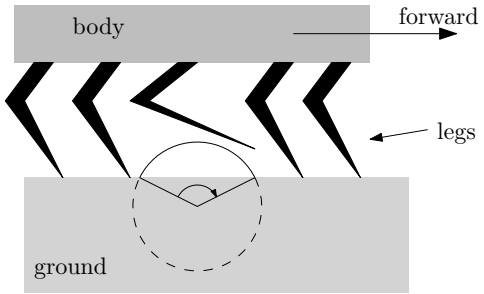

Figure 4.4: Kinematic diagram of the millipede spinal forward locomotion

Inspired by these characteristics, we consider a slender robot coupled with a substrate through a continuous distribution of compliant elements that mimic the legs of a millipede, see Figure 4.5. We use the deformability of the robot, modeleled as a con-

tinuous solid, to track the shape of the substrate similarly to the way the shape of the millipede morphs to curved shapes of the substrate on which it stands. By considering a continuous sequence of stiff elements aligned along a one dimensional support (axis), the natural choice for the mechanical model is the Timoshenko beam, that includes the axial displacement, the deflection, and the rotation of the the cross section. The calcified exoskeleton of millipedes is crucial in sustaining the typical forces involved during the motion. The density and Young's modulus of the exoskeleton of Nyssodesmus python millipedes are reported in [80] to be respectively $1660\,\mathrm{kg\,m^{-3}}$ and 17 GPa, for body mass varying between 2 g to 7 g. The mechanical model in this work is presented in terms of nondimensional parameters with bending and elastic supports stiffness normalized with respect to the shear stiffness of the Timoshenko beam. Results are obtained by specifying the ratio between bending stiffness and shear stiffness, and by considering the stiffness of the elastic supports to be a tunable parameter that influences the shape morphing.

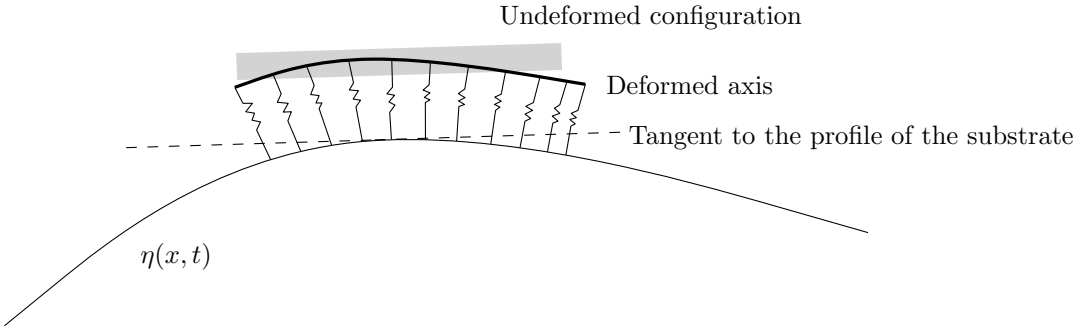

Figure 4.5: Sketch of the mechanism coupled with the substrate with profile described by the curve $\eta(x,t)$

4.4 Continuous Beam Model of the System

We present here the continuous model of a slender mechanism in which the flexibility of the body is used to detect the shape of the substrate on which the mechanism is deployed. The detection problem is formulated as a tracking problem where the coupling between the body of the mechanism and the substrate is given by a distributed system of compliant elements. This system is inspired by the mechanics of millipedes where the forward motion is achieved by a characteristic motion of the legs, and the adaptation to the shape of the substrate is achieved through the deformation of the body, see Section 4.3.

Here we specifically focus on the deformation of the body and the coupling with the substrate.

The mechanical model of a millipede spine can be considered as a kinematic chain of rigid bodies, with the length of each element comprising it being small as compared to the total length of the body. To characterize the flexibility of the system, each rigid element composing the body is mapped to the cross section of a Timoshenko beam [81] with support represented by a line that represent the idealization of the spine of the millipede. Therefore we consider the continuum to be represented by a one dimensional support (axis of the beam) with local Euclideian structure, which describes the local orientation of the cross section with respect to the axis. We assume that length and thickness of the mechanism are small as compared to the characteristic length and the environment in which it is deployed. Moreover we consider the variation of the curvature of the substrate to be small, and the mechanism to be locally parallel to the substrate, which implies that deformations are small [82]. Under these assumptions the components, with respect to a fixed rectangular Cartesian frame $\{x, y, z\}$, of the displacement of a point on the axis of the beam on the plane $\{x, z\}$ is given by

$$\begin{aligned} u_1(x, y, z, t) &= u(x, t) - z\psi(x, t) \\ u_2 &= 0 \\ u_3(x, y, z, t) &= w(x, t) \end{aligned}$$

where u is the axial displacement, ψ is the rotation angle of the cross section, and w is the transverse displacement with respect to the equilibrium state (assumed to be rectilinear with axis parallel to x), see Fig. 4.6. The linear Timoshenko beam model can be expressed by the following set of differential equations

$$\varrho A \frac{\partial^2 u}{\partial t^2} + c_u \frac{\partial u}{\partial t} = \frac{\partial}{\partial x}\left(EA\frac{\partial u}{\partial x}\right) + p_u \tag{4.1a}$$

$$\varrho A \frac{\partial^2 w}{\partial t^2} + c_w \frac{\partial w}{\partial t} = \frac{\partial}{\partial x}\left(kAG\left(\frac{\partial w}{\partial x} - \psi\right)\right) + p_w \tag{4.1b}$$

$$\varrho I \frac{\partial^2 \psi}{\partial t^2} + c_\psi \frac{\partial \psi}{\partial t} = \frac{\partial}{\partial x}\left(EI\frac{\partial \psi}{\partial x}\right) + kAG\left(\frac{\partial w}{\partial x} - \psi\right) + p_\psi \tag{4.1c}$$

where ϱ is the volume mass density, A the area of the cross section, I the moment of inertia, E and G Young's and shear elastic modulus, respectively, k is the Timoshenko shear modulus (nondimensional parameter that depends on the geometry), and p_u, p_w, and p_ψ are respectively distributed loads in the axial and transverse directions and a

distributed couple perpendicular to the plane of motion. Terms proportional to the first time derivatives through coefficients c_u, c_w, and c_ψ model the structural damping as equivalent viscous damping [81]. Structural damping accounts for hysteresis phenomena in elastic materials undergoing cyclic loading [81, 83], and therefore it depends on the frequency of excitation. In equivalent viscous damping models the dependency on the frequency of excitation $\bar{\omega}$ is included through the proportional coefficients by the inverse law $c_u = \bar{c}_u/(\pi\bar{\omega})$ (similarly for c_w and c_ϕ) [83], where $\bar{c}_u$ is a constant independent of $\bar{\omega}$. More refined viscous equivalent structural damping models for Timoshenko beams have been presented, among others, in Ref. [84] where adaptive structural damping parameters are introduced in the context of LQR control; in Ref. [85] where dependency to shear and bending angles is included; and in Ref. [86] where the response of nonlocal viscoelastic (Kelvin-Voigt) damped nanobeams is investigated. The governing equations (4.1) are obtained from the balance equations by using the following constitutive relations

$$N = EA\frac{\partial u}{\partial x}, \quad V = kAG\left(\frac{\partial w}{\partial x} - \psi\right), \quad M = EI\frac{\partial \psi}{\partial x} \tag{4.2}$$

where N, V, and M are respectively the axial, shear, and bending moment stress resultants.

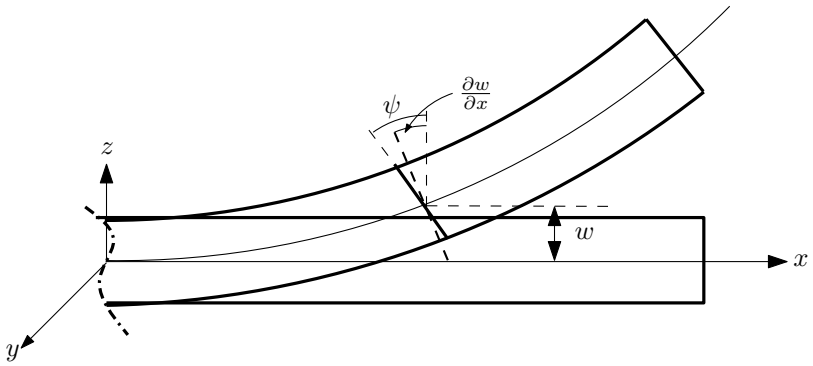

Figure 4.6: Sketch of the transverse kinematics of a linear Timoshenko beam

Let $(x, \eta(x,t))$ be a point on the substrate parametrized by x, see Fig. 4.5. The coupling between the body and the substrate is exerted by a distributed system of elastic elements (see the scheme in Fig. 4.5) that is modelled as an elastic foundation. The coupling elements are intended to be part of the moving robot, as they mimic the function of millipedes legs. We consider a two parameters elastic foundation models [11]; in the context of Timoshenko beam theory, the reaction of the coupling soft elastic system

is expressed by distributed forces and couples, that are constitutively related to the kinematic variables by

$$p_u(x,t) = -\kappa\,(u(x,t) - x) \tag{4.3a}$$

$$p_w(x,t) = -\kappa\,(w(x,t) - \eta(x,t)) \tag{4.3b}$$

$$p_\psi(x,t) = \kappa_\theta \left(\frac{\partial \psi}{\partial x} - \frac{\partial^2 \eta}{\partial x^2}\right) \tag{4.3c}$$

where κ and κ_θ (respectively with SI physical dimensions $\mathrm{N\,m^{-2}}$ and $\mathrm{N\,m^{-1}}$) quantify the linear and rotational stiffness of the legs, and are the two parameters of the elastic foundation model. By introducing the kinematic constraint $\psi \to \partial w/\partial x$ that characterized the Euler beam, we note that the constitutive relation for p_ψ depends on $\partial^2 w/\partial x^2$ consistently with two parameters foundation models [11]. The constitutive relation for p_w depends on the profile η, and the constitutive relation for p_ψ depends on the profile's curvature $\partial^2\eta/\partial x^2$; therefore within this model the coupling system acts as a distributed system of linear and rotational springs with bending moment interactions. Relations (4.3) do not include the deformability of the substrate, and are therefore valid when the coupling system is much softer than the substrate. Future refinements include the visco-elasticity of the substrate, leading to a three parameters generalized Vlazov-Jones foundation model [9, 10] to describe the interactions between the system and the environment in which it is deployed. We introduce the nondimensional variables

$$\hat{x} = \frac{x}{\ell}, \quad \hat{t} = \frac{t}{\tau}, \quad \hat{u} = \frac{u}{\ell}, \quad \hat{w} = \frac{w}{\ell}$$

where ℓ is the total length of the undeformed body, that by adopting the linearized beam theory equals the length of the deformed body (by neglecting second order terms), and τ is the characteristic time. By defining the characteristic time

$$\tau^2 = \frac{\varrho \ell^2}{kG}$$

we write the governing equations in nondimensional form as

$$\alpha_1 \frac{\partial^2 u}{\partial t^2} + \frac{\alpha_u}{\omega^\star}\frac{\partial u}{\partial t} - \frac{\partial^2 u}{\partial x^2} = 0 \tag{4.4a}$$

$$\frac{\partial^2 w}{\partial t^2} + \frac{\alpha_w}{\omega^\star}\frac{\partial w}{\partial t} - \frac{\partial^2 w}{\partial x^2} + \frac{\partial \psi}{\partial x} + \alpha_3 w = \alpha_3 \eta \tag{4.4b}$$

$$\alpha_1 \frac{\partial^2 \psi}{\partial t^2} + \frac{\alpha_\psi}{\omega^\star}\frac{\partial \psi}{\partial t} - \frac{\partial^2 \psi}{\partial x^2} - \alpha_4 \frac{\partial \psi}{\partial x} - \alpha_1\alpha_2 \left(\frac{\partial w}{\partial x} - \psi\right) = -\alpha_4 \frac{\partial^2 \eta}{\partial x^2} \tag{4.4c}$$

Here we have dropped the hat to indicate nondimensional quantities, we have introduced the nondimensional groups

$$\alpha_1 = \frac{kG}{E}, \quad \alpha_2 = \frac{A\ell^2}{I}, \quad \alpha_3 = \frac{\kappa\ell^2}{kAG}, \quad \alpha_4 = \frac{\kappa_\theta \ell}{EI}, \quad \omega^\star = \bar{\omega}\tau \tag{4.5a}$$

$$\alpha_u = \frac{\bar{c}_u \ell^2}{\pi EA}, \quad \alpha_w = \frac{\bar{c}_w \ell^2}{\pi kAG}, \quad \alpha_\psi = \frac{\bar{c}_\psi \ell^2}{\pi EI} \tag{4.5b}$$

Therefore $\alpha_1\alpha_2$ is a measure of the shear stiffness versus the bending stiffness, α_3 is a measure of the legs' linear stiffness versus the shear stiffness, α_4 measures the leg's bending stiffness with respect to the bending stiffness of the body, and α_u, α_u, and α_ψ are structural damping factors. The profile of the substrate $\eta(x,t)$ acts as a forcing term. Therefore one can use the elastic coupling to reconstruct $\eta(x,t)$ through the shape $w(x,t)$; in this case the device can act as a sensor to detect the time varying shape of the substrate.

The linear planar model presented here is a first approximation valid under the hypothesis that the length of the mechanism is small as compared to the radius of curvature of the substrate η that morphs the system. This model is suitable to capture the planar shape morphing, but it needs to be refined to describe the locomotion mechanics of bio-inspired millipedes. As discussed in [72] locomotion in unstructured terrains is often a combination on undulatory motions of the body coupled with with the synchronized motion of the legs. The coupling between the two mechanisms gives rise to a variety of gaits, that include lateral modes with respect to the planar motion studied in this paper. Experimental results in [72] for locomotion over sand of a multi-link robotic implementation of the combination of body and legs propulsion show that friction coefficients associated with undulatory motions are approximately equal to 0.5, with friction in the normal direction slightly higher than the one in the tangential direction, allowing for a net forward propulsion. Moreover, the maximum forces developed in the legs to sustain the centipede-mode motion are of the order of 10 N. This experimental data gives important indication in our current developments that include coupled forward locomotion and shape morphing, as it demonstrates the feasibility of centipede and millipede inspired propulsion, with values for friction and forces that set important constraints in the choice of materials and structures for the coupling mechanism.

4.5 Reduced Order Model

We obtain a reduced order model for the flexural and rotational motions by considering the Galerkin projections of fields w and ψ on suitable bases. By separation of variables, the displacement and rotation fields are expressed as

$$w(x,t) = \bar{\mathbf{w}}^{\mathsf{T}}(x)\mathbf{a}(t) \tag{4.6a}$$

$$\psi(x,t) = \bar{\boldsymbol{\psi}}^{\mathsf{T}}(x)\mathbf{b}(t) \tag{4.6b}$$

where $\bar{\mathbf{w}} = (\bar{w}_1 \cdots \bar{w}_n)^{\mathsf{T}}$ and $\bar{\boldsymbol{\psi}} = \left(\bar{\psi}_1 \cdots \bar{\psi}_n\right)^{\mathsf{T}}$ are $n-$dimensional sets of spatial basis functions, and $\mathbf{a} = (a_1 \cdots a_n)^{\mathsf{T}}$ and $\mathbf{b} = (b_1 \cdots b_n)^{\mathsf{T}}$ are time dependent vectors of amplitudes. The Galerkin projection technique dictates the substitution of (4.6) into the second and third equations (4.4) and premultiplication by the sets of test functions $\bar{\mathbf{w}}$ and $\bar{\boldsymbol{\psi}}$, respectively. Integration of the domain of the projected governing equations and integration by parts give

$$\begin{aligned}
\int_0^1 \bar{\mathbf{w}}\left(\bar{\mathbf{w}}^{\mathsf{T}}\ddot{\mathbf{a}} + \frac{\alpha_w}{\omega^\star}\bar{\mathbf{w}}^{\mathsf{T}}\dot{\mathbf{a}} + \alpha_3\bar{\mathbf{w}}^{\mathsf{T}}\mathbf{a}\right)\mathrm{d}x - \int_0^1 \frac{\mathrm{d}\bar{\mathbf{w}}}{\mathrm{d}x}\bar{\boldsymbol{\psi}}^{\mathsf{T}}\mathbf{b}\mathrm{d}x + \int_0^1 \frac{\mathrm{d}\bar{\mathbf{w}}}{\mathrm{d}x}\frac{\mathrm{d}\bar{\mathbf{w}}^{\mathsf{T}}}{\mathrm{d}x}\mathbf{a}\mathrm{d}x \\
- \bar{\mathbf{w}}\left(\frac{\mathrm{d}\bar{\mathbf{w}}^{\mathsf{T}}}{\mathrm{d}x}\mathbf{a} - \bar{\boldsymbol{\psi}}^{\mathsf{T}}\mathbf{b}\right)\Bigg|_0^1 = \int_0^1 \alpha_3\bar{\mathbf{w}}\eta\mathrm{d}x \\
\int_0^1 \bar{\boldsymbol{\psi}}\left(\bar{\boldsymbol{\psi}}^{\mathsf{T}}\ddot{\mathbf{b}} + \frac{\alpha_\psi}{\omega^\star}\bar{\boldsymbol{\psi}}^{\mathsf{T}}\dot{\mathbf{b}} - \alpha_1\alpha_2\left(\frac{\mathrm{d}\bar{\mathbf{w}}^{\mathsf{T}}}{\mathrm{d}x}\mathbf{a} - \bar{\boldsymbol{\psi}}^{\mathsf{T}}\mathbf{b}\right) - \alpha_4\frac{\mathrm{d}\bar{\boldsymbol{\psi}}^{\mathsf{T}}}{\mathrm{d}x}\mathbf{b}\right)\mathrm{d}x \\
+ \int_0^1 \frac{\mathrm{d}\bar{\boldsymbol{\psi}}}{\mathrm{d}x}\frac{\mathrm{d}\boldsymbol{\psi}^{\mathsf{T}}}{\mathrm{d}x}\mathbf{b}\mathrm{d}x - \bar{\boldsymbol{\psi}}\frac{\mathrm{d}\bar{\boldsymbol{\psi}}^{\mathsf{T}}}{\mathrm{d}x}\mathbf{b}\Bigg|_0^1 = -\int_0^1 \alpha_4\bar{\boldsymbol{\psi}}\frac{\partial^2\eta}{\partial x^2}\mathrm{d}x
\end{aligned}$$

By imposing the projected free end boundary conditions

$$\begin{aligned}
V(0) = V(1) = 0 \Rightarrow \frac{\mathrm{d}\mathbf{w}^{\mathsf{T}}}{\mathrm{d}x}(0)\mathbf{a}(t) - \boldsymbol{\psi}^{\mathsf{T}}(0)\mathbf{b}(t) = \frac{\mathrm{d}\mathbf{w}^{\mathsf{T}}}{\mathrm{d}x}(1)\mathbf{a}(t) - \boldsymbol{\psi}^{\mathsf{T}}(1)\mathbf{b}(t) = 0 \\
M(0) = M(1) = 0 \Rightarrow \frac{\mathrm{d}\boldsymbol{\psi}^{\mathsf{T}}}{\mathrm{d}x}(0)\mathbf{b}(t) = \frac{\mathrm{d}\boldsymbol{\psi}^{\mathsf{T}}}{\mathrm{d}x}(1)\mathbf{b}(t)
\end{aligned}$$

and by introducing the $n \times n$ matrices

$$\mathbf{M}_1 = \int_0^1 \bar{\mathbf{w}}\bar{\mathbf{w}}^{\mathsf{T}}\mathrm{d}x, \quad \mathbf{M}_2 = \int_0^1 \bar{\boldsymbol{\psi}}\bar{\boldsymbol{\psi}}^{\mathsf{T}}\mathrm{d}x \tag{4.7a}$$

$$\mathbf{K}_1 = \int_0^1 \frac{\mathrm{d}\bar{\mathbf{w}}}{\mathrm{d}x}\frac{\mathrm{d}\bar{\mathbf{w}}^{\mathsf{T}}}{\mathrm{d}x}\mathrm{d}x, \quad \mathbf{K}_2 = \int_0^1 \frac{\mathrm{d}\bar{\boldsymbol{\psi}}}{\mathrm{d}x}\frac{\mathrm{d}\bar{\boldsymbol{\psi}}^{\mathsf{T}}}{\mathrm{d}x}\mathrm{d}x \quad \mathbf{K}_3 = \int_0^1 \bar{\boldsymbol{\psi}}\frac{\mathrm{d}\bar{\boldsymbol{\psi}}^{\mathsf{T}}}{\mathrm{d}x}\mathrm{d}x \tag{4.7b}$$

$$\mathbf{K}_c = \int_0^1 \frac{\mathrm{d}\bar{\mathbf{w}}}{\mathrm{d}x}\bar{\boldsymbol{\psi}}^{\mathsf{T}}\mathrm{d}x, \quad \mathbf{F}_w(t) = \int_0^1 \bar{\mathbf{w}}\eta\mathrm{d}x, \quad \mathbf{F}_\psi(t) = \int_0^1 \bar{\boldsymbol{\psi}}\frac{\partial^2\eta}{\partial x^2}\mathrm{d}x \tag{4.7c}$$

we obtain the reduced order model in the form of the following coupled ordinary differential equations for the amplitudes $\mathbf{a}(t)$ and $\mathbf{b}(t)$

$$\mathbf{M}_1\frac{\mathrm{d}^2\mathbf{a}}{\mathrm{d}t^2}(t)+\frac{\alpha_w}{\omega^\star}\mathbf{M}_1\dot{\mathbf{a}}+(\mathbf{K}_1+\alpha_3\mathbf{M}_1)\mathbf{a}(t)-\mathbf{K}_c\mathbf{b}(t)=\alpha_3\mathbf{F}_w(t) \tag{4.8a}$$

$$\alpha_1\mathbf{M}_2\frac{\mathrm{d}^2\mathbf{b}}{\mathrm{d}t^2}(t)+\frac{\alpha_\psi}{\omega^\star}\mathbf{M}_2\dot{\mathbf{b}}+(\mathbf{K}_2+\alpha_1\alpha_2\mathbf{M}_2-\alpha_4\mathbf{K}_3)\mathbf{b}(t)$$
$$-\alpha_1\alpha_2\mathbf{K}_c^{\mathsf{T}}\mathbf{a}(t)=-\alpha_4\mathbf{F}_\psi(t) \tag{4.8b}$$

By introducing the state vector $\mathbf{q}=(\mathbf{a},\mathbf{b})$ and the block matrix operators

$$\mathbf{M}=\mathrm{diag}(\mathbf{M}_1,\mathbf{M}_2),\quad \mathbf{K}_\mathrm{D}=\frac{1}{\omega^\star}\mathrm{diag}(\alpha_w,\alpha_\psi)\otimes\mathbf{I}_n, \tag{4.9a}$$

$$\mathbf{K}=\begin{pmatrix}\mathbf{K}_1 & -\mathbf{K}_c\\ -\alpha_1\alpha_2\mathbf{K}_c & \mathbf{K}_2+\alpha_1\alpha_2\mathbf{M}_2\end{pmatrix},\quad \mathbf{K}_\mathrm{P}=\mathrm{diag}(\alpha_3,\alpha_4)\otimes\mathbf{I}_n, \tag{4.9b}$$

$$\bar{\mathbf{K}}=\mathrm{diag}(\mathbf{M}_1,-\mathbf{K}_3),\quad \mathbf{F}=\begin{pmatrix}\mathbf{F}_w\\ -\mathbf{F}_\psi\end{pmatrix} \tag{4.9c}$$

we rewrite the reduced order system as

$$\mathbf{M}\ddot{\mathbf{q}}+\mathbf{K}_\mathrm{D}\mathbf{M}\dot{\mathbf{q}}+\mathbf{K}\mathbf{q}=\mathbf{K}_\mathrm{P}\left(\mathbf{F}-\bar{\mathbf{K}}\mathbf{q}\right) \tag{4.10}$$

In eq. (4.9), $\mathbf{I}_n$ is the n-dimensional identity matrix and $\otimes$ is the Kronecker product [87] that maps the $d_1\times d_2$ matrix $\mathbf{A}$ and $d_3\times d_4$ matrix $\mathbf{B}$ into the $d_1d_2\times d_3d_4$ matrix $\mathbf{A}\otimes\mathbf{B}$ given by

$$\mathbf{A}\otimes\mathbf{B}:=\begin{pmatrix}A_{11}\mathbf{B} & A_{12}\mathbf{B} & \cdots & A_{1d_2}\mathbf{B}\\ A_{21}\mathbf{B} & A_{22}\mathbf{B} & \cdots & A_{2d_2}\mathbf{B}\\ \vdots & \vdots & \ddots & \vdots\\ A_{d_11}\mathbf{B} & A_{d_12}\mathbf{B} & \cdots & A_{d_1d_2}\mathbf{B}\end{pmatrix}$$

A suitable interpretation of (4.10) in the framework of closed loop control systems is given in Section 4.6.

4.5.1 Basis functions for the reduced order model

Here we set the basis functions for the reduced order model to be the linear eigenfunctions of a Timoshenko beam. In order to obtain the natural frequencies and associated eigenfunctions we follow the approach in [88], which is based on the solution of a vector

eigenvalues problem for the system of two coupled second order differential equations for the transverse displacement and for the the rotation of the cross section. In our case, the two equations are (4.4b) and (4.4c) with damping and forcing terms set to zero. The consideration of two separate evolution equations for w and ψ allows to enforce boundary conditions for free ends in a direct way. A different approach based on the derivation of one fourth order governing equation obtained by combining (4.4) is presented in the original work of Timoshenko [81]; however in this case the application of boundary conditions requires special attention [89].

To determine the eigenvalues, we follow the general procedure that consists on the time-space separation of variables followed by substitution in the homogeneous governing equations. The general solution of the second and third equations (4.4) with $\alpha_3 = \alpha_4 = 0$ (no forcing terms and no coupling with the substrate) is therefore assumed to be of the form

$$\begin{pmatrix} w(x,t) & \psi(x,t) \end{pmatrix}^{\mathsf{T}} = \exp(\mathrm{i}\omega t) \begin{pmatrix} W(x) & \Psi(x) \end{pmatrix}^{\mathsf{T}}$$

where ω is the frequency of oscillation, $i = \sqrt{-1}$ is the imaginary unit, and $W(x)$, $\Psi(x)$ are functions in $[0, 1]$ that express the dependency on x. By substituting into the second and third equations (4.4) with $\alpha_3 = \alpha_4 = 0$ and by separating the variables we obtain the spatial eigenvalue problem

$$\begin{aligned} \frac{\mathrm{d}^2 W}{\mathrm{d}x^2} + \omega^2 W - \frac{\mathrm{d}\Psi}{\mathrm{d}x} &= 0 \\ \frac{\mathrm{d}^2 \Psi}{\mathrm{d}x^2} + \alpha_1 \left(\omega^2 - \alpha_2\right) \Psi + \alpha_1 \alpha_2 \frac{\mathrm{d}W}{\mathrm{d}x} &= 0 \end{aligned}$$

The free ends boundary conditions dictated by the constitutive equations (4.2) are

$$\begin{aligned} \frac{\mathrm{d}\Psi}{\mathrm{d}x}(0) = \frac{\mathrm{d}\Psi}{\mathrm{d}x}(1) &= 0 \\ \frac{\mathrm{d}W}{\mathrm{d}x}(0) - \Psi(0) = \frac{\mathrm{d}W}{\mathrm{d}x}(1) - \Psi(1) &= 0 \end{aligned}$$

The general solution of the eigenvalues problem is sought by considering the vector evaluated function $\exp(\lambda x) \begin{pmatrix} \bar{W} & \bar{\Psi} \end{pmatrix}^{\mathsf{T}}$, where $\bar{W}$ and $\bar{\Psi}$ are constants. Such function is a solution for some positive constant λ if and only if

$$\begin{pmatrix} \lambda^2 + \beta_1 & -\lambda \\ \beta_3 \lambda & \lambda^2 + \beta_2 \end{pmatrix} \begin{pmatrix} \bar{W} \\ \bar{\Psi} \end{pmatrix} = \begin{pmatrix} 0 \\ 0 \end{pmatrix}$$

with nondimensional parameters β_i defined by

$$\beta_1 = \omega^2, \quad \beta_2 = \alpha_1\left(\omega^2 - \alpha_2\right), \quad \beta_3 = \alpha_1\alpha_2$$

The roots λ^2 of the characteristic polynomial $\lambda^4 + (\beta_1 + \beta_2 + \beta_3)\lambda^2 + \beta_1\beta_2 = 0$ are

$$\lambda_{1,2}^2 = -\frac{1}{2}\left(\beta_1 + \beta_2 + \beta_3\right)\left(1 \pm \sqrt{\Delta}\right)$$
$$\Delta = 1 - \frac{4\beta_1\beta_2}{\left(\beta_1 + \beta_2 + \beta_3\right)^2}$$

In order for λ^2 to be real it must be $\Delta > 0$, which is satisfied for $\beta_1\beta_2 < \gamma^2/4$, where $\gamma = \beta_1 + \beta_2 + \beta_3$. The special case $\lambda^2 = 0$ occurs when $\Delta = 1$, that is $\beta_1\beta_2 = 0$ or

$$\beta_1 = 0 \Rightarrow \omega^2 = 0,$$
$$\beta_2 = 0 \Rightarrow \omega^2 = \alpha_2 \text{ or } \alpha_1 = 0$$

This corresponds to rigid body motions of the system [88].

The condition $\Delta > 0$ dictates $\omega > 0$; therefore it must be $\gamma > 0$ since this is the case when γ is evaluated for $\omega > 0$. For $\Delta > 0$ and $\gamma > 0$ we have

$$\lambda_1 = \pm i\theta, \quad \theta^2 = \frac{\gamma}{2}\left(\sqrt{\Delta} + 1\right)$$

Moreover the condition $\Delta > 0$ implies

$$\beta_1\beta_2 = \alpha_1\omega^2\left(\omega^2 - \alpha_2\right)\begin{cases} < 0 & \text{for } \omega^2 < \alpha_2 \\ > 0 & \text{for } \omega^2 > \alpha_2 \end{cases}$$

For $\beta_1\beta_2 < 0$ we have $\sqrt{\Delta} > 1$ and

$$\lambda_2 = \pm\mu, \quad \mu^2 = \frac{\gamma}{2}\left(\sqrt{\Delta} - 1\right)$$

For this case the general solution is therefore given by [88]

$$\Phi(x) = C_1\begin{pmatrix} \sin\theta x \\ -\frac{\beta_1-\theta^2}{\theta}\cos\theta x \end{pmatrix} + C_2\begin{pmatrix} \cos\theta x \\ \frac{\beta_1-\theta^2}{\theta}\sin\theta x \end{pmatrix}$$
$$+C_3\begin{pmatrix} \sinh\mu x \\ \frac{\beta_1+\mu^2}{\mu}\cosh\mu x \end{pmatrix} + C_4\begin{pmatrix} \cosh\mu x \\ \frac{\beta_1+\mu^2}{\mu}\sinh\mu x \end{pmatrix}$$

Imposing the free end boundary conditions at $x = 0$ we obtain

$$C_1 = C_3\frac{\theta}{\mu}$$
$$C_2 = -C_4\frac{\beta_1 + \mu^2}{\beta_1 - \theta^2}$$

By imposing the free end boundary conditions at $x = 1$ we obtain the following linear algebraic relations involving C_3 and C_4

$$\mathbf{A}\begin{pmatrix} C_3 \\ C_4 \end{pmatrix} = \begin{pmatrix} 0 \\ 0 \end{pmatrix}$$

with coefficients matrix $\mathbf{A}$ given by

$$\mathbf{A} = \begin{pmatrix} \frac{\theta}{\mu}\left(\beta_1 - \theta^2\right)\sin\theta + \left(\beta_1 + \mu^2\right)\sinh\mu & \left(\beta_1 + \mu^2\right)\left(\cosh\mu - \cos\theta\right) \\ -\frac{\beta_1}{\mu}\cosh\mu & -\frac{\beta_1}{\mu}\sinh\mu \end{pmatrix}$$

The nontrivial solutions of the system are obtained by investigating the condition for rank deficiency of the coefficients matrix, which translates to the determinant being zero

$$-\cos\theta\cosh\mu + \frac{\theta(\theta^2 - \beta_1)}{\mu(\mu^2 + \beta_1)}\sin\theta\sinh\mu + 1 = 0 \tag{4.11}$$

All parameters in the characteristic equation depend on ω and on the material and geometric parameters of the system. Therefore, once the material and the geometry are defined the characteristic equation is a nonlinear function of ω only.

The first seven roots of the characteristic equation that determine the corresponding modes are given in Table 4.1. The roots are computed for $\alpha_1 = 0.1$ (shear modulus ten times smaller than the Young's modulus) and $\alpha_1\alpha_2 = 100$ (shear stiffness $kGA\ell^2$ to one hundred times larger than the bending stiffness EI). The mode shapes are normalized with respect to the maximum amplitude. The plots of the first three modes W and Ψ normalized with respect to the maximum value are given in Figure 4.7. Here we consider α_2 large enough so that all modes included as basis functions have eigenfrequency ω_n satisfying $\omega_n^2 < \alpha_2$; therefore we do not consider the general solution for $\omega^2 > \alpha_2$ for which $\sqrt{\Delta} < 1$ and $\lambda_2 = \pm i\bar{\mu}$, with $\bar{\mu}^2 = -\mu^2$.

Table 4.1: First seven roots of the characteristic equation (4.11) with nondimensional material parameters $\alpha_1 = 0.1$ and $\alpha_2 = 1000$

n	1	2	3	4	5	6	7
ω	2.07	4.96	8.32	11.8	15.3	18.7	22.0

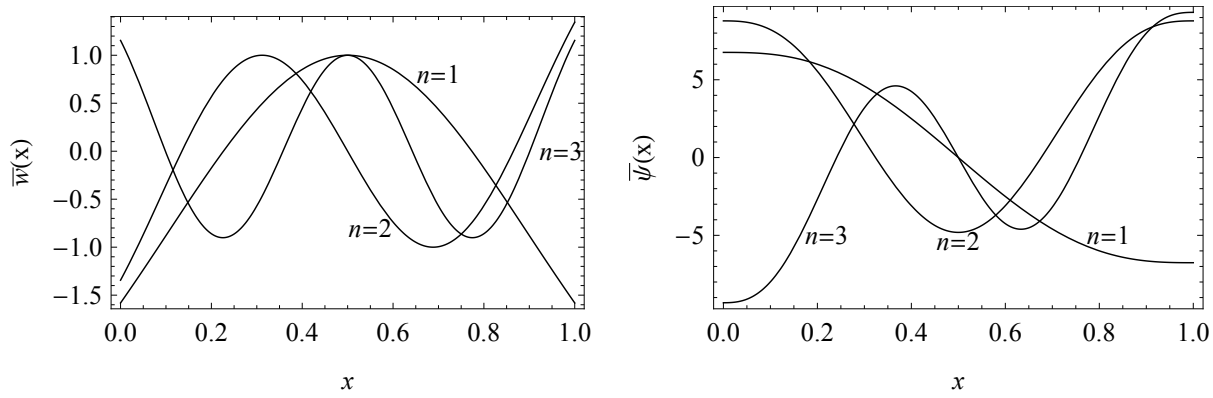

Figure 4.7: First three flexural (a) and rotational (b) modes, normalized with respect to the maximum value along the beam's span.

4.6 Formulation of the Tracking Control Problem

The reduced order model (4.8) is a system of ordinary differential equations that can be suitably interpreted in a control framework to formulate the problem of tracking a desired trajectory η with curvature $\partial^2\eta/\partial x^2$, with deformed shape described by the field w and curvature given by $\partial\psi/\partial x$. We consider homogeneous initial conditions; since the system is time-invariant (constant coefficients) we represent it in the Laplace domain by transforming the quantities in (4.10). By indicating the transformed variables with the same symbols we obtain

$$\left(s^2\mathbf{M} + \mathbf{K}\right)\mathbf{q}(s) = \mathbf{U}(s) \tag{4.12a}$$

$$\mathbf{U}(s) = -s\mathbf{K}_{\mathrm{D}}\mathbf{M}\mathbf{q}(s) + \mathbf{K}_{\mathrm{P}}\boldsymbol{\epsilon}(s) \tag{4.12b}$$

$$\boldsymbol{\epsilon} = \mathbf{F} - \bar{\mathbf{K}}\mathbf{q} \tag{4.12c}$$

where s is the Laplace variable, $\mathbf{U}$ is the control input determined by a Proportional + Derivative (PD) feedback law in which material parameters α_3 and α_4 that characterize the elasticity of the supporting layer (elastic foundation) are tunable proportional gains, and the structural damping parameters α_w and α_ψ are derivative control gains (see the definitions of $\mathbf{K}_{\mathrm{P}}$ and $\mathbf{K}_{\mathrm{D}}$ in (4.9)). The term $\boldsymbol{\epsilon}$ is the error within the reduced order system, with $\mathbf{F}$ representing the desired trajectory through the dependency on the profile η, see (4.9). Note that if the structural damping is constitutively assigned rather than being a tunable derivative gain, the feed-forward transfer function in (4.12)

becomes $(s^2\mathbf{M} + s\mathbf{K}_\mathrm{D}\mathbf{M} + \mathbf{K})^{-1}$, and the feedback $\mathbf{U}$ would be purely proportional. The closed loop transfer function of the system would however be the same, with different interpretation of the dissipation term.

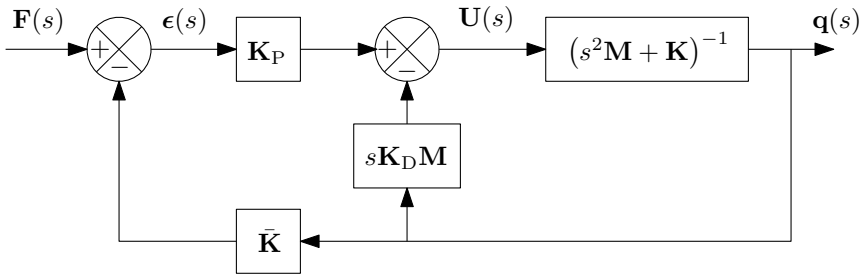

Figure 4.8: Block diagram for the system in (4.12).

The block diagram of (4.12) is shown in Figure 4.8.

4.7 Results and Discussions

We consider the body to be made of a material with shear modulus ten times smaller than the Young's modulus, and therefore $\alpha_1 = 0.1$; moreover, we consider the overall shear stiffness $kGA\ell^2$ to be one hundred times larger than the bending stiffness EI, and therefore $\alpha_1\alpha_2 = 100$, see definitions (4.5) (note that this is consistent with parameters adopted to compute the basis functions). Simulations do not require the specification of the scaling time τ; however, the choice of this parameter dictates the density and the length of the device once the shear modulus is given. Matrices for the reduced order model in equation (4.7) are computed by normalizing the modes with respect to the maximum value, so that the amplitudes $\mathbf{a}$ and $\mathbf{b}$ would represent the actual displacement with no necessity of rescaling. Simulation scenarios are always set with the undeformed shape to be parallel to the tangent of the substrate profile at the nearest point. This is consistent with the focus of the work on the shape adaptation to the substrate nonzero curvature around a given rigid body placement. Ongoing work includes the coupling of the shape tracking to the forward locomotion described for example by a rigid body placement.

Deflection field basis functions $\bar{w}_i(x)$ are even with respect to $x-1/2$ for $i = 1, 3, 5, \ldots$, and odd with respect to $x - 1/2$ for $i = 2, 4, 6, \ldots$, see Figure 4.7(a); on the other hand, the rotation spatial basis functions $\bar{\psi}_i$ are even with respect to $x - 1/2$ for $i = 2, 4, 6, \ldots$

and are odd with respect to $x - 1/2$ for $i = 1, 3, 5, \ldots$. This implies that entries ij in matrices $\mathbf{M}_1$, $\mathbf{M}_2$, $\mathbf{K}_1$, $\mathbf{K}_2$, and $\mathbf{K}_c$ are zero when $i + j$ is odd, whereas entries ij in matrix $\mathbf{K}_3$ are zero when $i+j$ is even, see (4.7). Therefore, in order to track the curvature $\partial^2\eta/\partial x^2$ we need $n \geq 2$, since for $n = 1$ the only entry of $\mathbf{K}_3$ is zero and therefore the position feedback $\mathbf{K}_3\mathbf{b}$ would be zero as well, implying that the second equation in (4.8) would be open loop. Unless otherwise stated, results below are therefore computed for $n = 2$.

The substrate shape tracking problem is first illustrated by considering the time-invariant shape

$$\eta(x) = 0.1\left(x^2 - x\right), \quad x \in [0, 1]$$

With this simulation we want to reproduce the scenario of the mechanism being deployed in a smooth valley, adapting the shape to follow the curved profile of the substrate. Since η is time invariant we have $\mathbf{F}_w = (-6.01 \times 10^{-3}, 0)$ and $\mathbf{F}_\psi = (0, 0.55)$, and therefore the reference input to the closed loop system is a step. For the static analysis the non-dimensional frequency $\omega^\star$ for the equivalent viscous coefficients is set equal to the fundamental frequency ω_1 (Table 4.1), based on the geometric assumption that the length of the mechanism is much smaller of the radius of curvature of the substrate, which implies that the fundamental mode is the most relevant one in describing the shape morphing with respect to η[1]. Typical values for the nondimensional structural damping factors (loss factors) related to commonly used materials can be found in the book [90, Chapter 2], as they are reported to range between 10^{-5} (pure aluminum) and 1 (hard rubber). We simulate one case in which α_w and α_ψ are chosen within this range, and one case in which they are set to larger values to demonstrate the effect of increasing damping. Different values are possible if the parameters are treated as tunable derivative gains.

For $\alpha_w = \alpha_\phi = 10$, results in Tables 4.2 and 4.3 show respectively the steady state values (calculated at $t = 50$) of the tracking errors $\|\boldsymbol{\epsilon}\|_w = \|\mathbf{F}_w - \mathbf{M}_1\mathbf{a}(t)\|$ and $\|\boldsymbol{\epsilon}\|_\psi = \|\mathbf{F}_\psi - \mathbf{K}_3\mathbf{b}(t)\|$ for different values of proportional gains α_3 and α_4, that are the parameters of the elastic foundation model associated with displacement and curvature tracking, respectively. The increased accuracy with increasing relative linear (α_3) and rotational (α_4) stiffness of the legs (relative with respect to the transverse and bending stiffness of the body, see (4.5)) clearly shows. We remark that for $\alpha_4 = 0$ the model for the distributed coupling system converges to Winkler foundation, see Eq. (4.3) and related

[1]This is a crude estimation since the structural damping is associated to cyclic loading [83].

discussion. For small proportional gain the steady-state error increases, as shown in Figure 4.9, where the tracking errors $\|\boldsymbol{\epsilon}\|_w = \|\mathbf{F}_w - \mathbf{M}_1\mathbf{a}(t)\|$ and $\|\boldsymbol{\epsilon}\|_\psi = \|\mathbf{F}_\psi - \mathbf{K}_3\mathbf{b}(t)\|$ are respectively plotted for the combinations of proportional gains corresponding to the first row and last column of Tables 4.2 and 4.3.

Table 4.2: Influence of the proportional gains on the steady state values of the tracking error $\|\boldsymbol{\epsilon}\|_w = \|\mathbf{F}_w - \mathbf{M}_1\mathbf{a}(t)\|$, for $\alpha_w = \alpha_\psi = 10$

α_4 \ α_3	1	10	100
0	4.91×10^{-3}	1.85×10^{-3}	0.25×10^{-3}
20	5.95×10^{-3}	2.33×10^{-3}	0.84×10^{-3}
50	4.47×10^{-3}	2.68×10^{-3}	1.53×10^{-3}

Table 4.3: Influence of the proportional gains on the steady state values of the tracking error $\|\boldsymbol{\epsilon}\|_\psi = \|\mathbf{F}_\psi - \mathbf{K}_3\mathbf{b}(t)\|$, for $\alpha_w = \alpha_\psi = 10$

α_4 \ α_3	1	10	100
0	34.2×10^{-2}	23.7×10^{-2}	54.1×10^{-2}
20	37.2×10^{-2}	16.2×10^{-2}	49.8×10^{-2}
50	11.3×10^{-2}	6.4×10^{-2}	37.5×10^{-2}

Deformed shapes along with the profile of the substrate are shown in Figure 4.10(a) for $\alpha_3 = (1, 10, 100)$ and $\alpha_4 = 0$, and in Figure 4.10(b) for $\alpha_3 = 100$ and $\alpha_4 = (0, 20, 50)$, and the same values for the nondimensional structural damping coefficients. With increasing proportional gain α_3 and relatively low α_4 the accuracy of the shape tracking increases and the deformed shape becomes a good indication of the substrate by reproducing the profile η accurately; however, for higher values of α_4 (mebrane stretching effect of the foundation becomes prominent) the model predictions of the deformed shape looses accuracy. The analogous set of results shown in Figure 4.9 is shown in Figure 4.11 for different damping parameters, namely $\alpha_w = \alpha_\psi = 3$. For smaller values of the structural damping attenuation factors numerical simulation are unstable for $\alpha_4 = 50$. From Figure 4.11 it is clear the transition from overdamped to underdamped response due to lower damping coefficient.

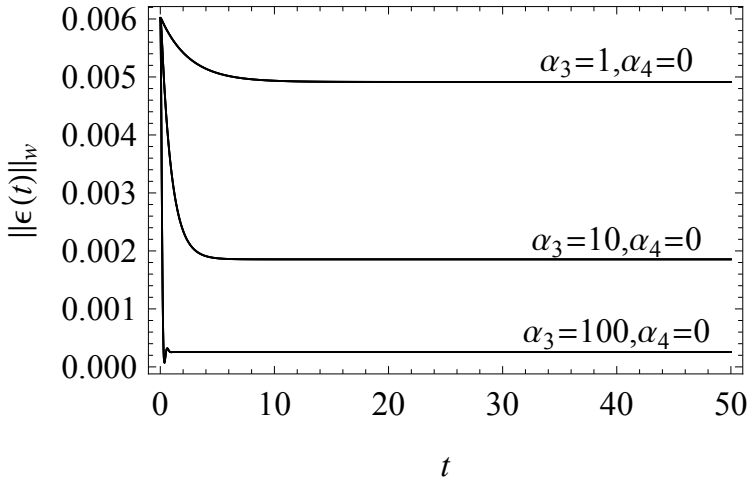

(a)

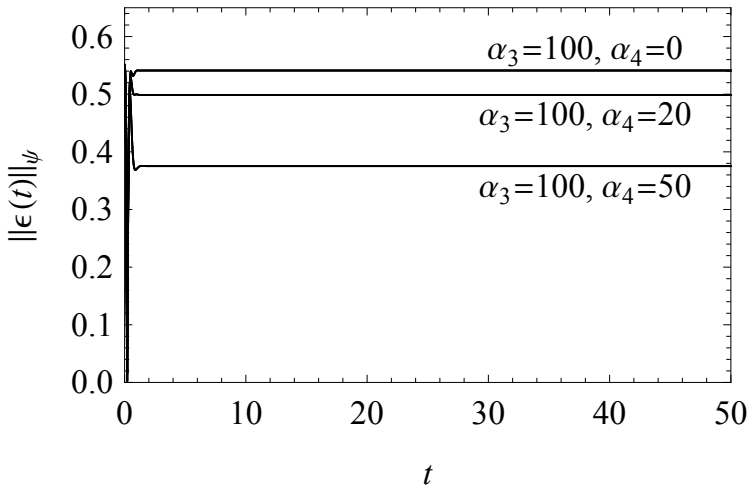

(b)

Figure 4.9: Tracking errors (a) $\|\boldsymbol{\epsilon}\|_w = \|\mathbf{F}_w - \mathbf{M}_1\mathbf{a}(t)\|$ and (b) $\|\boldsymbol{\epsilon}\|_\psi = \|\mathbf{F}_\psi - \mathbf{K}_3\mathbf{b}(t)\|$ for different values of the proportional gains and $\alpha_w = \alpha_\psi = 10$

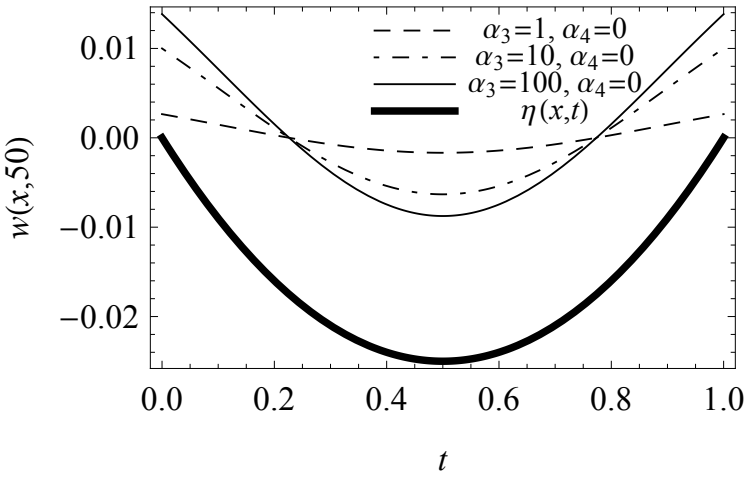

(a)

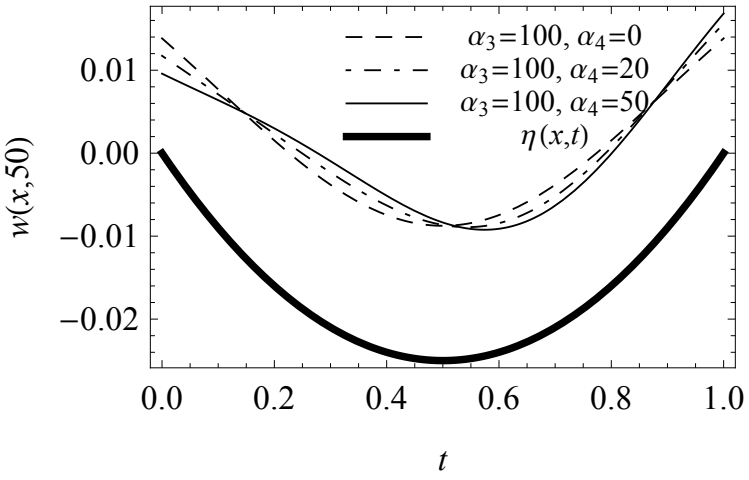

(b)

Figure 4.10: Deformed shapes for different values of the proportional gains along with the profile of the substrate, for $\alpha_w = \alpha_\psi = 10$

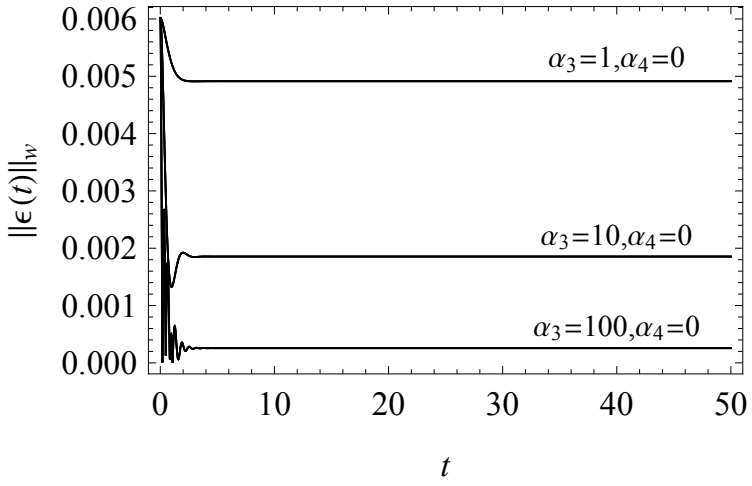

(a)

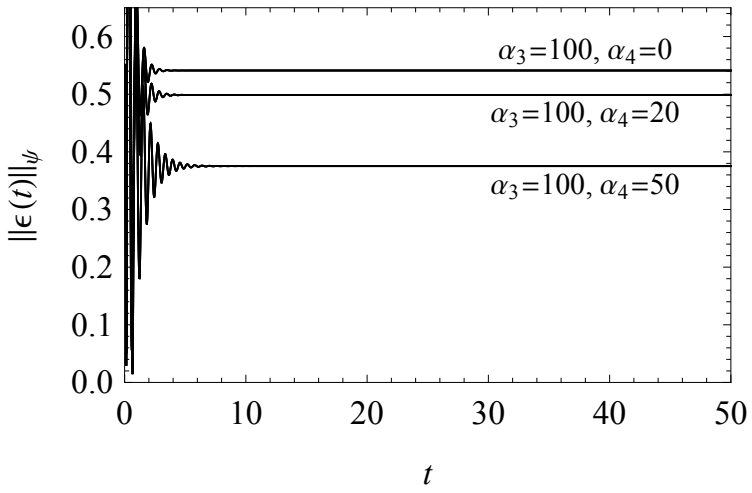

(b)

Figure 4.11: Tracking errors (a) $\|\boldsymbol{\epsilon}\|_w = \|\mathbf{F}_w - \mathbf{M}_1\mathbf{a}(t)\|$ and (b) $\|\boldsymbol{\epsilon}\|_\psi = \|\mathbf{F}_\psi - \mathbf{K}_3\mathbf{b}(t)\|$ for different values of the proportional gains and $\alpha_w = \alpha_\psi = 3$

n	$100\,\|w_n - \eta\|_{L^2}$	$100\,\|w_n - w_{n-2}\|_{H^1}$	$100\,\|\psi_n - \psi_{n-2}\|_{H^1}$
2	1.7	-	-
4	1.7	0.67	3.1
6	1.7	0.34	1.4
8	1.7	0.23	0.6

Table 4.4: L^2 and H^1 error norms (percentage) with increasing number of basis functions to approximate the solution

For the same profile $\eta(x)$, for $\alpha_3 = 100$, $\alpha_4 = 1$, $\alpha_w = \alpha_\psi = 10$ we show in Table 4.4 the L^2 and the H^1 error norms, respectively defined by

$$\|u - v\|_{L^2} := \left(\int_0^1 (u - v)^2 \, \mathrm{d}x \right)^{\frac{1}{2}} \tag{4.13a}$$

$$\|u - v\|_{H^1} := \left(\int_0^1 \left((u - v)^2 + \left(\frac{\partial u}{\partial x} - \frac{\partial v}{\partial x} \right)^2 \right) \mathrm{d}x \right)^{\frac{1}{2}} \tag{4.13b}$$

The L^2 norm measures the discrepancy between the shape η and the deformed axis of the mechanism w_n, where n is the number of basis functions. The H^1 errors are instead calculated between pairs of approximate solutions w_n and w_{n-2} and ψ_n and ψ_{n-2}. Basis functions labeled with even integers do not contribute since η is locally an even function of x, whereas the flexural basis functions with even indexes are odd functions of x. Regarding the rotation ψ the same argument applies except that the basis functions contributing to the solution are odd functions of x. The convergence in the H^1 error norm of the approximated solutions w_n and ψ_n is clear from numerical results in Table 4.4; moreover, the L^2 error norm between w_n and η shows the negligible contribution of higher modes to shape tracking. The deformed shapes obtained with one mode, two modes and three modes are shown in Figure 4.12, with the proximity between the curves confirming that the approximation based on the fundamental modes is accurate to describe the deflection within the class of geometries considered here. However, in order to include the curvature parameter in the elastic foundation model for the legs at least two basis functions need to be included.

As a second illustration we consider the time varying profile

$$\eta(x, t) = 0.1 \left(x^2 - x \right) \sin \frac{t}{2}, \quad x \in [0, 1],\, t \geq 0 \tag{4.14}$$

In this case the loading is cycling and therefore we set $\omega^\star = 1/2$ which is the nondimensional excitation frequency. Results are obtained by projecting along the fundamental

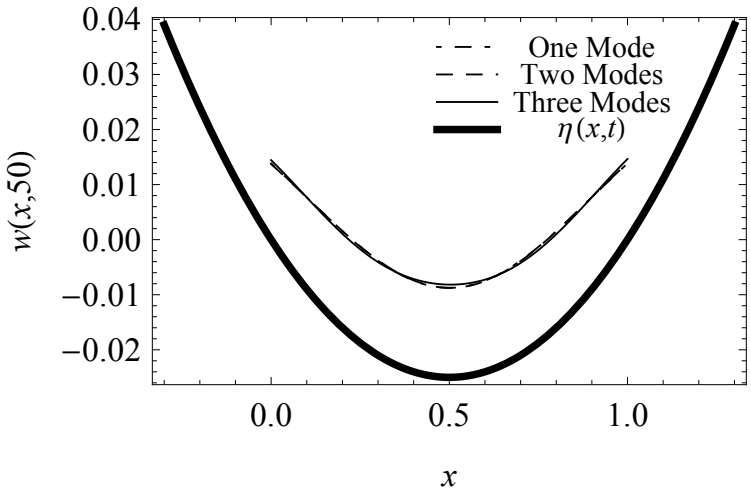

Figure 4.12: Deformed shape obtained with one and with three basis functions to approximate fields w and ψ

modes and for $\alpha_3 = 100$, $\alpha_4 = 1$, $\alpha_w = \alpha_\psi = 10$. As expected the steady-state error is non-zero since the time-varying profile cannot be tracked without a steady offset that depends on the transfer function of the system. The deformed shape at different snapshots is shown in Figure 4.13, from which it is clear that the system adapts to the substrate by tracking the fundamental features that are included in the model.

4.8 Conclusions

In this paper we have presented the model of a continuous slender mechanism that is the first step towards the modeling and design of a hyper-redundant autonomous robot with adaptive body shape. The model describes the coupling with a substrate represented by a smooth curve, with the physical connection between the body and the substrate represented by a distribution of linear compliant elements. The model is inspired by salient features of the spinal locomotion mechanism of centipedes and millipedes, in which the forward motion is achieved by a characteristic motion of the legs, and in which the shape of the body adapts to nonzero curvatures of the substrate by deforming accordingly. The initial-boundary values problem governing the deformation of the body of the mechanism is formulated as a Timoshenko beam on elastic foundation, and the action of the substrate is included as a forcing term on the deflection of the beam. The distributed parameters system is reduced to a time dependent system by projecting the

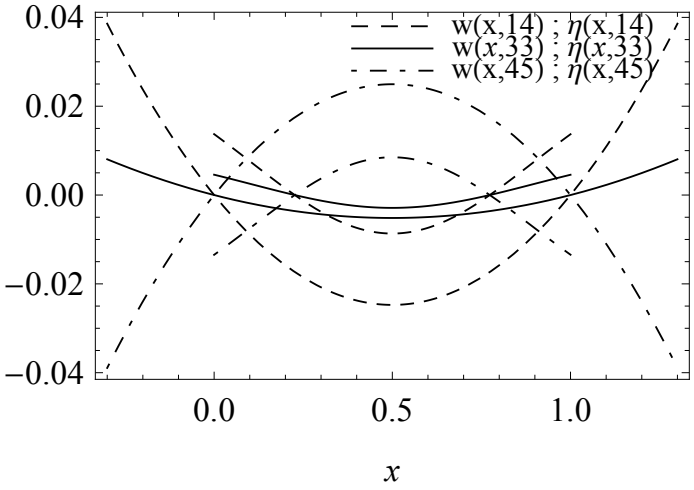

Figure 4.13: Deformed shape at different snapshots for the time-varying profile

spatial part of the deflection and rotation fields onto the linear modal basis functions. The time varying system is conveniently described in closed loop form with desired trajectory related to the shape of the substrate, so that the problem can be formulated as a tracking problem with the deformed shape of the robot morphing to the shape of the substrate.

Tracking results are shown for different values of control gains that represent tunable values of the elastic and dissipative characteristics of the coupling elements. Since the deformation is measured with respect to a locally parallel (to the substrate) undeformed configuration, a single degree of freedom system projected on the first mode shape accurately reproduce the class of substrates that are included within the characterizing assumptions of the model. By modeling the coupling deformable layer as a two parameters elastic foundation, curvature tracking is introduced. Results for a time-varying substrate are also presented, showing good qualitative morphing performance.

The model proposed here is suitable to describe the shape adaptation of slender flexible robotic devices coupled with a substrate that represent a generic environment. The presented linear planar model is valid to describe shape morphing when the length of the body of the elongated mechanism is small as compared to the radius of curvature of the substrate, and three dimensional effects associated with coupling with double curvature or generally unstructured terrains are neglected. The deployment on unstructured terrains could require three dimensional undulatory modes that require the extension of the planar model in this work. If the device is used as a sensor, the deformation can be used as a measure of the shape of an unknown substrate, and therefore to estimate

it. Part of ongoing work is the explicit inclusion of the rigid body motion with tracking of the position and orientation of the substrate to dictate the undeformed configuration of the system with respect to which one measures the deformation; moreover we are investigating the inverse problem to infer material properties of the substrate when it is modeled as elastic foundation.

References

[1] S. C. Dutta, R. Roy, A critical review on idealization and modeling for interaction among soil-foundation-structure system, Computers & Structures 80 (20-21) (2002) 1579–1594. doi:{10.1016/S0045-7949(02)00115-3}.

[2] D. N. Paliwal, S. N. Sinha, Static and dynamic behavior of shallow spherical-shells on Winkler foundation, Thin-Walled Structures 4 (6) (1986) 411–422. doi:{10.1016/0263-8231(86)90038-8}.

[3] M. M. Filonenko-Borodich, Some approximate theories of the elastic foundation, Uchenyie Zapiski Moskovskogo Gosudarstuennogo Universiteta Mechanika (46) (1940) 3–1, (in Russian).

[4] P. L. Pasternak, On a new method of analysis of an elastic foundation by means of two foundation constants, Gosudarsrvennoe Izdatelstvo Literaturi po Stroitelstvu i Arkhitekture(in Russian).

[5] I. Calio, A. Greco, Free vibrations of Timoshenko beam-columns on Pasternak foundations, Journal of Vibration and Control 19 (5) (2013) 686–696. doi:{10.1177/1077546311433609}.

[6] C. R. Briscoe, S. C. Mantell, J. H. Davidson, Buckling of a plate on a Pasternak foundation under uniform in-plane bending loads, International Journal of Structural Stability and Dynamics 13 (3). doi:{10.1142/S0219455412500708}.

[7] R. Jones, J. Xenophontos, The Vlasov foundation model, International Journal of Mechanical Sciences 19 (6) (1977) 317–23.

[8] V. Z. Vlasov, U. Leont'ev, Beams, plates, and shells on elastic foundation, Gosudarst vennoe lzdatel'st vo Ftziko-Matematicheskoi Literatury Moskva.

[9] M. Levinson, Generalized Vlasov-Jones foundation model - a foundation of grade-4, International Journal of Mechanical Sciences 25 (2) (1983) 149–154. doi:{10.1016/0020-7403(83)90007-3}.

[10] A. Shams, M. Porfiri, A generalized Vlasov-Jones foundation model for micromechanics studies of syntactic foams, Composite Structures 103 (2013) 168–178. doi:{10.1016/j.compstruct.2013.04.020}.

[11] F. Zhaohua, D. R. Cook, Beam elements on two-parameter elastic foundation, Journal of Engineering Mechanics 109 (6) (1983) 1390–1402.

[12] D. Avirovik, B. Butenhoff, S. Priya, Millipede-inspired locomotion through novel U-shaped piezoelectric motors, Smart Materials and Structures 23 (3). doi:{10.1088/0964-1726/23/3/037001}.

[13] M. Behl, K. Kratz, U. Noechel, T. Sauter, A. Lendlein, Temperature-memory polymer actuators, Proceedings of the National Academy of Sciences of the United States of America 110 (31) (2013) 12555–12559. doi:{10.1073/pnas.1301895110}.

[14] L. Hines, V. Arabagi, M. Sitti, Shape Memory Polymer-Based Flexure Stiffness Control in a Miniature Flapping-Wing Robot, IEEE Transactions on Robotics 28 (4) (2012) 987–990. doi:{10.1109/TRO.2012.2197313}.

[15] D. L. P. Bopearatchy, G. C. Hatanwala, State space control of a multi link robot manipulator by a translational modelling technique, in: Intelligent Control, 1990. Proceedings., 5th IEEE International Symposium on, 1990, pp. 285–290 vol.1. doi:10.1109/ISIC.1990.128470.

[16] T. Nanayakkara, K. Watanabe, K. Kiguchi, K. Izumi, Controlling multi-link manipulators by fuzzy selection of dynamic models, in: Industrial Electronics Society, 2000. IECON 2000. 26th Annual Confjerence of the IEEE, Vol. 1, 2000, pp. 638–643 vol.1. doi:10.1109/IECON.2000.973224.

[17] M. Moallem, K. Khorasani, R. Patel, An inverse dynamics sliding control technique for flexible multi-link manipulators, in: American Control Conference, 1997. Proceedings of the 1997, Vol. 3, 1997, pp. 1407–1411 vol.3. doi:10.1109/ACC.1997.610658.

[18] J.-X. Xu, Y.-J. Pan, T.-H. Lee, A gain shaped sliding mode control scheme using filtering techniques with applications to multi-link robotic manipulators, in: Proceedings of the American Control Conference, Vol. 6, 2001, pp. 4363–4368 vol.6. doi:10.1109/ACC.2001.945664.

[19] C. Wright, A. Johnson, A. Peck, Z. McCord, A. Naaktgeboren, P. Gianfortoni, M. Gonzalez-Rivero, R. Hatton, H. Choset, Design of a modular snake robot,

Proceedings of The IEEE/RSJ International Conference on Intelligent Robots and Systems 1 (2007) 2609–2614.

[20] M. Tesch, K. Lipkin, I. Brown, R. Hatton, A. Peck, J. Rembisz, , H. Choset, Parameterized and scripted gaits for modular snake robots, journal of advanced Robotics 23 (2009) 1131–1158.

[21] R. L. Hatton, H. Choset, Generating gaits for snake robots by annealed chain fitting and keyframe wave extraction, Proceedings of The IEEE/RSJ International Conference on Intelligent Robots and Systems 1 (2009) 840–845.

[22] F. Boyer, S. Ali, M. Porez, Macrocontinuous dynamics for hyperredundant robots: Application to kinematic locomotion bioinspired by elongated body animals, IEEE Transactions on Robotics 28 (2) (2012) 303–317. doi:10.1109/TRO.2011.2171616.

[23] J. C. Ower, J. Van de Vegte, Classical control design for a flexible manipulator: modeling and control system design, Journal of Robotics and Automation 3 (1987) 485–489.

[24] A. De Luca, B. Siciliano, Closed-form dynamic model of planar multilink lightweight robots, IEEE Transactions on Systems, Man and Cybernetics 21 (1991) 826–839.

[25] P. Tomei, A. v, Approximate modeling of robots having elastic links, IEEE Transactions on Systems, Man and Cybernetics 18 (1988) 831–840.

[26] Y. Chaolan, H. Jiazhen, C. Guoping, Modeling study of a flexible hub-beam system with large motion and with considering the effect of shear deformation, Journal of Sound and Vibration 295 (2006) 282–293.

[27] W. Chen, Dynamic modeling of multi-link flexible robotic manipulators, Journal of Computers and Structures 79 (2001) 183–195.

[28] B.-J. Lee, Geometrical Derivation of Differential Kinematics to Calibrate Model Parameters of Flexible Manipulator, International Journal of Advanced Robotic Systems 10. doi:10.5772/55592.

[29] L. Chen, H. Deng, Model reduction of rigid-flexible manipulators with experimental validation, in: Jiang, ZY and Liu, XH and Jiao, SH and Han, JT (Ed.), Engineering

Solutions for Manufacturing Processes, PTS 1-3, Vol. 655-657 of Advanced Materials Research, 2013, pp. 1101–1107, 3rd International Conference on Advances in Materials Manufacturing (ICAMMP 2012), Beihai, Peoples R China, Dec 22-23, 2012. doi:10.4028/www.scientific.net/AMR.655-657.1101.

[30] H. Esfandiar, S. Daneshmand, Complete dynamic modeling and approximate state space equations of the flexible link manipulator, Journal of Mechanical Science and Technology 26 (9) (2012) 2845–2856. doi:10.1007/s12206-012-0731-x.

[31] C. di Castri, A. Messina, Exact modeling for control of flexible manipulators, Journal of Vibration and Control 18 (10) (2012) 1526–1551. doi:10.1177/1077546311421796.

[32] M. H. Korayem, H. N. Rahimi, A. Nikoobin, Mathematical modeling and trajectory planning of mobile manipulators with flexible links and joints, Applied Mathematical Modelling 36 (7) (2012) 3223–3238. doi:10.1016/j.apm.2011.10.002.

[33] H. H. Lee, New dynamic modeling of flexible-link robots, Journal of Dynamic Systems, Measurement and Control 127 (1956) 307–309.

[34] X. Zhang, W. Xu, S. S. Nair, V. S. Chellaboina, Pde modeling and control of a flexible two-link manipulator, IEEE Transactions on Control Systems Technology 13 (2005) 301–312.

[35] R. I. Milford, S. F. Asokanthan, Configuration dependent eigenfrequencies for a two-link flexible manipulator: experimental verification, Journal of Sound and Vibration 222 (1999) 191–207.

[36] H. Ouyang, D. Richiedei, A. Trevisani, Pole assignment for control of flexible link mechanisms, Journal of Sound and Vibration 332 (12) (2013) 2884–2899. doi:10.1016/j.jsv.2013.01.004.

[37] J. C. P. Reis, J. S. da Costa, Motion planning and actuator specialization in the control of active-flexible link robots, Journal of Sound and Vibration 331 (14) (2012) 3255–3270. doi:10.1016/j.jsv.2012.03.004.

[38] Z.-C. Qiu, J.-D. Han, X.-M. Zhang, Y.-C. Wang, Z.-W. Wu, Active vibration control of a flexible beam using a non-collocated acceleration sensor and piezoelectric patch actuator, Journal of Sound and Vibration 326 (3-5) (2009) 438–455. doi:10.1016/j.jsv.2009.05.034.

[39] Z. J. Jia, Y. D. Song, W. C. Cai, Bio-inspired Approach for Smooth Motion Control of Wheeled Mobile Robots, Cognitive Computation 5 (2) (2013) 252–263. doi:10.1007/s12559-012-9186-8.

[40] H. Mahjoubi, K. Byl, Modeling Synchronous Muscle Function in Insect Flight: a Bio-Inspired Approach to Force Control in Flapping-Wing MAVs, Journal of Intelligent and Robotic Systems 70 (1-4, SI) (2013) 181–202. doi:10.1007/s10846-012-9746-x.

[41] B. Sun, D. Zhu, F. Ding, S. X. Yang, A novel tracking control approach for unmanned underwater vehicles based on bio-inspired neurodynamics, Journal of Marine Science and Technology 18 (1) (2013) 63–74. doi:10.1007/s00773-012-0188-8.

[42] Y. Park, D. Young, B. Chen, R. J. Wood, R. Nagpal, E. C. Goldfield, Networked Bio-Inspired Modules For Sensorimotor Control of Wearable Cyber-Physical Devices, in: 2013 International Conference on Computing, Networking and Communications (ICNC), 2013, San Diego, CA, Jan 28-31, 2013.

[43] J. Zhang, G. Qiao, G. Song, A. Wang, Design and Implementation of a Remote Control System for a Bio-inspired Jumping Robot, International Journal of Advanced Robotic Systems 9. doi:10.5772/51931.

[44] S. Tolu, M. Vanegas, N. R. Luque, J. A. Garrido, E. Ros, Bio-inspired adaptive feedback error learning architecture for motor control, Biological Cybernetics 106 (8-9) (2012) 507–522. doi:10.1007/s00422-012-0515-5.

[45] K. Abdelnour, A. Stinchcombe, M. Porfiri, J. Zhang, S. Childress, Bio-inspired hovering and locomotion via wirelessly powered ionic polymer metal composites, in: Proc. SPIE 7975, Bioinspiration, Biomimetics, and Bioreplication, 2011, pp. 79750R–79750R–9. doi:10.1117/12.881737.
+http://dx.doi.org/10.1117/12.881737

[46] A. Ijspeert, J. Hallam, D. Willshaw, From lampreys to salamanders: evolving neural controllers for swimming and walking, in: Pfeifer, R and Blumberg, B and Meyer, JA and Wilson, SW (Ed.), From Animals to Animats 5, From Animals to Animats Series, 1998, pp. 390–399, 5th International Conference on Simulation of Adaptive Behavior, Uuniversity of Zurich, Zurich, Switzerland, Aug 17-21, 1998.

[47] Z. Shiller, Y. GWO, Dynamic motion planning of autonomous vehicles, IEEE Transactions on Robotics and Automation 7 (2) (1991) 241–249. doi:10.1109/70.75906.

[48] B. Dandrea-Novel, G. Bastin, G. Campion, Modelling and control of non-holonomic wheeled mobile robots, in: 1991 IEEE International Conference on Robotics and Automation, VOLS 1-3, 1991, pp. 1130–1135, 1991 International Conference on Robotics and Automation, Sacramento, CA, Apr 09-11, 1991.

[49] J. Gray, H. Lissmann, Studies in animal locomotion VII. Locomotory reflexes in the earthworm, Journal of Experimental Biology 15 (4) (1938) 506–517.

[50] W. Yapp, Locomotion of Worms, Nature 177 (4509) (1956) 614–615. doi:10.1038/177614a0.

[51] J. Ostrowski, J. Burdick, The geometric mechanics of undulatory robotic locomotion, International Journal of Robotics Research 17 (7) (1998) 683–701. doi:10.1177/027836499801700701.

[52] P. Krishnaprasad, D. Tsakiris, Oscillations, SE(2)-snakes and motion control: a study of the Roller Racer, Dynamical Systems: An International Journal 16 (4) (2001) 347–397. doi:10.1080/14689360110090424.

[53] J. Martins, M. Botto, J. da Costa, A Newton-Euler model of a piezo-actuated nonlinear elastic manipulator link, in: Nunes, U and deAalmeida, AT and Bejczy, AK and Kosuge, K and Macgado, JAT (Ed.), Proceedings of the 11th International Conference on Advanced Robotics 2003, Vol. 1-3, Coimbra, Portugal, Jun 30-Jul 03, 2003, pp. 935–940.

[54] B. Jayne, Kinematics of Terrestrial Snake Locomotion , Copeia (4) (1986) 915–927.

[55] Y. Umetani, S. Hirose, Biomecanical study of serpentine locomotion, Proceedings of the 1st ROMANSY Symp Udine 177 (1974) 171–184.

[56] S. Hirose, Y. Umetani, Kinematic control of an active cord mechanism with tactile sensors, Proceedings of the CISM-ZFToM Symposium on Theory and Practice of Robots and manipulators (1976) 241–252.

[57] S. Hirose, K. Ikuta, M. Tsukamoto, , K. Sato, Considerations in design of the actuator based in the shape memory effect, Proceedings of the 6th IGToMM Congress (1987) 1549–1556.

[58] S. Hirose, Y. Umetani, The kinematics and control of a soft gripper for the handling of living and fragile objects, Proceedings of the IGToMM Congress (1979) 1549–1556.

[59] W. I. Clement, R. M. Inigo, Design of a snake-like manipulator, Journal Robotics and Autonomous Systems. 6 (1990) 265–282.

[60] S. Chiang, C. Crane, J. Duffy, Path planning for an articulated transporter manipulator system, Proc. of the 22nd ASME Mechanisms Conf. 45 (1992) 405–412.

[61] E. I. Verriest, Efficient motion planning for a planar multiple link robot, based on differential friction, Proc. of IEEE Decision and Control Conf. 3 (1989) 2364–2365.

[62] D. Sen, T. S. Mruthyunjays, Studies of a new snake-like manipulator, ASME Conf. Robotics, Spatial Mechanisms, and Mechanical Systems 45 (1992) 423–438.

[63] G. Chirikjian, J. Burdick, Kinematics of hyper-redundant manipulators, Proc. ASME Conf. of Mechanism (1990) 391–396.

[64] J. C. SIMO, A Finite Strain Beam Formulation - The 3-Dimensional Dynamic Problem. Part I: Formulation and Optimal Parametrization, Computer Methids in Applied Mechanics and Engineering 49 (1) (1985) 55–70. doi:{10.1016/0045-7825(85)90050-7}.

[65] J. C. Simo, L. Vu-Quoc, A three-dimensional finite-strain rod model. part II: Computational aspects, Computer Methods in Applied Mechanics and Engineering 58 (1) (1986) 79 – 116. doi:http://dx.doi.org/10.1016/0045-7825(86)90079-4.
http://www.sciencedirect.com/science/article/pii/0045782586900794

[66] E. Cosserat, F. Cosserat, Théorie des corps déformables, Hermann, Paris, 1909.

[67] R. J. Webster, III, J. S. Kim, N. J. Cowan, G. S. Chirikjian, A. M. Okamura, Nonholonomic modeling of needle steering, International Journal of Robotics Research 25 (5-6) (2006) 509–525. doi:{10.1177/0278364906065388}.

[68] D. C. Rucker, B. A. Jones, R. J. Webster, A geometrically exact model for externally loaded concentric-tube continuum robots, Robotics, IEEE Transactions on 26 (5) (2010) 769–780. doi:10.1109/TRO.2010.2062570.

[69] D. Trivedi, A. Lotfi, C. D. Rahn, Geometrically exact models for soft robotic manipulators, IEEE Transactions on Robotics 24 (4) (2008) 773–780. doi:{10.1109/TRO.2008.924923}.

[70] F. Boyer, M. Porez, W. Khalil, Macro-continuous computed torque algorithm for a three-dimensional eel-like robot, IEEE Transactions on Robotics 22 (4) (2006) 763–775. doi:{10.1109/TRO.2006.875492}.

[71] M. Sfakiotakis, D. P. Tsakiris, Undulatory and Pedundulatory Robotic Locomotion via Direct and Retrograde Body Waves, in: ICRA: 2009 IEEE International Conference on Robotics and Automation-ICRA, Vol. 1-7, Kobe, Japan, 2009, pp. 3404–3410.

[72] K. L. Hoffman, R. J. Wood, Passive undulatory gaits enhance walking in a myriapod millirobot, in: 2011 IEEE/RSJ International Conference on Intelligent Robots and Systems, 2011.

[73] R. Janssen, N.-M. Prpic, W. G. M. Damen, A review of the correlation of tergites, sternites, and leg pairs in diplopods, Frontiers in Zoology 3 (2006) 1–10.

[74] J. L. Capinera, Insects and Wildlife: Arthropods and their Relationships with Wild Vertebrate Animals, Wiley-Blackwell, 2010.

[75] J. L. Capinera, Encyclopedia of Entomology, Vol. 4, Springer, 2008.

[76] R. W. Cahn, Biomimetics: Biologically inspired technologies, Nature 444 (7118) (2006) 425–426. doi:10.1038/444425b.

[77] L. Drago, G. Fusco, E. Garollo, A. Minelli, Structural aspects of leg-to-gonopod metamorphosis in male helminthomorph millipedes (Diplopoda), Frontiers in Zoology 8. doi:10.1186/1742-9994-8-19.

[78] M. Golubitsky, I. Stewart, P. Buono, J. Collins, A modular network for legged locomotion, Phisica D 115 (1-2) (1998) 56–72. doi:10.1016/S0167-2789(97)00222-4.

[79] H. Enghpff, Adaptive radiation of the millipede genus Cylindroiulus om Madeira: habitat, body size, and morphology (Diplopoda, Julida: Julidae), Review of ecology and soil biology 20 (3) (1983) 403–415.

[80] B. Borrell, Mechanical properties of calcified exoskeleton from the neotropical millipede, Nyssodesmus python, Journal of Insect Physiology 50 (12) (2004) 1121–1126. doi:{10.1016/j.jinphys.2004.09.012}.

[81] S. Timoshenko, Vibration Problems In Engineering, D. Van Nostrand Company Inc., 1974.

[82] L. D. Landau, E. M. Lifshitz, Theory of Elasticity, Vol. 7 of A Course of Theoretical Physics, Pergamon Press, 1970.

[83] L. Meirovitch, Fundamentals of Vibrations, McGraw-Hill, 2001.

[84] E. Hernandez, D. Kalise, E. Otarola, A locking-free scheme for the LQR control of a Timoshenko beam, Journal of Computational and Applied Mathematics 235 (5) (2011) 1383–1393. doi:{10.1016/j.cam.2010.08.025}.

[85] J. Kauffman, G. Lesieutre, V. Babuska, Damping Models for Shear Beams with Applications to Spacecraft Wiring Harnesses, in: 53rd AIAA/ASME/ASCE/AHS/ASC Structures, Structural Dynamics and Materials Conference, Honolulu, Hawaii, 2012.

[86] Y. Lei, S. Adhikari, M. I. Friswell, Vibration of nonlocal Kelvin-Voigt viscoelastic damped Timoshenko beams, International Journal of Engineering Science 66-67 (2013) 1–13. doi:{10.1016/j.ijengsci.2013.02.004}.

[87] D. S. Bernstein, Matrix Mathematix: Theory, Facts, and Formulas, 2nd Edition, Princeton University Press, 2009.

[88] N. F. J. van Rensburg, A. J. van der Merwe, Natural frequencies and modes of a Timoshenko beam, Wave Motion 44 (1) (2006) 58–69. doi:10.1016/j.wavemoti.2006.06.008.

[89] L. Majkut, Free and forced vibrations of Timoshenko beam described by single differential equation, Journal of Theoretical and Applied Mechanics 47 (1) (2009) 193–210.

[90] C. F. Beards, Structural vibration: Analysis and Damping, Butterworth-Heinemann, 1996.

[91] J. Fattahi and D. Spinello, "A timoshenko beam reduced order model for shape tracking with a slender mechanism," *Journal of Sound and Vibration*, vol. 333, no. 20, pp. 5165 – 5180, 2014.

Chapter 5

Path following and shape morphing with a continuous slender robot

The work in this chapter is published in the Journal of Dynamic Systems, Measurement and Control. [81]

5.1 Abstract

We present the continuous model of a mobile slender mechanism that is intended to be the structure of an autonomous hyper-redundant slender robotic system. Rigid body degrees of freedom and deformability are coupled through a Lagrangian weak formulation that includes control inputs to achieve forward locomotion and shape tracking. The forward locomotion and the shape tracking are associated to the coupling with a substrate that models a generic environment with which the mechanism could interact. The assumption of small deformations around rigid body placements allows to adopt the floating reference kinematic description. By posing the distributed parameter control problem in a weak form we naturally introduce an approximate solution technique based on Galerkin projection on the linear mode shapes of the Timoshenko beam model, that is adopted to describe the body of the robot. Simulation results illustrate coupling among forward motion and shape tracking as described by the equations governing the system.

Keywords: Slender Flexible Mechanism Floating Frame Reduced Order Modeling Timoshenko Beam

5.2 Introduction

In this paper we present a model for the forward locomotion and shape morphing with a slender hyper-redundant mechanism. The mechanism is modeled as a Timoshenko beam in plane motion with natural (force) boundary conditions, which allows a rigid body motion of the system, kinematically described by three degrees of freedom. We adopt the modeling assumption that the characteristic length of the robot is small as compared to the radius of curvature of the substrate, which implies that the kinematics can be described by small deformations around rigid body placements. This leads to the adoption of the floating reference frame description [1, Chapter 5]. A similar framework has been adopted to study small vibrations in piezoelectric beams caused by prescribed rigid body motions [2]. By reproducing the scenario of a slender robot deployed in a generic environment, the shape-morphing problem is posed in terms of coupling with a substrate. This coupling is realized through a distributed system of compliant elements that, in terms of feedback, are represented by a distributed force. The forward locomotion is expressed in terms of the rigid body degrees of freedom tracking a moving point on the substrate, eventually with a given offset. The forward locomotion can therefore be described as a path following problem by employing a Frenet frame intrinsic description of the substrate as a parametrized curve in the two-dimensional environment [3]. The forward locomotion and shape morphing problems are coupled by posing the problem in a distributed control framework with minimization of a suitable action functional based on the Lagrangian function of the system. A simplified scenario is introduced by considering different time scales to describe the evolution of the rigid body motion and of the deformation field, with the assumption that the deformation field evolves much faster so that the shape morphing can be treated as a static problem coupled with the rigid body motion. The well posedness of the problem is stated in the appropriate product Hilbert space, and an approximate solution based on the Galerkin projection on the linear mode shapes is obtained. A passivity based feedback [4, Chapter 8] allows for the asymptotic tracking of the desired motion expressed in terms of the intrinsic geometric description of the path.

The dynamics of flexible hyper-redundant robotic systems is an active field of research. The dynamics of continuous robotic manipulators has been studied by many researchers [5–9], among others, the dynamics of a slewing flexible link is presented in [10, 11], and physical parameter estimation of the nonlinear dynamics of a single link robotic manipulator is proposed by [12]. In the same context, Lagrangian and Ritz

methods have been used by [13–15]. Multibody mobile mechanisms with large number of degrees of freedom can be modeled as one dimensional continua with local Euclideian structure (beam models), due to the slenderness of the system. Vibrations of a flexible manipulator based on the linear Euler-Bernoulli beam model are discussed in [16]. A flexible hub-beam system has been analyzed in [17] by accounting for the influence of shear and axial deformation. Modeling of flexible manipulators with different geometric and dynamic conditions can be found in [18–25], among others. The Lagrangian approach has been used in [26] to model bending of flexible robots modeled as Euler-Bernoulli beams, whereas an Hamiltonian formulation has been adopted in [27] to obtain the governing equations for the same class of systems and design associated controllers. The modal analysis of a two-link flexible manipulator modeled as a Timoshenko beam has been presented in [28]. In the study on active control of flexible structures a methodology based on system transfer matrix proposed by Hać in [29] that the location of sensor and actuators can be determined based on system's controllability and observability gramians, furthermore Book et al, addressed a feedback control for the flexible motion in the plane of two pinned beams in [30] and developed a recursive Lagrangian for a nonlinear flexible manipulator in [31].Control of linear Timoshenko beams is addressed in [32–35]. An overview on adaptive control of single rigid robotic manipulators interacting with dynamic environment is presented in [36].

Different control techniques for bio-inspired and bio-mimetic robots have been proposed by many researchers, among all Jia expressed a smoth motion control with the help of fuzzy rules in [37], and a prospective approach to agile flight control of insect-inspired is studied in [38]. Furthermore a hybrid control approach is presented for trajectory tracking control of unmanned underwater vehicles using a bio-inspired neurodynamics model has been presented in [39], and a multi-functional bio-inspired system with an active cyber-physical assistive device comprised in [40], which supports large deformation, and operates with its own on-board pneumatics and controllers. In the frame of remote control approach, an experimental model for a locust-like motion is designed and implemented in [41]. Neural locomotion controllers for a central pattern generator of lamprey is developed in [42, 43]. A survey to the focused section on bio-inspired mechatronics is presented in [44].

Beside the application of bio-inspired modeling in material fields such as, nanoparticle assembly [45], superoleophobic and smart materials [46], material with variable stiffness [47], polymer-inorganic study [48], and materials for biosensing [49], the multi segment and flexible slender robots find application in several fields such as medical instruments

like gastrointestinal tract tools [50] or endoscopic robots [51], industrial smart health monitoring [52, 53], and energy harvesting [54, 55], to name a few.

In [56–59] the locomotion mechanism and control of worm like robots are discussed. Other examples of bio-inspired robots are the ones that exploit the motion of snakes on various types of surfaces, the elastic elephant trunk like, soft grippers, tendon-driven robots and octopus, and tentacle-like grippers receptively in [60–66]. A Cosserat solid approach has been adopted in [6] to model the dynamics of several kinematically locomoted bio-inspired slender systems. Shape tracking and path tracking with multi-link manipulators is presented in [67–70], where high accuracy path tracking is achieved with high speed systems.

Vibration of flexible manipulators based on linearized Euler-Bernoulli beam is studied in [16]; stability of constrained multibody flexible mechanisms is investigated by [71]. When large displacements cannot be discarded, further complications are introduced by nonlinear strain-displacement relations, non-inertial body frame, and time-varying boundary conditions [72].

We consider a class of system in which propulsion and morphing are achieved by the action of a distributed system that in this respect mimics the action of legs in millipedes through a combination of undulatory and pendulatory motions. By adopting the nature of millipedes, legs movements makes an overall wave like forward motion in the system, that in the recent work [73] has been identified as analogous to a peristaltic wave, that typically propagate in the bodies of warm-like organisms. This mechanism is inherently redundant and robust as many contact points with the ground ensure persistent thrust for forward locomotion, and allows shape morphing with respect to nonzero curvature of the substrate, with filtering of local asperities through the coupling between the legs and the body. In general, this continuous model represents a better behavior of a dynamical system, however, it is mostly too difficult to model and solve a continuous system. For the understanding of an analytical concept of a flexible hyper-redundant autonomous robot, in this work we develop an appreciation of the robot's flexible body as a linearized planar Timoshenko beam theory which the forward locomotion and the shape tracking are associated to the coupling with a substrate that models a generic environment. A major advantage of the proposed method is generality of the model, could be applied to the continuum description of slender bio-mimetic robots to reconstruct the shape or sense the properties of the rigid, elastic or viscoelastic substrate profile like soil, muscle or inner member of a live body. The rest of the paper is organized as follows. In Section 5.3 we present the kinematics of the system. In Section 5.4 we present the weak form governing

the dynamics of a Timoshenko beam deforming around rigid body displacements, and formulate the control distributed parameters control problem with the characterization of the feedback that ensures asymptotic tracking of the desired path. The weak form is based on an action functional that includes point and distributed forces as possible control inputs. The reduced order model of the system based on Galerkin projection is presented in Section 5.5. Simulations that illustrate the path following locomotion coupled with the shape morphing are presented in Section 5.7, and conclusions and final remarks are drawn in Section 5.8.

5.3 Kinematics

We consider the planar motion of a slender robot, with flexible body modeled as a beam. The material body in the reference configuration has the form of a prism $\mathcal{P}_0$ of $\mathcal{E}$, where $\mathcal{E}$ is the Euclideian three-dimensional space, with associated space of translations $\mathcal{U}$. The reference configuration $\mathcal{P}_0$ is referred to the material coordinates $\mathbf{X} = \{X_1, X_2, X_3\}$ along the orthonormal Cartesian basis $\{\mathbf{E}_1, \mathbf{E}_2, \mathbf{E}_3\}$. The cross section of the beam-like body in the reference configuration is the rigid surface spanned by $\mathbf{E}_2$ and $\mathbf{E}_3$. For an undeformed length ℓ, the coordinate $X_1 \in [0, \ell]$ is the locus of the centroids of the cross sections, and $\mathbf{E}_1$ spans the tangent space to the axis (support) of the beam described by such coordinate.

We want to describe the motion of the robot as composed by a rigid body placement and by a small deformation about the rigid body placement. Therefore we adopt the concept of floating frame that is extensively described in [1, Chapter 5], and used in [2] to formulate the problem of vibrations of beams caused by a prescribed rigid motion. As it is illustrated schematically in Fig 5.1, the rigid body placement is described by the change of coordinates

$$\mathbf{x}(\mathbf{X}, t) = \mathbf{d}(t) + \mathbf{R}(\theta(t))\,(\mathbf{X} - \delta\ell\mathbf{E}_1) \tag{5.1}$$

that maps $\mathbf{X} \in \mathcal{P}_0$ to $\mathbf{x} \in \mathcal{P}_\mathrm{R}$, where $\mathcal{P}_\mathrm{R}$ is the region corresponding to the rigid body placement. The rigid change of coordinates is as usual composed of a rigid body displacement $\mathbf{d}$ that represents the time-varying position of a point in $\mathcal{P}_\mathrm{R}$ with respect to the origin of the fixed reference frame, and by the action of the rotation tensor $\mathbf{R}(\theta)$

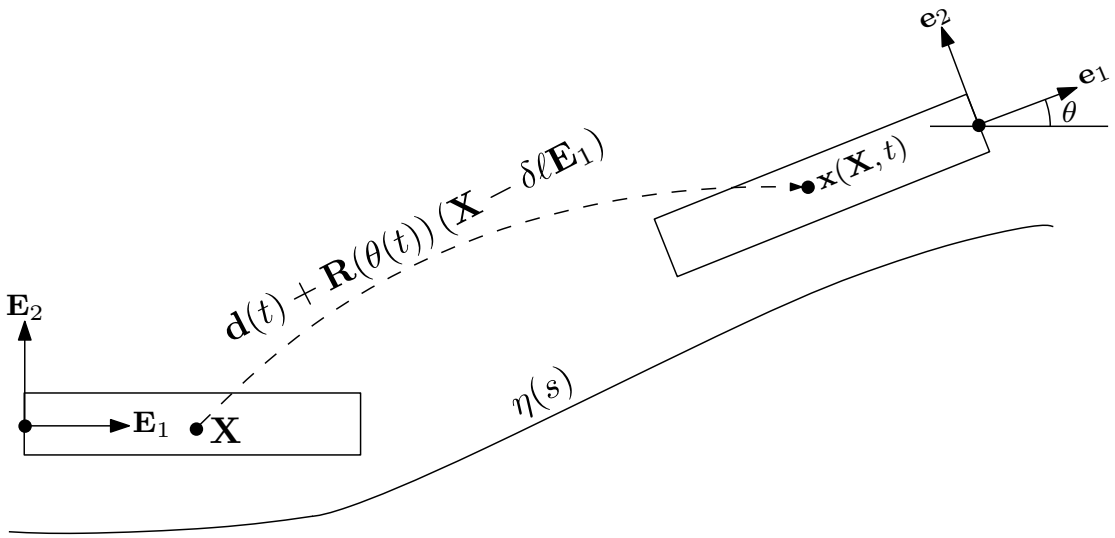

Figure 5.1: Schematic of floating frame concept which describes the system's motion by a rigid body placement and by a small deformation about the rigid body placement.

defined by (see for example [74])

$$\begin{aligned}\mathbf{R}(\theta) = \mathbf{E}_3 \otimes \mathbf{E}_3 + \cos\theta\,(\mathbf{E}_1 \otimes \mathbf{E}_1 + \mathbf{E}_2 \otimes \mathbf{E}_2) \\ - \sin\theta\,(\mathbf{E}_1 \otimes \mathbf{E}_2 - \mathbf{E}_2 \otimes \mathbf{E}_1)\end{aligned} \tag{5.2}$$

where $\otimes$ is the tensor product defined by the projection

$$(\mathbf{u} \otimes \mathbf{v})\mathbf{w} = (\mathbf{v} \cdot \mathbf{w})\mathbf{u} \tag{5.3}$$

for $\mathbf{u}$, $\mathbf{v}$, $\mathbf{w}$ in $\mathcal{U}$, with "$\cdot$" indicating the associated inner product. Moreover, $\delta \in [0,1]$ defines the point on the axis that is left unaltered by the action of $\mathbf{R}$, so that the rigid body motion is composed of a translation $\mathbf{d}$ and of a rotation around an axis passing through the point with position $\delta\ell\mathbf{E}_1$ with respect to the left boundary of the undeformed body. Note that $\mathbf{R}$ as defined in (5.2) is a rotation about $\mathbf{E}_3$, which is normal to the plane of the motion. Therefore the rotation tensor $\mathbf{R}$ can be equivalently be represented in the basis $\{\mathbf{E}_1, \mathbf{E}_2\}$ by the two-dimensional rotation matrix

$$\mathbf{R}(\theta) = \begin{pmatrix} \cos\theta & -\sin\theta \\ \sin\theta & \cos\theta \end{pmatrix} \tag{5.4}$$

The small deformation about the rigid body placement $\mathcal{P}_\mathrm{R}$ is described by a map $\boldsymbol{\chi} : \mathcal{P}_\mathrm{R} \to \mathcal{P}$ that takes points $\mathbf{x}$ and maps them to the point $\boldsymbol{\chi}$ in the current configuration

$\mathcal{P}$:

$$\boldsymbol{\chi}(\mathbf{x}, t, \tau) = \mathbf{x}(t) + \mathbf{U}(\mathbf{x}, t, \tau) \tag{5.5}$$

where $\mathbf{U}$ is a small deformation. In order to describe the two time scales that characterize respectively the rigid body degrees of freedom oscillations and the deformation oscillations, we have introduced the slow time

$$\tau = \epsilon t \tag{5.6}$$

with $\epsilon > 0$ [75, Chapter 11], to formalize the assumption that the morphing (shape adaptation) is much faster than the evolution of the rigid body degrees of freedom; therefore we will consider the quasi static shape adaptation obtained for $\epsilon \ll 1$. Consistently with the linearized planar Timoshenko beam theory [76] the deformation $\mathbf{U}$ is given by

$$\mathbf{U}(\mathbf{x}, t, \tau) = (u(x_1, \tau) - X_2\psi(x_1, \tau))\mathbf{e}_1(t) + w(x_1, \tau)\mathbf{e}_2(t) \tag{5.7}$$

where $\mathbf{e}_i = \mathbf{R}\mathbf{E}_i$ are rotated orthonormal basis vectors (floating reference frame [1]) that are used to describe the rigid body placement $\mathcal{P}_\mathrm{R}$, and $x_i = \mathbf{x} \cdot \mathbf{e}_i$. From (5.1) we have

$$\begin{aligned} x_1 = \mathbf{x} \cdot \mathbf{e}_1 = \mathbf{d} \cdot \mathbf{e}_1 + (X_1 - \delta\ell)\mathbf{e}_1 \cdot \mathbf{R}\mathbf{E}_1 \\ = \mathbf{d} \cdot \mathbf{e}_1 + (X_1 - \delta\ell)\mathbf{E}_1 \cdot \mathbf{R}^\mathsf{T}\mathbf{R}\mathbf{E}_1 = \mathbf{d} \cdot \mathbf{e}_1 + (X_1 - \delta\ell) \end{aligned} \tag{5.8}$$

$$x_2 = \mathbf{x} \cdot \mathbf{e}_2 = \mathbf{d} \cdot \mathbf{e}_2 + X_2\mathbf{e}_2 \cdot \mathbf{R}\mathbf{E}_2 = \mathbf{d} \cdot \mathbf{e}_2 + X_2 \tag{5.9}$$

where we have used the property $\mathbf{R}^{-1} = \mathbf{R}^\mathsf{T}$ (orthogonality of $\mathbf{R}$) and the definition of transpose $\mathbf{v}_2 \cdot \mathbf{R}\mathbf{v}_1 = \mathbf{v}_1 \cdot \mathbf{R}^\mathsf{T}\mathbf{v}_2$ for any two vectors $\mathbf{v}_1$ and $\mathbf{v}_2$.

In the floating reference frame, the material time derivative is performed by keeping $\mathbf{x}$ constant [2], and therefore $\mathcal{P}_\mathrm{R}$ is treated as the reference configuration with respect to the deformation. This approximation holds due to the hypothesis of small deformations around the rigid body placement. By accounting for the two time scales the material time derivative maps to

$$\dot{(\cdot)} = \frac{\partial}{\partial t} + \epsilon\frac{\partial}{\partial \tau} \tag{5.10}$$

for which we will use the compact notation $\partial_t + \epsilon\partial_\tau$. The velocity of a point $\boldsymbol{\chi}$ in $\mathcal{P}$ is obtained as its material time derivative, that is therefore given by

$$\begin{aligned} \dot{\boldsymbol{\chi}} = \partial_t\mathbf{d} + \partial_t\theta\mathbf{W}(\mathbf{x} - \mathbf{d}) + \dot{\mathbf{U}} \\ = \partial_t\mathbf{d} + \partial_t\theta\mathbf{W}((X_1 - \delta\ell)\mathbf{e}_1 + X_2\mathbf{e}_2) + \dot{\mathbf{U}} \end{aligned} \tag{5.11}$$

where $\mathbf{W}$ is the skew-symmetric tensor

$$\mathbf{W} = \mathbf{e}_2 \otimes \mathbf{e}_1 - \mathbf{e}_1 \otimes \mathbf{e}_2 \tag{5.12}$$

which allows to describe the time derivative of unit basis vectors rotating with angular velocity $\dot{\theta}$ as $\dot{\mathbf{e}}_i = \dot{\theta}\mathbf{W}\mathbf{e}_i$; this relation has bees used to derive the third therm on the right hand side of (5.11). In the rotating basis $\mathbf{W}$ has the matrix representation

$$\mathbf{W} = \begin{pmatrix} 0 & -1 \\ 1 & 0 \end{pmatrix} \tag{5.13}$$

with axial vector $\mathbf{e}_3 \equiv \mathbf{E}_3$, so that $\mathbf{W}\mathbf{a} = \mathbf{E}_3 \wedge \mathbf{a}$ for every vector $\mathbf{a}$, with operator $\wedge$ referring to the wedge product. This is consistent with the well known property that for planar motions the angular velocity is normal to the plane of the motion. The action of the skew symmetric tensor $\mathbf{W}$ on the floating basis vectors allows to write $\dot{\mathbf{x}}$ as $\partial_t \mathbf{d} + \partial_t\theta((X_1 - \delta\ell)\mathbf{e}_2 - X_2\mathbf{e}_1)$. In the floating reference frame the material derivative of $\mathbf{U}$ is given by

$$\begin{aligned} \dot{\mathbf{U}} &= \epsilon(\partial_\tau u - X_2\partial_\tau\psi)\mathbf{e}_1 + \epsilon\partial_\tau w\mathbf{e}_2 + \partial_t\theta\mathbf{W}\mathbf{U} \\ &= (\epsilon(\partial_\tau u - X_2\partial_\tau\psi) - w\partial_t\theta)\mathbf{e}_1 + (\epsilon\partial_t w + \partial_t\theta(u - X_2\psi))\mathbf{e}_2 \end{aligned} \tag{5.14}$$

The time derivative if the map $\boldsymbol{\chi}$ can therefore explicitly be written as

$$\begin{aligned} \dot{\boldsymbol{\chi}} = \partial_t\mathbf{d} &+ (\epsilon(\partial_\tau u - X_2\partial_\tau\psi) - \partial_t\theta(w + X_2))\,\mathbf{e}_1 \\ &+ (\epsilon\partial_\tau w + \partial_t\theta(u - X_2\psi + X_1 - \delta\ell))\,\mathbf{e}_2 \end{aligned} \tag{5.15}$$

Within the hypothesis of small deformations we consider the linearization

$$(\mathbf{I} + \nabla_{\mathbf{x}}\mathbf{U})^{\mathsf{T}}(\mathbf{I} + \nabla_{\mathbf{x}}\mathbf{U}) \simeq \mathbf{I} + \nabla_{\mathbf{x}}\mathbf{U} + \nabla_{\mathbf{x}}^{\mathsf{T}}\mathbf{U}$$

, so that the Green-Saint-Venant strain $\boldsymbol{\varepsilon}$ reduces to the symmetric part of $\nabla_{\mathbf{x}}\mathbf{U}$, and the gradient is represented in operator form as $\nabla_{\mathbf{x}} = \frac{\partial}{\partial x_j} \otimes \mathbf{e}_j$. Therefore we obtain

$$\nabla_{\mathbf{x}}\mathbf{U} = (u' - X_2\psi')\mathbf{e}_1 \otimes \mathbf{e}_1 + w'\mathbf{e}_2 \otimes \mathbf{e}_1 - \psi\mathbf{e}_1 \otimes \mathbf{e}_2 \tag{5.16}$$

$$\begin{aligned} \boldsymbol{\varepsilon} &= \mathrm{sym}\nabla_{\mathbf{x}}\mathbf{U} \\ &= (u' - X_2\psi')\mathbf{e}_1 \otimes \mathbf{e}_1 + \frac{1}{2}(w' - \psi)(\mathbf{e}_2 \otimes \mathbf{e}_1 + \mathbf{e}_1 \otimes \mathbf{e}_2) \end{aligned} \tag{5.17}$$

where $(\cdot)'$ means differentiation with respect to x_1.

5.4 Continuous model of a slender floating mechanism

5.4.1 Weak form

In this section we derive the weak form of the governing equations of a slender robot with kinematics described in the previous Section. The weak form allows to state the well posedness of a distributed parameters control problem with inputs suitably included in the variational form.

The kinetic energy of the system is then given by

$$\mathcal{K} = \frac{1}{2}\int_{\mathcal{P}} \varrho \dot{\boldsymbol{\chi}} \cdot \dot{\boldsymbol{\chi}} \mathrm{d}\mathcal{P} \tag{5.18}$$

where we have tacitly assumed that $\mathbf{d}$ is a boundary displacement. By relaxing this assumption the integral would have to be extended over regular regions with interfaces accounting for jump conditions. Given the geometry of $\mathcal{P}$, we consider the Cartesian product structure $\mathcal{P} = \mathcal{A} \times [0, \ell]$, where ℓ is the undeformed length of the beam and $\mathcal{A}$ is the two-dimensional Euclideian point space defining a rigid cross section. The axis of the beam is therefore spanned by the coordinate $x_1 \in [d_1 - \delta\ell, d_1 + \ell(1-\delta)]$, whereas x_2 and x_3 span the cross section. Therefore the integral in $\mathcal{P}$ is accordingly decomposed as $\int_{\mathcal{P}} = \int_{d_1-\delta\ell}^{d_1+\ell(1-\delta)} \int_{\mathcal{A}}$.

By writing explicitly the inner product $\dot{\boldsymbol{\chi}} \cdot \dot{\boldsymbol{\chi}}$ with the expression in (5.15) we obtain

$$\begin{aligned}\mathcal{K} = \frac{1}{2}\int_{d_1-\delta\ell}^{d_1+\ell(1-\delta)} \\ \int_{\mathcal{A}} \varrho \left(\left(\partial_t d_1 + \epsilon\partial_\tau u - w\partial_t\theta - X_2\left(\partial_t\theta + \epsilon\partial_\tau\psi\right)\right)^2 \right. \\ \left. + \left(\partial_t d_2 + \epsilon\partial_\tau w + \partial_t\theta\left(u + x_1 - X_2\psi\right)\right)^2 \right) \mathrm{d}\mathcal{A}\mathrm{d}x_1\end{aligned} \tag{5.19}$$

where we have introduced $d_i = \mathbf{d}\cdot\mathbf{e}_i$, that are the components of $\mathbf{d}$ in the body reference frame. We now operate the change of coordinate $x_1(X_1) = d_1 + X_1 - \delta\ell$ (see (5.8)) that clearly has unit determinant of the Jacobian (as expected being a rigid change of coordinate), and define the material descriptions of different scalar fields involved in the integration

$$u^\star(X_1, t) := u(x_1(X_1), t) = u(d_1 + X_1 - \delta\ell) \tag{5.20a}$$

$$w^\star(X_1, t) := w(d_1 + X_1 - \delta\ell) \tag{5.20b}$$

$$\psi^\star(X_1, t) := \psi(d_1 + X_1 - \delta\ell) \tag{5.20c}$$

Since the origins of coordinates $\{X_2, X_3\}$ are the centroids of the cross section (whose locus describes the axis of the beam) we have $\int_{\mathcal{A}} \varrho X_2 \mathrm{d}\mathcal{A} = 0$, and $\int_{\mathcal{A}} \varrho (X_2)^2 \mathrm{d}\mathcal{A} = I$, where I is the moment of inertia about X_3 (normal to the plane of motion). The expression for the kinetic energy therefore becomes

$$\begin{aligned}\mathcal{K} = \frac{1}{2}\int_0^\ell \big(\varrho A \left((\partial_t d_1 + \epsilon\partial_\tau u^\star)^2 + (\partial_t d_2 + \epsilon\partial_\tau w^\star)^2\right.\\ +(\partial_t\theta)^2\left((d_2+w^\star)^2 + (d_1+u^\star+X_1-\delta\ell)^2\right)\\ +2\partial_t\theta\left((d_1+u^\star+X_1-\delta\ell)(\partial_t d_2+\epsilon\partial_\tau w^\star)\right.\\ \left.-(d_2+w^\star)(\partial_t d_1+\epsilon\partial_\tau u^\star)\right))\\ \left.+I\left((\psi^\star\partial_t\theta)^2+(\partial_t\theta+\epsilon\partial_\tau\psi^\star)^2\right)\right)\mathrm{d}X_1\end{aligned} \tag{5.21}$$

Let $\boldsymbol{\sigma}$ be the Cauchy stress tensor in $\mathcal{P}$; the strain energy of the system is therefore given by

$$\begin{aligned}&\frac{1}{2}\int_{\mathcal{P}} \mathrm{tr}\left(\boldsymbol{\sigma}^\mathsf{T}\boldsymbol{\varepsilon}\right)\mathrm{d}\mathcal{P}\\ &= \frac{1}{2}\int_{d_1-\delta\ell}^{d_1+\delta(1-\ell)}\int_{\mathcal{A}}(\sigma_{11}\varepsilon_{11}+2\sigma_{12}\varepsilon_{12})\mathrm{d}\mathcal{A}\mathrm{d}x_1\\ &= \frac{1}{2}\int_{d_1-\delta\ell}^{d_1+\delta(1-\ell)}(Nu'+M\psi'+Q(w'-\psi))\,\mathrm{d}x_1\end{aligned} \tag{5.22}$$

where $\mathrm{tr}(\boldsymbol{\sigma}^\mathsf{T}\boldsymbol{\varepsilon})$ is the scalar product in the space of linear operators $\mathrm{Lin}(\mathcal{U},\mathcal{U})$, and the components of the tensors in the basis $\{\mathbf{e}_1, \mathbf{e}_2\}$ are obtained as $\varepsilon_{ij} = \mathbf{e}_i \cdot \boldsymbol{\varepsilon}\mathbf{e}_j$. Moreover, by integrating over the cross section we have introduced the stress resultants

$$N = \int_{\mathcal{A}} \sigma_{11}\mathrm{d}\mathcal{A},\; Q = \int_{\mathcal{A}} \sigma_{12}\mathrm{d}\mathcal{A},\; M = -\int_{\mathcal{A}} \sigma_{11}x_2\mathrm{d}\mathcal{A} \tag{5.23}$$

which are scalars representing respectively the normal and shear forces (projections along $\mathbf{e}_1$ and $\mathbf{e}_2$) and the bending moment (around $\mathbf{e}_3$). The potential energy of the system is then given by

$$\begin{aligned}\mathcal{V} = \int_{d_1-\delta\ell}^{d_1+\ell(1-\delta)}\Big(&\frac{1}{2}(Nu'+M\psi'+Q(w'-\psi))\\ &-b_N u - b_Q w - b_M\psi\Big)\,\mathrm{d}x_1 - f_1 d_1 - f_2 d_2 - f_3\theta\end{aligned} \tag{5.24}$$

where f_1, f_2, and f_3 are respectively the components of the external force and of the external torque that are dual of the rigid body degrees of freedom $\mathbf{d}$ and θ, and b_N, b_Q,

and b_M are distributed forces and a distributed torque that are dual of the deformations u, w, and ψ. All force components are along the floating basis axes. We assume the linear elastic material response, therefore adopting the following constitutive relations

$$N = AYu', \quad Q = kAG(w' - \psi), \quad M = IY\psi' \tag{5.25}$$

with Y, G, and k being constituive parameters for linear elastic homogeneous materials representing respectively Young's modulus, the shear modulus, and the shear shape factor ($k = 5/6$ for rectangular cross section). By using the constitutive relations it is immediate to introduce the material descriptions of the distributed force fields, so that the potential energy can be written as

$$\begin{aligned}\mathcal{V} = \int_0^\ell \Big(&\frac{1}{2}\left(AYu^{\star\prime 2} + kAG(w^{\star\prime} - \psi^\star)^2 + IY\psi^{\star\prime 2}\right) \\ &- b_N u^\star - b_Q w^\star - b_M \psi^\star \Big)\, \mathrm{d}X_1 - f_1 d_1 - f_2 d_2 - f_3 \theta \end{aligned} \tag{5.26}$$

We introduce the nondimensional kinematic variables X_1/ℓ, $u^\star/\ell$, and $w^\star/\ell$ with respect to the length ℓ, and the nondimensional forces $b_N\ell/kAG$, $b_Q\ell/kAG$, b_M/kAG, and f_i/kAG. Since no confusion arises, we indicate henceforth the nondimensional fields with the same symbols previously used for the the corresponding dimensional ones. Let

$$\mathbf{z} = (d_1, d_2, \theta, u^\star, w^\star, \psi^\star) \tag{5.27a}$$

$$\partial\mathbf{z} = (\partial_t d_1, \partial_t d_2, \partial_t \theta, \partial_\tau u^\star, \partial_\tau w^\star, \partial_\tau \psi^\star) \tag{5.27b}$$

be the state vector and its time derivative. With the introduction of the nondimensional parameters

$$\alpha_1 = \frac{Y}{kG}, \quad \alpha_2 = \frac{I}{A\ell^2}, \quad \bar{t}^2 = \frac{\varrho\ell^2}{kG} \tag{5.28}$$

where $\bar{t}$ is a characteristic time, we rewrite the kinetic energy in nondimensional form as

$$\begin{aligned}\mathcal{K} &= \frac{1}{2}\int_0^1 \partial\mathbf{z}^{\mathsf{T}}\mathbf{M}(\mathbf{z},\epsilon)\partial\mathbf{z}\mathrm{d}X_1 \\ &= \frac{1}{2}\int_0^1 M_{ij}(\mathbf{z},\epsilon)\partial z_i \partial z_j \mathrm{d}X_1 \end{aligned} \tag{5.29}$$

where we have adopted the convention of summing repeated indexes in their respective ranges. The non-zero entries of the 6×6 matrix $\mathbf{M}$ are

$$M_{11} = M_{22} = 1 \tag{5.30a}$$

$$M_{14} = M_{25} = M_{41} = M_{52} = \epsilon \tag{5.30b}$$
$$M_{44} = M_{55} = \epsilon^2 \tag{5.30c}$$
$$M_{66} = \alpha_2 \epsilon^2 \tag{5.30d}$$
$$M_{36} = M_{63} = \alpha_2 \epsilon \tag{5.30e}$$
$$M_{13} = M_{31} = -(d_2 + w^\star) \tag{5.30f}$$
$$M_{34} = M_{43} = -\epsilon(d_2 + w^\star) \tag{5.30g}$$
$$M_{23} = M_{32} = d_1 + u^\star + X_1 - \delta \tag{5.30h}$$
$$M_{35} = M_{53} = \epsilon(d_1 + u^\star + X_1 - \delta) \tag{5.30i}$$
$$M_{33} = \alpha_2(1 + \psi^\star)^2 + (d_1 + u^\star + X_1 - \delta)^2 + (d_2 + w^\star)^2 \tag{5.30j}$$

We define the collection of strain components $\bar{\boldsymbol{\varepsilon}}$, the collection of forces and torques $\boldsymbol{\tau}$, and the matrix $\mathbf{K}$ by

$$\bar{\boldsymbol{\varepsilon}} = (u^{\star\prime}, w^{\star\prime} - \psi^\star, \psi^{\star\prime}) \tag{5.31a}$$
$$\boldsymbol{\tau} = (f_1, f_2, f_3, b_N, b_Q, b_M) \tag{5.31b}$$
$$\mathbf{K} = \operatorname{diag}(\alpha_1, 1, \alpha_1\alpha_2) \tag{5.31c}$$

so that the nondimensional potential energy is rewritten as

$$\begin{aligned} \mathcal{V} &= \int_0^1 \left(\frac{1}{2} \bar{\boldsymbol{\varepsilon}}^\mathsf{T} \mathbf{K} \bar{\boldsymbol{\varepsilon}} - \boldsymbol{\tau}^\mathsf{T} \mathbf{z} \right) \mathrm{d}X_1 \\ &= \int_0^1 \left(\frac{1}{2} K_{ij} \bar{\varepsilon}_i \bar{\varepsilon}_j - \tau_i z_i \right) \mathrm{d}X_1 \end{aligned} \tag{5.32}$$

where the work term $\tau_i z_i$ is transported under the integral by dividing by the nondimensional length of the domain, that in this case is 1.

In order to obtain the weak form of the evolution equations we introduce the Lagrangian function

$$\mathcal{L}\left(\mathbf{z}, \partial\mathbf{z}, \bar{\boldsymbol{\varepsilon}}, \mathbf{b}, \boldsymbol{\tau}\right) = \mathcal{K}(\mathbf{z}, \partial\mathbf{z}) - \mathcal{V}(\mathbf{z}, \bar{\boldsymbol{\varepsilon}}, \boldsymbol{\tau}) \tag{5.33}$$

The external forces $\boldsymbol{\tau}$ can be interpreted as Lagrange multipliers if the corresponding displacements are prescribed (kinematic constraints); otherwise, in a control framework, they can be interpreted as control inputs to drive the corresponding dual kinematic quantities to desired values. The (strong) governing evolution equations are the cofactors of the variations $\tilde{\mathbf{z}}$, $\tilde{\boldsymbol{\tau}}$, that describe the evolution of the minimizers of the action

functional $\int_{t_1}^{t^2} \mathcal{L}\mathrm{d}t$ between two fixed points t_1 and t_2; this formulation can be generalized to include the initial conditions by considering Gurtin's convolution formulation, see [77]. Minimization of the action functional corresponds to the stationarity of its gradient (Gâteaux derivative) along the variations of its arguments. Here we consider the weak form, that is built by considering the cofactors of all arguments of the Lagrangian function; the weak form is suitable for numerical solution and it allows to pose the control problem in the appropriate Sobolev space. The stationarity of the gradient of the Lagrangian gives

$$\int_{t_1}^{t_2}\int_0^1 \Big(\partial\tilde{z}_k M_{kj}\partial z_j + \frac{1}{2}\tilde{z}_k\frac{\partial M_{ij}}{\partial z_k}\partial z_i\partial z_j \\ -K_{ij}\tilde{\bar{\varepsilon}}_i\bar{\varepsilon}_j + \tilde{z}_i\tau_i + \tilde{\tau}_i z_i)\,\mathrm{d}X_1\mathrm{d}t = 0 \tag{5.34}$$

Time integration by parts of the first term gives

$$\int_{t_1}^{t_2}\int_0^1 \Big(-\tilde{z}_k M_{kj}\partial^2 z_j - \tilde{z}_k\frac{\partial M_{kj}}{\partial z_i}\partial z_i\partial z_j + \tilde{z}_k\frac{1}{2}\frac{\partial M_{ij}}{\partial z_k}\partial z_i\partial z_j \\ -K_{ij}\tilde{\bar{\varepsilon}}_i\bar{\varepsilon}_j + \tilde{z}_i\tau_i + \tilde{\tau}_i z_i)\,\mathrm{d}X_1\mathrm{d}t = 0 \tag{5.35}$$

where, consistently with the Hamilton-Kirchhoff variational principle we have assumed that all fields are assigned at times t_1 and t_2, which implies that the boundary terms arising from the integration by parts in time are zero (since the corresponding variations of the fields are zero whenever the fields are assigned). The symbol ∂^2 means second time derivative. By introducing

$$c_{kij} = \frac{\partial M_{kj}}{\partial z_i} - \frac{1}{2}\frac{\partial M_{ij}}{\partial z_k} = \frac{1}{2}\left(\frac{\partial M_{kj}}{\partial z_i} + \frac{\partial M_{ki}}{\partial z_j} - \frac{\partial M_{ij}}{\partial z_k}\right) \tag{5.36}$$

(Christoffel symbols) we can define the 6×6 matrix

$$C_{kj} = c_{kij}\partial z_i \tag{5.37}$$

with nonzero entries given by

$$C_{13} = C_{31} = \partial_t d_2 + \frac{1+\epsilon}{2}\partial_\tau w^\star + \partial_t\theta(d_1 + u^\star + X_1 - \delta) \tag{5.38a}$$

$$C_{43} = C_{34} = \frac{1+\epsilon}{2}\partial_t d_2 + \epsilon\partial_\tau w^\star + \partial_t\theta(d_1 + u^\star + X_1 - \delta) \tag{5.38b}$$

$$C_{23} = C_{32} = -\partial_t d_1 - \frac{1+\epsilon}{2}\partial_\tau u^\star + \partial_t\theta(d_2 + w^\star) \tag{5.38c}$$

$$C_{53} = C_{35} = -\frac{1+\epsilon}{2}\partial_t d_1 - \epsilon\partial_\tau u^\star + \partial_t\theta(d_2 + w^\star) \tag{5.38d}$$

$$\begin{aligned} C_{33} = &-(\partial_t d_1 + \partial_\tau u^\star)(d_1 + u^\star + X_1 - \delta) \\ &-(\partial_t d_2 + \partial_\tau w^\star)(d_2 + w^\star) - \alpha_2\psi^\star\partial_\tau\psi^\star \end{aligned} \tag{5.38e}$$

$$C_{36} = C_{63} = \alpha_2\psi^\star\partial_t\theta \tag{5.38f}$$

By exploiting the arbitrariness of t_1 and t_2 the weak form of the problem is rewritten as

$$\begin{aligned} 0 &= \int_0^1 \left(\tilde{z}_i M_{ij}\partial^2 z_j + \tilde{z}_i C_{ij}\partial z_j + K_{ij}\tilde{\bar{\varepsilon}}_i\bar{\varepsilon}_j - \tilde{\tau}_i z_i + \tau_i\tilde{z}_i\right)\mathrm{d}X_1 \\ &= \int_0^1 \big(\tilde{\mathbf{z}}^\mathsf{T}\mathbf{M}(\mathbf{z},\epsilon)\partial^2\mathbf{z} + \tilde{\mathbf{z}}^\mathsf{T}\mathbf{C}(\mathbf{z},\partial\mathbf{z},\epsilon)\partial\mathbf{z} \\ &\qquad + \tilde{\bar{\boldsymbol{\varepsilon}}}^\mathsf{T}\mathbf{K}\bar{\boldsymbol{\varepsilon}} - \tilde{\boldsymbol{\tau}}^\mathsf{T}\boldsymbol{z} - \tilde{\mathbf{z}}^\mathsf{T}\boldsymbol{\tau}\big)\,\mathrm{d}X_1 \end{aligned} \tag{5.39}$$

5.4.2 Boundary Conditions and External Loads as Feedback

If forcing terms in the weak form (5.39) are not assigned they can be interpreted as Lagrange multipliers that are dual of enforced kinematic constraints. Here we are interested in modeling the system depicted in Figure 5.2, in which the beam is coupled with a smooth substrate by a distributed system of compliant elements, and the forward locomotion is dictated by the coupling of the point on the beam at $X_1 = \delta$ (that belongs to the undeformed axis of the beam rigidly displaced) with a moving point on the substrate described by the evolution of the arclength $s^*(t)$. Therefore the rigid motion can be set in the framework of a path tracking problem, in which the position and orientation of the undeformed body are respectively dictated by the position and orientation of a driving point on the substrate. Moreover, the shape of the system adapts to the shape of the substrate through the distributed coupling exerted by the system. We set $\delta = 1$ so that the point of the axis that is left unaltered by the action of the rotation tensor $\mathbf{R}$ is the extreme $X_1 = \ell$ (that is, the beam rotates about the extreme at $X_1 = \ell$). This point

that can be interpreted as the head of a slender robot whenever this model is applied such context.

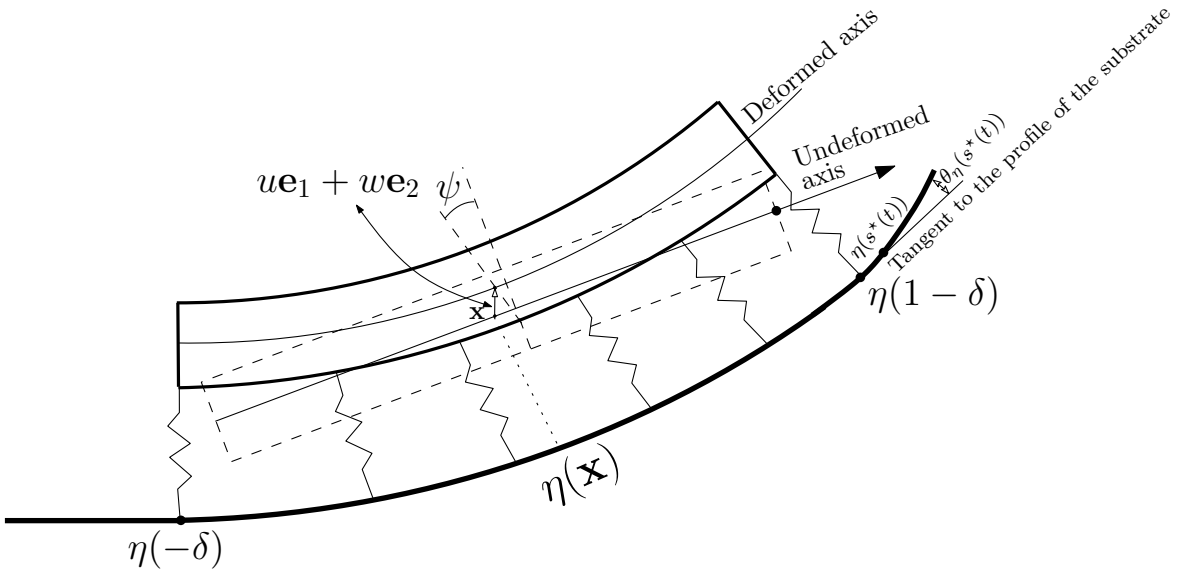

Figure 5.2: Sketch of the coupling between the flexible mechanism and a rigid substrate described by the curve $\boldsymbol{\eta}$. The coupling is exerted through a distributed system of compliant elements. The point $\boldsymbol{\eta}(s^*(t))$ is driven by the kinematics $s^*(t)$

We consider the distributed coupling with the substrate to be given by normal actions with respect to the axis of the beam, therefore dual of the transverse displacement w. This implies that $b_N = b_M = 0$ (no axial distributed forces and no distributed couples). In a control framework, the external forces are considered as inputs determined by suitable feedback laws. Therefore, given this characterization the nonzero components of the external forces are assigned as feedback and therefore $\tilde{\boldsymbol{\tau}} = \mathbf{0}$. Therefore the forcing term in the functional (5.39) becomes

$$\begin{aligned} &\int_0^1 \left(\tilde{\boldsymbol{\tau}}^\mathsf{T}\boldsymbol{z} + \tilde{\mathbf{z}}^\mathsf{T}\boldsymbol{\tau}\right) \mathrm{d}X_1 \\ &= f_1\tilde{d}_1 + f_2\tilde{d}_2 + f_3\tilde{\theta} + \int_0^1 b_Q\tilde{w}^\star \mathrm{d}X_1 \end{aligned} \tag{5.40}$$

with f_is applied at $X_1 = 1$ (head). The input vector is therefore redefined as

$$\boldsymbol{\tau} = (f_1, f_2, f_3, 0, b_Q, 0)\,. \tag{5.41}$$

5.4.3 Control problem statement

Let H be the product Hilbert space $\mathbb{R} \times \mathbb{R} \times \mathbb{R} \times S^1(0,1) \times S^1(0,1) \times S^1(0,1)$, where $\mathbb{R}$ is the set of real numbers and S^1 is the Sobolev space of functions with first derivative that is square summable in $(0,1)$, that is defined by the set

$$S^1(0,1) := \left\{ f : \int_0^1 f'(x_1,t)^2 \mathrm{d}x_1 < \infty \right\} \tag{5.42}$$

Therefore the the state $\mathbf{z}$ belongs to $\mathbb{R}^+ \times H$ and the input vector $\boldsymbol{\tau}$ belongs to $\mathbb{R}^+ \times \mathbb{R} \times \mathbb{R} \times \mathbb{R} \times S^0(0,1)$.

The variational formulation (5.39) includes the variations of the inputs, which implies that parameters (control gains) in the feedback loop can be included in the minimization process and therefore be determined adaptively by the evolution of the system. Here we consider the gains to be given constants, and therefore we formally consider the feedback $\boldsymbol{\tau}(\mathbf{z}, \mathbf{z}^{\mathrm{d}})$, where $\mathbf{z}^{\mathrm{d}}$ is a desired kinematic state that act as driving terms for the system. Although not explicitly shown, the feedback can include time derivatives of the desired state. The weak form (5.39) therefore specializes to

$$\begin{aligned} \int_0^1 \left(\tilde{\mathbf{z}}^{\mathsf{T}} \mathbf{M}(\mathbf{z}) \ddot{\mathbf{z}} + \tilde{\mathbf{z}}^{\mathsf{T}} \mathbf{C}(\mathbf{z}, \dot{\mathbf{z}}) \dot{\mathbf{z}} + \tilde{\bar{\boldsymbol{\varepsilon}}}^{\mathsf{T}} \mathbf{K} \bar{\boldsymbol{\varepsilon}} \right) \mathrm{d}X_1 \\ = \int_0^1 \tilde{\mathbf{z}}^{\mathsf{T}} \boldsymbol{\tau} \left(\mathbf{z}, \mathbf{z}^{\mathrm{d}} \right) \mathrm{d}X_1 \end{aligned} \tag{5.43}$$

with the right-hand side acting as a forcing term.

The control problem for the slender mechanism is then formulated as follows: find $\mathbf{z}$ that minimizes the action functional $\int_{t_1}^{t_2} \int_0^{\ell} \mathcal{L}$. This translates to the requirement of finding $\mathbf{z}$ that satisfy (5.43) for all $\tilde{\mathbf{z}}$.

5.5 Reduced order system

5.5.1 Galerkin projection

The reduced order model is obtained by separation of variables with respect to space and time. Since the rigid body displacement degrees of freedom are functions of time only the separation of variables for $\mathbf{d}$ and θ is trivial. The deformation fields are instead

decomposed as

$$u^\star(X_1,\tau) = \bar{\mathbf{u}}^\mathsf{T}(X_1)\mathbf{a}(\tau) \tag{5.44}$$

$$w^\star(X_1,\tau) = \bar{\mathbf{w}}^\mathsf{T}(X_1)\mathbf{b}(\tau) \tag{5.45}$$

$$\psi(X_1,\tau) = \bar{\boldsymbol{\psi}}^\mathsf{T}(X_1)\mathbf{c}(\tau) \tag{5.46}$$

where $\bar{\mathbf{u}} = (\bar{u}_1,\ldots,\bar{u}_n)^\mathsf{T}$, $\bar{\mathbf{w}} = (\bar{w}_1,\ldots,\bar{w}_n)^\mathsf{T}$, and $\bar{\boldsymbol{\psi}} = \left(\bar{\psi}_1,\ldots,\bar{\psi}_n\right)^\mathsf{T}$ are $n-$dimensional sets of spatial basis functions, and $\mathbf{a} = (a_1,\ldots,a_n)^\mathsf{T}$, $\mathbf{b} = (b_1,\ldots,b_n)^\mathsf{T}$, and $\mathbf{c} = (c_1,\ldots,c_n)^\mathsf{T}$ are time dependent vectors of amplitudes. We introduce

$$\bar{\mathbf{z}} = \begin{pmatrix} I_{3\times3} & 0_{3\times n} \\ & \bar{\mathbf{u}}^\mathsf{T}(X_1) \\ 0_{3\times3} & \bar{\mathbf{w}}^\mathsf{T}(X_1) \\ & \bar{\boldsymbol{\psi}}^\mathsf{T}(X_1) \end{pmatrix}, \quad \boldsymbol{\zeta} = (d_1, d_2, \theta, \mathbf{a}, \mathbf{b}, \mathbf{c}) \tag{5.47}$$

so that $\mathbf{z} = \bar{\mathbf{z}}\boldsymbol{\zeta}$ and $\tilde{\mathbf{z}} = \bar{\mathbf{z}}\tilde{\boldsymbol{\zeta}}$. Therefore (5.43) can be rewritten as

$$\tilde{\boldsymbol{\zeta}}^\mathsf{T}\left(\boldsymbol{\mu}_\mathbf{M}(\boldsymbol{\zeta},\epsilon)\partial^2\boldsymbol{\zeta} + \boldsymbol{\mu}_\mathbf{C}(\boldsymbol{\zeta},\partial\boldsymbol{\zeta},\epsilon)\partial\boldsymbol{\zeta} + \boldsymbol{\mu}_\mathbf{K}\boldsymbol{\zeta} = \mathbf{F}\left(\boldsymbol{\zeta},\mathbf{z}^\mathrm{d}\right)\right) = \mathbf{0} \tag{5.48}$$

where $(\partial\boldsymbol{\zeta})_i = \partial_t\zeta_i$ for $i = 1,2,3$ and $(\partial\boldsymbol{\zeta})_i = \partial_\tau\zeta_i$ for $i > 3$. The expression (5.48) has to hold for all $\tilde{\boldsymbol{\zeta}}$, which implies the reduced order system evolution of the $3n+3$ coefficients in $\boldsymbol{\zeta}$

$$\boldsymbol{\mu}_\mathbf{M}(\boldsymbol{\zeta},\epsilon)\partial^2\boldsymbol{\zeta} + \boldsymbol{\mu}_\mathbf{C}(\boldsymbol{\zeta},\partial\boldsymbol{\zeta},\epsilon)\partial\boldsymbol{\zeta} + \boldsymbol{\mu}_\mathbf{K}\boldsymbol{\zeta} = \mathbf{F}\left(\boldsymbol{\zeta},\mathbf{z}^\mathrm{d}\right) \tag{5.49}$$

where $3n+3\times3n+3$ operators $\boldsymbol{\mu}_\mathbf{M}$, $\boldsymbol{\mu}_\mathbf{C}$, and $\boldsymbol{\mu}_\mathbf{K}$ and the $3n+3$ load vector $\mathbf{F}$ are given by

$$\boldsymbol{\mu}_\mathbf{M}(\boldsymbol{\zeta},\epsilon) = \int_0^1 \bar{\mathbf{z}}^\mathsf{T}\mathbf{M}(\bar{\mathbf{z}}\boldsymbol{\zeta},\epsilon)\bar{\mathbf{z}}\mathrm{d}X_1 \tag{5.50a}$$

$$\boldsymbol{\mu}_\mathbf{C}(\boldsymbol{\zeta},\partial\boldsymbol{\zeta},\epsilon) = \int_0^1 \bar{\mathbf{z}}^\mathsf{T}\mathbf{C}(\bar{\mathbf{z}}\boldsymbol{\zeta},\bar{\mathbf{z}}\partial\boldsymbol{\zeta},\epsilon)\bar{\mathbf{z}}\mathrm{d}X_1 \tag{5.50b}$$

$$\boldsymbol{\mu}_\mathbf{K} = \int_0^1 \begin{pmatrix} 0_{3\times3+3n} \\ 0_{3+3n\times3} \quad \bar{\mathbf{K}} \end{pmatrix} \mathrm{d}X_1 \tag{5.50c}$$

$$\bar{\mathbf{K}} = \begin{pmatrix} \alpha_1\bar{\mathbf{u}}'^\mathsf{T}\bar{\mathbf{u}}' & 0_{n\times n} & 0_{n\times n} \\ 0_{n\times n} & \bar{\mathbf{w}}'^\mathsf{T}\bar{\mathbf{w}}' & -\bar{\mathbf{w}}'^\mathsf{T}\bar{\boldsymbol{\psi}} \\ 0_{n\times n} & -\bar{\boldsymbol{\psi}}^\mathsf{T}\bar{\mathbf{w}}' & \alpha_1\alpha_2\bar{\boldsymbol{\psi}}'^\mathsf{T}\bar{\boldsymbol{\psi}}' + \bar{\boldsymbol{\psi}}^\mathsf{T}\bar{\boldsymbol{\psi}} \end{pmatrix} \tag{5.50d}$$

$$\mathbf{F}\left(\boldsymbol{\zeta},\mathbf{z}^\mathrm{d}\right) = \int_0^1 \tilde{\mathbf{z}}^\mathsf{T}\boldsymbol{\tau}\left(\bar{\mathbf{z}}\boldsymbol{\zeta},\mathbf{z}^\mathrm{d}\right)\mathrm{d}X_1 \tag{5.50e}$$

5.5.2 Basis functions

The set of basis functions for the deformation fields of the beam is obtained by solving the following homogeneous system for the nondimensionalized Timoshenko beam with free ends boundary conditions and a distributed system of supporting springs with stiffness per unit length κ

$$\ddot{u} - \alpha_1 u'' = 0 \tag{5.51a}$$

$$\ddot{w} - (w' - \psi)' + \alpha_3 w = 0 \tag{5.51b}$$

$$\alpha_2 \ddot{\psi} - \alpha_1 \alpha_2 \psi'' - (w' - \psi) = 0 \tag{5.51c}$$

$$u'(0,t) = u'(1,t) = 0, \tag{5.51d}$$

$$w'(0,t) - \psi(0,t) = w'(1,t) - \psi(1,t) = 0 \tag{5.51e}$$

$$\psi'(0,t) = \psi'(1,t) = 0 \tag{5.51f}$$

where α_1 and α_2 are defined in (5.28), and

$$\alpha_3 = \frac{\kappa \ell^2}{kGA} \tag{5.52}$$

is a nondimensional measure of the stiffness of the supporting spring with respect to the shear stiffness of the body. The solution is obtained by the usual separation of variables $u(X_1,\tau) = \bar{u}(X_1)\exp(\mathrm{I}\omega\tau)$, $w(X_1,\tau) = \bar{w}(X_1)\exp(\mathrm{I}\omega\tau)$, and $\psi(X_1,\tau) = \bar{\psi}(X_1)\exp(\mathrm{I}\omega\tau)$, where $\omega > 0$ is the angular frequency and I is the imaginary unit. Since (5.51a) is uncoupled the solution for $\bar{u}$ is easily obtained as

$$\bar{u}_i(X_1) = B\cos(i\pi X_1) \tag{5.53}$$

To obtain the natural frequencies and associated eigenfunctions for w and ψ we follow the approach in [78], which is based on the solution of a vector eigenvalues problem for the system of two coupled second order differential equations for the transverse displacement and for the the rotation of the cross section. In our case, the two equations are (5.51b) and (5.51b). This allows to enforce boundary conditions for free ends in a direct way. A different approach based on the derivation of one fourth order governing equation obtained by combining (5.51b) and (5.51b) is presented in the original work of Timoshenko [76]. However in this case the application of boundary conditions requires special attention [79]. The vector eigenvalues problem has different general solutions depending on the choice of material parameters [78]. The general solution of the eigenvalues problem is

sought by considering the vector evaluated function $\exp(\lambda x)\begin{pmatrix} \bar{W} & \bar{\Psi} \end{pmatrix}^{\mathsf{T}}$, where $\bar{W}$ and $\bar{\Psi}$ are constants. Such function is a solution for some positive constant λ if and only if

$$\begin{pmatrix} \lambda^2+\beta_1 & -\lambda \\ \beta_3\lambda & \lambda^2+\beta_2 \end{pmatrix}\begin{pmatrix} \bar{W} \\ \bar{\Psi} \end{pmatrix} = \begin{pmatrix} 0 \\ 0 \end{pmatrix} \tag{5.54}$$

with nondimensional parameters β_i defined by

$$\beta_1 = \omega^2 - \alpha_3, \quad \beta_2 = \frac{1}{\alpha_1}\left(\omega^2 - \frac{1}{\alpha_2}\right), \quad \beta_3 = \frac{1}{\alpha_1\alpha_2} \tag{5.55}$$

The roots λ^2 of the characteristic polynomial $\lambda^4 + (\beta_1+\beta_2+\beta_3)\lambda^2 + \beta_1\beta_2 = 0$ are

$$\lambda^2_{1,2} = -\frac{1}{2}(\beta_1+\beta_2+\beta_3)\left(1 \pm \sqrt{\Delta}\right) \tag{5.56}$$

$$\Delta = 1 - \frac{4\beta_1\beta_2}{(\beta_1+\beta_2+\beta_3)^2} \tag{5.57}$$

In order for λ^2 to be real it must be $\Delta > 0$, which is satisfied for $\beta_1\beta_2 < \gamma^2/4$, where $\gamma = \beta_1+\beta_2+\beta_3$. The special case $\lambda^2 = 0$ occurs when $\Delta = 1$, that is $\beta_1\beta_2 = 0$ or

$$\beta_1 = 0 \Rightarrow \omega^2 = \alpha_3, \tag{5.58}$$

$$\beta_2 = 0 \Rightarrow \omega^2 = \alpha_2 \text{ or } \alpha_1 = 0 \tag{5.59}$$

This corresponds to rigid body motions of the system [79]. Here we consider the system made of a material with shear modulus ten times smaller than the Young's modulus, and we consider the overall shear stiffness $kGA\ell^2$ to be one hundred times larger than the bending stiffness YI. Moreover we set the supporting springs to be softer than the beam (with ratio 1/2). Therefore parameters α_i are assigned to the numerical values in Table 5.1.

Table 5.1: Nondimensional parameters of the Timoshenko beam

α_1	$\alpha_1\alpha_2$	α_3
10	10^{-2}	0.5

Let ω_Δ be the root of $\Delta = 0$ and ω_γ be the root of $\gamma = 0$; with the choice of parameters listed above we have $\omega_\Delta = 0.707$ and $\omega_\gamma = 0.674$. Moreover, $\omega_\lambda = 0.707$ is the root of $\beta_1\beta_2 = 0$. The condition $\Delta > 0$ implies $\omega > \omega_\Delta$; therefore it must be $\gamma > 0$ since this is the case for $\gamma(\omega > \omega_\gamma) > 0$, and in this case $\omega_\gamma < \omega_\Delta$. For $\Delta > 0$ and $\gamma > 0$ we have

$\lambda_1 = \pm \mathrm{I}\nu_1$ with $\nu_1^2 = \frac{\gamma}{2}\left(\sqrt{\Delta}+1\right)$; $\Delta > 0$ also implies $\beta_1\beta_2 < 0$, since this is the case for $\beta_1\beta_2$ evaluated at $\omega > \omega_\lambda$, and $\omega_\lambda = \omega_\Delta$. Therefore $\sqrt{\Delta} > 1$ with $\lambda_2 = \pm\nu_2$ and $\nu_2^2 = \frac{\gamma}{2}\left(\sqrt{\Delta}-1\right)$. Here $\Delta > 0$ dictates $\omega > \omega_\Delta$. The general solution is therefore given by

$$\begin{aligned}\Phi(x) = C_1 \begin{pmatrix} \sin\nu_1 X_1 \\ -\frac{\beta_1-\nu_1^2}{\nu_1}\cos\nu_1 X_1 \end{pmatrix} + C_2 \begin{pmatrix} \cos\nu_1 X_1 \\ \frac{\beta_1-\nu_1^2}{\nu_1}\sin\nu_1 X_1 \end{pmatrix} \\ + C_3 \begin{pmatrix} \sinh\nu_2 X_1 \\ \frac{\beta_1+\nu_2^2}{\nu_2}\cosh\nu_2 X_1 \end{pmatrix} + C_4 \begin{pmatrix} \cosh\nu_2 X_1 \\ \frac{\beta_1+\nu_2^2}{\nu_2}\sinh\nu_2 X_1 \end{pmatrix}\end{aligned} \tag{5.60}$$

By imposing the free end boundary conditions at $X_1 = 0$ and $X_1 = 1$ we obtain the linear algebraic relations involving C_3 and C_4 and coefficient matrix. The nontrivial solutions of the system are obtained by investigating the condition for rank deficiency of the coefficients matrix, which translates into the following condition for the determinant

$$-\cos\nu_1\cosh\nu_2 + \frac{\nu_1(\nu_1^2-\beta_1)}{\nu_2(\nu_2^2+\beta_1)}\sin\nu_1\sinh\nu_2 + 1 = 0 \tag{5.61}$$

All parameters in the characteristic equation depend on ω and on the material and geometric parameters of the system. Therefore, once the material and the geometry are defined the characteristic equation is a nonlinear function of ω only. The first seven roots of the characteristic equation that determine the corresponding modes are given in Table 5.2. The mode shapes are normalized with respect to the maximum amplitude for $x \in (0,1)$ (boundaries not included). The corresponding dimensional values of the frequencies are obtained from the ones in Table 5.2 as $\omega/\bar{t} = \frac{\omega}{\ell}\sqrt{\frac{kG}{\varrho}}$.

Table 5.2: First seven roots of the characteristic equation for the linear modes

n	1	2	3	4	5	6	7
ω	2.184	5.004	8.351	11.81	15.28	18.68	22.02

5.6 Feedback and Control Law

Let $\boldsymbol{\eta}(s^*) = \eta_1(s^*)\mathbf{E}_1 + \eta_2(s^*)\mathbf{E}_2$ be the position in the global frame of a point on the substrate in which the mechanism is deployed, parametrized by the arclength s^*. Moreover, let

$$\mathbf{p}(X_1) = \mathbf{x} - X_2\mathbf{e}_2 = \mathbf{d} + (X_1 - 1)\mathbf{e}_1 \tag{5.62}$$

be the point on the undeformed axes for $\delta = 1$, and $\mathbf{g}$ be a vector with constant components in the body reference frame so that $\dot{\mathbf{g}} = \mathbf{W}\mathbf{g}$. The desired state is defined by

$$\mathbf{z}^{\mathrm{d}} = \begin{pmatrix} (\boldsymbol{\eta}(s^*) - \mathbf{g}) \cdot \mathbf{e}_1 \\ (\boldsymbol{\eta}(s^*) - \mathbf{g}) \cdot \mathbf{e}_2 \\ \theta_{\boldsymbol{\eta}}(s^*) \\ 0 \\ (\boldsymbol{\eta}(\bar{s}(X_1)) - \mathbf{g}) \cdot \mathbf{e}_2 \\ 0 \end{pmatrix}, \tag{5.63}$$

where $\tan\theta_{\boldsymbol{\eta}} = \frac{\boldsymbol{\eta}' \cdot \mathbf{e}_2}{\boldsymbol{\eta}' \cdot \mathbf{e}_1}$, so that $\theta_{\boldsymbol{\eta}}$ is the global orientation of the tangent vector $\boldsymbol{\eta}'$, and $\bar{s}(X_1)$ is the arclength that defines a point on the curve corresponding to the solution of the minimization problem $\bar{s}(X_1) = \arg\min_s \|\mathbf{p}(X_1) - \boldsymbol{\eta}(s)\|$, which is solved by the roots s of the scalar equation $(\mathbf{p}(X_1) - \boldsymbol{\eta}(s)) \cdot \boldsymbol{\eta}'(s) = 0$.

We consider the rigid body motion to be much slower than the shape morphing with respect to the rigid substrate. Therefore we restrict the analysis to a class of hyper-redundant slender mechanisms that are soft enough to morph continuously when moving forward with respect to the substrate. This hypothesis is formalized by considering the limit case $\epsilon \ll 1$, so that fields that depend on the slow time τ are nearly steady-state with respect to the evolution in t. Within this framework, the only nonzero entries of the nonlinear matrix operator in (5.30) are those defined by M_{ij}, $i, j \leq 3$ (they still depend on deformaiton fields $u^\star$, $w^\star$, and $\psi^\star$), and $\mathbf{M}$ can be represented in block form as

$$\mathbf{M} = \begin{pmatrix} \mathbf{M}_{\mathbf{x}} & \mathbf{0}_{3\times 3} \\ \mathbf{0}_{3\times 3} & \mathbf{0}_{3\times 3} \end{pmatrix} \tag{5.64}$$

with entries of the 3×3 block $\mathbf{M}_{\mathbf{x}}$ given in (5.30). The operator $\boldsymbol{\mu}_{\mathbf{M}}$ can be correspondingly block partitioned, with the only nonzero block being the upper left 3×3 one given by

$$\boldsymbol{\mu}_{\mathbf{M}_{\mathbf{x}}} = \int_0^1 \mathbf{M}_{\mathbf{x}} \mathrm{d}X_1 \tag{5.65}$$

as follows from the definition of the basis functions in (5.47) and by the definition in (5.50). For $\epsilon \ll 1$ the matrix operator $\mathbf{C}$ can be partitioned as

$$\mathbf{C} = \begin{pmatrix} \mathbf{C}_{\mathbf{x}} & \mathbf{C}_{\mathbf{xU}} \\ \mathbf{C}_{\mathbf{xU}}^{\mathsf{T}} & \mathbf{0}_{3\times 3} \end{pmatrix} \tag{5.66}$$

with nonzero 3×3 blocks following from (5.38) for $\epsilon \ll 1$. Correspondingly we can define the 3×3 and the $3 \times 3n$ operators $\boldsymbol{\mu}_{\mathbf{C_x}}$ and $\boldsymbol{\mu}_{\mathbf{C_{xU}}}$ following from the induced block partition of the operator $\boldsymbol{\mu}_{\mathbf{C}}$ in (5.50)

$$\boldsymbol{\mu}_{\mathbf{C}} = \begin{pmatrix} \boldsymbol{\mu}_{\mathbf{C_x}} & \boldsymbol{\mu}_{\mathbf{C_{xU}}} \\ \boldsymbol{\mu}_{\mathbf{C_{xU}}}^{\mathsf{T}} & \mathbf{0}_{3n\times 3n} \end{pmatrix} \tag{5.67}$$

Passivity based controller is a design technique that achieves system stabilization via the route of passivation, that is, rendering the closedloop system passive with a desired storage function (that usually qualifies as a Lyapunov function for the stability analysis.)[80]. It involves in controlling a system with the intention at making the closed-loop system passive. The block diagram of passivity based control is shown in Fig 5.3. Therefore, by partition the state vector as $\boldsymbol{\zeta}(t) = (\boldsymbol{\xi}(t), \mathbf{q}(0))$, where the first block collects the 3 rigid body degrees of freedom and the second block collects the $3n$ deformation degrees of freedom, we rewrite the system (5.49) as

$$\boldsymbol{\mu}_{\mathbf{M_x}}\ddot{\boldsymbol{\xi}} + \boldsymbol{\mu}_{\mathbf{C_x}}\dot{\boldsymbol{\xi}} = \mathbf{F}_{\boldsymbol{\xi}} \tag{5.68}$$

$$\boldsymbol{\mu}_{\mathbf{C_{xU}}}^{\mathsf{T}}\dot{\boldsymbol{\xi}} + \bar{\mathbf{K}}\mathbf{q} = \mathbf{F}_{\mathbf{q}} \tag{5.69}$$

where $\bar{\mathbf{K}}$ is defined in (5.50) and $\mathbf{F}_{\boldsymbol{\xi}}$ and $\mathbf{F}_{\mathbf{q}}$ are the 3 and $3n$ blocks induced by the partition of $\mathbf{F}$ in (5.50). In order to set the shape morphing as a static deformation, we choose the nonlinear feedback

$$\mathbf{F}_{\mathbf{q}} = \boldsymbol{\mu}_{\mathbf{C_{xU}}}^{\mathsf{T}}\dot{\boldsymbol{\xi}} + \alpha_3(\mathbf{H}\mathbf{q} - \mathbf{f}_{\mathbf{q}}(\mathbf{q}^{\mathrm{d}})), \tag{5.70}$$

$$\mathbf{H} = \int_0^1 \boldsymbol{\varphi}^{\mathsf{T}}\boldsymbol{\varphi}\mathrm{d}X_1, \quad \mathbf{f}_{\mathbf{q}}(\mathbf{q}^{\mathrm{d}}) = \int_0^1 \boldsymbol{\varphi}^{\mathsf{T}}\mathbf{q}^{\mathrm{d}}\mathrm{d}X_1 \tag{5.71}$$

where the $3 \times n$ matrix $\boldsymbol{\varphi}$ is given by $(\bar{\mathbf{u}}, \bar{\mathbf{w}}, \bar{\boldsymbol{\psi}})^{\mathsf{T}}$ (lower right block of $\mathbf{z}$ in (5.47)), and $\mathbf{q}^{\mathrm{d}} = (0, (\boldsymbol{\eta}(\bar{s}(X_1)) - \mathbf{g}) \cdot \mathbf{e}_2, 0)$ is the desired state for the deformation field. Therefore, in a finite dimensional subset of L^2 the nonlinear feedback $\mathbf{F}_{\mathbf{q}}$ dictates the shape morphing of the slender mechanism to the substrate to which it is coupled, and α_3 defined in (5.52) can be considered as a tuning parameter (proportional gain in the time varying case) that measures the stiffness of the elastic supports with respect to the stiffness of the body. Therefore a large value of α_3 means that the supports are much stiffer that the body and the shape morphs to the substrate in a passive way, since the actuation provided by the surface through the supports overcomes the elastic resistance of the body. For very large α_3 the second term becomes dominant (as long as the state $\boldsymbol{\xi}$ and its time derivative

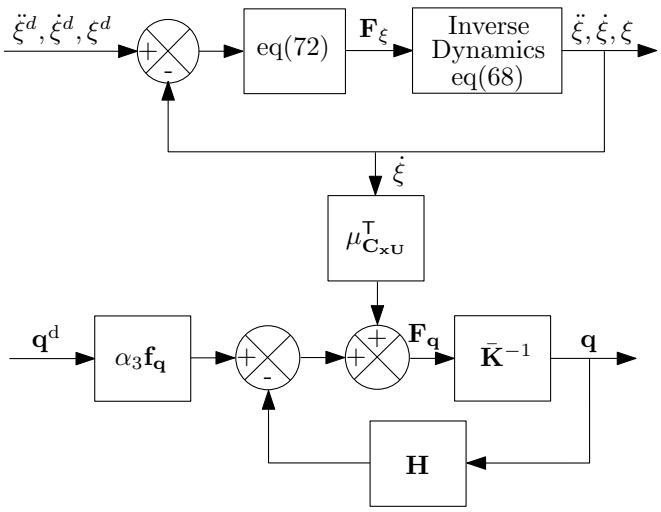

Figure 5.3: Block diagram of the passivity based control system.

are bounded) and the feedback ensures convergence of $\mathbf{q}$ to the desired state in a finite dimensional subset of L^2.

The loop for the path tracking problem (rigid body motion) is closed by considering the following passivity based feedback [4, Chapter 8]

$$\mathbf{F}_{\boldsymbol{\xi}} = \boldsymbol{\mu}_{\mathbf{M_x}}(\ddot{\boldsymbol{\xi}}^d + \boldsymbol{\Lambda}\dot{\boldsymbol{\gamma}}) + \boldsymbol{\mu}_{\mathbf{C_x}}(\dot{\boldsymbol{\xi}}^d + \boldsymbol{\Lambda}\boldsymbol{\gamma}) + \mathbf{L}(\dot{\boldsymbol{\gamma}} + \boldsymbol{\Lambda}\boldsymbol{\gamma}) \tag{5.72}$$

where $\boldsymbol{\Lambda}$ and $\mathbf{L}$ are 3×3 symmetric positive definite gain matrices, and $\boldsymbol{\gamma} = \boldsymbol{\xi}^{\mathrm{d}} - \boldsymbol{\xi}$ is the error with desired state $\boldsymbol{\xi}^{\mathrm{d}}$ given by the first three components of $\mathbf{z}^{\mathrm{d}}$ in (5.63). The time derivatives of the desired state are

$$\dot{\boldsymbol{\xi}}^{\mathrm{d}} = \begin{pmatrix} \left(\dot{s^*}\boldsymbol{\eta}'(s^*) - \dot{\mathbf{g}}\right) \cdot \mathbf{e}_1 \\ \left(\dot{s^*}\boldsymbol{\eta}'(s^*) - \dot{\mathbf{g}}\right) \cdot \mathbf{e}_2 \\ \dot{s^*}\kappa_{\boldsymbol{\eta}}(s^*) \end{pmatrix}, \tag{5.73}$$

$$\ddot{\boldsymbol{\xi}}^{\mathrm{d}} = \begin{pmatrix} \left(\ddot{s^*}\boldsymbol{\eta}'(s^*) + \dot{s^*}^2\boldsymbol{\eta}''(s^*) - \ddot{\mathbf{g}}\right) \cdot \mathbf{e}_1 \\ \left(\ddot{s^*}\boldsymbol{\eta}'(s^*) + \dot{s^*}^2\boldsymbol{\eta}''(s^*) - \ddot{\mathbf{g}}\right) \cdot \mathbf{e}_2 \\ \ddot{s^*}\kappa_{\boldsymbol{\eta}}(s^*) + \dot{s^*}^2\kappa'_{\boldsymbol{\eta}}(s^*) \end{pmatrix} \tag{5.74}$$

where $\dot{s^*}$ can be interpreted as the forward speed of the system since $s^*(t)$ is the prescribed trajectory of the arclength on the path that drives the path tracking, $\kappa_{\boldsymbol{\eta}} = \theta'_{\boldsymbol{\eta}} = \|\boldsymbol{\eta}''\|$ is the curvature of the substrate, and $\boldsymbol{\eta}'' = \kappa_{\boldsymbol{\eta}}\mathbf{N}$, with $\mathbf{N}$ normal to the path. The closed

loop system can therefore be written as

$$\boldsymbol{\mu}_{\mathbf{M_x}}(\boldsymbol{\xi},\mathbf{q})(\ddot{\boldsymbol{\gamma}}+\boldsymbol{\Lambda}\dot{\boldsymbol{\gamma}})+(\boldsymbol{\mu}_{\mathbf{C_x}}(\boldsymbol{\xi},\mathbf{q})+\mathbf{L})(\dot{\boldsymbol{\gamma}}+\boldsymbol{\Lambda}\boldsymbol{\gamma})=\mathbf{0} \tag{5.75}$$

$$(\bar{\mathbf{K}}+\alpha_3\mathbf{H})\mathbf{q}=\alpha_3\mathbf{f_q}(\mathbf{q}^{\mathrm{d}}) \tag{5.76}$$

We can now establish global asymptotic stability of the error $\boldsymbol{\gamma}$.

Proposition 1. *The error $\boldsymbol{\gamma}$ and error rate $\dot{\boldsymbol{\gamma}}$ in the closed loop system* (5.75) *are globally asymptotically stable.*

Proof. Let $\boldsymbol{\beta}=\dot{\boldsymbol{\gamma}}+\boldsymbol{\Lambda}\boldsymbol{\gamma}$. Consider the candidate Lyapunov function

$$V=\frac{1}{2}\boldsymbol{\beta}^{\mathsf{T}}\boldsymbol{\mu}_{\mathbf{M_x}}\boldsymbol{\beta}+\boldsymbol{\gamma}^{\mathsf{T}}\boldsymbol{\Lambda}\mathbf{L}\boldsymbol{\gamma} \tag{5.77}$$

The time derivative along the trajectories defined by (5.75) gives

$$\begin{aligned}\dot{V}&=\boldsymbol{\beta}^{\mathsf{T}}\boldsymbol{\mu}_{\mathbf{M_x}}\dot{\boldsymbol{\beta}}+\frac{1}{2}\boldsymbol{\beta}^{\mathsf{T}}\dot{\boldsymbol{\mu}}_{\mathbf{M_x}}\boldsymbol{\beta}+2\boldsymbol{\gamma}^{\mathsf{T}}\boldsymbol{\Lambda}\mathbf{L}\dot{\boldsymbol{\gamma}}\\&=\frac{1}{2}\boldsymbol{\beta}^{\mathsf{T}}(\dot{\boldsymbol{\mu}}_{\mathbf{M_x}}-2\boldsymbol{\mu}_{\mathbf{C_x}})\boldsymbol{\beta}-\boldsymbol{\beta}^{\mathsf{T}}\mathbf{L}\boldsymbol{\beta}+2\boldsymbol{\gamma}^{\mathsf{T}}\boldsymbol{\Lambda}\mathbf{L}\dot{\boldsymbol{\gamma}}\end{aligned} \tag{5.78}$$

From the definition of $\mathbf{C}$ in (5.36) and (5.37) it follows that the matrix $\dot{\boldsymbol{\mu}}_{\mathbf{M_x}}-2\boldsymbol{\mu}_{\mathbf{C_x}}$ is skew symmetric; therefore the first term on the right hand side is zero. Moreover, by using the definition of $\boldsymbol{\beta}$

$$\dot{V}=-\dot{\boldsymbol{\gamma}}^{\mathsf{T}}\mathbf{L}\dot{\boldsymbol{\gamma}}-\boldsymbol{\gamma}^{\mathsf{T}}\boldsymbol{\Lambda}^{\mathsf{T}}\mathbf{L}\boldsymbol{\Lambda}\boldsymbol{\gamma}\leq 0 \tag{5.79}$$

with the equality holding for $\boldsymbol{\gamma}=\mathbf{0}$ and $\dot{\boldsymbol{\gamma}}=\mathbf{0}$, that therefore define a globally asymptotically stable equilibrium. □

5.7 Simulation Results and Numerical Examples

We consider a system made of a material with shear modulus ten times smaller than the Young's modulus ($\alpha_1=0.1$). Moreover, we consider the overall shear stiffness $kGA\ell^2$ to be one hundred times larger than the bending stiffness EI ($\alpha_1\alpha_2=100$). As emerged from the theoretical analysis, two key parameters are the kinematics $s^*(t)$ of the driving arclength on the path, and the value of α_3; specifically, $s^*(t)$ determines how fast is the rigid body motion of the system, and therefore the validity of the simplifying hypothesis $\epsilon\ll 1$ (upon which we have discarded terms in $O(\epsilon)$) that characterizes the slow time,

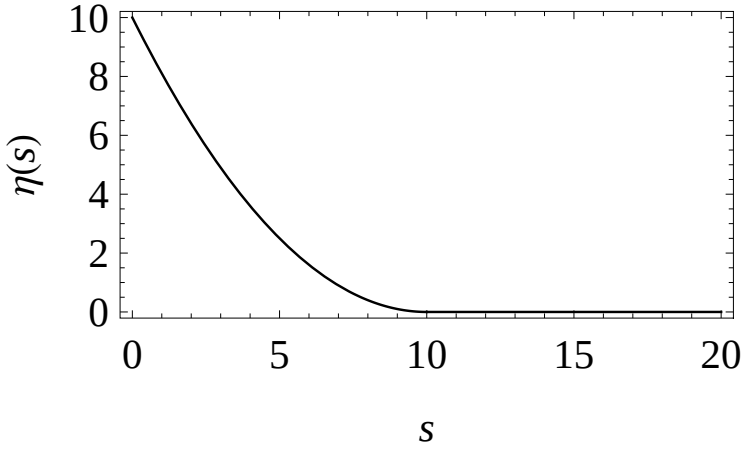

Figure 5.4: Sketch of the geometry of the path defining the rigid substrate.

while α_3 determines how rigid is the support with respect to the body. We illustrate this by considering different combinations.

We set the gap function $\mathbf{g}$ to zero, set $\mathbf{\Lambda}$ to be the identity matrix, and $\mathbf{L} = \text{diag}(4, 10, 20)$. The path profile $\boldsymbol{\eta}$ is parametrized as

$$\boldsymbol{\eta}(s) = s\mathbf{E}_1 + 0.1(s-10)^2(\mathfrak{u}(s) - \mathfrak{u}(s-10))\mathbf{E}_2, \tag{5.80}$$

where $\mathfrak{u}$ is the unit step function, which evaluates to 1 whenever its argument is greater than 0. As shown in Fig. 5.4 the path is the merge of a parabolic profile and of a straight profile.

As a first illustration we consider a system with relatively stiff supports with respect to the stiffness of the body ($\alpha_3 = 20$, see eq. (5.52)). In this case we consider the family of driving parameters $s^*(t) = vt$, where v is assigned and determines how fast is the rigid body motion. We consider one degree of freedom for each deformation field, and therefore the dimension of $\mathbf{q}$ is 3. Tracking errors $\|\mathbf{e}_i \cdot \boldsymbol{\eta}(s^*(t)) - d_i(t)\|$, $i = 1, 2$, and $|\theta_{\boldsymbol{\eta}}(s^*(t)) - \theta(t)|$ are shown in Figures 5.5 and 5.6 for $v = 0.005$ and 0.03 to characterize slow and fast motions, respectively. Consistently with theoretical predictions, the Figures reveal that the tracking error corresponding to fast motion is in general larger on the part of the portion of the path with nonzero curvature. For $s^*(t) = 0.03t$, Figure 5.7(a) shows four snapshots of the system: the initial condition $t = 0$; an intermediate state on the parabolic portion of the path at point $s = 1.5$, a state across the point $s = 10$ where the change of curvature occurs, and the final state where the head overlaps to the last defined point of the path ($s = 15$). The zoom of the snapshot around $s = 10$ is shown in

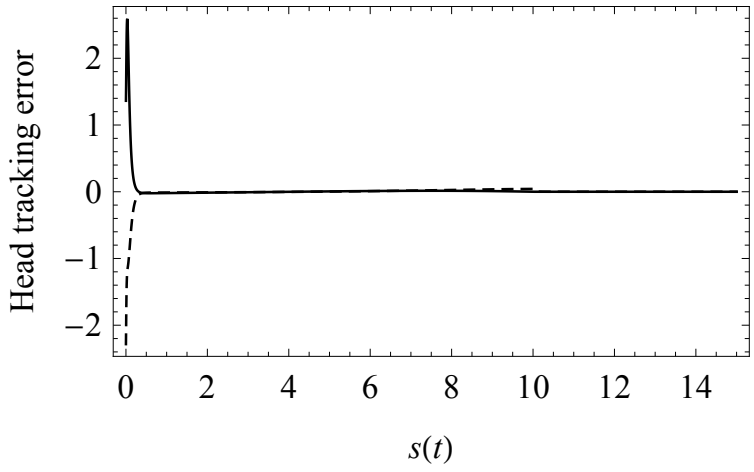

(a)

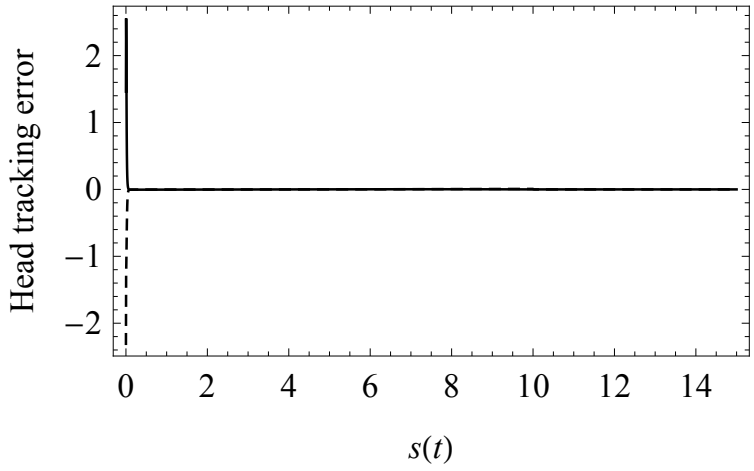

(b)

Figure 5.5: Head tracking errors $|\mathbf{e}_1 \cdot \boldsymbol{\eta}(s^*(t)) - d_1(t)|$ (solid line) and $|\mathbf{e}_2 \cdot \boldsymbol{\eta}(s^*(t)) - d_2(t)|$ (dashed line) for $s(t) = 0.005t$; (a) $\alpha_3 = 20$ and $s^*(t) = 0.03t$ and (b) $\alpha_3 = 20$ and $s^*(t) = 0.005t$.

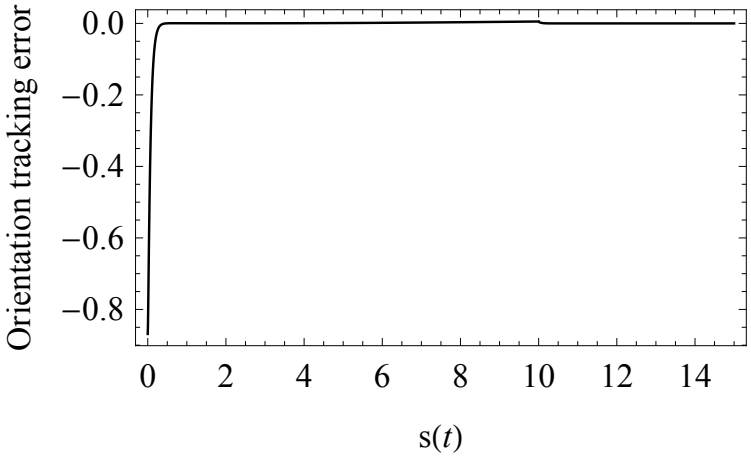

(a)

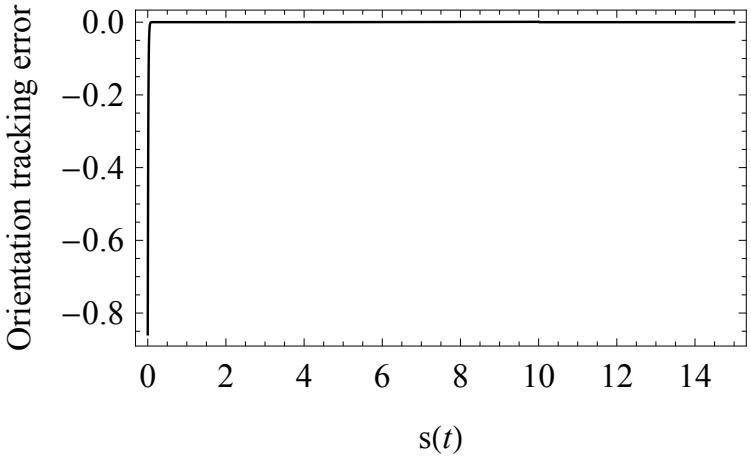

(b)

Figure 5.6: (a) Orientation tracking errors for $\alpha_3 = 20$ and $s^*(t) = 0.03t$; (b) Orientation tracking errors for $\alpha_3 = 20$ and $s^*(t) = 0.005t$.

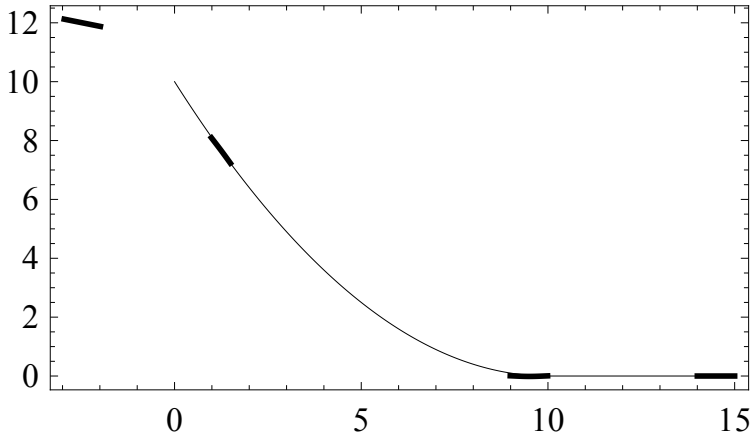

(a)

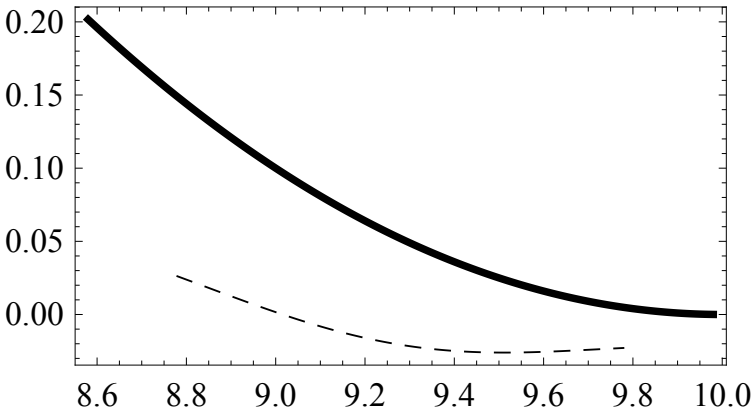

(b)

Figure 5.7: For $\alpha_3 = 20$ and $s^*(t) = 0.03t$ (a) four snapshots of the system and (b) snapshot around $s = 10$, with substrate represented by continuous line.

Fig. 5.7(b).

To illustrate the effect of the relative stiffness α_3, we consider the driving kinematics $s^*(t) = 0.03t$ and two values of α_3. As shown in Figure 5.8 this parameter does not affect the rigid body motion (head tracking error), which is expected (see equation (5.75)) since α_3 is a relative measure of stiffness of the supports with respect to the stiffness of the beam. Note that Fig. 5.8(a) is the same as Fig. 5.5(a) but zoomed near $s = 0$ to enhance the variation of the error. Same consideration applies to the orientation tracking error as shown by Fig. 5.9 when compared with Fig. 5.6(a) (same $s^*(t)$). On the other hand, the shape morphing is affected by α_3 (see equation (5.75)) as qualitatively shown in Fig. 5.10 in which the same snapshot in Fig. 5.7(b) is represented for $\alpha_3 = 0.5$ ($\alpha_3 = 20$ in Fig. 5.7(b)). Indeed with increasing α_3 the actuation from the rigid surface through the elastic supports becomes relatively higher than the stiffness of the body that tends to react against the shape change.

For the same profile $\boldsymbol{\eta}$, for $\alpha_3 = 20$ and $s^*(t) = 0.03$, Fig. 5.11(a) shows the time histories of the the the L^2 error norms defined by

$$\|\boldsymbol{\eta} \cdot \mathbf{e}_2 - w^\star\|_{L^2} := \left(\int_0^1 (\boldsymbol{\eta} \cdot \mathbf{e}_2 - w^\star)^2 \, \mathrm{d}X_1 \right)^{\frac{1}{2}} \tag{5.81}$$

with increasing number of basis functions to approximate the spatial fields. Curves are virtually overlapped, which reveals that within the simplified model considered here the first mode captures the salient features of the system in terms of shape morphing, as expected by the hypothesis that the radius of curvature of the substrate is much larger that the length of the mechanism, and therefore locally it is not expected to have sharp changes of curvature. To further show the matching between curves, the difference in the L^2 norm for three pairs of consecutive odd number of basis functions is shown in Fig. 5.11. For the class of systems considered here one mode is therefore sufficient to describe the shape morphing.

The deformed shapes obtained with one mode and with seven modes are shown in Figure 5.12, with the proximity between the two curves confirming that the approximation based on the fundamental modes is accurate within the class of problems considered here.

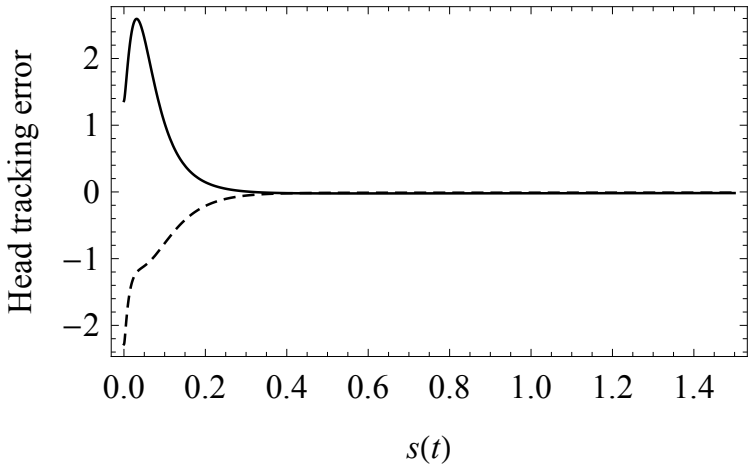

(a)

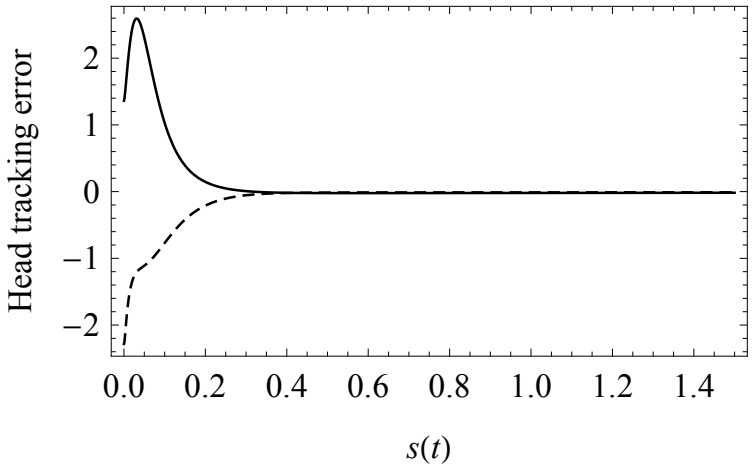

(b)

Figure 5.8: Head tracking errors $|\mathbf{e}_1 \cdot \boldsymbol{\eta}(s^*(t)) - d_1(t)|$ (solid line) and $|\mathbf{e}_2 \cdot \boldsymbol{\eta}(s^*(t)) - d_2(t)|$ (dashed line) for $s^*(t) = 0.03t$; (a) $\alpha_3 = 20$; (b) $\alpha_3 = 0.5$. Results are computed for $0 \leq s \leq 15$, but they are plotted only for $0 \leq s \leq 1.5$ in order to zoom on the variation of the tracking error.

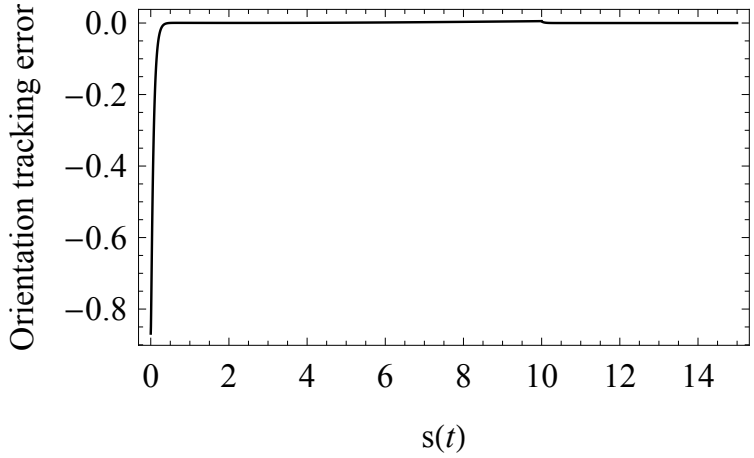

Figure 5.9: Orientation tracking error for $\alpha_3 = 0.5$ and $s^*(t) = 0.03t$.

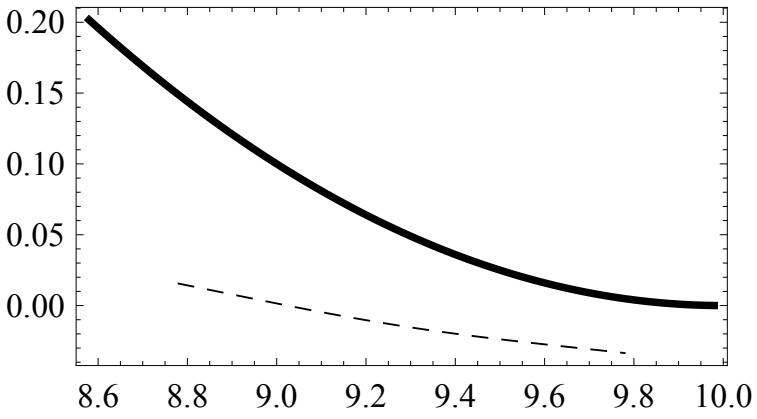

Figure 5.10: For $\alpha_3 = 0.5$, snapshot of the deformed shape (dashed line) with a near portion of the rigid substrate represented by the continuous line.

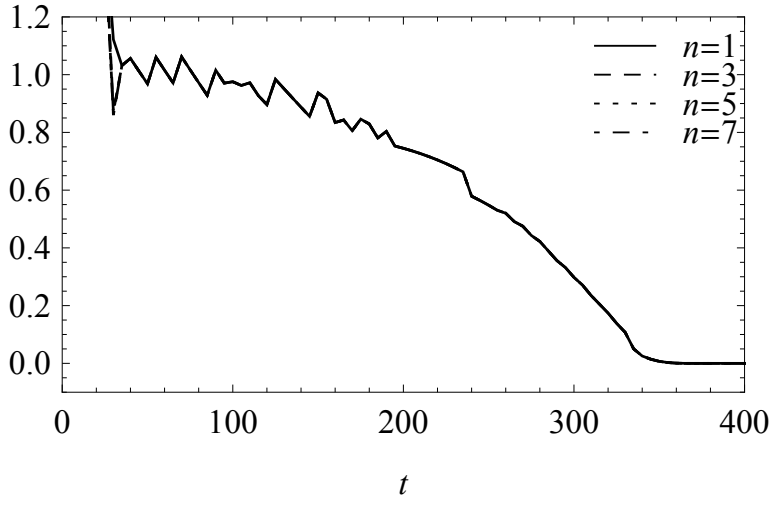

(a)

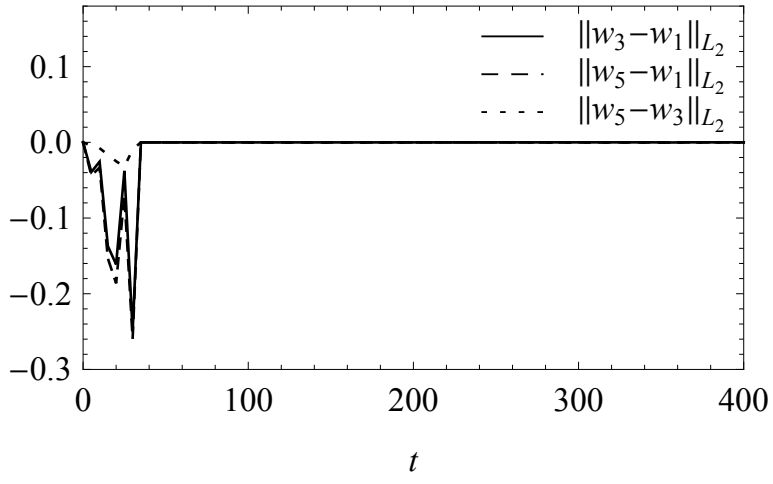

(b)

Figure 5.11: (a) L_2 error norm, $\|w_n^\star - \boldsymbol{\eta} \cdot \mathbf{e}_2\|_{L^2}$ with number of basis functions $n = 1, 3, 5, 7$; (b) L_2 error norms $\left\|w_n^\star - w_{n-2}^\star\right\|_{L^2}$ for $n = 1, 3, 5$.

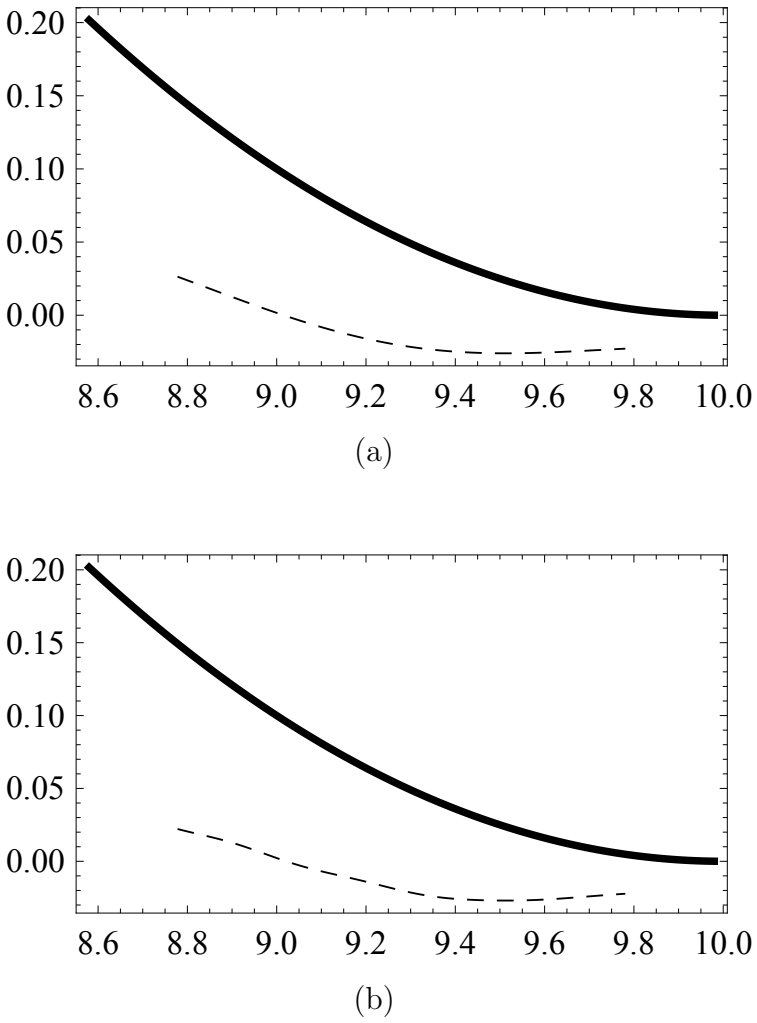

Figure 5.12: Snapshot of the system for $\alpha_3 = 20$ and $s^*(t) = 0.03t$ at $s = 10$; (a) deflection field approximated with one basis function; (b) deflection field approximated with seven basis functions.

5.8 Conclusions

We have presented a distributed parameters model for the forward locomotion and shape morphing of a slender hyper-redundant mechanism. The mechanism is coupled with a rigid substrate by a distributed system of compliant elements, and the deformability of the system is modeled by adopting the planar linear Timoshenko beam theory. Two time scales are introduced to formalize the modeling assumption that the evolution of the rigid body motion is much slower than the evolution of the shape adaptation with respect to a coupled substrate. The control problem is posed in the appropriate product Hilbert space in terms of a suitable weak form that encodes the coupling between rigid body motion and deformation. A reduced order model is introduced, based on space-time separation and projection on spatial mode shapes of Timoshenko beams. The L^2 norm convergence of the approximate solution is assessed, which reveals that for this class of systems one spatial basis function gives accurate results. The influence of key parameters is illustrated by numerical simulations.

Current and future work include the consideration of deformable substrate models and the formulation of the inverse problem to use the device as a sensor with respect to geometry and constitutive parameters of the environment in which it is deployed. Future plans include the hardware realization of a hyper-redundant robotic device for autonomous operation in a variety of environments.

Acknowledgement

This work was supported by the Natural Sciences and Engineering Research Council of Canada (NSERC) through the Discovery Program.

References

[1] A. A. Shabana, Dynamics of Multibody Systems, 3rd Edition, Cambridge University Press, 2010.

[2] C. Zehetner, H. Irschik, Displacement compensation of beam vibrations caused by rigid-body motions, Smart Materials and Structures 14 (4) (2005) 862. http://stacks.iop.org/0964-1726/14/i=4/a=046

[3] C. Altafini, Following a path of varying curvature as an output regulation problem, IEEE Transactions on Automatic Control 47 (9) (2002) 1551–1556. doi:{10.1109/TAC.2002.802750}.

[4] M. W. Spong, S. Hutchinson, M. Vidyasagar, Robot Modeling and Control, Wiley, 2006.

[5] L. Gaul, J. Becker, Model-based piezoelectric hysteresis and creep compensation for highly-dynamic feedforward rest-to-rest motion control of piezoelectrically actuated flexible structures, International Journal of engineeing Science 47 (11-12) (2009) 1193–1207. doi:{10.1016/j.ijengsci.2009.07.006}.

[6] F. Boyer, S. Ali, M. Porez, Macrocontinuous Dynamics for Hyperredundant Robots: Application to Kinematic Locomotion Bioinspired by Elongated Body Animals, IEEE Transactions on Robotics 28 (2) (2012) 303–317. doi:{10.1109/TRO.2011.2171616}.

[7] F. Boyer, D. Primault, The Poincare-Chetayev equations and flexible multibody systems, PMM Journal of Applied Mathematics and Mechanics 69 (6) (2005) 925–942. doi:{10.1016/j.jappmathmech.2005.11.015}.

[8] F. Boyer, M. Porez, A. Leroyer, M. Visonneau, Fast Dynamics of an Eel-Like Robot-Comparisons With Navier-Stokes Simulations, IEEE Transaction on Robotics 24 (6) (2008) 1274–1288. doi:{10.1109/TRO.2008.2006249}.

[9] S.-M. Kim, H. Kim, K. Boo, M. J. Brennan, Demonstration of non-collocated vibration control of a flexible manipulator using electrical dynamic absorbers, Smart Materials and Structures 22 (12). doi:{10.1088/0964-1726/22/12/127001}.

[10] F. Bellezza, L. Lanari, G. Ulivi, Exact modeling of the slewing flexible link, Proceedings of the IEEE International Conference on Robotics and Automation (1999) 734–739.

[11] M. W. D. White, G. R. Heppler, Timoshenko model of a flexible slewing link, Proceedings of the American Control Conference (1995) 2815–2819.

[12] S. DanielBerhe, H. Unbehauen, Physical parameter estimation of the nonlinear dynamics of a single link robotic manipulator with flexible joint using the HMF-method, in: Proceedings of the 1997 American Control Conference, Vols 1-6, 1997, pp. 1504–1508, Albuquerque, NM, Jun 04-06.

[13] P. Tomei, A. Tornambe, Approximate modeling of robots having elastic links, IEEE Transactions on Systems, Man and Cybernetics 18 (1988) 831–840.

[14] R. Tarumi, Y. Oshita, Free-vibration acoustic resonance of a nonlinear elastic bar, Philosophical Magazine 91 (5) (2011) 772–786. doi:{10.1080/14786435.2010.530614}.

[15] S. H. Arshad, M. N. Naeem, N. Sultana, A. G. Shah, Z. Iqbal, Vibration analysis of bi-layered FGM cylindrical shells, Archive of Applied Mechanics 81 (3) (2011) 319–343. doi:{10.1007/s00419-010-0409-8}.

[16] J. C. Ower, J. Van de Vegte, Classical control design for a flexible manipulator: modeling and control system design, Journal of Robotics and Automation 3 (1987) 485–489.

[17] Y. Chaolan, H. Jiazhen, C. Guoping, Modeling study of a flexible hub-beam system with large motion and with considering the effect of shear deformation, Journal of Sound and Vibration 295 (2006) 282–293.

[18] W. Chen, Dynamic modeling of multi-link flexible robotic manipulators, Journal of Computers and Structures 79 (2001) 183–195.

[19] B.-J. Lee, Geometrical Derivation of Differential Kinematics to Calibrate Model Parameters of Flexible Manipulator, International Journal of Advanced Robotic Systems 10, article number 106. doi:{10.5772/55592}.

[20] L. Chen, H. Deng, Model reduction of rigid-flexible manipulators with experimental validation, in: Jiang, ZY and Liu, XH and Jiao, SH and Han, JT (Ed.), Engineering Solutions for Manufacturing Processes, PTS 1-3, Vol. 655-657 of Advanced Materials Research, 2013, pp. 1101–1107. doi:{10.4028/www.scientific.net/AMR.655-657.1101}.

[21] H. Esfandiar, S. Daneshmand, Complete dynamic modeling and approximate state space equations of the flexible link manipulator, Journal of Mechanical Science and Technology 26 (9) (2012) 2845–2856. doi:{10.1007/s12206-012-0731-x}.

[22] C. di Castri, A. Messina, Exact modeling for control of flexible manipulators, Journal of Vibration and Control 18 (10) (2012) 1526–1551. doi:{10.1177/1077546311421796}.

[23] M. H. Korayem, H. N. Rahimi, A. Nikoobin, Mathematical modeling and trajectory planning of mobile manipulators with flexible links and joints, Applied Mathematical Modelling 36 (7) (2012) 3223–3238. doi:{10.1016/j.apm.2011.10.002}.

[24] S. B. Choi, S. C. Kim, H. K. Kim, Position and force control of a two-link flexible manipulator with piezoelectric actuators (1999) 73–80.

[25] P.-B. Nguyen, S.-B. Choi, Open-loop position tracking control of a piezoceramic flexible beam using a dynamic hysteresis compensator, Smart Materials and Structures 19 (12). doi:{10.1088/0964-1726/19/12/125008}.

[26] H. H. Lee, New dynamic modeling of flexible-link robots, Journal of Dynamic Systems, Measurement and Control 127 (1956) 307–309.

[27] X. Zhang, W. Xu, S. S. Nair, V. S. Chellaboina, Pde modeling and control of a flexible two-link manipulator, IEEE Transactions on Control Systems Technology 13 (2005) 301–312.

[28] R. I. Milford, S. F. Asokanthan, Configuration dependent eigenfrequencies for a two-link flexible manipulator: experimental verification, Journal of Sound and Vibration 222 (1999) 191–207.

[29] A. Hać, L. Liu, Sensor and actuator location in motion control of flexible structures, Journal of Sound and Vibration 167 (2) (1993) 239–261.

[30] W. J. Book, O. Maizza-Neto, D. Whitney, Feedback control of two beam, two joint systems with distributed flexibility, Journal of Dynamic Systems, Measurement, and Control 97 (4) (1975) 424–431.

[31] W. J. Book, Recursive lagrangian dynamics of flexible manipulator arms, The International Journal of Robotics Research 3 (3) (1984) 87–101.

[32] C. di Castri, A. Messina, Exact modeling for control of flexible manipulators, Journal of Vibration and Control 18 (10) (2012) 1526–1551. doi:{10.1177/1077546311421796}.

[33] J. Meek, H. Liu, Nonlinear dynamics analysis of flexible beams under large overall motions and the flexible manipulator simulation, Computers and Structures 56 (1) (1995) 1–14. doi:{10.1016/0045-7949(94)00542-B}.

[34] K. Yuan, C. Hu, Nonlinear modeling and partial linearizing control of a slewing Timoshenko-beam, Journal of Dynamic Systems, Measurement, and Control-Transactions of the ASME 118 (1) (1996) 75–83. doi:{10.1115/1.2801154}.

[35] A. Zuyev, O. Sawodny, Observer design for a flexible manipulator model with a payload, in: Proceedings of the 45th IEEE Conference on Decision and Control, Vols 1-14, 2006, pp. 4490–4495, San Diego, CA, DEC 13-15. doi:{10.1109/CDC.2006.376770}.

[36] M. Vukobratovic, A. Tuneski, Adaptive control of single rigid robotic manipulators interacting with dynamic environment - An overview, Journal of Intelligent and Robotic Systems 17 (1) (1996) 1–30. doi:{10.1007/BF00435714}.

[37] Z. J. Jia, Y. D. Song, W. C. Cai, Bio-inspired Approach for Smooth Motion Control of Wheeled Mobile Robots, Cognitive Computation 5 (2) (2013) 252–263. doi:{10.1007/s12559-012-9186-8}.

[38] H. Mahjoubi, K. Byl, Modeling Synchronous Muscle Function in Insect Flight: a Bio-Inspired Approach to Force Control in Flapping-Wing MAVs, Journal of Intelligent and Robotic Systems 70 (1-4, SI) (2013) 181–202. doi:{10.1007/s10846-012-9746-x}.

[39] B. Sun, D. Zhu, F. Ding, S. X. Yang, A novel tracking control approach for unmanned underwater vehicles based on bio-inspired neurodynamics, Jour-

nal of Marine Science and Technology 18 (1) (2013) 63–74. doi:{10.1007/s00773-012-0188-8}.

[40] Y. Park, D. Young, B. Chen, R. J. Wood, R. Nagpal, E. C. Goldfield, Networked Bio-Inspired Modules For Sensorimotor Control of Wearable Cyber-Physical Devices, in: 2013 International Conference on Computing, Networking and Communications (ICNC), 2013, San Diego, CA.

[41] J. Zhang, G. Qiao, G. Song, A. Wang, Design and Implementation of a Remote Control System for a Bio-inspired Jumping Robot, International Journal of Advanced Robotic Systems 9, article number 117. doi:{10.5772/51931}.

[42] J. L. González-Mora, A. Rodríguez-Hernández, L. F. Rodríguez-Ramos, L. Díaz-Saco, N. Sosa, Development of a new space perception system for blind people, based on the creation of a virtual acoustic space, in: J. Mira, J. Sánchez-Andrés (Eds.), Engineering Applications of Bio-Inspired Artificial Neural Networks, Vol. 1607 of Lecture Notes in Computer Science, Springer Berlin Heidelberg, 1999, pp. 321–330. doi:10.1007/BFb0100499.
http://dx.doi.org/10.1007/BFb0100499

[43] S. Tolu, M. Vanegas, N. R. Luque, J. A. Garrido, E. Ros, Bio-inspired adaptive feedback error learning architecture for motor control, Biological Cybernetics 106 (8-9) (2012) 507–522. doi:{10.1007/s00422-012-0515-5}.

[44] A. J. Ijspeert, J. Hallam, D. Willshaw, From lampreys to salamanders: evolving neural controllers for swimming and walking, in: Pfeifer, R and Blumberg, B and Meyer, JA and Wilson, SW (Ed.), From Animals to Animats 5, From Animals to Animats Series, 1998, pp. 390–399, 5th International Conference on Simulation of Adaptive Behavior, University of Zurich, Zurich, Switzerland.

[45] S. Yang, X. Jin, K. Liu, L. Jiang, Nanoparticles assembly-induced special wettability for bio-inspired materials, Particuology 11 (4, SI) (2013) 361–370. doi:{10.1016/j.partic.2013.02.001}.

[46] K. Liu, Y. Tian, L. Jiang, Bio-inspired superoleophobic and smart materials: Design, fabrication, and application, Progress in Materials Science 58 (4) (2013) 503–564. doi:{10.1016/j.pmatsci.2012.11.001}.

[47] F. Saavedra, I. Erick, M. I. Friswell, Y. Xia, Variable stiffness biological and bio-inspired materials, Journal of Intelligent Material Systems and Structures 24 (5) (2013) 529–540. doi:{10.1177/1045389X12461722}.

[48] A. Sugawara-Narutaki, Bio-inspired synthesis of polymer-inorganic nanocomposite materials in mild aqueous systems, Polymer Journal 45 (3) (2013) 269–276. doi:{10.1038/pj.2012.171}.

[49] M. M. Stevens, G. Mecklenburg, Bio-inspired materials for biosensing and tissue engineering, Polymer International 61 (5) (2012) 680–685. doi:{10.1002/pi.4183}.

[50] A. Menciassi, P. Dario, Bio-inspired solutions for locomotion in the gastrointestinal tract: background and perspectives, Philosophical Transactions of the Royal Society A:-Mathematical, Physical and Engineering Sciences 361 (1811) (2003) 2287–2298. doi:{10.1098/rsta.2003.1255}.

[51] P. Dario, P. Ciarletta, A. Menciassi, B. Kim, Modelling and experimental validation of the locomotion of endoscopic robots in the colon, in: Siciliano, B and Dario, P (Ed.), Experimental RoboticsS VIII, Vol. 5 of Springer Tracts in Advanced Robotics, 2003, pp. 445–453, 8th International Symposium on Experimental Robotics (ISER 02), Sant'Angelo, Italy, Jul 08-11, 2002.

[52] D. Huston, J. Miller, B. Esser, Adaptive, robotic and mobile sensor systems for structural assessment, in: Liu, SC (Ed.), Smart Structures and Materials 2004: Sensors and Smart Structures Technologies for Civil, Mechanical, and Aerospace Systems, Vol. 5391, 2004, pp. 189–196, San Diego, CA. doi:{10.1117/12.546606}.

[53] B. Esser, D. R. Huston, Versatile robotic platform for structural health monitoring and surveillance, Smart Structures and Systems 1 (4) (2005) 325–338.

[54] Y. Cha, H. Kim, M. Porfiri, Energy harvesting from underwater base excitation of a piezoelectric composite beam, Smart Materials and Structures 22 (11) (2013) 115026.
http://stacks.iop.org/0964-1726/22/i=11/a=115026

[55] Y. Cha, L. Shen, M. Porfiri, Energy harvesting from underwater torsional vibrations of a patterned ionic polymer metal composite, Smart Materials and Structures

22 (5) (2013) 055027.
http://stacks.iop.org/0964-1726/22/i=5/a=055027

[56] J. Gray, H. W. Lissmann, Studies in animal locomotion VII. Locomotory reflexes in the earthworm, Journal of Experimental Biology 15 (4) (1938) 506–517.

[57] K. M. Dorgan, C. J. Law, G. Rouse, Meandering worms: mechanics of undulatory burrowing in muds, Proceedings of the Royal Society B Biological Sciences 280 (1757). doi:{10.1098/rspb.2012.2948}.

[58] K. A. Daltorio, A. S. Boxerbaum, A. D. Horchler, K. M. Shaw, H. J. Chiel, R. D. Quinn, Efficient worm-like locomotion: slip and control of soft-bodied peristaltic robots, Bioinspiration & Biomimetics 8 (3). doi:{10.1088/1748-3182/8/3/035003}.

[59] W. B. Yapp, Locomotion of Worms, Nature 177 (4509) (1956) 614–615. doi:{10.1038/177614a0}.

[60] J. M. Martins, M. A. Botto, J. M. S. da Costa, A Newton-Euler model of a piezoactuated nonlinear elastic manipulator link, in: Nunes, U and deAalmeida, AT and Bejczy, AK and Kosuge, K and Macgado, JAT (Ed.), Proceedings of the 11th International Conference on Advanced Robotics 2003, Vol 1-3, 2003, pp. 935–940, Coimbra, Portugal.

[61] B. C. Jayne, Kinematics of Terrestrial Snake Locomotion , Copeia 1986 (4) (1986) 915–927.

[62] Y. Umetani, S. Hirose, Biomecanical study of serpentine locomotion, Proceedings of the 1st ROMANSY Symp Udine 177 (1974) 171–184.

[63] S. Hirose, Connected differential mechanism and its applications, Proceedings of the 2nd International Conference in Advances in Robotics (1985) 319–326.

[64] S. Hirose, Y. Umetani, Kinematic control of an active cord mechanism with tactile sensors, Proceedings of the CISM-ZFToM Symposium on Theory and Practice of Robots and manipulators (1976) 241–252.

[65] S. Hirose, K. Ikuta, M. Tsukamoto, , K. Sato, Considerations in design of the actuator based in the shape memory effect, Proceedings of the 6th IGToMM Congress (1987) 1549–1556.

[66] S. Hirose, Y. Umetani, The kinematics and control of a soft gripper for the handling of living and fragile objects, Proceedings of the IGToMM Congress (1979) 1549–1556.

[67] D. L. P. Bopearatchy, G. C. Hatanwala, State space control of a multi link robot manipulator by a translational modelling technique, in: Intelligent Control, 1990. Proceedings., 5th IEEE International Symposium on, 1990, pp. 285–290 vol.1. doi:10.1109/ISIC.1990.128470.

[68] T. Nanayakkara, K. Watanabe, K. Kiguchi, K. Izumi, Controlling multi-link manipulators by fuzzy selection of dynamic models, in: Industrial Electronics Society, 2000. IECON 2000. 26th Annual Confjerence of the IEEE, Vol. 1, 2000, pp. 638–643 vol.1. doi:10.1109/IECON.2000.973224.

[69] M. Moallem, K. Khorasani, R. Patel, An inverse dynamics sliding control technique for flexible multi-link manipulators, in: American Control Conference, 1997. Proceedings of the 1997, Vol. 3, 1997, pp. 1407–1411 vol.3. doi:10.1109/ACC.1997.610658.

[70] J.-X. Xu, Y.-J. Pan, T.-H. Lee, A gain shaped sliding mode control scheme using filtering techniques with applications to multi-link robotic manipulators, in: American Control Conference, 2001. Proceedings of the 2001, Vol. 6, 2001, pp. 4363–4368 vol.6. doi:10.1109/ACC.2001.945664.

[71] S. K. Ider, Stability analysis of constraints in flexible multibody systems dynamics, International Journal of engineeing Science 28 (12) (1990) 1277–1290. doi:{10.1016/0020-7225(90)90075-T}.

[72] M. Pascal, Some open problems in dynamic analysis of flexible multi-body systems, Journal of Multibody System Dynamics 5 (2001) 315–334.

[73] S. Kuroda, I. Kunita, Y. Tanaka, A. Ishiguro, R. Kobayashi, T. Nakagaki, Common mechanics of mode switching in locomotion of limbless and legged animals, Journal of The Royal Society Interface 11 (95) (2014) 20140205.

[74] P. Chadwick, Continuum Mechanics: Concise Theory and Problems, 1st Edition, Dover Publications, 1998.

[75] C. M. Bender, S. A. Orszag, Advanced Mathematical Methods for Scientists and Engineers I, Springer, 1999.

[76] S. Timoshenko, Vibration Problems In Engineering, D. Van Nostrand Company Inc., 1974.

[77] R. B. Hetnarski, J. Ignaczak, The Mathematical Theory of Elasticity, 2nd Edition, CRC Press, 2010.

[78] N. F. J. van Rensburg, A. J. van der Merwe, Natural frequencies and modes of a Timoshenko beam, Wave Motion 44 (1) (2006) 58–69. doi:{10.1016/j.wavemoti.2006.06.008}.

[79] L. Majkut, Free and forced vibrations of Timoshenko beam Described by single differential equation, Journal of Theoretical and Applied Mechanics 47 (1) (2009) 193–210.

[80] C. Batlle, A. Dòria-Cerezo, G. Espinosa-Pérez, R. Ortega, Simultaneous interconnection and damping assignment passivity-based control: Two practical examples, in: Lagrangian and Hamiltonian Methods for Nonlinear Control 2006, Springer, 2007, pp. 157–169.

[81] J. S. Fattahi and D. Spinello, "Path following and shape morphing with a continuous slender mechanism," *Journal of Dynamic Systems, Measurement, and Control*, 2015.

Chapter 6

Sensing linear viscoelastic constitutive parameters with a Timoshenko beam on a multi-layer foundation: modeling and simulation

The work in this chapter is published in the Journal of Sensing and BioSensing Research.[74]

6.1 Abstract

We present a sensor model comprised of a Timoshenko beam coupled with a linear viscoelastic substrate via a distributed system of compliant elements. The system of governing equations includes the evolution of the kinematic descriptors of the Timoshenko beam and of the interface between the coupling elements and the viscoelastic substrate. This model is used to pose an inverse problem aimed at estimating the constitutive parameters of the substrate from deformation measurements of the beam induced by different input forces and torques. The sensing model is demonstrated by comparing its prediction with published experimentally obtained constitutive parameters identifying standard linear viscoelastic material models, showing good agreement between model estimations and experimental results.

Keywords: Viscoelastic response Sensor model Distributed parameters system Inverse problem

6.2 Introduction

In this work we propose a model for a continuous deformable system that can be used as a sensor to estimate constitutive parameters of a substrate to which it is coupled. The sensor is comprised of a planar Timoshenko beam, and of a distributed system of compliant elements that exert the coupling with the substrate. The system is a sensor in the sense that kinematic quantities (that is, deflections and rotations along the axis of the beam) are acquired through measurements; the model of the system allows then to define a cost function that encodes least square residuals between measurements and model displacements, including constitutive parameters that can be estimated by minimizing the cost function. This leads naturally to an inverse problem formulation, in which the action or external forces (from the substrate) that determine a given kinematics (measured) has to be found. One important application of this work is the estimation of material parameters for soft biological tissues, which is demonstrated by comparison of the predictions of the proposed model with published results.

Inverse problems deal in general with the determination of unknown parameters in a wide range of engineering and science applications [1–5]. Inverse problems for hyper redundant mechanisms with different geometric and dynamic conditions can be found in [6–11]. For elongated hyper-redundant systems models of one dimensional continua with local Euclideian structure (beam models) are often naturally adopted, due to their suitability in describing the features associated with the slenderness. Among all, many studies have been dedicated to inverse problems applied to structural health monitoring, crack identification, or to the estimation of material properties of soils [12–25]. Additionally, the mechanical properties play a key role in stability, development, and remodeling of biological tissues, and the constitutive response of biomaterials can be correlated to the physical structure of living tissues and with eventual abnormalities, resulting into diagnosing techniques [26, 27]. The links between biomechanics and human diseases have been the subject of considerable scientific research efforts [28–31]. Recent developments of the study of biological systems has reached a point where it can benefit considerably from contributions from continuum mechanics, which have provided a framework to analyze and predict the behavior of biomechanical mechanisms without specifically modeling the properties at the cellular and molecular levels [32–34].

In inverse problem solutions, different optimization techniques are used to estimate time dependent parameters, often related to root searching iterative methods belonging to the family of steepest descent and scaled steepest descent methods. Textbook [35] present

general methods of solution of inverse problems for vibrating systems; the application of different optimization methods to the solution of inverse problems for linear and nonlinear vibrating and static systems can be found in [36–42]. In this work we use the least squares error method to reconstruct smooth beam deformed shapes from discrete measurements along the axis, and to estimate time dependent material parameters in the constitutive models of soft tissues coupled with the sensor. This class of numerical optimization tools has been used in [43, 44] to estimate time dependent material parameters, and in [45–47] to solve inverse problems in linear and non-linear vibrating systems.

The rest of paper is organized as follows. In Section 6.3 we present the continuous model of a linear Timoshenko beam coupled with a viscoelastic foundation by a continuous distribution of compliant elements. The viscoelastic foundation represents linear viscoelastic materials for which we want to estimate constitutive parameters. This setting allows to formulate the problem as the one of a beam on a multi-layer foundation. A reduced order model for the beam on viscoelastic foundation is then derived, to allow to solve the coupled system of governing partial differential equations. In Section 6.4 we formulate the inverse problem to estimate constitutive parameters of the substrate. Results and discussions are presented in Section 6.5.

6.3 Mechanical model of the coupled system

In this section we present the mechanical model of a deformable body coupled with a viscoelastic substrate through a distributed system of deformable elements. The deformable body along with the distributed system of coupling elements is inspired by a class of organisms that move on unstructured substrates by adapting the shape of their bodies to non-zero curvatures of the substrates (shape morphing) and by forward locomoting through a traveling wave-like motion transmitted by the legs in contact with the substrate. These features have been used in [48, 49] to model and simulate shape morphing and forward locomotion. Here, these ideas are extended to exploit the system's features as a sensor, in which case the shape morphing parameters are observable (measured) and suitable characteristics of the substrate are reconstructed based on the model presented below. Specifically, we consider an elastic elongated body on a generalized foundation, where the two layers of the foundation are provided by the coupling system and by the substrate, see schematics in Fig. 6.1. The governing equations of the system include the evolution of the Timoshenko beam and of the interface between the substrate and the coupling elements.

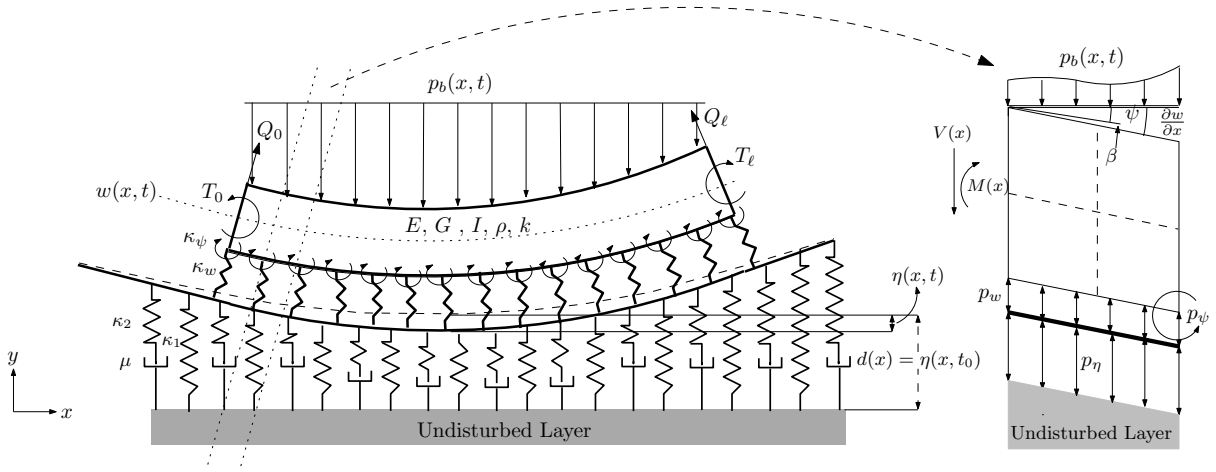

Figure 6.1: Sensor mechanism analogy model on viscoelastic foundation, and detail of the free body diagram of a portion of the beam.

6.3.1 Sensor's body model

We are interested in describing the kinematics of a deformable body that can be considered as the limit of a sequence of rigid elements connected through soft elements acting as spherical joints. This reproduces the salient characteristics of the bodies of millipedes [50–52] that specifically characterizes their peculiar shape morphing coupled with forward locomotion. In order to retain the independent relative rotational motion between two contiguous elements, it is natural to adapt a Timoshenko beam model that is a one dimensional continuum (axis) with a local Euclideian structure describing the state of cross section [49]. We consider the variation of the curvature of the substrate to be small, and the mechanism to be locally parallel to the substRrate, which implies that deformations are small [53]. Let $\{x, y, z\}$ be a fixed rectangular Cartesian frame with $x \in [0, L]$ spanning the initially rectilinear axis of the beam, and $\{y, z\}$ spanning the beam's cross section. By referring to Fig. 6.1, let u be the axial displacement, ψ be the rotation angle of the cross section, and w be the transverse displacement. The linear

planar Timoshenko beam is then described by the following set of evolution equations

$$\varrho A\frac{\partial^2 u}{\partial t^2}+c_u\frac{\partial u}{\partial t}=\frac{\partial}{\partial x}\left(EA\frac{\partial u}{\partial x}\right)+p_u \tag{6.1a}$$

$$\varrho A\frac{\partial^2 w}{\partial t^2}+c_w\frac{\partial w}{\partial t}=\frac{\partial}{\partial x}\left(kAG\left(\frac{\partial w}{\partial x}-\psi\right)\right)+p_w \tag{6.1b}$$

$$\varrho I\frac{\partial^2 \psi}{\partial t^2}+c_\psi\frac{\partial \psi}{\partial t}=\frac{\partial}{\partial x}\left(EI\frac{\partial \psi}{\partial x}\right)+kAG\left(\frac{\partial w}{\partial x}-\psi\right)+p_\psi \tag{6.1c}$$

where ϱ is the volume mass density, A the area of the cross section, I the moment of inertia, E and G respectively Young's and shear elastic moduli, k is the shear modulus (nondimensional parameter that depends on the geometry), and p_u, p_w, and p_ψ are distributed loads (per unit length) in the axial and transverse directions and a distributed couple perpendicular to the plane of motion. Terms proportional to the first time derivatives through coefficients c_u, c_w, and c_ψ model the structural damping as equivalent viscous damping [54]. Structural damping accounts for hysteresis phenomena in elastic materials undergoing cyclic loading [54, 55], and therefore it depends on the frequency of excitation. In equivalent viscous damping models the dependency on the frequency of excitation $\bar{\omega}$ is included through the proportional coefficients by the inverse law $c_u=\bar{c}_u/(\pi\bar{\omega})$ (similarly for c_w and c_ϕ) [55], where $\bar{c}_u$ is a constant independent of $\bar{\omega}$.

We consider the following force (von Neuman) boundary conditions

$$\text{At } x=0: \quad kAG\left(\frac{\partial w}{\partial x}-\psi\right)+Q_0=0, \quad EI\frac{\partial \psi}{\partial x}+T_0=0 \tag{6.2a}$$

$$\text{At } x=\ell: \quad -kAG\left(\frac{\partial w}{\partial x}-\psi\right)+Q_\ell=0, \quad -EI\frac{\partial \psi}{\partial x}+T_\ell=0 \tag{6.2b}$$

where Q_0, Q_ℓ and T_0, T_ℓ are respectively shear forces and bending moments applied at the boundaries $x=0$ and $x=\ell$, see Fig. 6.1.

6.3.2 Substrate model

Figure 6.1, shows a Timoshenko beam as sensor which is supported by a system of distributed compliant elements connected with a substrate with viscoelastic response. Several foundation models can be found in the literature to describe thin structures on continua. For linear viscoelastic materials, the relation between stress and strain is a function of strain and strain rate. With reference to Fig. 6.2, typical linear viscoelastic responses have lumped representations described by Kelvin-Voigt, Maxwell, and standard linear models. The standard linear model is used to describe the linear viscoelastic

response of a number of soft and biological materials, among others. The constitutive relation for the standard solid model is [56]

$$\kappa_1 \sigma + \mu \dot{\sigma} = \kappa_1 \kappa_2 \varepsilon + \mu \left(\kappa_1 + \kappa_2 \right) \dot{\varepsilon} \tag{6.3}$$

where σ is the normal stress, ε is the normal strain, a superimposed dot means material time differentiation, and κ_1, κ_2, and μ are stiffness and damping parameters of the elements represented in Fig. 6.2, having the physical dimensions of elastic and viscous moduli, respectively. Here we defined normal stress and normal strain by considering a continuous distribution of lumped elements. By referring to Fig. 6.1 we define the undeformed profile of the substrate to be $d(x)$, and the deformation of the same profile with respect to the undeformed configuration to be $\eta(x,t)$. The profile $d(x)$ can be interpreted as the thickness of a viscoelastic layer with respect to the depth of a layer that is not affected by the interaction with the beam, so that the normal strain ε in the viscoelastic model can be expressed as $\varepsilon = \eta / d$. Considering p_η as the normal force per unit width of the substrate exerted by the viscoelastic layer, we can rewrite the balance in (6.3) as

$$\kappa_1 p_\eta + \mu \dot{p}_\eta = \kappa_1 \kappa_2 \frac{\eta}{d} + \mu \left(\kappa_1 + \kappa_2 \right) \frac{\dot{\eta}}{d} \tag{6.4}$$

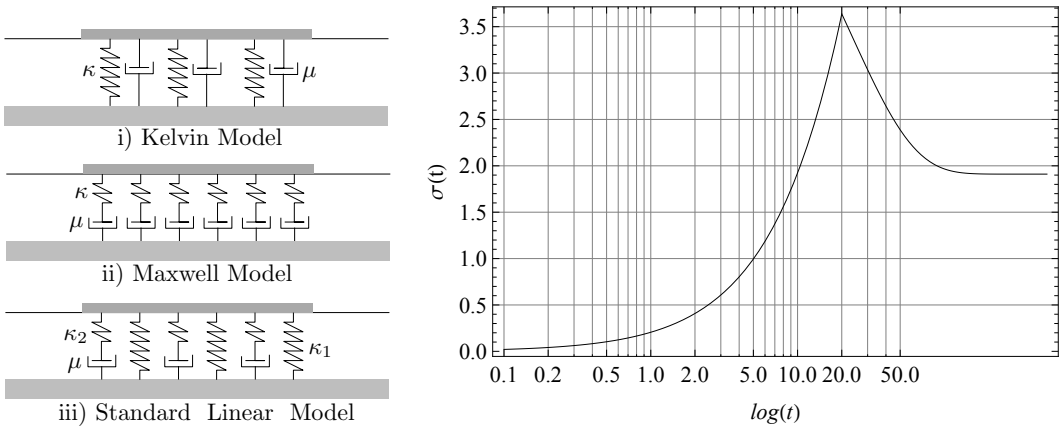

Figure 6.2: (a) Three linear viscoelastic models and (b) stress-relaxation response of an standard linear viscoelastic model with $\kappa_1 = 2\,\mathrm{N\,m^{-1}}$, $\kappa_2 = 1.5\,\mathrm{N\,m^{-1}}$, $\mu = 20\,\mathrm{N\,s\,m^{-1}}$.

6.3.3 Model of the coupled system

The sensing system modelled in this work is comprised of a deformable body coupled with a substrate through a distributed set of compliant elements. In order to describe the coupling between the different parts we adopt a multi-layer foundation model with a beam resting on it. Specifically, the foundation model is comprised of two layers respectively representing the coupling elements and the visco-elastic substrate. Following [57] we obtain an evolution equation for the interface between the two layers that is coupled with the evolution of the body described as a Timoshenko beam. The solution of the evolution of the interface describes the profile of the substrate to which the sensor is deployed. Different elastic and visco-elastic foundation models have been introduced to appropriately describe relevant scenarios [57]. The simplest is the Wrinkler model, in which the foundation is described as a system of independent springs reacting to the deflection of the body [58, 59]. Two parameters extensions of the Wrinkler model have been proposed by Filolenko-Borodich [60] and Pasternak [61–63] respectively by considering membrane like interactions (with constant tension) and shear interactions among springs. Alternatively to this family of models that are based on interactions between mechanical elements, continuum medium based model have been proposed based on variational formulations that include assumed kinematics of the foundation elastic medium [58, 64]. The Vlasov model [65] is based on the assumption that the in-plane displacement of the structure is identically zero, and the displacement on the transverse direction is controlled by the structure's deflection through a shape function that expresses the dependency on the depth of the elastic medium. A rigorous derivation of the shape function of the Vlasov model is presented in [64]. The generalized Vlazov-Jones model is presented in [66] to account for non-vanishing in-plane structural displacements, and adapted in [67] to to describe the isotropic matrix material in syntactic foams particulate composites. All two parameter models are equivalent in the sense that they are described by the same constitutive relation, except for the computation of the parameters [68].

To describe the interaction between the coupling elements and the body we adopt a generalized foundation model [68], in which the coupling elements transfer a distributed force and a distributed couple constitutively related to the kinematics of the Timoshenko beam and to the interface deformation descriptor η. By introducing the external body forces p_b and external body couples p_c we specify the forces and couples in (6.1) by

$$p_w = p_b - \kappa_w(w - \eta), \quad p_\psi = p_c - \kappa_\psi \left(\psi - \frac{\partial \eta}{\partial x}\right) \tag{6.5}$$

where κ_w and κ_ψ (respectively with SI physical dimensions $\mathrm{N\,m^{-2}}$ and $\mathrm{N\,m^{-1}}$) are elastic constants associated to linear and rotational distributed springs. Therefore the coupling elements relate the profile η and its slope to the kinematics of the Timoshenko beam. In the sensing framework p_b and p_c can be considered as inputs to the system that allow to estimate constitutive parameters, as specified below. The reactions $-\kappa_w(w-\eta)$ and $\kappa_\psi(\psi-\partial\eta/\partial x)$ are measured with respect to the static reactions $-\kappa_w d$ and $\kappa_\psi \partial d/\partial x$, and therefore $d(x)$ can be considered as the initial undisturbed profile under static equilibrium conditions. Additionally, we assume $p_u = 0$ as we focus on the deflection of the body. To obtain the evolution of the interface we assume that only normal interactions are transmitted through it, that is the coupling elements and the substrate interacts only through normal forces. More general multi-layer foundations consider shear interactions as well [69]. The balance of normal forces at the interface gives

$$-\kappa_w(w-\eta) + p_\eta = 0 \tag{6.6}$$

Substituting (6.6) into (6.4) we obtain the evolution equation for the interface that has initial undisturbed profile $d(x)$

$$\kappa_1\kappa_w(w-\eta) + \mu\kappa_w(\dot{w}-\dot{\eta}) - \kappa_1\kappa_2\frac{\eta}{d} - \mu\left(\kappa_1+\kappa_2\right)\frac{\dot{\eta}}{d} = 0 \tag{6.7}$$

6.3.4 Nondimensional Governing Equations

We introduce the nondimensional variables

$$\hat{x} = \frac{x}{\ell}, \quad \hat{t} = \frac{t}{\tau}, \quad \hat{w} = \frac{w}{\ell}, \quad \hat{p}_b = \frac{p_b}{\kappa_w\ell}, \quad \hat{p}_c = \frac{p_c}{\kappa_\psi\ell}, \quad \hat{\eta} = \frac{\eta}{\ell}, \quad \hat{d} = \frac{d}{\ell} \tag{6.8}$$

where ℓ is the total length of the undeformed body, and τ is the characteristic time that is given by

$$\tau^2 = \frac{\varrho\ell^2}{kG} \tag{6.9}$$

By substituting (6.5) into (6.1b),(6.1c) and (6.7), we rewrite the governing equations in nondimensional form as

$$\frac{\partial^2 w}{\partial t^2} + \frac{\alpha_w}{\omega^\star}\frac{\partial w}{\partial t} - \frac{\partial^2 w}{\partial x^2} + \frac{\partial\psi}{\partial x} + \alpha_3 w = p_b + \alpha_3\eta \tag{6.10a}$$

$$\alpha_1\frac{\partial^2\psi}{\partial t^2} + \frac{\alpha_\psi}{\omega^\star}\frac{\partial\psi}{\partial t} - \frac{\partial^2\psi}{\partial x^2} + \alpha_4\psi - \alpha_1\alpha_2\left(\frac{\partial w}{\partial x} - \psi\right) = p_c + \alpha_4\frac{\partial\eta}{\partial x} \tag{6.10b}$$

$$\beta_1(w-\eta) + \beta_\mu(\dot{w}-\dot{\eta}) - \beta_1\beta_2\frac{\eta}{d} - \beta_\mu\left(\beta_1+\beta_2\right)\frac{\dot{\eta}}{d} = 0 \tag{6.10c}$$

Here we have dropped the hat to indicate nondimensional quantities, and we have introduced the nondimensional groups

$$\alpha_1 = \frac{kG}{E}, \quad \alpha_2 = \frac{A\ell^2}{I}, \quad \alpha_3 = \frac{\kappa_w \ell^2}{kAG}, \quad \alpha_4 = \frac{\kappa_\psi}{EI} \tag{6.11a}$$

$$\omega^\star = \bar{\omega}\tau, \quad \alpha_w = \frac{\bar{c}_w \ell^2}{\pi kAG}, \quad \alpha_\psi = \frac{\bar{c}_\psi \ell^2}{\pi EI} \tag{6.11b}$$

$$\beta_1 = \frac{\kappa_1}{\kappa\ell}, \quad \beta_2 = \frac{\kappa_2}{\kappa\ell}, \quad \beta_\mu = \frac{\mu}{\kappa\ell\tau}. \tag{6.11c}$$

Therefore $\alpha_1\alpha_2$ is a measure of the shear stiffness versus the bending stiffness, α_3 is a measure of the legs' linear stiffness versus the shear stiffness, α_4 measures the leg's bending stiffness with respect to the bending stiffness of the body, and α_w and α_ψ are structural damping factors.

The nondimensional version of boundary conditions (6.2) is

$$\text{At } x = 0: \quad \frac{\partial w}{\partial x} - \psi + \hat{Q}_0 = 0, \quad \frac{\partial \psi}{\partial x} + \hat{T}_0 = 0 \tag{6.12a}$$

$$\text{At } x = \ell: \quad -\left(\frac{\partial w}{\partial x} - \psi\right) + \hat{Q}_1 = 0, \quad -\frac{\partial \psi}{\partial x} + \hat{T}_1 = 0 \tag{6.12b}$$

where nondimensional forces and torques $\hat{Q}$ and $\hat{T}$ are obtained from the corresponding dimensional ones respectively by dividing by kAG and by EI. Since no ambiguity arises, in the following we will drop the hat for the nondimensional boundary forces and torques. By assuming that only the portion of the substrate in contact with the sensor experiences deformation, we adopt the following boundary conditions for the field η

$$\eta(x,t) = 0 \text{ at } x = 0 \text{ and } x = 1. \tag{6.13}$$

6.3.5 Reduced Order Model

We obtain a reduced order model for the flexural and rotational motions through Galerkin projections of the fields w, ψ, and η on suitable bases. By separation of variables, the kinematic fields are expressed as

$$w(x,t) = \bar{\mathbf{w}}^{\mathsf{T}}(x)\mathbf{a}(t) \tag{6.14a}$$

$$\psi(x,t) = \bar{\boldsymbol{\psi}}^{\mathsf{T}}(x)\mathbf{b}(t) \tag{6.14b}$$

$$\eta(x,t) = \bar{\eta}(x)c(t) \tag{6.14c}$$

where $\bar{\mathbf{w}} = (\bar{w}_1 \cdots \bar{w}_n)^{\mathsf{T}}$, $\bar{\boldsymbol{\psi}} = \left(\bar{\psi}_1 \cdots \bar{\psi}_n\right)^{\mathsf{T}}$, and $\bar{\eta}$ are spatial basis functions. Basis functions $\bar{\mathbf{w}}$ and $\bar{\boldsymbol{\psi}}$ are obtained by solving the vector eigenvalues problem associated

with a planar Timoshenko beam with free end boundary conditions, see [49] and the Appendix for details. The mode shapes are normalized with respect to the maximum amplitude. The plots of the first three modes $\bar{\mathbf{w}}$, and $\bar{\boldsymbol{\psi}}$ normalized with respect to the maximum value are given in Figure 6.3. The interface η is considered as a perturbation of the undeformed profile $d(x)$, and the basis function $\bar{\eta}$ is chosen to be a quadratic polynomial satisfying homogeneous boundary conditions

$$\bar{\eta}(x) = x(x-1) \tag{6.15}$$

Coefficients $\mathbf{a} = (a_1 \cdots a_n)^\mathsf{T}$, $\mathbf{b} = (b_1 \cdots b_n)^\mathsf{T}$ and $c(t)$ represent unknowns time dependent amplitudes. By introducing the matrices (see Appendix 6.6 for more details)

$$\mathbf{M}_1 = \int_0^1 \bar{\mathbf{w}}\bar{\mathbf{w}}^\mathsf{T}\mathrm{d}x, \quad \mathbf{M}_2 = \int_0^1 \bar{\boldsymbol{\psi}}\bar{\boldsymbol{\psi}}^\mathsf{T}\mathrm{d}x, \quad M_3 = \int_0^1 \bar{\eta}^2\mathrm{d}x \tag{6.16a}$$

$$\mathbf{K}_1 = \int_0^1 \frac{\mathrm{d}\bar{\mathbf{w}}}{\mathrm{d}x}\frac{\mathrm{d}\bar{\mathbf{w}}^\mathsf{T}}{\mathrm{d}x}\mathrm{d}x, \quad \mathbf{K}_2 = \int_0^1 \frac{\mathrm{d}\bar{\boldsymbol{\psi}}}{\mathrm{d}x}\frac{\mathrm{d}\bar{\boldsymbol{\psi}}^\mathsf{T}}{\mathrm{d}x}\mathrm{d}x, \quad K_3 = \int_0^1 \frac{\bar{\eta}^2}{d}\mathrm{d}x \tag{6.16b}$$

$$\mathbf{K}_{w\psi} = \int_0^1 \frac{\mathrm{d}\bar{\mathbf{w}}}{\mathrm{d}x}\bar{\boldsymbol{\psi}}^\mathsf{T}\mathrm{d}x, \quad \mathbf{K}_{\eta w} = \int_0^1 \bar{\eta}\bar{\mathbf{w}}\mathrm{d}x, \quad \mathbf{K}_{\psi\eta} = \int_0^1 \bar{\boldsymbol{\psi}}^\mathsf{T}\frac{\mathrm{d}\bar{\eta}}{\mathrm{d}x}\mathrm{d}x \tag{6.16c}$$

we obtain the reduced order model in the form of the following coupled ordinary differential equations for the amplitudes $\mathbf{a}(t)$, $\mathbf{b}(t)$ and $c(t)$

$$\mathbf{M}_1\ddot{\mathbf{a}}(t) + \frac{\alpha_w}{\omega^\star}\mathbf{M}_1\dot{\mathbf{a}}(t) + (\mathbf{K}_1 + \alpha_3\mathbf{M}_1)\,\mathbf{a}(t) - \mathbf{K}_{w\psi}\mathbf{b}(t) - \alpha_3\mathbf{K}_{\eta w}^\mathsf{T}c(t) = \mathbf{F}_w(t) \tag{6.17a}$$

$$\alpha_1\mathbf{M}_2\ddot{\mathbf{b}}(t) + \frac{\alpha_\psi}{\omega^\star}\mathbf{M}_2\dot{\mathbf{b}}(t) + (\mathbf{K}_2 + (\alpha_1\alpha_2 + \alpha_4)\,\mathbf{M}_2)\mathbf{b}(t) - \alpha_1\alpha_2\mathbf{K}_{w\psi}^\mathsf{T}\mathbf{a}(t) - \alpha_4\mathbf{K}_{\psi\eta}c(t) = \mathbf{F}_\psi(t) \tag{6.17b}$$

$$\beta_\mu\,(M_3 + (\beta_1+\beta_2)K_3)\,\dot{c}(t) + \beta_1\,(M_3 + \beta_2 K_3)\,c(t) - \mathbf{K}_{\eta w}\,(\beta_1\mathbf{a}(t) + \beta_\mu\dot{\mathbf{a}}(t)) = 0 \tag{6.17c}$$

where forcing terms $\mathbf{F}_w$ and $\mathbf{F}_\psi$ are given by

$$\mathbf{F}_w = -\,(Q_0\bar{\mathbf{w}}(0) + Q_1\bar{\mathbf{w}}(1)) + \int_0^1 p_b\bar{\mathbf{w}}\mathrm{d}x \tag{6.18a}$$

$$\mathbf{F}_\psi = -\,\big(T_0\bar{\boldsymbol{\psi}}(0) + T_1\bar{\boldsymbol{\psi}}(1)\big) + \int_0^1 p_c\bar{\boldsymbol{\psi}}\mathrm{d}x \tag{6.18b}$$

Forces and moments in (6.18) can be considered as inputs to the sensor system, with corresponding deformations and internal forces obtained by measurements.

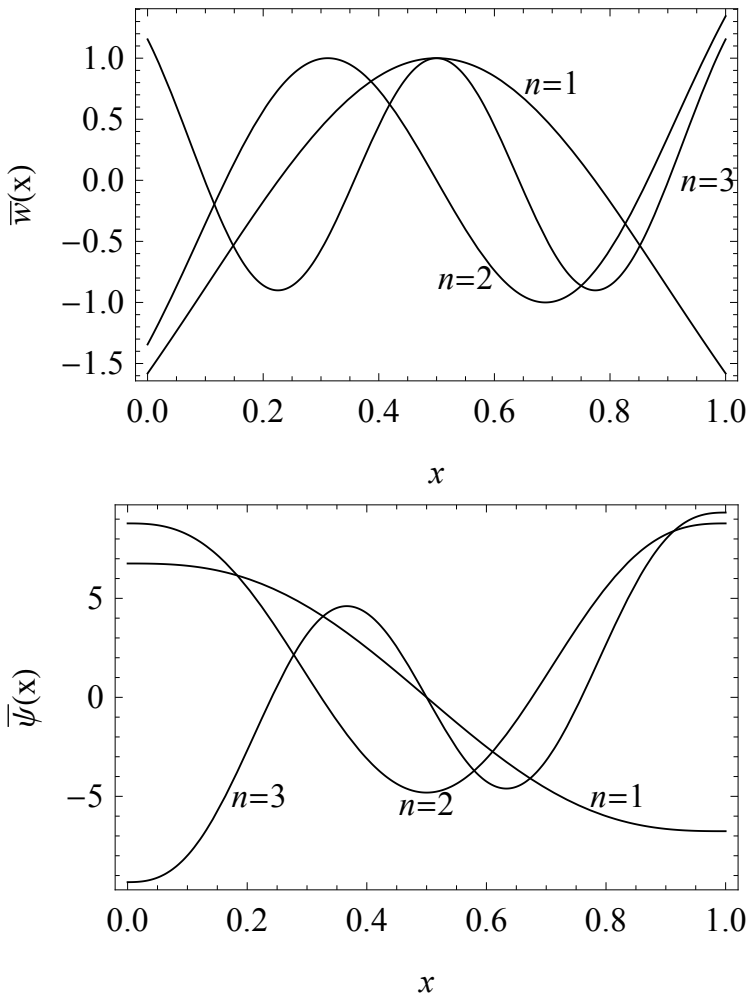

Figure 6.3: First three flexural and rotational modes, normalized with respect to the maximum value along the beam's span.

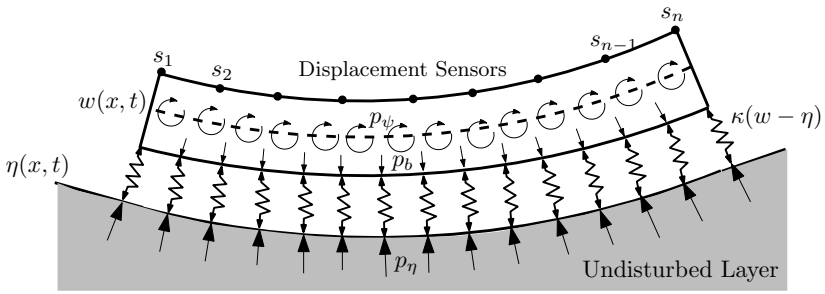

Figure 6.4: Schematic for the sensor system with set of observation points $(s_1, s_2, \cdots, s_n)$ along the beam axis.

6.4 Inverse Problem

In this section we present a procedure to use the model described in Section 6.3 to estimate the material properties of the viscoelastic layer, see Fig. 6.4. The model for the coupled system is given by the set of equations (6.10), which describe the coupled evolution of the beam and of the interface between the substrate and the coupling elements. We formulate an inverse problem based on the model (6.10) to estimate the material parameters of the substrate given displacement and/or force measurements of the beam.

The general structure of the inverse problem is schematized in Fig. 6.5, where a least squares residuals cost function is build from measurements and the model, and material parameters are selected as minimizers of such cost function. As specified below, different cost functions can be defined based on the nature of measurements, that is weather considering a displacement sensor or a force sensor.

6.4.1 Displacement sensor

When using the system as a displacement sensor, a time series of displacements of the beam are taken at a set of observation points $x_1, \ldots, x_n$ along the axis of the beam. Such time series measurements can be typically collected by a system of strain gauges or other common strain sensors while the system responds to a suitable excitation. At time t, the spatial sets of displacements are denoted by the collections

$$\tilde{\mathbf{w}}(t) = (\tilde{w}_1(t), \ldots, \tilde{w}_n(t))^\mathsf{T} \tag{6.19a}$$

$$\tilde{\boldsymbol{\psi}}(t) = \left(\tilde{\psi}_1(t), \ldots, \tilde{\psi}_n(t)\right)^\mathsf{T} \tag{6.19b}$$

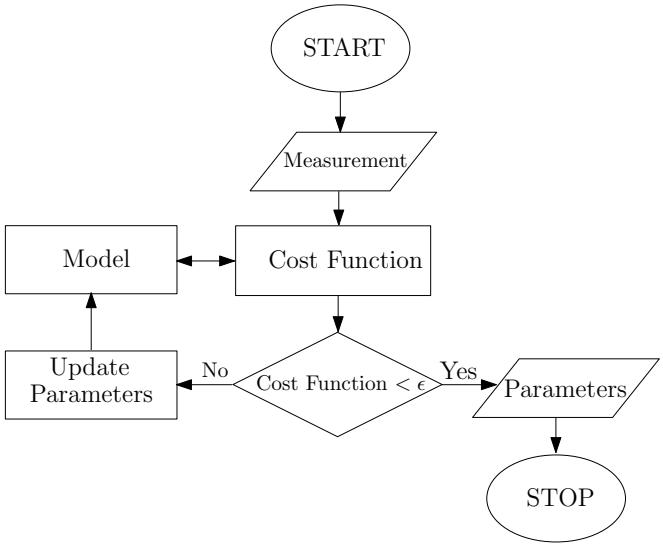

Figure 6.5: General flowchart of inverse problem.

In order to estimate the material parameters corresponding to the model (6.10) we define the least square residuals cost function by

$$\mathscr{R}(\hat{\mathbf{g}}) = \frac{1}{2}\sum_{j=1}^{N}\Big(\left(\tilde{\mathbf{w}}(t_j) - \mathbf{w}(\hat{\mathbf{g}}, t_j)\right)^{\mathsf{T}}\left(\tilde{\mathbf{w}}(t_j) - \mathbf{w}(\hat{\mathbf{g}}, t_j)\right) + \Big(\tilde{\boldsymbol{\psi}}(t_j) - \boldsymbol{\psi}(\hat{\mathbf{g}}, t_j)\Big)^{\mathsf{T}}\Big(\tilde{\boldsymbol{\psi}}(t_j) - \boldsymbol{\psi}(\hat{\mathbf{g}}, t_j)\Big)\Big) \tag{6.20}$$

where $\hat{\mathbf{g}}$ is a set of estimated parameters, that in this case include the viscoelastic constitutive parameters of the substrate, that is $\hat{\mathbf{g}} = (\hat{\beta}_{f_1}, \hat{\beta}_{f_2}, \hat{\beta}_{\mu})$;

$$\mathbf{w}(\hat{\mathbf{g}}, t) = (w(x_1, t), \ldots, w(x_n, t))^{\mathsf{T}}, \quad \boldsymbol{\psi}(\hat{\mathbf{g}}, t) = (\psi(x_1, t), \ldots, \psi(x_n, t))^{\mathsf{T}} \tag{6.21}$$

are n-collections obtained by evaluating at the observation points a solution of (6.10) for a given set of parameters $\hat{\mathbf{g}}$.

The cost function is minimized through a Nelder-Mead method which is natively implemented in a Matlab© routine solver [70]. This method is based on an iterative technique to solve nonlinear inverse problems for parameter estimation. By referring to Fig. 6.5 the routine stops when the residual $\mathscr{R}$ is smaller than a user defined parameter, which in this work is set to 10^{-7}. The default value from the solver is 10^{-4}.

6.5 Results and Discussions

6.5.1 Geometry and material parameters

We consider a beam with rectangular cross section. The structural damping parameters are set to $\alpha_w = \alpha_\psi = 10$, see Section 6.3.1 for details. The material is characterized by shear modulus ten times smaller than the Young's modulus, and therefore $\alpha_1 = 0.1$. Moreover, we consider the overall shear stiffness $kGA\ell^2$ to be one hundred times larger than the bending stiffness EI, and therefore $\alpha_1\alpha_2 = 100$. Simulations do not require the specification of the scaling time τ; however, the choice of this parameter dictates the density and the length of the device once the shear modulus is given. Simulation scenarios are always set with measuring dataset for the vertical and rotational deflection of the system with $\alpha_3 = 10$, meaning that the stiffness of the coupling elements is ten times larger than the shear stiffness of the body so that the body of the sensor morphs according to the shape of the substrate, see [49]. The undisturbed depth of the substrate is set to $d = 1$. The sensor model presented in this work was tested by estimating the viscoelastic parameters of specimens tested in [71], where standard linear viscoelastic material parameters where obtained from experimental data through material response fit.

Fields w and ψ in the reduced order model are both projected on the first two bases functions; this choise is dictated by the necessity to capture even and odd characteristics of forcing terms, see Fig. 6.3.

6.5.2 Displacement sensor

In this section we present simulation results for the system deployed as a displacement sensor. The implementation of this scenario requires a set of N observation points along the axis of the beam on which strain and/or displacement sensors are installed (typically strain gauges). To induce a deformation of the beam coupled with the substrate we consider two different force inputs. In the first case we consider in (6.18) $Q_0 = Q_1 = -Q$, while all the other forcing terms are zero. The forces are applied for 20 nondimensional time units, so that the forcint term becomes

$$\mathbf{F}_w(t) = Q(\bar{\mathbf{w}}(0) + \bar{\mathbf{w}}(1))(\mathfrak{u}(t) - \mathfrak{u}(t-20)) \tag{6.22}$$

where $\mathfrak{u}$ is the unit step function which evaluates to 1 whenever its argument is greater than 0. In the second case we considered a distributed torque p_c in (6.18), while the

remaining forcing parameters in (6.18) are zero. The distributed torque is nonzero in the nondimensional time interval $[0, 20]$, so that the expression for p_c is

$$p_c = -T\left(\mathfrak{u}(x) - 2\mathfrak{u}\left(x - \frac{1}{2}\right)\right)(\mathfrak{u}(t) - \mathfrak{u}(t-20)) \tag{6.23}$$

where T is the nondimensional amplitude of the distributed torque.

Table 6.1: Standard linear viscoelastic material parameters experimentally obtained in [71] for different specimens.

Specimen	β_1	β_2	μ
PH45	0.68	0.39	2.14
PH56	0.56	0.48	5.54
PH76	0.80	0.19	3.76

Simulated measurements for the cost function (6.19) were generated by solving (6.17) for the deformation of the beam when a given set of material parameters are assigned. Simulated measurements are taken with sample rate 1 Hz, and unless otherwise specified white noise with standard deviation 4% is added. Material parameters for the beam system are described above, whereas for the substrate we adopted the ones published in [71] and reported in Table 6.1 in nondimensional form. The actual measurements are obtained from the displacements by adding white noise. All numerical examples refer to a system with two observaton points at the abscissaee $x = 0.5$ and $x = 0.75$ along the axes of the beam. The set of nondimensional beam parameters is completed by considering three cases with $\alpha_4 = (1, 10, 20)$, meaning that the rotational stiffness of the coupling springs could be in the order of the bending stiffness of the body or stiffer. When the displacement is projected on the first two bases functions, the input force (6.22) with $Q_0 = Q_1 = 1$ is

$$\mathbf{F}_w = \begin{pmatrix} -3.16233 \\ 0 \end{pmatrix}(\mathfrak{u}(t) - \mathfrak{u}(t-20)) \tag{6.24}$$

Dots and solid lines in Fig. 6.6 show simulated measurements and displacement solutions for vertical and rotational displacements of the Timoshenko beam from the reduced order model, with $\alpha_3 = 10$ and $\alpha_4 = 10$. The corresponding estimated material properties are shown in the first row of Table. 6.2. These results are in good agreement with the measurements from [71] reported in Table 6.1 in nondimensional form for comparison.

Corresponding deflection $\eta(x)$ of the substrate at $x = 0.5$ is shown in Fig. 6.7(a) revealing a typical creep response due to a step load history; three snapshots ($t = 16$, $t = 20$ and $t = 100$) of the deflections of the beam and of the substrate obtained as the solution of the reduced order model are shown in Fig. 6.7(b), where the horizontal configuration corresponds to unloaded specimen after 80 nondimensional time units the force is released.

Table 6.2: Estimated material properties of a standard linear viscoelastic substrate with step input forces 6.24.

α_3	α_4	β_1	β_1	β_μ
10	1	0.81	0.19	3.77
10	10	0.79	0.22	3.72
10	20	0.78	0.22	3.71

For different values of the coupling elements stiffeness $\alpha_4 = (1, 10, 20)$ and for $\alpha_3 = 10$, the converged estimated viscoelastic parameters are summarized in Table 6.2. Corresponding deflections of the substrate at $x = 0.5$ are shown in Fig. 6.8(a), and deformed shapes of the beam and of the substrate at $t = 20$ are shown in Fig. 6.8(b). For the simulated sensor system increase in α_4 causes an increasing in the beam deflection and consequently in the induced deflection viscoleastic substrate, but material parameters estimation is not significantly affected. On the other hand, increase in α_3 means increasing the stiffness of the cupling springs with respect to the stiffness of the beam, which implies smaller deflections w and η for the same input force. At the limit, for very large α_3, the deflection of the beam would morph on the profile $d(x)$, and therefore very stiff coupling elements would compromise the functioning of the sensor deployed on an initially flat substrate.

As a second example we consider the input torque (6.23). For $T = 5$, the projected input torque $\mathbf{F}_\psi$ in (6.18) is

$$\mathbf{F}_\psi = \begin{pmatrix} 14.04 \\ 0 \end{pmatrix} (\mathfrak{u}(t) - \mathfrak{u}(t - 20)) \tag{6.25}$$

Table. 6.3 shows the corresponding converged estimated parameters for $\alpha_3 = 10$ and $\alpha_4 = (1, 10, 20)$; also in this case the estimated parameters are in good agreement with the ones reported by [71], and no significant difference is observed with respect to the input considered above. Dots and solid lines in Fig. 6.9 show simulated measurements

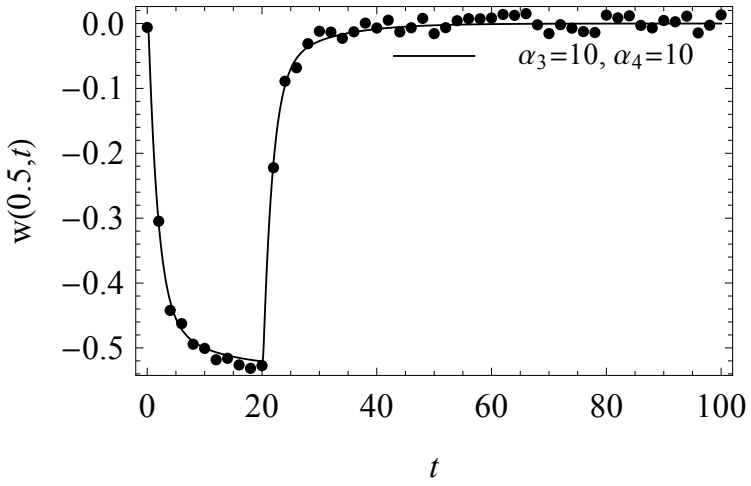

(a)

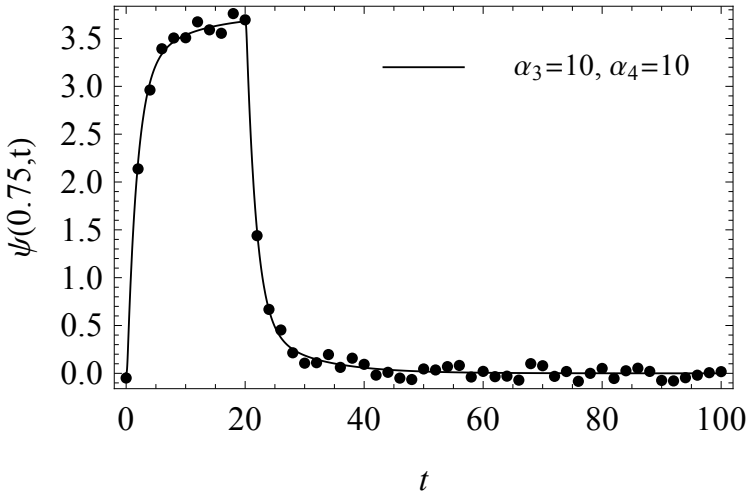

(b)

Figure 6.6: Simulated measurements (dots) and displacement solutions (solid line) of governing equations of the coupled system (6.17) for $\alpha_3 = 10$ and $\alpha_4 = 10$ and step input force (6.24), for (a) vertical displacement, and (b) rotational displacement.

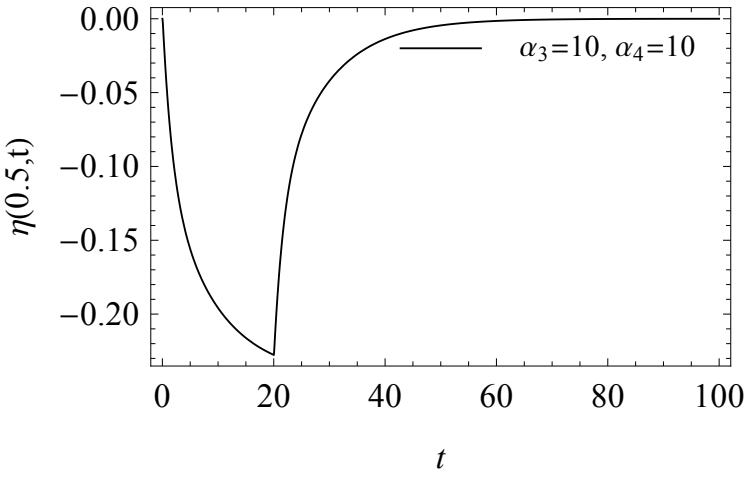

(a)

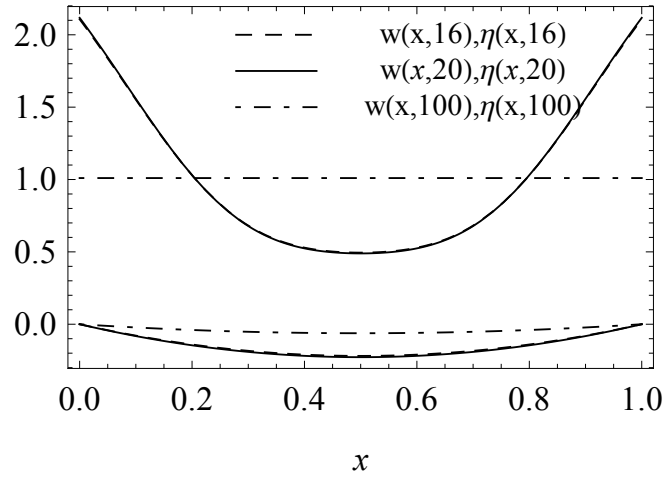

(b)

Figure 6.7: Plot of (a) time history of the deflection of the substrate at $x = 0.5$; (b) beam and substrate deformed shapes at nondimensional times $t = 16$, $t = 20$, $t = 100$, for $\alpha_3 = 10$ and $\alpha_4 = 10$ and step input force (6.24).

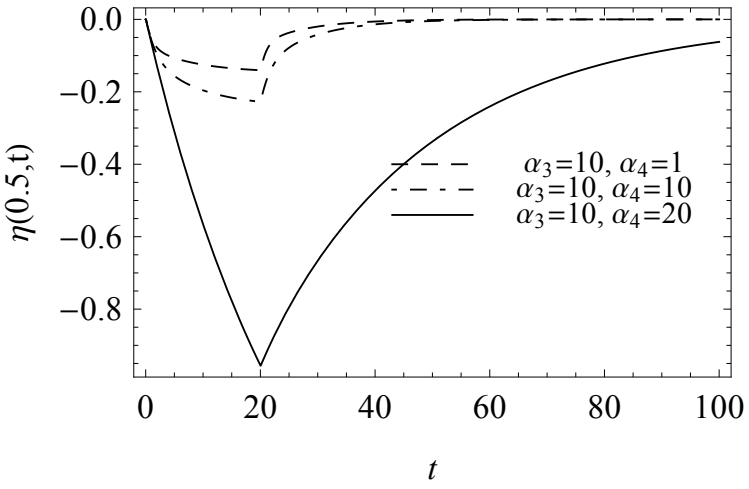

(a)

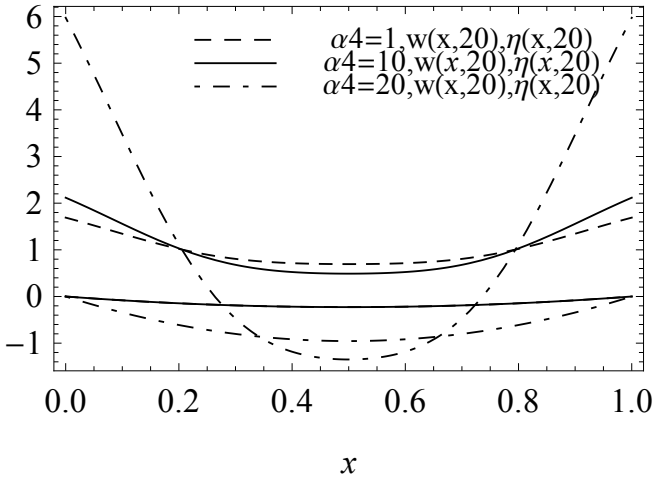

(b)

Figure 6.8: Plot of (a) Time history of the deflection of the substrate at $x = 0.5$; (b) Beam and substrate deformed shapes at ondimensional times $t = 16$, $t = 20$, $t = 100$, for $\alpha_3 = 10$ and $\alpha_4 = (1, 10, 20)$ and step input force (6.24).

Table 6.3: Estimated material properties of a standard linear viscoelastic substrate with step input distributed torque (6.25).

α_3	α_4	β_1	β_1	β_μ
10	1	0.81	0.19	3.77
10	10	0.81	0.19	3.76
10	20	0.79	0.182	3.76

and displacement solutions from the reduced order model, for $\alpha_3 = 10$ and $\alpha_4 = 10$; as before, measurements are simulated with material properties from Table 6.1, and time history of the displacement is plotted with estimated material parameters from Table 6.3. Corresponding deflection η of the substrate at $x = 0.5$ is shown in Fig. 6.10(a), and Fig. 6.10(b) shows three snapshots ($t = 16$, $t = 20$ and $t = 100$) of the deflections of the beam and of the substrate obtained as solutions of the reduced order model. Deflection of the substrate at $x = 0.5$ for $\alpha_3 = 10$, $\alpha_4 = (1, 10, 20)$, and estimated parameters, which are summarized Table 6.3, are shown in Fig. 6.11(a), and deflections of the beam and of the substrate for the governing equations of the coupled system for $t = 20$ are shown in Fig. 6.11(b). Also in this case the displacements are consistent with the expected creep response.

Simulation results were repeated by simulating strain measurements with three different white noise levels and applying the input force in (6.24), in order to check the robustness of the method with respect to noise. Specifically, measurements were simulated by adding to the model output displacement white noise terms sampled from Gaussian distributions with 2%, 6%, and 10% standard deviations. Noisy displacements for 6% and 10% cases are shown as dots in Fig. 6.12, along with solid lines showing their common expected values. Estimated material parameters for the three cases are shown in Table 6.4, revealing a close agreement regardless of the different noises considered. Further increasing of the noise would require the inclusion of noise elimination techniques [72].

In order to check the consistence of the sensor with respect to different specimens, the material property estimation has been repeated by simulating strain measurements with three different specimens presented in Table I of [71] (see Table 6.1 above). Considering the input force (6.24) and for $\alpha_3 = 10$ and $\alpha_4 = 10$, Table 6.5 presents the converged estimated parameters for three specimens, that are in good agreement with the ones experimentally obtained in [71]. Deflections η of these specimens at $x = 0.5$, corresponding

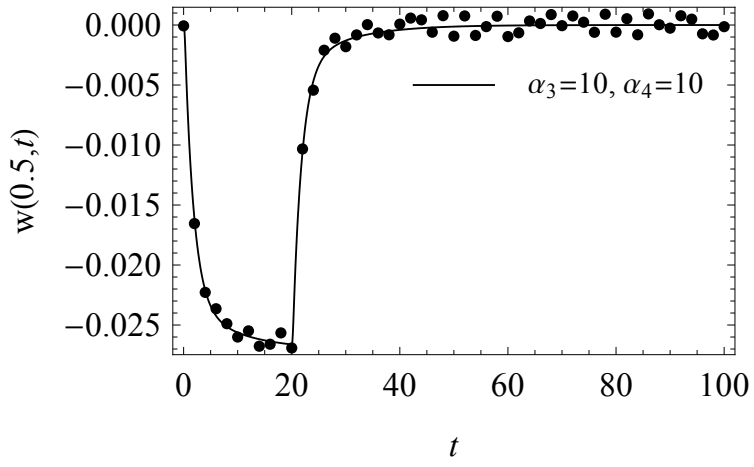

(a)

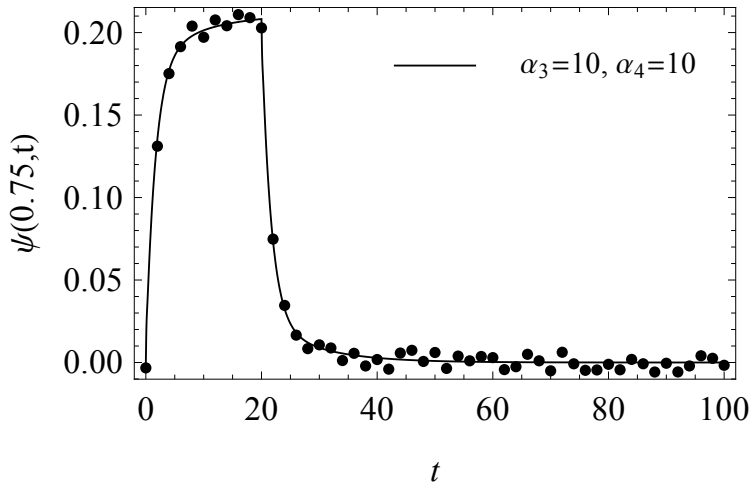

(b)

Figure 6.9: Simulated measurements (dots) and displacement solutions (solid line) of governing equations of the coupled system (6.17) for $\alpha_3 = 10$ and $\alpha_4 = 10$ and step torque (6.25), for (a) vertical displacement, and (b) rotational displacement.

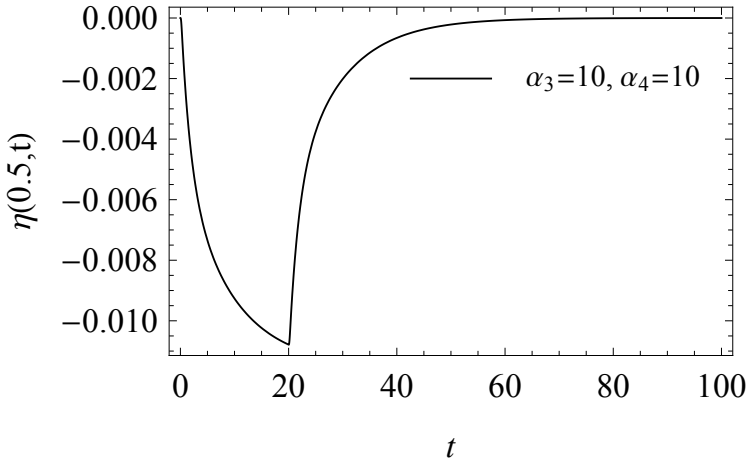

(a)

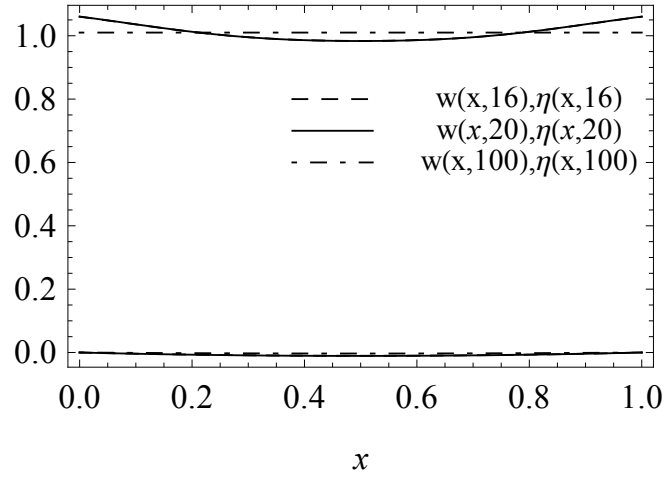

(b)

Figure 6.10: Plot of (a) time history of the deflection of the substrate at $x = 0.5$; (b) beam and substrate deformed shapes at nondimensional times $t = 16$, $t = 20$, $t = 100$, for $\alpha_3 = 10$ and $\alpha_4 = 10$ and step torque (6.25).

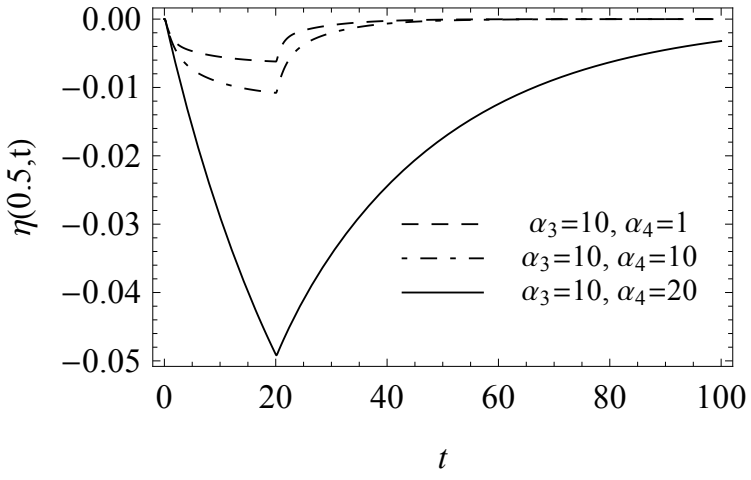

(a)

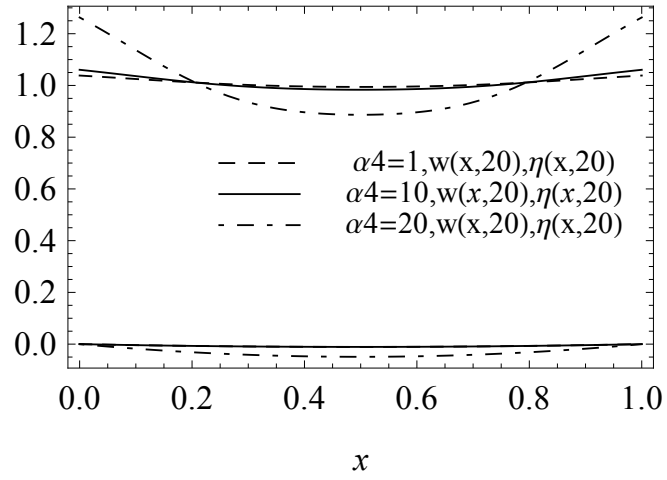

(b)

Figure 6.11: Plot of (a) time history of the deflection of the substrate at $x = 0.5$; (b) beam and substrate deformed shapes at nondimensional time $t = 20$, for $\alpha_3 = 10$ and $\alpha_4 = (1, 10, 20)$ and step torque (6.25).

Table 6.4: Estimated material properties for the standard linear viscoelastic substrate with respect different noise standard deviations for simulated measurements, $\alpha_3 = 10$, $\alpha_4 = 10$, and step input force (6.24).

Noise standard deviation	β_1	β_1	β_μ
2%	0.81	0.19	3.76
6%	0.81	0.19	3.77
10%	0.84	0.21	3.82

to estimated parameters in Table 6.5, are shown in Fig. 6.13.

Table 6.5: Estimated material properties for different specimens in [71]. Simulated measurements are obtained for $\alpha_3 = 10$, $\alpha_4 = 10$, and step input force (6.24).

Material	β_1	β_1	β_μ
PH45	0.67	0.38	2.13
PH56	0.56	0.47	5.54
PH76	0.81	0.19	3.76

6.6 Conclusion

We derived the initial boundary values problem governing the evolution of a Timoshenko beam and of the profile of a linear viscoelastic substrate that are coupled through a system of compliant elements. This system has been used as the model to pose an inverse problem for the estimation of the constitutive parameters of the viscoelastic substrate, with material response modeled as standard linear viscoelastic. Material parameters are the minimizing set of a least square cost function encoding the residuals between displacement measurements and model predicted displacements.

Predictions of the sensing apparatus are obtained by simulating the estimation of material parameters for specimens that have been experimentally characterized. Simulated measurements are based on the published values of constitutive viscoelastic parameters. Predictions of the model accurately reproduce published experimental characterizations of standard linear viscoelastic materials, and they show robustness with respect to relatively high white noise added to the simulated measurements.

Current and future work include the hardware realization of the system proposed

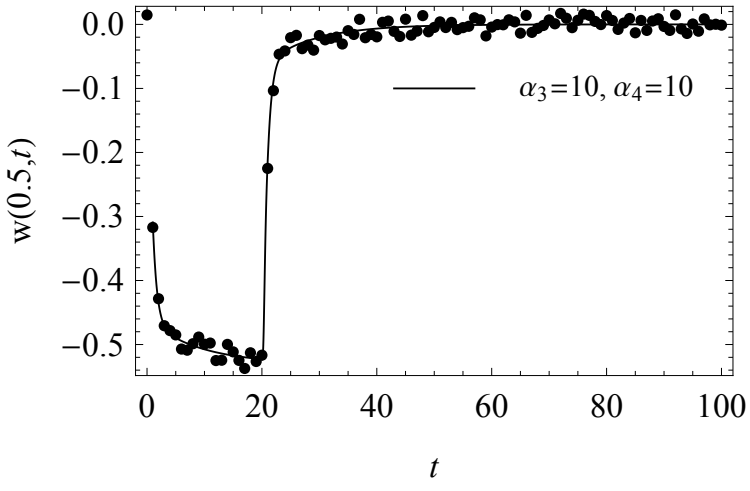

(a)

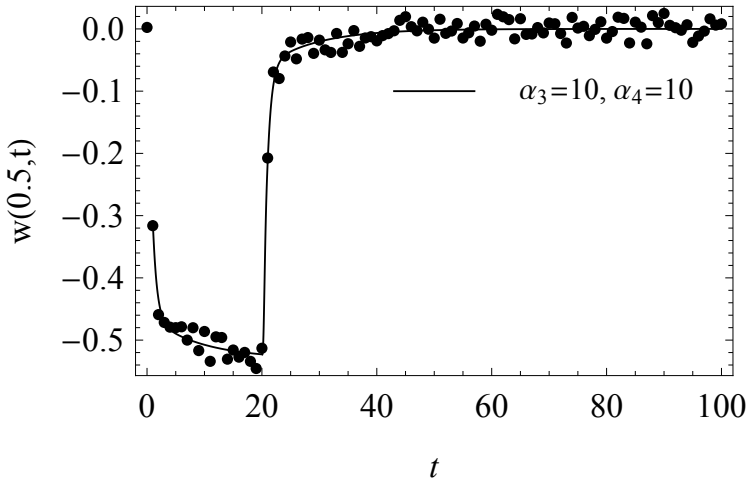

(b)

Figure 6.12: Simulated measurements (dots) and displacement solutions (solid line) based on estimated parameters in Table 6.5 with step input force (6.24) for (a) noisy measurements with standard deviation ±6%, and (b) noisy measurements with standard deviation ±10%.

here, and the experimental testing on soft and biological tissues that typically exhibit viscoelastic responses. The sensor model is being merged with a locomotion and shape

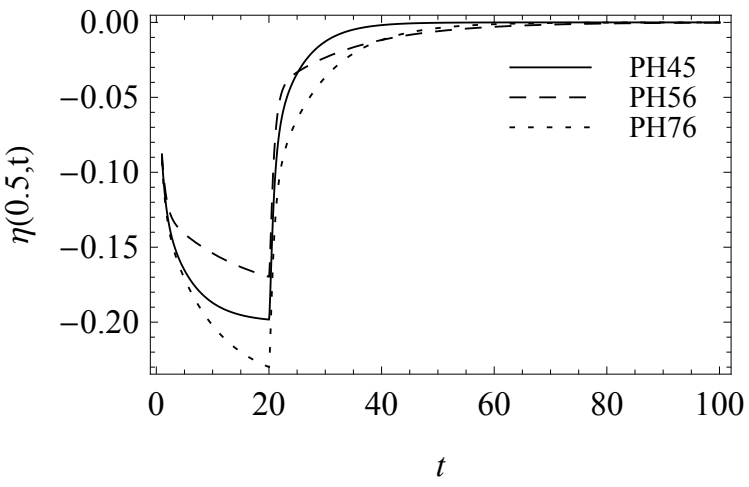

Figure 6.13: Simulated substrate displacement at point $x = 0.5$, based on estimated parameters in Table 6.4 with step input force (6.24).

morphing model for the same system, with the goal of realizing an autonomous hyper-redundant robotic system that can be deployed in non-structured environments and can be used for sensing, monitoring, and exploring. Device miniaturization allow for sensing of biological tissues with diagnosis related applications.

References

[1] C. Huang, C. Shih, S. Kim, An inverse vibration problem in estimating the spatial and temporal-dependent external forces for cutting tools, Applied Mathematical Modelling 33 (6) (2009) 2683–2698.

[2] W. Chen, Y. Yang, W. Chang, H. Lee, Inverse problem of estimating transient heat transfer rate on external wall of forced convection pipe, Energy Conversion and Management 49 (8) (2008) 2117–2123.

[3] D. T. W. Lin, W. Yan, H. Li, Inverse problem of unsteady conjugated forced convection in parallel plate channels, International Journal of Heat and Mass Transfer 51 (5-6) (2008) 993–1002.

[4] M. Girault, D. Petit, Resolution of linear inverse forced convection problems using model reduction by the Modal Identification Method: application to turbulent flow in parallel-plate duct, International Journal of Heat and Mass Transfer 47 (17-18) (2004) 3909–3925.

[5] C. Huang, W. Chen, A three-dimensional inverse forced convection problem in estimating surface heat flux by conjugate gradient method, International Journal of Heat and Mass Transfer 43 (17) (2000) 3171–3181.

[6] W. Chen, Dynamic modeling of multi-link flexible robotic manipulators, Journal of Computers and Structures 79 (2001) 183–195.

[7] B.-J. Lee, Geometrical Derivation of Differential Kinematics to Calibrate Model Parameters of Flexible Manipulator, International Journal of Advanced Robotic Systems 10.

[8] L. Chen, H. Deng, Model reduction of rigid-flexible manipulators with experimental validation, in: 3rd International Conference on Advances in Materials Manufacturing(ICAMMP 2012),, Vol. 655-657, pp. 1101–1107, Beihai, Peoples R China, Dec 22-23, 2012.

[9] H. Esfandiar, S. Daneshmand, Complete dynamic modeling and approximate state space equations of the flexible link manipulator, Journal of Mechanical Science and Technology 26 (9) (2012) 2845–2856.

[10] C. di Castri, A. Messina, Exact modeling for control of flexible manipulators, Journal of Vibration and Control 18 (10) (2012) 1526–1551.

[11] M. H. Korayem, H. N. Rahimi, A. Nikoobin, Mathematical modeling and trajectory planning of mobile manipulators with flexible links and joints, Applied Mathematical Modelling 36 (7) (2012) 3223–3238. doi:{10.1016/j.apm.2011.10.002}.

[12] H. Lee, C. Richards, R. Richards, Experimental and numerical study of microchannel heater/evaporators for thermal phase-change actuators, Sensors and Actuators A: Physical 195 (2013) 7–20.

[13] H. V. Thakur, S. M. Nalawade, Y. Saxena, K. Grattan, All-fiber embedded pm-pcf vibration sensor for structural health monitoring of composite, Sensors and Actuators A: Physical 167 (2) (2011) 204–212.

[14] K. M. Dolatshahi, F. R. Rofooei, Inverse vibration problem for un-damped 3-dimensional multi-story shear building models, Journal of Sound and Vibration 333 (1) (2014) 99–113. doi:{10.1016/j.jsv.2013.08.045}.

[15] C. Liu, An iterative GL(n, R) method for solving non-linear inverse vibration problems, Nonlinear Dynamics 74 (3) (2013) 685–699. doi:{10.1007/s11071-013-0997-2}.

[16] A. Maciag, A. Pawinska, Solving direct and inverse problems of plate vibration by using the Trefftz functions, Journal of Theoretical and Applied Mechanics 51 (3) (2013) 543–552.

[17] G. F. Safina, Analysis of Direct and Inverse Problems on Transverse Vibrations of a Supported Shaft, Russian Journal of Nondestructive Testing 46 (4) (2010) 302–313. doi:{10.1134/S106183091004008X}.

[18] W. Q., W. Y., Z. L., Inverse Mode Problem in the Discrete Model of Circular Plate Axial Symmetry Vibration, in: International Conference on Mechanical Engineering and Green Manufacturing (MEGM), 2010, pp. 71–78.

[19] B. N. Datta, V. Sokolov, Quadratic Inverse Eigenvalue Problems, Active Vibration Control and Model Updating, Applied and Computational Mathematics 8 (2) (2009) 170–191.

[20] L. D. Chiwiacowsky, H. F. De Campos Velho, P. Gasbarri, A variational approach for solving an inverse vibration problem, Inverse Problems in Science and Engineering 14 (5) (2006) 557–577, Symposium on Inverse Problems, Design and Optimization, Rio de Janeiro, Brazil, Mar 17-19, 2004. doi:{10.1080/17415970600574237}.

[21] H. Ressing, M. Gadala, A practical investigation to solving the inverse problem of crack identification through vibration measurements, Engineering Computations 23 (1-2) (2006) 32–56. doi:{10.1108/02644400610638961}.

[22] N. Khiem, Crack detection for structure based on the dynamic stiffness model and the inverse problem of vibration, Inverse Problems in Science and Engineering 14 (1) (2006) 85–96. doi:{10.1080/17415970500272908}.

[23] C. Huang, A generalized inverse force vibration problem for simultaneously estimating the time-dependent external forces, Applied Mathematical Modelling 29 (11) (2005) 1022–1039. doi:{10.1016/j.apm.2005.02.006}.

[24] C. Huang, A nonlinear inverse problem in estimating simultaneously the external forces for a vibration system with displacement-dependent parameters, Journal of The Franklin Institute. Engineering and Applied Mathematics 342 (7) (2005) 793–813. doi:{10.1016/j.jfranklin.2005.06.006}.

[25] C. Huang, A non-linear inverse vibration problem of estimating the external forces for a system with displacement-dependent parameters, Journal of Sound and Vibration 248 (5) (2001) 789–807. doi:{10.1006/jsvi.2001.3838}.

[26] J. Humphrey, Continuum biomechanics of soft biological tissues, Proceedings of the Royal Society A: Mathematical, Physical and Engineering Sciences 459 (2029) (2003) 3–46. doi:{10.1098/rspa.2002.1060}.

[27] Y. Fung, Biomechanics: Mechanical Properties of Living Tissues, Biomechanics, Springer, 1993.
http://books.google.ca/books?id=4HaMStTGOHwC

[28] M. D. Maestro, F. Cecchi, S. M. Serio, C. Laschi, P. Dario, Sensing device for measuring infants grasping actions, Sensors and Actuators A-physical 165 (2011) 155–163. doi:10.1016/j.sna.2010.08.016.

[29] M. Morris, F. Huxham, J. McGinley, K. Dodd, R. Iansek, The biomechanics and motor control of gait in Parkinson disease, Clinical Biomechanics 16 (6) (2001) 459–470. doi:{10.1016/S0268-0033(01)00035-3}.

[30] G. Y. H. Lee, C. T. Lim, Biomechanics approaches to studying human diseases, Trends in Biotechnology 25 (3) (2007) 111–118. doi:{10.1016/j.tibtech.2007.01.005}.

[31] E. J. Weinberg, D. Shahmirzadi, M. Mofrad, On the multiscale modeling of heart valve biomechanics in health and disease, Biomechanics and Modeling in Mechanobiology 9 (4) (2010) 373–387. doi:{10.1007/s10237-009-0181-2}.

[32] M. K. Rausch, E. Kuhl, On the effect of prestrain and residual stress in thin biological membranes, Journal of the Mechanics and Physics of Solids 61 (9) (2013) 1955–1969. doi:{10.1016/j.jmps.2013.04.005}.

[33] L. M. Sander, Alignment Localization in Nonlinear Biological Media, Journal of Biomechanical Engineering, Transactions of the ASME 135 (7). doi:{10.1115/1.4024199}.

[34] A. M. Zoellner, A. B. Tepole, E. Kuhl, On the biomechanics and mechanobiology of growing skin, Journal of Theoretical Biology 297 (2012) 166–175. doi:{10.1016/j.jtbi.2011.12.022}.

[35] G. Gladwell, Inverse Problems in Vibration, Mechanics, Dynamical Systems, Vol 9, Kluwer, 1986.
http://books.google.ca/books?id=uAvr4s9JTTAC

[36] D. Moss, H. Benaroya, A discrete inverse vibration problem with parameter uncertainty, Applied Mathematics and Computation 69 (2-3) (1995) 313–333. doi:{10.1016/0096-3003(94)00140-Y}.

[37] L. Starek, D. Iman, A. Kress, A Symmetric Inverse Vibration Problem, Journal of Vibration and Acoustics 114 (4) (1992) 564–568. doi:{10.1115/1.2930299}.

[38] M. Yamamoto, Inverse eigenvalue problem for a vibration of a string with viscous drag, Journal of Mathematical Analysis and Applications 152 (1) (1990) 20–34. doi:{10.1016/0022-247X(90)90090-3}.

[39] H. Banks, R. Powers, I. Rosen, Inverse problems in the modeling of vibrations of flexible beams, Lecture Notes in Control and Information Sciences 102 (1987) 1–22.

[40] A. Tsaune, V. Golovko, Anharmonic vibration-rotation inverse problem with reconstruction of Hamiltonian terms, Journal of Molecular Spectroscopy 108 (1) (1984) 82–98. doi:{10.1016/0022-2852(84)90288-1}.

[41] M. Hamada, Y. Seguchi, Y. Tada, Shape Determination Problems of Structures by the Inverse Variational Principle : 2nd Report, Buckling and Vibration Problems, The Japan Society of Mechanical EngineersBulletin of the JSME 23 (184) (1980) 1581–1588.

[42] N. Stepanov, G. Koptev, Y. Panchenko, Uniqueness of solution of an inverse vibration problem, Optika i spektroskopiya 38 (4) (1975) 657–662.

[43] W. Liu, D. Li, J. Shen, Least-squares solutions of constrained inverse eigenproblem and associated optimal approximation problem, International Journal of Computer Mathematics 90 (3) (2013) 641–650. doi:{10.1080/00207160.2012.735662}.

[44] M. S. Gockenbach, A. A. Khan, An abstract framework for elliptic inverse problems: Part 1. An output least-squares approach, Mathematics and Mechanics of Solids 12 (3) (2007) 259–276. doi:{10.1177/1081286505055758}.

[45] R. Forke, D. Scheibner, K. Hiller, T. Gessner, W. Dötzel, J. Mehner, Fabrication and characterization of a force coupled sensor–actuator system for adjustable resonant low frequency vibration detection, Sensors and Actuators A: Physical 145 (2008) 245–256.

[46] C. Yang, Solution of an inverse vibration problem using a linear least-squares error method, Applied Mathematical Modelling 20 (10) (1996) 785–788.

[47] D. Hua, P. Lancaster, Linear matrix equations from a non-linear inverse vibration problem of estimating the time-dependent stiffness coefficnverse problem of vibration theory, Linear Algebra and its Applications 246 (1996) 31–47.

[48] J. Fattahi, D. Spinello, Timoshenko Beam Model for Exploration and Sensing with a Continuum Centipede Inspired Robot, in: Proceedings of 2013 ASME Dynamic Systems and Control Conference, Vol. 5391, 2013, pp. 189–196. doi:{10.1117/12.546606}.

[49] J. Fattahi, D. Spinello, A Timoshenko beam reduced order model for shape tracking with a slender mechanism, Journal of Sound and Vibration 333 (20) (2014) 5165 – 5180. doi:http://dx.doi.org/10.1016/j.jsv.2014.05.040. http://www.sciencedirect.com/science/article/pii/S0022460X14004490

[50] R. W. Cahn, Biomimetics: Biologically inspired technologies, Nature 444 (7118) (2006) 425–426. doi:{10.1038/444425b}.

[51] L. Drago, G. Fusco, E. Garollo, A. Minelli, Structural aspects of leg-to-gonopod metamorphosis in male helminthomorph millipedes (Diplopoda), Frontiers in Zoology 8. doi:{10.1186/1742-9994-8-19}.

[52] M. Golubitsky, I. Stewart, P. Buono, J. Collins, A modular network for legged locomotion, Phisica D 115 (1-2) (1998) 56–72. doi:{10.1016/S0167-2789(97)00222-4}.

[53] L. D. Landau, E. M. Lifshitz, Theory of Elasticity, Vol. 7 of A Course of Theoretical Physics, Pergamon Press, 1970.

[54] S. Timoshenko, Vibration Problems In Engineering, D. Van Nostrand Company Inc., 1974.

[55] L. Meirovitch, Fundamentals of Vibrations, McGraw-Hill, 2001.

[56] A. Plaseied, A. Fatemi, Deformation response and constitutive modeling of vinyl ester polymer including strain rate and temperature effects, Journal of Materials Science 43 (4) (2008) 1191–1199. doi:10.1007/s10853-007-2297-z. http://dx.doi.org/10.1007/s10853-007-2297-z

[57] A. D. Kerr, Elastic and viscoelastic foundation models, Journal of Applied Mechanics 31 (1964) 491. doi:10.1115/1.3629667.

[58] S. C. Dutta, R. Roy, A critical review on idealization and modeling for interaction among soil-foundation-structure system, Computers & Structures 80 (20-21) (2002) 1579–1594. doi:{10.1016/S0045-7949(02)00115-3}.

[59] D. N. Paliwal, S. N. Sinha, Static and dynamic behavior of shallow spherical-shells on Winkler foundation, Thin-Walled Structures 4 (6) (1986) 411–422. doi:{10.1016/0263-8231(86)90038-8}.

[60] M. M. Filonenko-Borodich, Some approximate theories of the elastic foundation, Uchenyie Zapiski Moskovskogo Gosudarstuennogo Universiteta Mechanika (46) (1940) 3–1, (in Russian).

[61] P. L. Pasternak, On a new method of analysis of an elastic foundation by means of two foundation constants, Gosudarsrvennoe Izdatelstvo Literaturi po Stroitelstvu i Arkhitekture(in Russian).

[62] I. Calio, A. Greco, Free vibrations of Timoshenko beam-columns on Pasternak foundations, Journal of Vibration and Control 19 (5) (2013) 686–696. doi:{10.1177/1077546311433609}.

[63] C. R. Briscoe, S. C. Mantell, J. H. Davidson, Buckling of a plate on a Pasternak foundation under uniform in-plane bending loads, International Journal of Structural Stability and Dynamics 13 (3). doi:{10.1142/S0219455412500708}.

[64] R. Jones, J. Xenophontos, The Vlasov foundation model, International Journal of Mechanical Sciences 19 (6) (1977) 317–23.

[65] V. Z. Vlasov, U. Leont'ev, Beams, plates, and shells on elastic foundation, Gosudarst vennoe lzdatel'st vo Ftziko-Matematicheskoi Literatury Moskva.

[66] M. Levinson, Generalized Vlasov-Jones foundation model - a foundation of grade-4, International Journal of Mechanical Sciences 25 (2) (1983) 149–154. doi:{10.1016/0020-7403(83)90007-3}.

[67] A. Shams, M. Porfiri, A generalized Vlasov-Jones foundation model for micromechanics studies of syntactic foams, Composite Structures 103 (2013) 168–178. doi:{10.1016/j.compstruct.2013.04.020}.

[68] F. Zhaohua, D. R. Cook, Beam elements on two-parameter elastic foundation, Journal of Engineering Mechanics 109 (6) (1983) 1390–1402.

[69] M. Kneifati, Analysis of plates on a kerr foundation model, Journal of Engineering Mechanics 111 (11) (1985) 1325–1342. doi:10.1061/(ASCE)0733-9399(1985)111:11(1325).

[70] M. Works, fminsearch, http://www.mathworks.com/help/matlab/ref/fminsearch.html (Release 12).

[71] D. Craiem, F. J. Rojo Pérez, J. M. Atienza Riera, G. V. Guinea Tortuero, R. L. Armentano, Fractional calculus applied to model arterial viscoelasticity, Latin American applied research 38 (2) (2008) 141–145.

[72] R. Myers, Classical and Modern Regression With Applications, Duxbury classic series, Duxbury/Thompson Learning, 1990.
http://books.google.ca/books?id=LOHHKQAACAAJ

[73] N. F. J. van Rensburg, A. J. van der Merwe, Natural frequencies and modes of a Timoshenko beam, Wave Motion 44 (1) (2006) 58–69. doi:{10.1016/j.wavemoti.2006.06.008}.

[74] J. Fattahi and D. Spinello, "Sensing linear viscoelastic constitutive parameters with a timoshenko beam on a multi-layer foundation: Modeling and simulation," *Sensing and Bio-Sensing Research*, vol. 4, pp. 78–89, 2015.

Appendix 1: Basis functions

To obtain the natural frequencies and associated eigenfunctions for w and ψ we follow the approach in [73], which is based on the solution of a vector eigenvalues problem for the system of two coupled second order differential equations for the transverse displacement and for the the rotation of the cross section. For the analytical expressions we follow the general procedure that consists on the time-space separation of variables followed by substitution in the homogeneous governing equations. The general solution of the second and third equations (6.10) with $\alpha_3 = \alpha_4 = 0$ (no forcing terms and no coupling with the substrate) is therefore assumed to be of the form

$$\begin{pmatrix} w(x,t) & \psi(x,t) \end{pmatrix}^{\mathsf{T}} = \exp(\mathrm{i}\omega t) \begin{pmatrix} W(x) & \Psi(x) \end{pmatrix}^{\mathsf{T}}$$

where ω is the frequency of oscillation, $i = \sqrt{-1}$ is the imaginary unit, and $W(x)$, $\Psi(x)$ are functions in $[0,1]$ that express the dependency on x. By separating the variables and considering the vector evaluated function $\exp(\lambda x) \begin{pmatrix} \bar{W} & \bar{\Psi} \end{pmatrix}^{\mathsf{T}}$, where $\bar{W}$ and $\bar{\Psi}$ are constants, in the spatial eigenvalue problem. Spatial eigenvalue function is a solution for some positive constant λ if and only if

$$\begin{pmatrix} \lambda^2 + \beta_1 & -\lambda \\ \beta_3 \lambda & \lambda^2 + \beta_2 \end{pmatrix} \begin{pmatrix} \bar{W} \\ \bar{\Psi} \end{pmatrix} = \begin{pmatrix} 0 \\ 0 \end{pmatrix}$$

with nondimensional parameters β_i defined by

$$\beta_1 = \omega^2, \quad \beta_2 = \alpha_1 \left(\omega^2 - \alpha_2\right), \quad \beta_3 = \alpha_1 \alpha_2$$

In order the root of the characteristic polynomial $\lambda^4 + (\beta_1 + \beta_2 + \beta_3)\lambda^2 + \beta_1\beta_2 = 0$ to be real it must be $\Delta > 0$, which is satisfied for $\beta_1\beta_2 < \gamma^2/4$, where $\gamma = \beta_1 + \beta_2 + \beta_3$. The condition $\Delta > 0$ dictates $\omega > 0$; therefore it must be $\gamma > 0$ since this is the case when γ is evaluated for $\omega > 0$. For $\Delta > 0$ and $\gamma > 0$ we have

$$\lambda_1 = \pm i\theta, \quad \theta^2 = \frac{\gamma}{2}\left(\sqrt{\Delta} + 1\right)$$

For $\beta_1\beta_2 < 0$ we have $\sqrt{\Delta} > 1$ and

$$\lambda_2 = \pm\mu, \quad \mu^2 = \frac{\gamma}{2}\left(\sqrt{\Delta} - 1\right)$$

For this case the general solution is therefore given by [73]

$$\Phi(x) = C_1 \begin{pmatrix} \sin\theta x \\ -\frac{\beta_1-\theta^2}{\theta}\cos\theta x \end{pmatrix} + C_2 \begin{pmatrix} \cos\theta x \\ \frac{\beta_1-\theta^2}{\theta}\sin\theta x \end{pmatrix} + C_3 \begin{pmatrix} \sinh\mu x \\ \frac{\beta_1+\mu^2}{\mu}\cosh\mu x \end{pmatrix} + C_4 \begin{pmatrix} \cosh\mu x \\ \frac{\beta_1+\mu^2}{\mu}\sinh\mu x \end{pmatrix}$$

Imposing the free end boundary conditions at $x = 0$ we obtain

$$C_1 = C_3\frac{\theta}{\mu} \quad C_2 = -C_4\frac{\beta_1+\mu^2}{\beta_1-\theta^2}$$

By imposing the free end boundary conditions at $x = 1$ we obtain the following linear algebraic relations involving C_3 and C_4

$$\mathbf{A}\begin{pmatrix} C_3 \\ C_4 \end{pmatrix} = \begin{pmatrix} 0 \\ 0 \end{pmatrix}$$

with coefficients matrix $\mathbf{A}$ given by

$$\mathbf{A} = \begin{pmatrix} \frac{\theta}{\mu}\left(\beta_1-\theta^2\right)\sin\theta + \left(\beta_1+\mu^2\right)\sinh\mu & \left(\beta_1+\mu^2\right)\left(\cosh\mu-\cos\theta\right) \\ -\frac{\beta_1}{\mu}\cosh\mu & -\frac{\beta_1}{\mu}\sinh\mu \end{pmatrix}$$

The nontrivial solutions of the system are obtained by investigating the condition for rank deficiency of the coefficients matrix, which translates to the determinant being zero

$$-\cos\theta\cosh\mu + \frac{\theta(\theta^2-\beta_1)}{\mu(\mu^2+\beta_1)}\sin\theta\sinh\mu + 1 = 0 \tag{6.26}$$

All parameters in the characteristic equation depend on ω and on the material and geometric parameters of the system. Therefore, once the material and the geometry are defined the characteristic equation is a nonlinear function of ω only.

Appendix 2: Galerkin projection

The Galerkin projection technique dictates the substitution of (6.14) into the second and third equations (6.10) and premultiplication by the sets of test functions $\bar{\mathbf{w}}$, $\bar{\boldsymbol{\psi}}$, and $\bar{\eta}$ respectively. Integration of the domain of the projected governing equations and

integration by parts give

$$\int_0^1 \bar{\mathbf{w}}\left(\bar{\mathbf{w}}^\mathsf{T}\ddot{\mathbf{a}} + \frac{\alpha_w}{\omega^\star}\bar{\mathbf{w}}^\mathsf{T}\dot{\mathbf{a}} + \alpha_3\bar{\mathbf{w}}^\mathsf{T}\mathbf{a}\right)\mathrm{d}x - \int_0^1 \frac{\mathrm{d}\bar{\mathbf{w}}}{\mathrm{d}x}\bar{\boldsymbol{\psi}}^\mathsf{T}\mathbf{b}\mathrm{d}x + \int_0^1 \frac{\mathrm{d}\bar{\mathbf{w}}}{\mathrm{d}x}\frac{\mathrm{d}\bar{\mathbf{w}}^\mathsf{T}}{\mathrm{d}x}\mathbf{a}\mathrm{d}x$$
$$- \bar{\mathbf{w}}\left(\frac{\mathrm{d}\bar{\mathbf{w}}^\mathsf{T}}{\mathrm{d}x}\mathbf{a} - \bar{\boldsymbol{\psi}}^\mathsf{T}\mathbf{b}\right)\Big|_0^1 - \int_0^1 \alpha_3\bar{\mathbf{w}}\bar{\eta}\mathrm{d}x = \int_0^1 \bar{\mathbf{w}}p_b\mathrm{d}x \tag{6.27}$$

$$\int_0^1 \bar{\boldsymbol{\psi}}\left(\bar{\boldsymbol{\psi}}^\mathsf{T}\ddot{\mathbf{b}} + \frac{\alpha_\psi}{\omega^\star}\bar{\boldsymbol{\psi}}^\mathsf{T}\dot{\mathbf{b}} - \alpha_1\alpha_2\left(\frac{\mathrm{d}\bar{\mathbf{w}}^\mathsf{T}}{\mathrm{d}x}\mathbf{a} - \bar{\boldsymbol{\psi}}^\mathsf{T}\mathbf{b}\right) - \alpha_4\frac{\mathrm{d}\bar{\boldsymbol{\psi}}^\mathsf{T}}{\mathrm{d}x}\mathbf{b}\right)\mathrm{d}x$$
$$+ \int_0^1 \frac{\mathrm{d}\bar{\boldsymbol{\psi}}}{\mathrm{d}x}\frac{\mathrm{d}\boldsymbol{\psi}^\mathsf{T}}{\mathrm{d}x}\mathbf{b}\mathrm{d}x - \bar{\boldsymbol{\psi}}\frac{\mathrm{d}\bar{\boldsymbol{\psi}}^\mathsf{T}}{\mathrm{d}x}\mathbf{b}\Big|_0^1 + \int_0^1 \alpha_4\bar{\boldsymbol{\psi}}\frac{\partial\bar{\eta}}{\partial x}\mathrm{d}x = \int_0^1 \bar{\boldsymbol{\psi}}p_c\mathrm{d}x \tag{6.28}$$

$$\int_0^1 \bar{\eta}\left((\beta_\mu\bar{\eta} + \beta_\mu(\beta_1+\beta_2)\frac{\bar{\eta}}{d})\dot{\mathbf{c}} + (\beta_1\bar{\eta} + \beta_1\beta_2\frac{\bar{\eta}}{d})\mathbf{c}\right)\mathrm{d}x$$
$$- \int_0^1 \bar{\eta}\left(\beta_1\bar{\mathbf{w}}\dot{\mathbf{a}} + \beta_2\bar{\mathbf{w}}\mathbf{a}\right)\mathrm{d}x = 0 \tag{6.29}$$

Part III

Conclusion

Chapter 7

Summary and Conclusions

7.1 Summary

The first part of the thesis has served as an introduction about organization and motivation of this work. A detailed introduction has been proposed to describe the robotic modelling in general. A literature review in the field of hyper redundant mechanisms and robotics is given Chapter 1. An overview of significant modeling frameworks used in the attached papers has been given in the rest of Part I.

In Chapter 4 we presented the model of a continuous slender mechanism that is the first step towards the modeling and design of a hyper-redundant autonomous with adaptive body shape. The model describes the coupling with a substrate represented by a smooth curve, with the physical connection between the body and the substrate represented by a distribution of linear compliant elements. The time varying system is conveniently described in closed loop form with desired trajectory related to the shape of the substrate. We formulated the problem as a tracking system with the deformed shape of the robot reproducing the shape of the substrate. The model proposed here is suitable to describe the shape adaptation of slender flexible robotic devices coupled with the substrate. If the device is used as a sensor, the deformation can be used as a measure of the shape of an unknown substrate, and therefore to estimate it.

Chapter 5 included the explicit inclusion of the rigid body motion with tracking of the position and orientation of the substrate to dictate the undeformed configuration of the system with respect to which one measures the deformation. Considering the floating frame description, the forward locomotion is expressed in terms of the rigid body degrees of freedom tracking a moving point on the substrate.

Chapter 6 described a sensor model for a hyper redundant slender mechanism for estimating the properties of a viscoelastic substrate. A constitutive model has been introduced for a system of beam with distributed compliant elements which are coupled with the viscoelastic profile. The governing equations for this coupled system has been addressed, and the sensor model was based on numerical inverse problem method, which used the reduced order form of the governing equation as referenced model. The presented inverse problem is based on residual least square error method, which used a system of distributed displacement sensors as measurements.

7.2 Contributions

The contributions of the candidate's research cover the objectives set out for this thesis. These objectives were:

Developing a continuous, hyper redundant model for a slender robot: We developed an appreciation of the robot's flexible body as a linearized planar Timoshenko beam theory, where the shape morphing is associated to the coupling with a substrate that models a generic environment in which the system could be deployed. This mechanical model mimics the spinal locomotion mechanisms of millipedes and centipedes in which the flexible body morphs with respect to the curvature of the substrate. The interaction with the environment has been described by a continuous distribution of spring elements mimicking the robot legs.

Developing an inverse problem for a slender mechanism: We Developed a study of distributed sensor in order to find the properties of the environment that system has been deployed in. Since distributed compliant elements can act as a distributed sensor to reconstruct the kinematics of the substrate to which the robot is coupled. This work performs an inverse problem for continuous systems using distributed strain gauges. By exploiting this relation and the possible generalization, one can model the robot as a sensor to infer certain material properties of the substrate.

Developing a model of a slender robot for path tracking: We developed a study on spinal and forward motion control algorithms, in which proposed system's Lagrangian gives an algorithm for classical and modern control framework, in order to tune the system deformability and control the forward motion. To describe the motion of the robot, we adopt the concept of floating frame that is composed of a rigid body placement and by deformation about the rigid body placement. We proposed mathematical models, which analytically deal with both shape adaptation and forward motion modelling of a

slender robot mechanism through linear Timoshenko beam theory. Systems modelled in this manner are referred to as distributed parameter (continuous) systems, in which, both forces and deformabilty are distributed throughout the extent of the system which is treated as continuous.

Developing a bio-inspired model for a slender robot: We developed a study of millipede's locomotion. In order to cover all essential steps in the analysis of the system, we propose mathematical models, which analytically deal with both shape adaptation and forward motion modelling of a slender robot mechanism through linear Timoshenko beam theory. Systems modelled in this manner are referred to as distributed parameter (continuous) systems, in which, both forces and deformabilty are distributed throughout the extent of the system which is treated as continuous.

7.3 Future Work

Possible future research directions developing from this study are:

Shape Reconstruction Sensor: Considering the concept of the first paper (Chapter 4), the presented model can be used as shape sensor to reconstruct the shape of curvy substrates, which are out of reach to measure, like gastrointestinal organs inside the body, body's vessels or even pipes in hazardous area. Also, it can be used as a health monitoring sensor in order to check the deformation of the gas pipe or dams, which are hard to measure technically.

Shape Morphing Robot using Smart Materials: Considering the work presented in Chapter 5 , by adding layer of Shape Memory Polymer, which creates a high deformation with low electric consumption, we can develop the presented model as a tunable system with respect to different environments.

Force Sensor: Considering the work presented in Chapter 6, we can consider the system of compliant elements as distributed force sensors. Then, the presented model can be used as a sensor to estimate other properties of a viscoelastic substrate like relaxation moduli.

Complete Bibliography

[1] D. Craiem, F. J. Rojo Pérez, J. M. Atienza Riera, G. V. Guinea Tortuero, and R. L. Armentano, "Fractional calculus applied to model arterial viscoelasticity," *Latin American applied research*, vol. 38, no. 2, pp. 141–145, 2008.

[2] R. Bogue, "Exoskeletons and robotic prosthetics: a review of recent developments," *Industrial Robot- An International Journal*, vol. 36, no. 5, pp. 421–427, 2009.

[3] M. Kassler, "Robotics for health care: a review of the literature," *Robotica*, vol. 11, pp. 495–516, NOV-DEC 1993.

[4] K. Doty, C. Melchiorri, and C. Bonivento, "A theory of generalized inverses applied to robotics," *International Journal of Robotics Research*, vol. 12, pp. 1–19, FEB 1993.

[5] S. Dubowsky and E. Papadopoulos, "The kinematics, dynamics, and control of free-flying and free-floating space robotic systems," *IEEE Transactions on Robotics and Automation*, vol. 9, pp. 531–543, OCT 1993.

[6] R. Van Ham, T. G. Sugar, B. Vanderborght, K. W. Hollander, and D. Lefeber, "Compliant Actuator Designs Review of Actuators with Passive Adjustable Compliance/Controllable Stiffness for Robotic Applications," *IEEE Robotics & Automation Magazine*, vol. 16, pp. 81–94, SEP 2009.

[7] P. Darie, E. Guglielmelli, B. Allotta, and M. Carrozza, "Robotics for medical applications," *IEEE Robotics & Automation Magazine*, vol. 3, pp. 44–56, SEP 1996.

[8] M. Hoffmann, H. G. Marques, A. H. Arieta, H. Sumioka, M. Lungarella, and R. Pfeifer, "Body Schema in Robotics: A Review," *IEEE Transactions on Autonomous Mental Development*, vol. 2, pp. 304–324, DEC 2010.

[9] N. Tejima, "Rehabilitation robotics: a review," *Advance Robotic*, vol. 14, no. 7, pp. 551–564, 2000.

[10] S. A. Green, M. Billinghurst, X. Chen, and J. G. Chase, "Human-Robot Collaboration: A Literature Review and Augmented Reality Approach In Design," *International Journal of Advanced Robotic Systems*, vol. 5, pp. 1–18, MAR 2008.

[11] R. Janssen, N.-M. Prpic, and W. G. M. Damen, "A review of the correlation of tergites, sternites, and leg pairs in diplopods," *Frontiers in Zoology*, vol. 3, pp. 1–10, Feb 2006.

[12] A. A. Shabana, *Dynamics of Multibody Systems*. Cambridge University Press, 3 ed., 2010.

[13] C. Altafini, "Following a path of varying curvature as an output regulation problem," *IEEE Transactions on Automatic Control*, vol. 47, pp. 1551–1556, Sep 2002.

[14] F. L. Lewis, D. M. Dawson, and C. T. Abdallah, *Robot manipulator control: theory and practice*. CRC Press, 2003.

[15] M. Wojtyra and J. Fraczek, "Comparison of Selected Methods of Handling Redundant Constraints in Multibody Systems Simulations," *Journal of Computational and Nonlinear Dynamics*, vol. 8, APR 2013.

[16] M. A. Sherman, A. Seth, and S. L. Delp, "Simbody: multibody dynamics for biomedical research," in *IUTAM Symposium on Human Body Dynamics* (McPhee, J and Kovecses, J, ed.), vol. 2 of *Procedia IUTAM*, pp. 241–261, Int Union Theoret & Appl Mech (IUTAM), 2011. IUTAM Symposium on Human Body Dynamics - From Multibody Systems to Biomechanics, Univ Waterloo, Waterloo, CANADA, JUN 05-08, 2011.

[17] G. Schultz and K. Mombaur, "Modeling and Optimal Control of Human-Like Running," *IEEE/ASME Transactions on Mechatronics*, vol. 15, pp. 783–792, OCT 2010.

[18] A. Carvalho and A. Suleman, "Multibody simulation of the musculoskeletal system of the human hand," *Multibody System Dynamics*, vol. 29, pp. 271–288, MAR 2013.

[19] T. M. Guess, "Forward dynamics simulation using a natural knee with menisci in the multibody framework," *Multibody System Dynamics*, vol. 28, pp. 37–53, AUG 2012.

[20] A. Stops, R. Wilcox, and Z. Jin, "Computational modelling of the natural hip: a review of finite element and multibody simulations," *Computer Methods in Biomechanics and Biomedical Engineering*, vol. 15, no. 9, pp. 963–979, 2012.

[21] M. E. Lund, M. de Zee, M. S. Andersen, and J. Rasmussen, "On validation of multibody musculoskeletal models," *Proceedings of the Institution of Mechanical Engineers Part H Journal of Engineering in Medicine*, vol. 226, no. H2, SI, pp. 82–94, 2012.

[22] F. Naets, T. Tamarozzi, G. H. K. Heirman, and W. Desmet, "Real-time flexible multibody simulation with Global Modal Parameterization," *Multibody System Dynamics* , vol. 27, pp. 267–284, MAR 2012.

[23] V. Sonneville and O. Bruls, "Sensitivity analysis for multibody systems formulated on a Lie group," *Multibody System Dynamics*, vol. 31, pp. 47–67, JAN 2014.

[24] A. Muller and Z. Terze, "On the choice of configuration space for numerical Lie group integration of constrained rigid body systems," *Journal of Computational and Applied Mathematics*, vol. 262, pp. 3–13, MAY 15 2014. 13th Seminar Numerical Solution of Differential and Differential-Algebraic Equations (NUMDIFF), Martin Luther Univ Halle Wittenberg, Halle, GERMANY, SEP 10-14, 2012.

[25] Z. Terze, M. Vrdoljak, and D. Zlatar, "Geometric Mathematical Framework for Multibody System Dynamics," in *Numerical Analysis and Applied Mathematics, VOLS I-III* (Psihoyios, G and Tsitouras, C, ed.), vol. 1281 of *AIP Conference Proceedings*, pp. 1288–1291, European Soc Comp Methods Sci & Engn, 2010. International Conference on Numerical Analysis and Applied Mathematics, Rhodes, GREECE, SEP 19-25, 2010.

[26] O. Bruls and A. Cardona, "On the Use of Lie Group Time Integrators in Multibody Dynamics," *Journal of Computational and Nonlinear Dynamics*, vol. 5, JUL 2010.

[27] A. Wynn, Y. Wang, R. Palacios, and P. J. Goulart, "An energy-preserving description of nonlinear beam vibrations in modal coordinates," *Journal of Sound and Vibration*, vol. 332, pp. 5543–5558, OCT 14 2013.

[28] J. Ding and Z. Pan, "Higher Order Variational Integrators for Multibody System Dynamics with Constraints," *Advances in Mechanical Engineering*, 2014.

[29] P. Betsch, C. Hesch, N. Saenger, and S. Uhlar, "Variational Integrators and Energy-Momentum Schemes for Flexible Multibody Dynamics," *Journal of Computational and Nonlinear Dynamics*, vol. 5, JUL 2010.

[30] M. Pascal, "Some open problems in dynamic analysis of flexible multi-body systems," *Journal of Multibody System Dynamics*, vol. 5, pp. 315–334, 2001.

[31] F. Bellezza, L. Lanari, and G. Ulivi, "Exact modeling of the slewing flexible link," *Proceedings of the IEEE International Conference on Robotics and Automation*, pp. 734–739, 1999.

[32] M. W. D. White and G. R. Heppler, "Timoshenko model of a flexible slewing link," *Proceedings of the American Control Conference*, pp. 2815–2819, 1995.

[33] J. C. Ower and J. Van de Vegte, "Classical control design for a flexible manipulator: modeling and control system design," *Journal of Robotics and Automation*, vol. 3, pp. 485–489, 1987.

[34] A. De Luca and B. Siciliano, "Closed-form dynamic model of planar multilink lightweight robots," *IEEE Transactions on Systems, Man and Cybernetics*, vol. 21, pp. 826–839, 1991.

[35] P. Tomei and A. v, "Approximate modeling of robots having elastic links," *IEEE Transactions on Systems, Man and Cybernetics*, vol. 18, pp. 831–840, 1988.

[36] Y. Chaolan, H. Jiazhen, and C. Guoping, "Modeling study of a flexible hub-beam system with large motion and with considering the effect of shear deformation," *Journal of Sound and Vibration*, vol. 295, pp. 282–293, 2006.

[37] W. Chen, "Dynamic modeling of multi-link flexible robotic manipulators," *Journal of Computers and Structures*, vol. 79, pp. 183–195, 2001.

[38] H. H. Lee, "New dynamic modeling of flexible-link robots," *Journal of Dynamic Systems, Measurement and Control*, vol. 127, pp. 307–309, 1956.

[39] X. Zhang, W. Xu, S. S. Nair, and V. S. Chellaboina, "Pde modeling and control of a flexible two-link manipulator," *IEEE Transactions on Control Systems Technology*, vol. 13, pp. 301–312, 2005.

[40] R. I. Milford and S. F. Asokanthan, "Configuration dependent eigenfrequencies for a two-link flexible manipulator: experimental verification," *Journal of Sound and Vibration*, vol. 222, pp. 191–207, 1999.

[41] C. di Castri, A. Messina, and G. Reina, "Modeling effects on free vibration of a two-link flexible manipulator," *Proceedings of The Eighteenth CISM-IFToMM Symposium*, vol. 524, pp. 99–107, 2010.

[42] P. Pai and A. Palazotto, "Large-deformation analysis of flexible beams," *International Journal of Solids and Structures*, vol. 33, pp. 1335–1353, APR 1996.

[43] S. Von Dombrowski, "Analysis of large flexible body deformation in multibody systems using absolute coordinates," *Multibody System Dynamics*, vol. 8, pp. 409–432, NOV 2002.

[44] J. Gerstmayr and H. Irschik, "On the correct representation of bending and axial deformation in the absolute nodal coordinate formulation with an elastic line approach," *Journal of Sound and Vibration*, vol. 318, pp. 461–487, DEC 9 2008.

[45] H. Yoo, R. Ryan, and R. Scott, "Dynamics of flexible beams undergoing overall motions," *Journal of Sound and Vibration*, vol. 181, pp. 261–278, MAR 23 1995.

[46] R. Kang, D. T. Branson, T. Zheng, E. Guglielmino, and D. G. Caldwell, "Design, modeling and control of a pneumatically actuated manipulator inspired by biological continuum structures," *Bioinspiration & Biomimetics*, vol. 8, Sep 2013.

[47] G. Chirikjian and J. Burdick, "Kinematically optimal hyper-redundant manipulator configurations," *IEEE Transactions on Robotics and Automation*, vol. 11, pp. 794–806, Dec 1995.

[48] B. Atakan, A. Erkmen, and I. Erkmen, "3-D grasping during serpentine motion with a snake-like robot," in *Proceedings of the Sixth IASTED International Conference on Robotics and Applications* (Gerhardt, LA, ed.), pp. 46–51, Int Assoc Sci & Technol Dev, Oct 31-Nov 02 2005. Cambridge, MA.

[49] D. L. P. Bopearatchy and G. C. Hatanwala, "State space control of a multi link robot manipulator by a translational modelling technique," in *Intelligent Control, 1990. Proceedings., 5th IEEE International Symposium on*, pp. 285–290 vol.1, 1990.

[50] T. Nanayakkara, K. Watanabe, K. Kiguchi, and K. Izumi, "Controlling multi-link manipulators by fuzzy selection of dynamic models," in *Industrial Electronics Society, 2000. IECON 2000. 26th Annual Confjerence of the IEEE*, vol. 1, pp. 638–643 vol.1, 2000.

[51] M. Moallem, K. Khorasani, and R. Patel, "An inverse dynamics sliding control technique for flexible multi-link manipulators," in *American Control Conference, 1997. Proceedings of the 1997*, vol. 3, pp. 1407–1411 vol.3, 1997.

[52] J.-X. Xu, Y.-J. Pan, and T.-H. Lee, "A gain shaped sliding mode control scheme using filtering techniques with applications to multi-link robotic manipulators," in *Proceedings of the American Control Conference*, vol. 6, pp. 4363–4368 vol.6, 2001.

[53] C. Wright, A. Johnson, A. Peck, Z. McCord, A. Naaktgeboren, P. Gianfortoni, M. Gonzalez-Rivero, R. Hatton, and H. Choset, "Design of a modular snake robot," *Proceedings of The IEEE/RSJ International Conference on Intelligent Robots and Systems*, vol. 1, pp. 2609–2614, 2007.

[54] M. Tesch, K. Lipkin, I. Brown, R. Hatton, A. Peck, J. Rembisz, , and H. Choset, "Parameterized and scripted gaits for modular snake robots," *journal of advanced Robotics*, vol. 23, pp. 1131–1158, 2009.

[55] R. L. Hatton and H. Choset, "Generating gaits for snake robots by annealed chain fitting and keyframe wave extraction," *Proceedings of The IEEE/RSJ International Conference on Intelligent Robots and Systems*, vol. 1, pp. 840–845, 2009.

[56] Z. Shiller and Y. GWO, "Dynamic motion planning of autonomous vehicles," *IEEE Transactions on Robotics and Automation*, vol. 7, pp. 241–249, APR 1991.

[57] B. Dandrea-Novel, G. Bastin, and G. Campion, "Modelling and control of non-holonomic wheeled mobile robots," in *1991 IEEE International Conference on Robotics and Automation, VOLS 1-3*, pp. 1130–1135, 1991. 1991 International Conference on Robotics and Automation, Sacramento, CA, Apr 09-11, 1991.

[58] J. Gray and H. Lissmann, "Studies in animal locomotion VII. Locomotory reflexes in the earthworm," *Journal of Experimental Biology*, vol. 15, pp. 506–517, Oct 1938.

[59] J. Martins, M. Botto, and J. da Costa, "A Newton-Euler model of a piezo-actuated nonlinear elastic manipulator link," in *Proceedings of the 11th International Conference on Advanced Robotics 2003* (Nunes, U and deAalmeida, AT and Bejczy, AK and Kosuge, K and Macgado, JAT, ed.), vol. 1-3, (Coimbra, Portugal, Jun 30-Jul 03), pp. 935–940, 2003.

[60] B. Jayne, "Kinematics of Terrestrial Snake Locomotion ," *Copeia*, pp. 915–927, Dec 23 1986.

[61] Y. Umetani and S. Hirose, "Biomecanical study of serpentine locomotion," *Proceedings of the 1st ROMANSY Symp Udine*, vol. 177, pp. 171–184, 1974.

[62] S. Hirose, K. Ikuta, M. Tsukamoto, , and K. Sato, "Considerations in design of the actuator based in the shape memory effect," *Proceedings of the 6th IGToMM Congress*, pp. 1549–1556, 1987.

[63] S. Hirose and Y. Umetani, "The kinematics and control of a soft gripper for the handling of living and fragile objects," *Proceedings of the IGToMM Congress*, pp. 1549–1556, 1979.

[64] W. I. Clement and R. M. Inigo, "Design of a snake-like manipulator," *Journal Robotics and Autonomous Systems.*, vol. 6, pp. 265–282, 1990.

[65] S. Chiang, C. Crane, and J. Duffy, "Path planning for an articulated transporter manipulator system," *Proc. of the 22nd ASME Mechanisms Conf.*, vol. 45, pp. 405–412, 1992.

[66] E. I. Verriest, "Efficient motion planning for a planar multiple link robot, based on differential friction," *Proc. of IEEE Decision and Control Conf.*, vol. 3, pp. 2364–2365, 1989.

[67] D. Sen and T. S. Mruthyunjays, "Studies of a new snake-like manipulator," *ASME Conf. Robotics, Spatial Mechanisms, and Mechanical Systems*, vol. 45, pp. 423–438, 1992.

[68] G. Chirikjian and J. Burdick, "Kinematics of hyper-redundant manipulators," *Proc. ASME Conf. of Mechanism*, pp. 391–396, 1990.

[69] *Biologically inspired robots: Snake-like locomotors and manipulators*, vol. 64. University of Oxford Press, first ed., 1993.

[70] H. Yamada, S. Chigisaki, M. Mori, K. Takita, K. Ogami, and S. Hirose, "Development of amphibious snake-like robot acm-r5," *Proc. ISR2005*, 2005.

[71] A. Motahari, H. Zohoor, and M. H. Korayem, "A New Inverse Kinematic Algorithm For Discretely Actuated Hyper-redundant Manipulators," *Latin American applied research*, vol. 43, pp. 161–168, APR 2013.

[72] A. Chibani, C. Mahfoudi, T. Chettibi, and R. Merzouki, "Conceptual Study of a Class of Hybrid Hyper-Redundant Robot," in *IEEE International Conference on Robotics and Biomimetics (ROBIO)*. Guangzhou, P R China, DEC 11-14, 2012.

[73] M. G. Marcos, J. A. T. Machado, and T. P. Azevedo-Perdicoulis, "A fractional approach for the motion planning of redundant and hyper-redundant manipulators," *Signal Processing*, vol. 91, pp. 562–570, MAR 2011.

[74] S. Yahya, H. A. F. Mohamed, M. Moghavvemi, and S. S. Yang, "A Geometrical Inverse Kinematics Method for Hyper-Redundant Manipulators," in *10th International Conference on Control, Automation, Robotics and Vision, VOLS 1-4*, pp. 1954–1958. Hanoi, Vietnam, DEC 17-20, 2008.

[75] F. Fahimi, H. Ashrafiuon, and C. Nataraj, "An improved inverse kinematic and velocity solution for spatial hyper-redundant robots," *IEEE Transactions on Robotics and Automation*, vol. 18, pp. 103–107, FEB 2002.

[76] H. Mochiyama, E. Shimemura, and H. Kobayashi, "Shape control of manipulators with hyper degrees of freedom," *International Journal of Robotics Research*, vol. 18, pp. 584–600, JUN 1999.

[77] G. Chirikjian and J. Burdick, "A modal approach to hyper-redundant manipulator kinematics," *IEEE Transactions on Robotics and Automation*, vol. 10, pp. 343–354, JUN 1994.

[78] C. Huang, C. Shih, and S. Kim, "An inverse vibration problem in estimating the spatial and temporal-dependent external forces for cutting tools," *Applied Mathematical Modelling*, vol. 33, pp. 2683–2698, Jun 2009.

[79] W. Chen, Y. Yang, W. Chang, and H. Lee, "Inverse problem of estimating transient heat transfer rate on external wall of forced convection pipe," *Energy Conversion and Management*, vol. 49, pp. 2117–2123, Aug 2008.

[80] D. T. W. Lin, W. Yan, and H. Li, "Inverse problem of unsteady conjugated forced convection in parallel plate channels," *International Journal of Heat and Mass Transfer*, vol. 51, pp. 993–1002, MAR 2008.

[81] M. Girault and D. Petit, "Resolution of linear inverse forced convection problems using model reduction by the Modal Identification Method: application to turbulent flow in parallel-plate duct," *International Journal of Heat and Mass Transfer*, vol. 47, pp. 3909–3925, AUG 2004.

[82] C. Huang and W. Chen, "A three-dimensional inverse forced convection problem in estimating surface heat flux by conjugate gradient method," *International Journal of Heat and Mass Transfer*, vol. 43, pp. 3171–3181, SEP 2000.

[83] L. Righetti, J. Buchli, M. Mistry, M. Kalakrishnan, and S. Schaal, "Optimal distribution of contact forces with inverse-dynamics control," *International Journal of Robotics Research*, vol. 32, pp. 280–298, MAR 2013.

[84] K. Nagasaka, Y. Kawanami, S. Shimizu, T. Kito, T. Tsuboi, A. Miyamoto, T. Fukushima, and H. Shimomura, "Whole-body Cooperative Force Control for a Two-Armed and Two-Wheeled Mobile Robot Using Generalized Inverse Dynamics and Idealized Joint Units," IEEE International Conference on Robotics and Automation ICRA, pp. 3377–3383. AK, May 03-08, 2010.

[85] C. Guarino L Bianco and O. Gerelli, "Trajectory scaling for a manipulator inverse dynamics control subject to generalized force derivative constraints," in *IEEE/RSJ International Conference on Intelligent Robots and Systems*, pp. 5749–5754. St Louis, MO, Oct 10-15, 2009.

[86] S. Ider, "Inverse dynamics of redundant manipulators using a minimum number of control forces," *Journal of Robotic Systems*, vol. 12, pp. 569–579, Aug 1995.

[87] K. M. Dolatshahi and F. R. Rofooei, "Inverse vibration problem for un-damped 3-dimensional multi-story shear building models," *Journal of Sound and Vibration*, vol. 333, pp. 99–113, Jan 6 2014.

[88] C. Liu, "An iterative GL(n, R) method for solving non-linear inverse vibration problems," *Nonlinear Dynamics*, vol. 74, pp. 685–699, Nov 2013.

[89] A. Maciag and A. Pawinska, "Solving direct and inverse problems of plate vibration by using the Trefftz functions," *Journal of Theoretical and Applied Mechanics*, vol. 51, no. 3, pp. 543–552, 2013.

[90] G. F. Safina, "Analysis of Direct and Inverse Problems on Transverse Vibrations of a Supported Shaft," *Russian Journal of Nondestructive Testing*, vol. 46, pp. 302–313, APR 2010.

[91] W. Q., W. Y., and Z. L., "Inverse Mode Problem in the Discrete Model of Circular Plate Axial Symmetry Vibration," in *International Conference on Mechanical Engineering and Green Manufacturing (MEGM)*, pp. 71–78, 2010.

[92] B. N. Datta and V. Sokolov, "Quadratic Inverse Eigenvalue Problems, Active Vibration Control and Model Updating," *Applied and Computational Mathematics*, vol. 8, no. 2, pp. 170–191, 2009.

[93] L. D. Chiwiacowsky, H. F. De Campos Velho, and P. Gasbarri, "A variational approach for solving an inverse vibration problem," *Inverse Problems in Science and Engineering*, vol. 14, no. 5, pp. 557–577, 2006. Symposium on Inverse Problems, Design and Optimization, Rio de Janeiro, Brazil, Mar 17-19, 2004.

[94] H. Ressing and M. Gadala, "A practical investigation to solving the inverse problem of crack identification through vibration measurements," *Engineering Computations*, vol. 23, no. 1-2, pp. 32–56, 2006.

[95] N. Khiem, "Crack detection for structure based on the dynamic stiffness model and the inverse problem of vibration," *Inverse Problems in Science and Engineering*, vol. 14, pp. 85–96, Jan 2006.

[96] C. Huang, "A generalized inverse force vibration problem for simultaneously estimating the time-dependent external forces," *Applied Mathematical Modelling*, vol. 29, pp. 1022–1039, Nov 2005.

[97] C. Huang, "A nonlinear inverse problem in estimating simultaneously the external forces for a vibration system with displacement-dependent parameters," *Journal of The Franklin Institute. Engineering and Applied Mathematics*, vol. 342, pp. 793–813, NOV 2005.

[98] C. Huang, "A non-linear inverse vibration problem of estimating the external forces for a system with displacement-dependent parameters," *Journal of Sound and Vibration*, vol. 248, pp. 789–807, Dec 13 2001.

[99] C. Huang, "An inverse non-linear force vibration problem of estimating the external forces in a damped system with time-dependent system parameters," *Journal of Sound and Vibration*, vol. 242, pp. 749–765, May 17 2001.

[100] D. Moss and H. Benaroya, "A discrete inverse vibration problem with parameter uncertainty," *Applied Mathematics and Computation*, vol. 69, pp. 313–333, May 1995.

[101] L. Starek, D. Iman, and A. Kress, "A Symmetric Inverse Vibration Problem," *Journal of Vibration and Acoustics*, vol. 114, pp. 564–568, OCT 1992.

[102] M. Yamamoto, "Inverse eigenvalue problem for a vibration of a string with viscous drag," *Journal of Mathematical Analysis and Applications*, vol. 152, pp. 20–34, OCT 1990.

[103] H. Banks, R. Powers, and I. Rosen, "Inverse problems in the modeling of vibrations of flexible beams," *Lecture Notes in Control and Information Sciences*, vol. 102, pp. 1–22, 1987.

[104] A. Tsaune and V. Golovko, "Anharmonic vibration-rotation inverse problem with reconstruction of Hamiltonian terms," *Journal of Molecular Spectroscopy*, vol. 108, no. 1, pp. 82–98, 1984.

[105] M. Hamada, Y. Seguchi, and Y. Tada, "Shape Determination Problems of Structures by the Inverse Variational Principle : 2nd Report, Buckling and Vibration Problems," *The Japan Society of Mechanical EngineersBulletin of the JSME*, vol. 23, no. 184, pp. 1581–1588, 1980.

[106] N. Stepanov, G. Koptev, and Y. Panchenko, "Uniqueness of solution of an inverse vibration problem," *Optika i spektroskopiya*, vol. 38, no. 4, pp. 657–662, 1975.

[107] C. Yang, "Solution of an inverse vibration problem using a linear least-squares error method," *Applied Mathematical Modelling*, vol. 20, pp. 785–788, Oct 1996.

[108] D. Hua and P. Lancaster, "Linear matrix equations from a non-linear inverse vibration problem of estimating the time-dependent stiffness coefficnverse problem

of vibration theory," *Linear Algebra and its Applications* , vol. 246, pp. 31–47, Oct 1996.

[109] S. Kuroda, I. Kunita, Y. Tanaka, A. Ishiguro, R. Kobayashi, and T. Nakagaki, "Common mechanics of mode switching in locomotion of limbless and legged animals," *Journal of The Royal Society Interface*, vol. 11, no. 95, p. 20140205, 2014.

[110] J. Fattahi and D. Spinello, "A timoshenko beam reduced order model for shape tracking with a slender mechanism," *Journal of Sound and Vibration*, vol. 333, no. 20, pp. 5165 – 5180, 2014.

[111] J. L. Capinera, *Insects and Wildlife: Arthropods and their Relationships with Wild Vertebrate Animals*. Wiley-Blackwell, 2010.

[112] J. L. Capinera, *Encyclopedia of Entomology*, vol. 4. Springer, 2008.

[113] R. W. Cahn, "Biomimetics: Biologically inspired technologies," *Nature*, vol. 444, pp. 425–426, NOV 23 2006.

[114] L. Drago, G. Fusco, E. Garollo, and A. Minelli, "Structural aspects of leg-to-gonopod metamorphosis in male helminthomorph millipedes (Diplopoda)," *Frontiers in Zoology*, vol. 8, Aug 22 2011.

[115] M. Golubitsky, I. Stewart, P. Buono, and J. Collins, "A modular network for legged locomotion," *Phisica D*, vol. 115, pp. 56–72, APR 15 1998.

[116] H. Enghpff, "Adaptive radiation of the millipede genus Cylindroiulus om Madeira: habitat, body size, and morphology (Diplopoda, Julida: Julidae)," *Review of ecology and soil biology*, vol. 20, no. 3, pp. 403–415, 1983.

[117] D. Avirovik, B. Butenhoff, and S. Priya, "Millipede-inspired locomotion through novel U-shaped piezoelectric motors," *Smart Materials and Structures*, vol. 23, Mar 2014.

[118] F. Boyer and S. Ali, "Recursive inverse dynamics of mobile multibody systems with joints and wheels," *IEEE Transactions on Robotics*, vol. 27, pp. 215–228, 2011.

[119] S. Timoshenko, *Vibration Problems In Engineering*. D. Van Nostrand Company Inc., 1974.

[120] E. Kausel, "Nonclassical modes of unrestrained shear beams," *Journal of engineering mechanics*, vol. 128, no. 6, pp. 663–667, 2002.

[121] A. D. Kerr, "Elastic and viscoelastic foundation models," *Journal of Applied Mechanics*, vol. 31, no. 3, pp. 491–498, 1964.

[122] Y. Shin, J. Yun, K. Seong, J. Kim, and S. Kang, "Natural frequencies of euler-bernoulli beam with open cracks on elastic foundations," *Journal of mechanical science and technology*, vol. 20, no. 4, pp. 467–472, 2006.

[123] M.-H. Hsu, "Vibration analysis of edge-cracked beam on elastic foundation with axial loading using the differential quadrature method," *Computer Methods in Applied Mechanics and Engineering*, vol. 194, no. 1, pp. 1–17, 2005.

[124] M. De Rosa, "Free vibrations of timoshenko beams on two-parameter elastic foundation," *Computers & Structures*, vol. 57, no. 1, pp. 151–156, 1995.

[125] S. Lee, Y. Kuo, and F. Lin, "Stability of a timoshenko beam resting on a winkler elastic foundation," *Journal of sound and vibration*, vol. 153, no. 2, pp. 193–202, 1992.

[126] Z. Wang, S. Ma, B. Li, and Y. Wang, "Stability and Adaptability of Passive Creeping of a Snake-like Robot," in *IEEE/RSJ 2010 International Conference on Intelligent Robots and Systems (IROS 2010)*, pp. 395–400, 2010. Taipei, Taiwan, Oct 18-22.

[127] A. G. Razaqpur and K. Shah, "Exact analysis of beams on two-parameter elastic foundations," *International Journal of Solids and Structures*, vol. 27, no. 4, pp. 435–454, 1991.

[128] M. Kargarnovin and D. Younesian, "Dynamics of timoshenko beams on pasternak foundation under moving load," *Mechanics Research Communications*, vol. 31, no. 6, pp. 713–723, 2004.

[129] L. G. Arboleda-Monsalve, D. G. Zapata-Medina, and J. D. Aristizabal-Ochoa, "Timoshenko beam-column with generalized end conditions on elastic foundation: Dynamic-stiffness matrix and load vector," *Journal of Sound and Vibration*, vol. 310, no. 4, pp. 1057–1079, 2008.

[130] X. Ma, J. Butterworth, and G. Clifton, "Static analysis of an infinite beam resting on a tensionless pasternak foundation," *European Journal of Mechanics-A/Solids*, vol. 28, no. 4, pp. 697–703, 2009.

[131] J. Vincent, *Structural biomaterials*. Princeton University Press, 2012.

[132] H. T. Banks, S. Hu, and Z. R. Kenz, "A brief review of elasticity and viscoelasticity," tech. rep., DTIC Document, 2010.

[133] N. F. J. van Rensburg and A. J. van der Merwe, "Natural frequencies and modes of a Timoshenko beam," *Wave Motion*, vol. 44, pp. 58–69, NOV 2006.

[134] S. C. Dutta and R. Roy, "A critical review on idealization and modeling for interaction among soil-foundation-structure system," *Computers & Structures*, vol. 80, pp. 1579–1594, Aug 2002.

[135] D. N. Paliwal and S. N. Sinha, "Static and dynamic behavior of shallow spherical-shells on Winkler foundation," *Thin-Walled Structures*, vol. 4, no. 6, pp. 411–422, 1986.

[136] M. M. Filonenko-Borodich, "Some approximate theories of the elastic foundation," *Uchenyie Zapiski Moskovskogo Gosudarstuennogo Universiteta Mechanika*, no. 46, pp. 3–1, 1940. (in Russian).

[137] P. L. Pasternak, "On a new method of analysis of an elastic foundation by means of two foundation constants," *Gosudarsrvennoe Izdatelstvo Literaturi po Stroitelstvu i Arkhitekture*, 1954. (in Russian).

[138] I. Calio and A. Greco, "Free vibrations of Timoshenko beam-columns on Pasternak foundations," *Journal of Vibration and Control*, vol. 19, pp. 686–696, APR 2013.

[139] C. R. Briscoe, S. C. Mantell, and J. H. Davidson, "Buckling of a plate on a Pasternak foundation under uniform in-plane bending loads," *International Journal of Structural Stability and Dynamics*, vol. 13, Apr 2013.

[140] R. Jones and J. Xenophontos, "The Vlasov foundation model," *International Journal of Mechanical Sciences*, vol. 19, no. 6, pp. 317–23, 1977.

[141] V. Z. Vlasov and U. Leont'ev, "Beams, plates, and shells on elastic foundation," *Gosudarst vennoe lzdatel'st vo Ftziko-Matematicheskoi Literatury Moskva*, 1966.

[142] M. Levinson, "Generalized Vlasov-Jones foundation model - a foundation of grade-4," *International Journal of Mechanical Sciences*, vol. 25, no. 2, pp. 149–154, 1983.

[143] A. Shams and M. Porfiri, "A generalized Vlasov-Jones foundation model for micromechanics studies of syntactic foams," *Composite Structures*, vol. 103, pp. 168–178, Sep 2013.

[144] F. Zhaohua and D. R. Cook, "Beam elements on two-parameter elastic foundation," *Journal of Engineering Mechanics*, vol. 109, no. 6, pp. 1390–1402, 1983.

[145] M. Behl, K. Kratz, U. Noechel, T. Sauter, and A. Lendlein, "Temperature-memory polymer actuators," *Proceedings of the National Academy of Sciences of the United States of America*, vol. 110, pp. 12555–12559, Jul 30 2013.

[146] L. Hines, V. Arabagi, and M. Sitti, "Shape Memory Polymer-Based Flexure Stiffness Control in a Miniature Flapping-Wing Robot," *IEEE Transactions on Robotics*, vol. 28, pp. 987–990, Aug 2012.

[147] F. Boyer, S. Ali, and M. Porez, "Macrocontinuous dynamics for hyperredundant robots: Application to kinematic locomotion bioinspired by elongated body animals," *IEEE Transactions on Robotics*, vol. 28, pp. 303–317, April 2012.

[148] B.-J. Lee, "Geometrical Derivation of Differential Kinematics to Calibrate Model Parameters of Flexible Manipulator," *International Journal of Advanced Robotic Systems*, vol. 10, FEB 7 2013.

[149] L. Chen and H. Deng, "Model reduction of rigid-flexible manipulators with experimental validation," in *Engineering Solutions for Manufacturing Processes, PTS 1-3* (Jiang, ZY and Liu, XH and Jiao, SH and Han, JT, ed.), vol. 655-657 of *Advanced Materials Research*, pp. 1101–1107, 2013. 3rd International Conference on Advances in Materials Manufacturing (ICAMMP 2012), Beihai, Peoples R China, Dec 22-23, 2012.

[150] H. Esfandiar and S. Daneshmand, "Complete dynamic modeling and approximate state space equations of the flexible link manipulator," *Journal of Mechanical Science and Technology*, vol. 26, pp. 2845–2856, Sep 2012.

[151] C. di Castri and A. Messina, "Exact modeling for control of flexible manipulators," *Journal of Vibration and Control*, vol. 18, pp. 1526–1551, Sep 2012.

[152] M. H. Korayem, H. N. Rahimi, and A. Nikoobin, "Mathematical modeling and trajectory planning of mobile manipulators with flexible links and joints," *Applied Mathematical Modelling*, vol. 36, pp. 3223–3238, Jul 2012.

[153] H. Ouyang, D. Richiedei, and A. Trevisani, "Pole assignment for control of flexible link mechanisms," *Journal of Sound and Vibration*, vol. 332, pp. 2884–2899, Jun 10 2013.

[154] J. C. P. Reis and J. S. da Costa, "Motion planning and actuator specialization in the control of active-flexible link robots," *Journal of Sound and Vibration*, vol. 331, pp. 3255–3270, Jul 2 2012.

[155] Z.-C. Qiu, J.-D. Han, X.-M. Zhang, Y.-C. Wang, and Z.-W. Wu, "Active vibration control of a flexible beam using a non-collocated acceleration sensor and piezoelectric patch actuator," *Journal of Sound and Vibration*, vol. 326, pp. 438–455, Oct 9 2009.

[156] Z. J. Jia, Y. D. Song, and W. C. Cai, "Bio-inspired Approach for Smooth Motion Control of Wheeled Mobile Robots," *Cognitive Computation*, vol. 5, pp. 252–263, Jun 2013.

[157] H. Mahjoubi and K. Byl, "Modeling Synchronous Muscle Function in Insect Flight: a Bio-Inspired Approach to Force Control in Flapping-Wing MAVs," *Journal of Intelligent and Robotic Systems*, vol. 70, pp. 181–202, APR 2013.

[158] B. Sun, D. Zhu, F. Ding, and S. X. Yang, "A novel tracking control approach for unmanned underwater vehicles based on bio-inspired neurodynamics," *Journal of Marine Science and Technology*, vol. 18, pp. 63–74, Mar 2013.

[159] Y. Park, D. Young, B. Chen, R. J. Wood, R. Nagpal, and E. C. Goldfield, "Networked Bio-Inspired Modules For Sensorimotor Control of Wearable Cyber-Physical Devices," in *2013 International Conference on Computing, Networking and Communications (ICNC)*, 2013. San Diego, CA, Jan 28-31, 2013.

[160] J. Zhang, G. Qiao, G. Song, and A. Wang, "Design and Implementation of a Remote Control System for a Bio-inspired Jumping Robot," *International Journal of Advanced Robotic Systems*, vol. 9, OcT 10 2012.

[161] S. Tolu, M. Vanegas, N. R. Luque, J. A. Garrido, and E. Ros, "Bio-inspired adaptive feedback error learning architecture for motor control," *Biological Cybernetics*, vol. 106, pp. 507–522, OcT 2012.

[162] K. Abdelnour, A. Stinchcombe, M. Porfiri, J. Zhang, and S. Childress, "Bio-inspired hovering and locomotion via wirelessly powered ionic polymer metal composites," in *Proc. SPIE 7975, Bioinspiration, Biomimetics, and Bioreplication*, pp. 79750R–79750R–9, 2011.

[163] A. Ijspeert, J. Hallam, and D. Willshaw, "From lampreys to salamanders: evolving neural controllers for swimming and walking," in *From Animals to Animats 5* (Pfeifer, R and Blumberg, B and Meyer, JA and Wilson, SW, ed.), From Animals to Animats Series, pp. 390–399, 1998. 5th International Conference on Simulation of Adaptive Behavior, Uuniversity of Zurich, Zurich, Switzerland, Aug 17-21, 1998.

[164] W. Yapp, "Locomotion of Worms," *Nature*, vol. 177, no. 4509, pp. 614–615, 1956.

[165] J. Ostrowski and J. Burdick, "The geometric mechanics of undulatory robotic locomotion," *International Journal of Robotics Research*, vol. 17, pp. 683–701, Jul 1998.

[166] P. Krishnaprasad and D. Tsakiris, "Oscillations, SE(2)-snakes and motion control: a study of the Roller Racer," *Dynamical Systems: An International Journal*, vol. 16, pp. 347–397, Dec 2001.

[167] S. Hirose and Y. Umetani, "Kinematic control of an active cord mechanism with tactile sensors," *Proceedings of the CISM-ZFToM Symposium on Theory and Practice of Robots and manipulators*, pp. 241–252, 1976.

[168] J. C. SIMO, "A Finite Strain Beam Formulation - The 3-Dimensional Dynamic Problem. Part I: Formulation and Optimal Parametrization," *Computer Methids in Applied Mechanics and Engineering*, vol. 49, no. 1, pp. 55–70, 1985.

[169] J. C. Simo and L. Vu-Quoc, "A three-dimensional finite-strain rod model. part II: Computational aspects," *Computer Methods in Applied Mechanics and Engineering*, vol. 58, no. 1, pp. 79 – 116, 1986.

[170] E. Cosserat and F. Cosserat, *Théorie des corps déformables*. Paris: Hermann, 1909.

[171] R. J. Webster, III, J. S. Kim, N. J. Cowan, G. S. Chirikjian, and A. M. Okamura, "Nonholonomic modeling of needle steering," *International Journal of Robotics Research*, vol. 25, pp. 509–525, May-Jun 2006.

[172] D. C. Rucker, B. A. Jones, and R. J. Webster, "A geometrically exact model for externally loaded concentric-tube continuum robots," *Robotics, IEEE Transactions on*, vol. 26, pp. 769–780, Oct 2010.

[173] D. Trivedi, A. Lotfi, and C. D. Rahn, "Geometrically exact models for soft robotic manipulators," *IEEE Transactions on Robotics*, vol. 24, pp. 773–780, Aug 2008.

[174] F. Boyer, M. Porez, and W. Khalil, "Macro-continuous computed torque algorithm for a three-dimensional eel-like robot," *IEEE Transactions on Robotics*, vol. 22, pp. 763–775, Aug 2006.

[175] M. Sfakiotakis and D. P. Tsakiris, "Undulatory and Pedundulatory Robotic Locomotion via Direct and Retrograde Body Waves," in *ICRA: 2009 IEEE International Conference on Robotics and Automation-ICRA*, vol. 1-7, (Kobe, Japan), pp. 3404–3410, May 12-17 2009.

[176] K. L. Hoffman and R. J. Wood, "Passive undulatory gaits enhance walking in a myriapod millirobot," in *2011 IEEE/RSJ International Conference on Intelligent Robots and Systems*, 2011.

[177] B. Borrell, "Mechanical properties of calcified exoskeleton from the neotropical millipede, Nyssodesmus python," *Journal of Insect Physiology*, vol. 50, pp. 1121–1126, Dec 2004.

[178] L. D. Landau and E. M. Lifshitz, *Theory of Elasticity*, vol. 7 of *A Course of Theoretical Physics*. Pergamon Press, 1970.

[179] L. Meirovitch, *Fundamentals of Vibrations*. McGraw-Hill, 2001.

[180] E. Hernandez, D. Kalise, and E. Otarola, "A locking-free scheme for the LQR control of a Timoshenko beam," *Journal of Computational and Applied Mathematics*, vol. 235, pp. 1383–1393, Jan 1 2011.

[181] J. Kauffman, G. Lesieutre, and V. Babuska, "Damping Models for Shear Beams with Applications to Spacecraft Wiring Harnesses," in *53rd*

AIAA/ASME/ASCE/AHS/ASC Structures, Structural Dynamics and Materials Conference, (Honolulu, Hawaii), April 23-25 2012.

[182] Y. Lei, S. Adhikari, and M. I. Friswell, "Vibration of nonlocal Kelvin-Voigt viscoelastic damped Timoshenko beams," *International Journal of Engineering Science*, vol. 66-67, pp. 1–13, May-Jun 2013.

[183] D. S. Bernstein, *Matrix Mathematix: Theory, Facts, and Formulas*. Princeton University Press, second ed., 2009.

[184] L. Majkut, "Free and forced vibrations of Timoshenko beam described by single differential equation," *Journal of Theoretical and Applied Mechanics*, vol. 47, no. 1, pp. 193–210, 2009.

[185] C. F. Beards, *Structural vibration: Analysis and Damping*. Butterworth-Heinemann, 1996.

[186] J. S. Fattahi and D. Spinello, "Path following and shape morphing with a continuous slender mechanism," *Journal of Dynamic Systems, Measurement, and Control*, 2015.

[187] C. Zehetner and H. Irschik, "Displacement compensation of beam vibrations caused by rigid-body motions," *Smart Materials and Structures*, vol. 14, no. 4, p. 862, 2005.

[188] M. W. Spong, S. Hutchinson, and M. Vidyasagar, *Robot Modeling and Control*. Wiley, 2006.

[189] L. Gaul and J. Becker, "Model-based piezoelectric hysteresis and creep compensation for highly-dynamic feedforward rest-to-rest motion control of piezoelectrically actuated flexible structures," *International Journal of engineeing Science*, vol. 47, pp. 1193–1207, Nov-Dec 2009.

[190] F. Boyer, S. Ali, and M. Porez, "Macrocontinuous Dynamics for Hyperredundant Robots: Application to Kinematic Locomotion Bioinspired by Elongated Body Animals," *IEEE Transactions on Robotics*, vol. 28, pp. 303–317, Apr 2012.

[191] F. Boyer and D. Primault, "The Poincare-Chetayev equations and flexible multibody systems," *PMM Journal of Applied Mathematics and Mechanics*, vol. 69, no. 6, pp. 925–942, 2005.

[192] F. Boyer, M. Porez, A. Leroyer, and M. Visonneau, "Fast Dynamics of an Eel-Like Robot-Comparisons With Navier-Stokes Simulations," *IEEE Transaction on Robotics*, vol. 24, pp. 1274–1288, Dec 2008.

[193] S.-M. Kim, H. Kim, K. Boo, and M. J. Brennan, "Demonstration of non-collocated vibration control of a flexible manipulator using electrical dynamic absorbers," *Smart Materials and Structures*, vol. 22, Dec 2013.

[194] S. DanielBerhe and H. Unbehauen, "Physical parameter estimation of the non-linear dynamics of a single link robotic manipulator with flexible joint using the HMF-method," in *Proceedings of the 1997 American Control Conference, Vols 1-6*, pp. 1504–1508, 1997. Albuquerque, NM, Jun 04-06.

[195] R. Tarumi and Y. Oshita, "Free-vibration acoustic resonance of a nonlinear elastic bar," *Philosophical Magazine*, vol. 91, no. 5, pp. 772–786, 2011.

[196] S. H. Arshad, M. N. Naeem, N. Sultana, A. G. Shah, and Z. Iqbal, "Vibration analysis of bi-layered FGM cylindrical shells," *Archive of Applied Mechanics*, vol. 81, pp. 319–343, Mar 2011.

[197] S. B. Choi, S. C. Kim, and H. K. Kim, "Position and force control of a two-link flexible manipulator with piezoelectric actuators," pp. 73–80, 1999.

[198] P.-B. Nguyen and S.-B. Choi, "Open-loop position tracking control of a piezoceramic flexible beam using a dynamic hysteresis compensator," *Smart Materials and Structures*, vol. 19, Dec 2010.

[199] X. Zhang, W. Xu, S. S. Nair, and V. S. Chellaboina, "Pde modeling and control of a flexible two-link manipulator," *IEEE Transactions on Control Systems Technology*, vol. 13, pp. 301–312, 2005.

[200] A. Hać and L. Liu, "Sensor and actuator location in motion control of flexible structures," *Journal of Sound and Vibration*, vol. 167, no. 2, pp. 239–261, 1993.

[201] W. J. Book, O. Maizza-Neto, and D. Whitney, "Feedback control of two beam, two joint systems with distributed flexibility," *Journal of Dynamic Systems, Measurement, and Control*, vol. 97, no. 4, pp. 424–431, 1975.

[202] W. J. Book, "Recursive lagrangian dynamics of flexible manipulator arms," *The International Journal of Robotics Research*, vol. 3, no. 3, pp. 87–101, 1984.

[203] C. di Castri and A. Messina, "Exact modeling for control of flexible manipulators," *Journal of Vibration and Control*, vol. 18, pp. 1526–1551, Sep 2012.

[204] J. Meek and H. Liu, "Nonlinear dynamics analysis of flexible beams under large overall motions and the flexible manipulator simulation," *Computers and Structures*, vol. 56, pp. 1–14, Jul 1995.

[205] K. Yuan and C. Hu, "Nonlinear modeling and partial linearizing control of a slewing Timoshenko-beam," *Journal of Dynamic Systems, Measurement, and Control-Transactions of the ASME*, vol. 118, pp. 75–83, Mar 1996.

[206] A. Zuyev and O. Sawodny, "Observer design for a flexible manipulator model with a payload," in *Proceedings of the 45th IEEE Conference on Decision and Control, Vols 1-14*, pp. 4490–4495, 2006. San Diego, CA, DEC 13-15.

[207] M. Vukobratovic and A. Tuneski, "Adaptive control of single rigid robotic manipulators interacting with dynamic environment - An overview," *Journal of Intelligent and Robotic Systems*, vol. 17, pp. 1–30, Sep 1996.

[208] J. González-Mora, A. Rodríguez-Hernández, L. Rodríguez-Ramos, L. Díaz-Saco, and N. Sosa, "Development of a new space perception system for blind people, based on the creation of a virtual acoustic space," in *Engineering Applications of Bio-Inspired Artificial Neural Networks* (J. Mira and J. Sánchez-Andrés, eds.), vol. 1607 of *Lecture Notes in Computer Science*, pp. 321–330, Springer Berlin Heidelberg, 1999.

[209] S. Yang, X. Jin, K. Liu, and L. Jiang, "Nanoparticles assembly-induced special wettability for bio-inspired materials," *Particuology*, vol. 11, pp. 361–370, Aug 2013.

[210] K. Liu, Y. Tian, and L. Jiang, "Bio-inspired superoleophobic and smart materials: Design, fabrication, and application," *Progress in Materials Science*, vol. 58, pp. 503–564, May 2013.

[211] E. I. Saavedra F., M. I. Friswell, and Y. Xia, "Variable stiffness biological and bio-inspired materials," *Journal of Intelligent Material Systems and Structures*, vol. 24, pp. 529–540, Mar 2013.

[212] A. Sugawara-Narutaki, "Bio-inspired synthesis of polymer-inorganic nanocomposite materials in mild aqueous systems," *Polymer Journal*, vol. 45, pp. 269–276, Mar 2013.

[213] M. M. Stevens and G. Mecklenburg, "Bio-inspired materials for biosensing and tissue engineering," *Polymer International*, vol. 61, pp. 680–685, May 2012.

[214] A. Menciassi and P. Dario, "Bio-inspired solutions for locomotion in the gastrointestinal tract: background and perspectives," *Philosophical Transactions of the Royal Society A:-Mathematical, Physical and Engineering Sciences*, vol. 361, pp. 2287–2298, OcT 15 2003. International Workshop on Biologically Inspired Robotics, Hewlett-Packard Lab, Bristol, UK, Aug, 2002.

[215] P. Dario, P. Ciarletta, A. Menciassi, and B. Kim, "Modelling and experimental validation of the locomotion of endoscopic robots in the colon," in *Experimental RoboticsS VIII* (Siciliano, B and Dario, P, ed.), vol. 5 of *Springer Tracts in Advanced Robotics*, pp. 445–453, 2003. 8th International Symposium on Experimental Robotics (ISER 02), Sant'Angelo, Italy, Jul 08-11, 2002.

[216] D. Huston, J. Miller, and B. Esser, "Adaptive, robotic and mobile sensor systems for structural assessment," in *Smart Structures and Materials 2004: Sensors and Smart Structures Technologies for Civil, Mechanical, and Aerospace Systems* (Liu, SC, ed.), vol. 5391 of *Proceedings of SPIE-The International Society for Optical Engineering*, pp. 189–196, 2004.

[217] B. Esser and D. Huston, "Versatile robotic platform for structural health monitoring and surveillance," *Smart Structures and Systems*, vol. 1, pp. 325–338, OcT 2005.

[218] Y. Cha, H. Kim, and M. Porfiri, "Energy harvesting from underwater base excitation of a piezoelectric composite beam," *Smart Materials and Structures*, vol. 22, no. 11, p. 115026, 2013.

[219] Y. Cha, L. Shen, and M. Porfiri, "Energy harvesting from underwater torsional vibrations of a patterned ionic polymer metal composite," *Smart Materials and Structures*, vol. 22, no. 5, p. 055027, 2013.

[220] K. M. Dorgan, C. J. Law, and G. Rouse, "Meandering worms: mechanics of undulatory burrowing in muds," *Proceedings of the Royal Society B Biological Sciences*, vol. 280, Apr 2013.

[221] K. A. Daltorio, A. S. Boxerbaum, A. D. Horchler, K. M. Shaw, H. J. Chiel, and R. D. Quinn, "Efficient worm-like locomotion: slip and control of soft-bodied peristaltic robots," *Bioinspiration & Biomimetics*, vol. 8, Sep 2013.

[222] S. Hirose, "Connected differential mechanism and its applications," *Proceedings of the 2nd International Conference in Advances in Robotics*, pp. 319–326, 1985.

[223] S. K. Ider, "Stability analysis of constraints in flexible multibody systems dynamics," *International Journal of engineeing Science*, vol. 28, no. 12, pp. 1277–1290, 1990.

[224] P. Chadwick, *Continuum Mechanics: Concise Theory and Problems*. Dover Publications, 1 ed., 1998.

[225] C. M. Bender and S. A. Orszag, *Advanced Mathematical Methods for Scientists and Engineers I*. Springer, 1999.

[226] R. B. Hetnarski and J. Ignaczak, *The Mathematical Theory of Elasticity*. CRC Press, 2 ed., 2010.

[227] C. Batlle, A. Dòria-Cerezo, G. Espinosa-Pérez, and R. Ortega, "Simultaneous interconnection and damping assignment passivity-based control: Two practical examples," in *Lagrangian and Hamiltonian Methods for Nonlinear Control 2006*, pp. 157–169, Springer, 2007.

[228] J. Fattahi and D. Spinello, "Sensing linear viscoelastic constitutive parameters with a timoshenko beam on a multi-layer foundation: Modeling and simulation," *Sensing and Bio-Sensing Research*, vol. 4, pp. 78–89, 2015.

[229] H. Lee, C. Richards, and R. Richards, "Experimental and numerical study of microchannel heater/evaporators for thermal phase-change actuators," *Sensors and Actuators A: Physical*, vol. 195, pp. 7–20, 2013.

[230] H. V. Thakur, S. M. Nalawade, Y. Saxena, and K. Grattan, "All-fiber embedded pm-pcf vibration sensor for structural health monitoring of composite," *Sensors and Actuators A: Physical*, vol. 167, no. 2, pp. 204–212, 2011.

[231] J. Humphrey, "Continuum biomechanics of soft biological tissues," *Proceedings of the Royal Society A: Mathematical, Physical and Engineering Sciences*, vol. 459, pp. 3–46, Jan 8 2003.

[232] Y. Fung, *Biomechanics: Mechanical Properties of Living Tissues*. Biomechanics, Springer, 1993.

[233] M. D. Maestro, F. Cecchi, S. M. Serio, C. Laschi, and P. Dario, "Sensing device for measuring infants grasping actions," *Sensors and Actuators A-physical*, vol. 165, pp. 155–163, 2011.

[234] M. Morris, F. Huxham, J. McGinley, K. Dodd, and R. Iansek, "The biomechanics and motor control of gait in Parkinson disease," *Clinical Biomechanics*, vol. 16, pp. 459–470, Jul 2001.

[235] G. Y. H. Lee and C. T. Lim, "Biomechanics approaches to studying human diseases," *Trends in Biotechnology*, vol. 25, pp. 111–118, Mar 2007.

[236] E. J. Weinberg, D. Shahmirzadi, and M. Mofrad, "On the multiscale modeling of heart valve biomechanics in health and disease," *Biomechanics and Modeling in Mechanobiology*, vol. 9, pp. 373–387, AUG 2010.

[237] M. K. Rausch and E. Kuhl, "On the effect of prestrain and residual stress in thin biological membranes," *Journal of the Mechanics and Physics of Solids*, vol. 61, pp. 1955–1969, SEP 2013.

[238] L. M. Sander, "Alignment Localization in Nonlinear Biological Media," *Journal of Biomechanical Engineering, Transactions of the ASME*, vol. 135, Jul 2013.

[239] A. M. Zoellner, A. B. Tepole, and E. Kuhl, "On the biomechanics and mechanobiology of growing skin," *Journal of Theoretical Biology*, vol. 297, pp. 166–175, MAR 21 2012.

[240] G. Gladwell, *Inverse Problems in Vibration*. Mechanics, Dynamical Systems, Vol 9, Kluwer, 1986.

[241] W. Liu, D. Li, and J. Shen, "Least-squares solutions of constrained inverse eigenproblem and associated optimal approximation problem," *International Journal of Computer Mathematics*, vol. 90, pp. 641–650, Mar 1 2013.

[242] M. S. Gockenbach and A. A. Khan, "An abstract framework for elliptic inverse problems: Part 1. An output least-squares approach," *Mathematics and Mechanics of Solids*, vol. 12, pp. 259–276, Jun 2007.

[243] R. Forke, D. Scheibner, K. Hiller, T. Gessner, W. Dötzel, and J. Mehner, "Fabrication and characterization of a force coupled sensor–actuator system for adjustable resonant low frequency vibration detection," *Sensors and Actuators A: Physical*, vol. 145, pp. 245–256, 2008.

[244] S. J. Fattahi and D. Spinello, "Timoshenko Beam Model for Exploration and Sensing with a Continuum Centipede Inspired Robot," in *Proceedings of 2013 ASME Dynamic Systems and Control Conference*, vol. 5391, pp. 189–196, 2013. Stanford, CA, Oct.

[245] J. Fattahi and D. Spinello, "A Timoshenko beam reduced order model for shape tracking with a slender mechanism," *Journal of Sound and Vibration*, vol. 333, no. 20, pp. 5165 – 5180, 2014.

[246] A. Plaseied and A. Fatemi, "Deformation response and constitutive modeling of vinyl ester polymer including strain rate and temperature effects," *Journal of Materials Science*, vol. 43, no. 4, pp. 1191–1199, 2008.

[247] A. D. Kerr, "Elastic and viscoelastic foundation models," *Journal of Applied Mechanics*, vol. 31, p. 491, 1964.

[248] M. Kneifati, "Analysis of plates on a kerr foundation model," *Journal of Engineering Mechanics*, vol. 111, no. 11, pp. 1325–1342, 1985.

[249] M. Works, "fminsearch." `http://www.mathworks.com/help/matlab/ref/fminsearch.html`, Release 12.

[250] R. Myers, *Classical and Modern Regression With Applications*. Duxbury classic series, Duxbury/Thompson Learning, 1990.

Glossary of Terms

H : Hilbert Space.

L : Lebesgue Space.

t : the deformation oscillations time.

τ : rigid body degrees of freedom oscillations time.

$w(x,t)$: transverse displacement of the beam compared to the centerline.

u : represent the components of displacement parallel to x direction.

v : represent the components of displacement parallel to y direction.

w : represent the components of displacement parallel z direction.

$p_u(x,t)$: external distributed axial force.

$p_w(x,t)$: external distributed vertical force.

$p_\psi(x,t)$: external distributed torque.

$M(x,t)$: bending moment.

$V(x,t)$: shear force.

A : $[m^2]$, cross sectional area $A = y.z$.

ρ : $[kg\ m^{-3}]$, density of the beam.

δ : variation inintegrating; used in Hamilton's Principle.

π : strain energy.

$\mathcal{K}$: kinetic energy.

$\boldsymbol{\sigma}$: Cauchy stress tensor.

ε_{ij} : strain component.

σ_{ij} : stress component.

G : $[Pa]$, shear modulus.

k : shear correction factor.

E : $[Pa]$, Young's modulus.

I : $[m^4]$, moment of inertia with respect to the y axis.

g : $[m\ s^{-2}]$, gravitational acceleration.

ℓ : $[m]$, length of the beam.

β : shear angle

ν : linear velocity.

ω : angular velocity.

$p_\eta(x,t)$: force per unit length exerted by the elastic foundation.

M_η : induced moment by the elastic foundation.

κ_w : foundation elastic coefficient.

κ_{w_1} : second elastic foundation.

E_s : Young's modulus of foundation.

ν_s : Poisson's ratio of foundation.

κ_G : shear modulus of foundation.

μ : damping parameter of viscoelastic model.

R : position of the reference frame origin (X_1', X_2', X_3') with respect to the inertial reference (X_1, X_2, X_3).

θ : orientation of the body reference with respect to the inertial reference.

$\bar{u}$: position vector of the arbitrary point.

$\mathbf{A}$: transformation matrix between the floating and inertial reference frame.

$\mathbf{S}$: space-dependent shape matrix,

$\mathbf{q}_f$: time-dependent vector, generalized coordinates of the deformable body.

$\mathbf{U}$: system deformation in a floating frame.

$\{\mathbf{E}_1, \mathbf{E}_2, \mathbf{E}_3\}$: orthonormal Cartesian basis.

$\mathbf{X} = \{X_1, X_2, X_3\}$: material coordinates.

$\mathbf{R}$: rigid body rotation matrix.

$\mathbf{d}$: rigid body translation matrix.

$\bar{\mathbf{u}}$, $\bar{\mathbf{w}}$, $\bar{\boldsymbol{\psi}}$: $n-$ dimensional sets of spatial basis functions.

Appendix A

Floating Frame Approach

To present a flexible multi-body system in the motion, we can use different approach like; Inertial frame, Co-rotational frame and Floating frame of references. In the Inertial frame approach; an absolute nodal co-ordinates is defined in an absolute reference frame, and no distinction between the rigid and elastic coordinates is exist. In Co-rotational frame; the motion will be separated into the gross motion and small deformation motion of the finite elements which follow the gross motion. In the concept of floating frame of reference we use a reference frame that follows the motion of the flexible body, in which the reference motion is not the rigid body motion. Therefore, different coordinate systems can be selected for a deformable body. The floating frame does not lead to a separation between the gross motion and the small deformation. In this study the floating frame concept is being used to develop the dynamic equations of a mobile flexible slender mechanism. In order to solve dynamic equations using Galerkin approximation; a shape function should be taken into account, and naturally the isoparametric elements for the shape functions should satisfy the kinetic boundaries and also describe the arbitrary rigid body translations and infinitesimal rotations. On the other hand; in the Floating frame, the motion of the flexible body can be represented by two sets of reference and elastic coordinates. The reference coordinates show the position and orientation of the floating reference origin and the elastic coordinates identify the displacements of the deformable body with respect to the body reference. The reference frame configuration can be expressed as,

$$\mathbf{q}_r = \begin{bmatrix} \mathbf{R}^T & \theta^T \end{bmatrix}^T \tag{A.1}$$

where $\mathbf{R}$ is a vector that describes the position of the reference frame origin (X_1', X_2', X_3'), with respect to the inertial reference (X_1, X_2, X_3), and θ represents the orientation of the

system's body reference with respect to the inertial reference. Therefore, the position vector $\mathbf{r}$ can be considered in the inertial reference frame as the position vector of an arbitrary point on flexible body with respect to the inertial origin,

$$\mathbf{r} = \mathbf{R} + \mathbf{A}\mathbf{u} \tag{A.2}$$

where $\mathbf{u}$ is the local position vector of the arbitrary point $\mathcal{P}$, and $\mathbf{A}$ is the transformation matrix between the floating and inertial reference frame,

$$\mathbf{A} = \begin{bmatrix} \cos\theta & -\sin\theta & 0 \\ \sin\theta & \cos\theta & 0 \\ 0 & 0 & 1 \end{bmatrix} \tag{A.3}$$

Considering the gross as a rigid body; the components of relevant vector for any two arbitrary points on the body coordinate system remain unchanged, but considering relative motion, in flexible bodies the distance between two arbitrary points on the deformable body does not remain constant, and local position vector of point $\mathcal{P}$ can be redefine as,

$$\mathbf{u} = \mathbf{u}_0 + \mathbf{u}_f \tag{A.4}$$

where $\mathbf{u}_0$ is the position vector of point $\mathcal{P}$ in the undeformed state, and $\mathbf{u}_f$ is the displacement vector of point $\mathcal{P}$ with respect to undeformed state, which is a *space-time* dependent vector, and it can be defined by projection method as partial sums of the series of the base functions and time dependant coefficient. Therefore, the equation (A.4) can be rewritten as

$$\mathbf{u} = \mathbf{u}_0 + \mathbf{S}\mathbf{q}_f \tag{A.5}$$

where $\mathbf{S}$ is a space-dependent shape matrix, and $\mathbf{q}_f$ is the vector of time-dependent elastic generalized coordinates of the deformable body. Then we can rewrite the global position of an arbitrary point $\mathcal{P}$ (equation (A.2)) in the planar case,

$$\mathbf{r} = \mathbf{R} + \mathbf{A}\left(\mathbf{u}_0 + \mathbf{S}\mathbf{q}_f\right) \tag{A.6}$$

The velocity equation can be obtained by differentiating (A.2) with respect to time,

$$\dot{\mathbf{r}} = \dot{\mathbf{R}} + \dot{\mathbf{A}}\mathbf{u} + \mathbf{A}\dot{\mathbf{u}} \tag{A.7}$$

where, considering time derivatives of the elastic coordinates of body the $\dot{\mathbf{u}}_0 = 0$, and $\dot{\mathbf{u}} = \mathbf{S}\dot{\mathbf{q}}_f$, therefore (A.7) can be rewritten as;

$$\dot{\mathbf{r}} = \dot{\mathbf{R}} + \dot{\mathbf{A}}\mathbf{u} + \mathbf{A}\mathbf{S}\dot{\mathbf{q}}_f \tag{A.8}$$

By rewriting $\dot{\mathbf{A}}\mathbf{u} = \mathbf{B}\dot{\boldsymbol{\theta}}$, we can isolate the velocity term, in which $\boldsymbol{\theta}$ is here the vector which elements $\dot{\boldsymbol{\theta}}$ are the time derivatives of the rotational coordinates of the body reference, and $\mathbf{B} = \mathbf{B}(\theta, \mathbf{q}_f)$ can be defined

$$\mathbf{B} = \left[\frac{\partial}{\partial \theta_1} (\mathbf{A}\mathbf{u}) , \frac{\partial}{\partial \theta_2} (\mathbf{A}\mathbf{u}) \dots \frac{\partial}{\partial \theta_{n_r}} (\mathbf{A}\mathbf{u}) \right] \tag{A.9}$$

where the n_r is the total number of rotational coordinates of the reference of body, and using chain rule, equation (A.9) can be rewrite

$$\mathbf{B} = \sum_{k=1}^{n_r} \frac{\partial}{\partial \boldsymbol{\theta}_k} (\mathbf{A}\mathbf{u}) \, \dot{\boldsymbol{\theta}}_k \tag{A.10}$$

then by substitution $\dot{\mathbf{A}}\mathbf{u} = \mathbf{B}\dot{\boldsymbol{\theta}}$ into (A.8), the partitioned form of the absolute velocity vector can be found

$$\dot{r} = \begin{bmatrix} \mathbf{I} & \mathbf{B} & \mathbf{A}\mathbf{S} \end{bmatrix} \begin{bmatrix} \dot{\mathbf{R}} \\ \dot{\boldsymbol{\theta}} \\ \dot{\mathbf{q}}_f \end{bmatrix} \tag{A.11}$$

where $\mathbf{I}$ is a 3×3 identity matrix.

As it stated in Paper B, using velocity equation and developing expressions for the kinetic energy and considering virtual work principles the mass matrix, the quadratic velocity vector for the elastic and external forces can be derived.

Appendix B

Copyright Permission

Dear Mr. Fattahi,

It is our pleasure to grant you permission to use all or any part of the ASME paper "Path Following and Shape Morphing With a Continuous Slender Mechanism, by Javad S. Fattahi; Davide Spinello, J. Dyn. Sys., Meas., Control. 2015; 137(10), cited in your letter for inclusion in a PhD thesis entitled Locomotion and Morphing of a Coupled Bio-Inspired Flexible System: Modeling and Simulation to be published by University of Ottawa.

Permission is granted for the specific use as stated herein and does not permit further use of the materials without proper authorization. Proper attribution must be made to the author(s) of the materials. Please note: if any or all of the figures and/or Tables are of another source, permission should be granted from that outside source or include the reference of the original source. ASME does not grant permission for outside source material that may be referenced in the ASME works.

As is customary, we request that you ensure full acknowledgment of this material, the author(s), source and ASME as original publisher. Acknowledgment must be retained on all pages printed and distributed.

Many thanks for your interest in ASME publications.

Sincerely,

Beth Darchi
Publishing Administrator
ASME
2 Park Avenue, 6th Floor
New York, NY 10016-5990